Freeze Concentration of Aqueous Solutions by Clathration

A Thesis submitted for the
Degree of Doctor of Philosophy
in the University of London

by

Stuart Wilson Aaron, B.Sc.(Eng), A.C.G.I.

Department of Chemical Engineering
and Chemical Technology,
City and Guilds College,
Imperial College,
London, S. W. 7.

October 1968

Abstract

Current interest in direct-contact heat transfer, in which a volatile dispersed phase evaporates into a continuous medium, has stimulated a study into the possible use of this technique for concentrating liquid foodstuffs. The immiscible refrigerant selected for its low toxicity, difluorodichloromethane, combines with water to form a crystalline clathrate, or hydrate.

Bench-scale tests were conducted with aqueous sucrose solutions in a well-stirred 5 litre reactor which was operated both batchwise and as a flow reactor. Hydrate equilibrium data and agent solubility for the sucrose system have been determined in the batch reactor. Material and energy balances have been established and the degree and rate of concentration effectively analysed in terms of the experimental variables - power input, sucrose concentration, reactor temperature and pressure and slurry viscosity.

The process offers a convenient method of concentrating aqueous feedstocks. 20% of the water contained in the sucrose feed may be removed as hydrate in a single stage and the hydrate crystals may be washed free of occluded mother liquor.

The experimental results show that the rate-controlling mechanism is the transfer of agent through the continuous-phase boundary layer surrounding the agent bubbles. A correlation for the volumetric liquid-film mass-transfer coefficient has been derived, which makes it possible to predict the performance of a single stage reactor.

Comparative tests were conducted in the same equipment with propane as the hydrating agent. A comparison of the results suggests that the correlation developed for the Freon-12 system may not be extended to include other hydrate formers. The experimental coefficients also differ substantially from those predicted by established two-phase correlations and it is considered that these differences are due to the effects of the boiling liquid phase and the reactor pressure. Tests with growth and decomposition of the hydrate indicate a fundamental dependence on operating pressure.

Acknowledgements

The author's thanks and appreciation are due to Dr. A. P. Shahbenderian for his invaluable stimulation and advice throughout the course of this work.

Thanks are due to Mr. J. S. Oakley and his staff for the technical advice and assistance in construction of the apparatus.

Finally the author would like to thank the Science Research Council for providing the necessary maintenance grant.

Contents

		Page
1.	Introduction	1
	1.2 Choice of process	7
2.	Introduction to hydrate process	9
	2.1 The hydrate process - phase diagram	9
	2.2 Commercial process for desalination	12
	2.3 The hydrate process for sucrose concentration	16
	2.4 Primary experimental investigation	18
	2.5 Proposed experimental project	21
3.	Experimental hydrate process	23
	3.1 Reactor operation	23
	3.2 The hydrate reactor	26
	3.3 Freon cycle design	39
	3.4 Glycol bath and constant temperature bath	43
	3.5 Decomposition vessel and filter unit	48
	3.6 Design of experiments	49
	3.7 Operating procedure	55
4.	Equilibrium and freon solubility data	
	4.1 Phase diagram for freon-12 hydrate in sucrose solution	63
	4.2 Hydrate equilibrium analysis	69
	4.3 Solubility of freon-12 in sucrose solution	79
	4.4 Proposed solubility model	84

Contents (continued) Page

5. Theory and literature review 89

5.1 Hydrate growth in autorefrigerated reactors 89

5.2 Hydrate kinetic studies 100

5.3 Effect of mixing on over-all mass transfer coefficients 107

5.4 Heat transfer considerations 122

5.5 Batch hydrate kinetics 133

5.6 Heat and mass balance for steady-state runs.....143

6. Experimental results 145

6.1 Calculation of temperature-time curves.....145

6.2 Batch runs as an approximation to steady-state conditions 155

6.3 Analysis of steady-state data 184

6.4 Propane hydrate experiments 196

7. Nucleation, decomposition and filtration results 198

7.1 The onset of spontaneous nucleation 198

7.2 Decomposition studies 206

7.3 Results of wash studies 216

8. Discussion of results and design criteria 221

8.1 The hydrate growth model 221

8.2 Comparison of the over-all mass transfer coefficient with published data 224

8.3 Comparison with propanes and methyl bromide as hydrate formers 229

8.4 Reactor performance as a concentration stage 233

8.5 Scale-up considerations 234

8.6 Recommendations for further work 238

Contents (continued)

Appendices		Page
A	Batch hydrate results	240
B	Flow reactor results	279
C	Propane hydrate data	286
D	Decomposition results	298
E	Solubility and equilibrium data	305
F	Filtration data	313
G	Calibrations and physical constants	326
Notation		334
References		337

1. Introduction

The special aspect of this study was to investigate a process for the concentration of aqueous heat sensitive potable liquids by freezing out ice using a direct contact cooling medium to effect heat transfer. Concentrates of heat sensitive liquids such as fruit and vegetable juices are in most cases juices which, when rediluted, resemble the original juice in composition and flavour. Table 1.1, (1) gives some examples of products and the particular cases for concentration. Concentration at elevated temperatures results in loss of nutritive and organoleptic stability. The relative heat sensitivity of juices is controlled not only by the temperature of concentration, but also by the time of holding at this temperature (2).

Product	Purpose
Orange Juice	Reduce shipping, storage, container costs
Fruit Syrups	Raise sugar content of comestibles to such a level as to retard spoilage
Instant or Soluble Coffee	Concentrated liquid which can then be economically subjected to complete dehydration (e.g. freeze drying)
Beer	Reduce liquid volume for handling and storage in plant

Table 1.1 Case for concentration of aqueous solutions

Concentration by evaporation, which may strip volatile aromatic compounds that contribute to the flavour of the juice, is often carried out in turbulent film single-pass vacuum evaporators. Such film evaporation techniques give suitable short-contact, low temperature characteristics. Additional equipment is required for aromatics recovery and subsequent blending.

Concentration by freezing is the most satisfactory method for removing water from fruit juices without altering the natural flavour (3). The Linde-Krause (4) freeze technique was one of the first continuous processes for concentrate production: ice was formed on the surface of a refrigerated drum rotating in a trough of juice. The successor to this process is the scraped surface heat exchanger (5,6) which can produce concentrates of markedly superior flavour to the evaporation process. Fruit juices, coffee extract and vinegar are slush frozen in the freezer, e.g. The Chemetron Corporation 'Votator' (7), and the fine uniform ice crystals are centrifuged and washed. For most materials 50% of the water is removed as ice in a single stage, and the loss of solids in the ice phase

is kept as low as 0.5 to 1%. The viscosity of the cold concentrated liquid with a hold-up of many fine crystals is quite high; agitation and the separation of small crystals from viscous mother liquor becomes difficult. In general with all liquids a viscosity limit constrains operating conditions before the eutectic composition is reached. Freeze concentration by this technique is more expensive than evaporation, Dooley (7) indicates a factor of two, but it is justified in terms of product quality.

The importance of the desalination projects of the Office of Saline Water (8) has renewed interest in novel methods of freeze concentration. Since the advent of improved slurry reflux washing techniques (9), it seems likely that freeze concentration may now be a more competitive proposition. In common with the 'Votator' process, freeze concentrates produced commercially invariably employ a secondary metallic surface for indirect heat transfer. This additional resistance demands a larger equivalent transfer area and imposes the mechanical problems of scraping a surface upon which ice crystals are seeded.

When, on the other hand, a cooling agent is dispersed within the bulk of the aqueous phase, a

large transfer area is established, and controlled nucleation and growth is more readily achieved than with the higher thermal driving forces associated with secondary surfaces. The higher crystallization temperature results in a lower energy consumption, and the smaller subcooling will tend to form cubic crystals rather than dendrites which occlude mother liquor.

A search through the available literature and patents indicates four areas of interest which warrant investigation.

1.11 Heat transfer without change of phase (10)

A process in which the solvent freezes out in the form of a crust on the surface of a cold immiscible non-volatile liquid particle immersed in the aqueous sclution. Little interest has been shown in this method, but liquid-liquid heat exchangers are being investigated as heat recovery units (11). A survey of the heat transfer characteristics of this system is given by Sideman and Shabtai (12).

Since the latent heat of fusion is to be converted into a sensible heat gain of the immiscible agent, the required initial subcooling of the agent will be

sufficient to nucleate ice rapidly in the neighbourhood of the drops and produce many small occluded crystals. The process is still costly, and losses of solute are realised with crystals grown under high thermal driving forces.

1.12 Freezing Point Depression Technique (13)

A soluble gas is dissolved in the aqueous solution under pressure, thereby lowering the freezing temperature. The solution is then cooled below its original freezing temperature with no ice formation on the cooling surface. A release of the pressure causes partial freezing out of ice. Work carried out by Stinchfield (14) on this process using CO_2 as the gaseous agent, shows that a ten cycle process needed for effective concentration is not only very expensive but in fact contra-indicated. The main criticism is that the heat of fusion of ice must be absorbed by the solution as sensible heat, and this requires that very high pressures are used to dissolve sufficient agent to achieve realistic per-stage concentrations.

1.13 Heat Transfer with change of phase (15)

The aqueous solution is mixed with an immiscible volatile liquid, which flashes off in one or more evaporation stages. Ice grown in the stage is separated and the cycle completed by condensing the refrigerant on the washed ice. This process is attracting investigation by several desalination authorities, many of them use butane as the immiscible refrigerant (16). The vacuum freezer (17), in which ice is frozen out from sea water under vacuum at the triple point, also comes under this category, water behaving as the refrigerant.

1.14 Heat Transfer with change of phase accompanied by reaction (18)

This involves a chemical process in which a clathrating agent and water combine to form insoluble crystals. A classification of the types and structure of clathrates, more commonly and loosely referred to as hydrates, is presented by von Stackelberg (35). The crystals are separated and the hydrating agent, which evaporates to remove the heat of reaction, is condensed on the washed crystals. The initial survey of this process has been described, from the desalination aspect in several publications which also discuss the relative merits of the fluorocarbon and paraffin hydrate formers (19,20).

1.2 Choice of Process

With these considerations in mind, the investigation of a process utilizing a boiling liquid refrigerant seems most interesting. For this case the heat of fusion is transferred through a very small temperature differential to the boiling agent. As the temperature differential decreases, so the process becomes more ideal; hence energy for conversion is minimised. The choice of the best refrigerant is important since many otherwise suitable agents would strip the liquid food of flavour, or impart some taste to the concentrate. The Freon family are generally very insoluble, non-toxic and innocuous, and of these FREON-12, difluorodichloromethane, is a commercially familiar and reasonably priced refrigerant. Freon-12 is also a hydrating agent and, since there is a definite shortage of data on hydrate kinetics compared with the work undertaken by the Office of Saline Water on ice growth, the hydrate process was chosen for study. It was decided to use sucrose solution as the aqueous medium. For experimental purposes, sucrose was desirable since it has high purity for a low cost and its physical properties are well documented.

An alternative scheme for the production of ice in fruit juices could have employed octofluorocyclobutane, C-318, an inert fluorocarbon refrigerant which does not behave as an hydrating agent. The cost of C-318 is very high, but agent losses from a well-designed commercial plant should be very small.

1.21 Reverse Osmosis

Recent developments with plastic membranes have drawn attention to the possibility of reverse osmosis as a competitive means of concentration. Sourinajan (21) has applied this technique to the concentration of sucrose in aqueous solutions using a porous cellulose-acetate membrane. The batch apparatus is described as a practical concentration technique for natural maple syrup and other industrial sugar solutions. The main advances in this field will be sought in the development of membrane technology.

2. Introduction to Hydrate Process

2.1 The Hydrate Process Phase Diagram

Pure water is separated from an aqueous solution by a reaction with a suitable agent to produce a solid hydrate. The process can achieve 100% solute recovery since the solid phase is completely selective towards water. The heat of reaction is transferred to the evaporating agent dispersed in the solution. Reference to the phase diagram gives an insight into the mechanism of hydrate growth. The diagram defines the pressures and temperatures at which hydrate exists and characterises the departure from phase equilibrium which exists in a hydrate reactor.

A conventional phase diagram is used to represent the equilibrium conditions. Figure 1 shows the two component system Freon-12 and water where line AD is the vapour pressure curve. Area I, below the condensation line, represents liquid water containing dissolved freon and freon vapour. Above line ED, Area III represents the liquid phases water and freon. When the system is cooled below EBC a crystalline hydrate appears. EB is the equilibrium line between the solid hydrate and liquid freon: it approximates to a vertical line (19). In Area II all water is

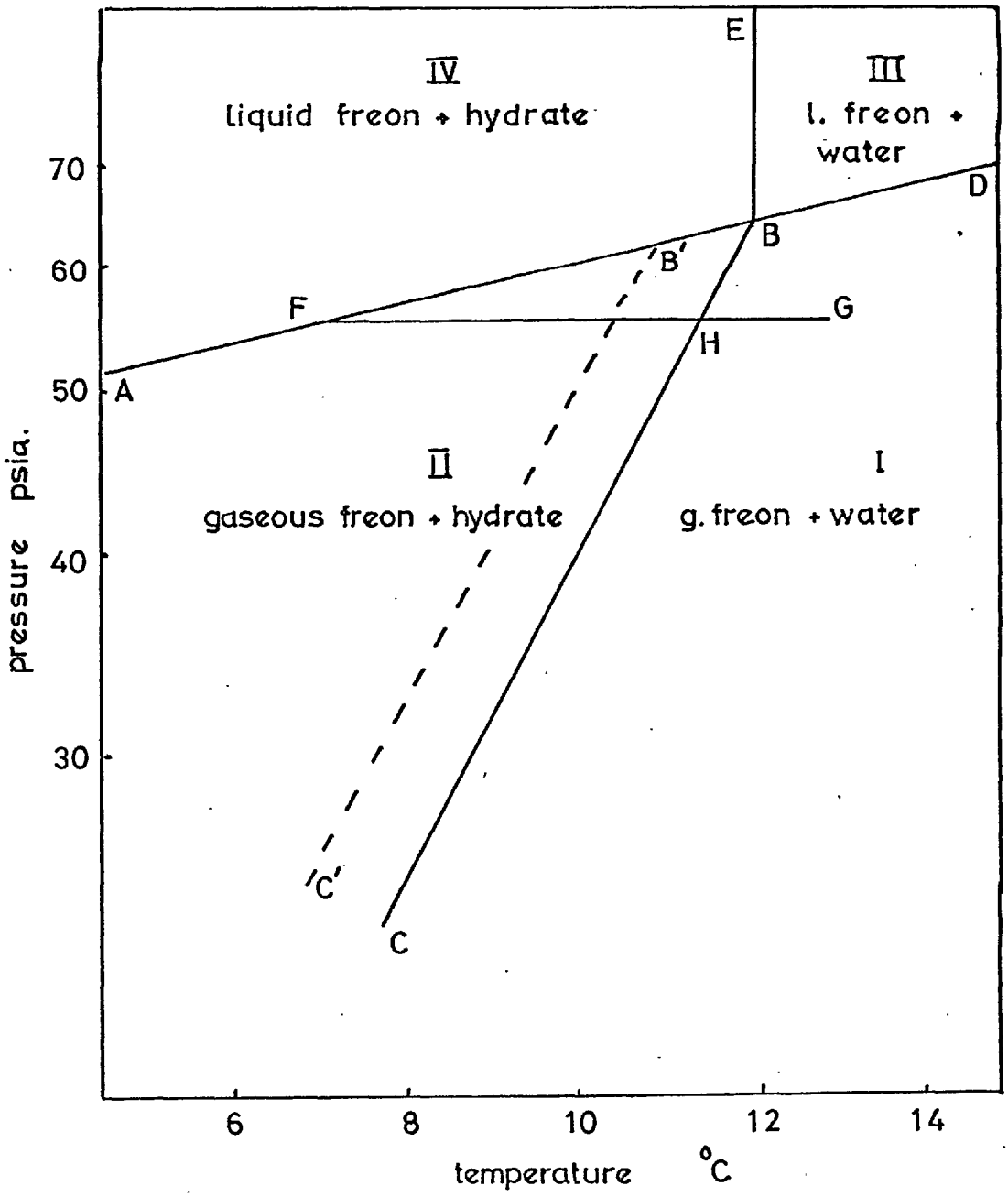


figure 1 Phase diagram, Freon-12 hydrate

converted to hydrate if there is an excess of freon, or in the case of an excess of water, all freon is converted to hydrate. Line BC denotes the equilibrium between hydrate and water in an atmosphere of gaseous freon.

The quadruple point B is an invariant point and the pressure and temperature characterising this transition are referred to as the critical decomposition pressure and temperature. At the critical pressure four phases co-exist in the two component system: Hence, by the phase rule, there are zero degrees of freedom.

If the hydrate reactor conditions are represented by position G on figure 1 and the reactor is cooled at constant pressure, hydrate should appear as FG crosses the hydrate line BC at H. The temperature stays constant as hydrate is formed and the solution cooled. In practice there is a tendency for the aqueous solution to supercool a definite extent before growth of hydrate occurs; this period is equivalent to the metastable limit of Ostwald. The temperature of the reactor contents must fall below this limit in order that spontaneous nucleation may occur, but the growth process can take place within the limit.

Consider the practical case in which cooling is obtained by the evaporation of freon in the reactor, at a constant pressure corresponding to FHG. As the solution is cooled the temperature falls below H and at some temperature in Area II the solution nucleates spontaneously. The production of hydrate is accompanied by a generation of heat and the reactor temperature rises. The temperature increases to a steady value at which the rate of heat generation is equal to the rate of cooling (section 6.2). Flooding of the reactor with liquid agent will take place if the saturated liquid temperature corresponding to point F is greater than the spontaneous nucleation temperature. The effect of sucrose on the system described above is to shift EC to the left of the diagram to E'C' by an increment of temperature equal to the freezing point depression.

2.2 Commercial Hydrate Process for Desalination

Current research and development projects concerned with crystallization processes for desalination are reviewed by Barduhn (22). Two large scale plants employing hydrating agents have been constructed for the Office of Saline Water. Sweetwater (23) have a

plant of 20m. gal./day capacity using propane and Koppers (24) use difluorodichloromethane as hydrating agent in a 10m. gal./day plant.

The hydrate reactors have, in each case, operated successfully; most commissioning problems have arisen due to malfunctioning of the crystal-brine separators. Sweetwater developed liquid cyclones to separate crystals from the brine, whereas Koppers relied on a reflux washer in which a moving bed of crystals was contacted with a counterflow of wash water. The trouble stems from the small crystal size produced in the reactor. It has been suggested that a more soluble agent may give a larger crystal size.

2.21 Research in Desalination by Hydration

The design of the reactors of the pilot plants mentioned in the preceeding section was based on experimental work conducted by Koppers (24). The principal agent used in this bench-scale project for the desalination of 4% salt solution was propane, but comparative studies were undertaken with freon-12 and freon-11. An autorefrigerated 10-gallon vessel fitted with a three blade agitator was used as the

hydrate reactor. The main variables considered were power input, residence time and thermal driving force. Detailed conclusions drawn from the investigation are discussed later in section 5.2; the criterion for scale-up was found to be the power input per unit reactor volume.

A two phase reactor was also studied to discover whether or not conventional crystallisation techniques could be applied to hydrate reactor design. In the Oslo crystallizer, for example, supersaturation is developed in the circulating stream in one part of the unit and released in another. Supersaturation is restricted to a level at which spontaneous nucleation does not occur. Koppers experimented with a system in which water was saturated by contacting it with liquid agent, cooled to become supersaturated and then pumped up through a bed of hydrate crystals. No increase in the size of the suspended particles was observed. It was concluded that at least three phases must be present in the reactor for hydrate formation to occur.

Collot d'Escury (25) has described experiments in which the rate of production of monofluorodichloromethane

hydrate (F-21) was measured in a stirred cell. Gaseous agent was absorbed through an unbroken gas-liquid interface into salt solution. The solution was stirred at such a rate as to prevent the surface becoming covered with a skin of hydrate. These experiments were followed by de Graauw (26) with a study of propane and chlorine hydrates. Again the experimental work was restricted to a three phase batch system, with the reaction vessel immersed in a thermostat bath.

Pangborn et al (27) have studied the formation rate of methyl bromide hydrate from sea water and liquid agent in a well-stirred one gallon reactor. Methyl bromide was used as the combined direct contact refrigerant and hydrating agent. This project covers a wider range of aqueous solution and operating conditions than Koppers, and gives a more detailed experimental analysis of an autorefrigerated hydrate reactor.

The conclusions drawn from these experimental projects and their relevance to the present study are discussed in section 5.2.

2.3 The Hydrate Process for Sucrose Concentration

The design for a commercial freeze concentration process is based on the Koppers process for desalination after the Donath patent (18). A flowsheet for the process is shown in figure 2. Sucrose feed, initially precooled by the product stream, enters the reactor and contacts the dispersed liquid agent. Hydrate slurry is fed to a centrifuge where mother liquor and crystals are separated. Part of the mother liquor is recycled to control the fractional hold-up of crystals in the reactor (See section 8.5). Washed crystals are transported to the condenser-melter where agent is condensed, decomposing the hydrate.

2.31 The Refrigeration Cycle

The refrigeration cycle is a two-stage compression system, a common feature of hydrate and ice desalination plant. The primary compressor handles vapour generated in the reactor; most is condensed on the washed crystals. Excess vapour is compressed further in the secondary compressor and condensed by heat exchange in an indirect-contact condenser. The thermodynamic principles involved in this cycle are discussed in section 8.5.

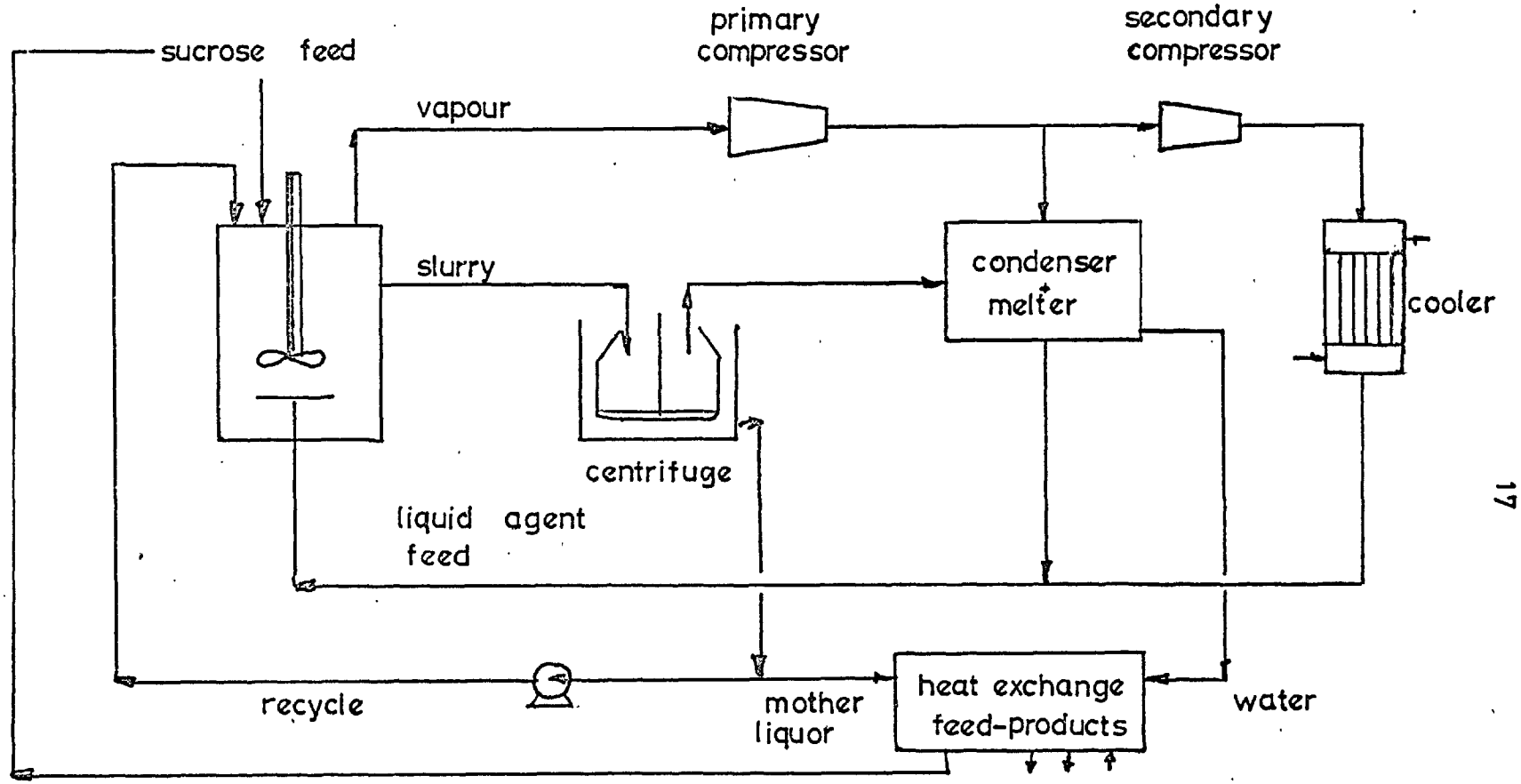


figure 2 Flowsheet for hydrate process: single stage concentration

2.4 Primary Experimental Investigation

Since no data were available for hydrate growth in systems other than solutions of sodium chloride, tests were initially run with a small glass cell, figure 12, immersed in a constant temperature bath. Problems of nucleation and growth pertaining to sucrose solutions were investigated. Quantitative results were limited to the determination of phase equilibrium, section 4.2, but some trends in the behaviour of the hydrate cell under different conditions were established, as described in the following sections.

2.41 Nucleation of the Hydrate Phase

A 250 ml. sample of sucrose solution was cooled in the cell to temperatures below the hydrate formation temperature by adding ice to the water bath. The sample was deaerated and about 10% by volume of liquid freon was introduced. At subcoolings of up to 10°C, nucleation did not occur at either the liquid-liquid interface or the gas-liquid interface. When, however, the pressure in the cell was reduced by venting freon gas to the atmosphere, and liquid freon was caused to evaporate in contact with the aquecus solution,

nucleation occurred at subcoolings in the range 6-8°C. This response was in agreement with other workers; the behaviour seems no different for 10%-35% w/w sucrose solutions. The temperature at which the onset of nucleation was observed appeared to be random. This was consistent with the fact that poor mixing caused random local temperature differences during the period of evaporation of the dispersed phase.

To confirm that nucleation did not occur at an agitated gas-liquid interface in the absence of liquid agent, gas was bubbled into the cell through a sintered disc distributor. No nucleation was observed in sucrose solutions with a maximum subcooling of 10°C during two-hour induction periods.

2.42 Hydrate Growth

Growth rates and crystal characteristics were both most irregular in this first experimental cell. If the quantity of liquid freon at nucleation was small, only a small quantity of single crystals were produced. Such crystals tended to be delicate and to fracture easily. For example, a single 'whisker ' crystal was nucleated in a site on the steel thermocouple probe immersed in the solution. The crystal was curved,

following the streamlines in the stirred solution; the dimensions were approximately 1 cm. long by 1 mm. wide. A cathetometer was used in an endeavour to follow the growth of such crystals, but they sheared at even the lowest agitation rates. Several experiments were carried out to find a suitable technique for growing a single crystal in the cell. A small flow of gaseous freon was dispersed continuously into the system containing hydrate nuclei, but in no way was it possible to observe the growth rate of one crystal. Control of the cell temperature during these runs was rather poor since heat generated in the cell was transferred through a glass wall to the constant temperature bath. The size range of crystals was of the order of 50 to 100 microns. These figures were calculated from setting velocity observations, assuming the crystals to be spheres.

If an excess of liquid freon was available at nucleation, growth occurred around the rising bubbles. The cell consequently became packed with bubbles 'frozen' by a thin hydrate film.

A sampling probe, the prototype of those described in section 3.43, was installed to test a method for

withdrawing a sample of mother liquor free of hydrate. The concentration of the sucrose solution in equilibrium with hydrate crystals was compared with the feedstock concentration.

2.5 Proposed Experimental Project

The above experiments confirmed that concentration of sucrose solutions may be effected by the formation of the hydrate of Freon-12. It was decided not to pursue further the technique for growing single crystals. Even if such a technique could be devised, and Koppers (24) indicated from the failure of their two-phase reactor that the problem did not fall into the usual category of unit operations, the conditions of growth would not compare with the conditions existing in a four phase reactor. Thus any mathematical model describing the growth of a single hydrate crystal would not apply to a commercial reactor in which the dispersed agent is boiling vigorously. Basically the project called for operating data from a realistically scaled four phase well-stirred reactor for a range of sucrose solutions.

In general the purpose of the experiments was to predict the most favourable operating conditions for concentrating a particular sucrose solution at a given throughput. Now operation under the most favourable conditions implies an optimum state, i.e. a maximum yield of concentrated sucrose for a given throughput from equipment of fixed design or optimum economic design and operation of equipment. However the experimental scheme was designed not to optimise hydrate yield and hence the degree of sucrose concentration, but to determine the mechanism of the physical and chemical changes that occur in the system. After establishing a model resulting from experimentation with sucrose, it is possible to predict future performance of the reactor and compare the process both technically and economically with established processes.

3. Experimental Hydrate Process

A simplified flow sheet for the experimental reactor system is shown in figure 3. Liquid freon was gravity fed from the condenser C to the reactor V and dispersed in a suspension of hydrate crystals and sucrose solution by the action of a turbine impeller. As fresh hydrate phase was formed, the heat of reaction caused the dispersed liquid agent to evaporate. Vapour generated in this way was condensed in the shell and coil condenser C.

Luyben (28) and Weisser (29) have both described similarly integrated reactor-condenser systems, referred to by Luyben as autorefrigerated reactors, and previously used in the control of polymerization reactions.

3.1 Reactor Operation

The freeze concentration plant envisaged in section 2.3 employs a continuous stirred tank reactor. Operation of the experimental system as a flow reactor was achieved by keeping constant both the rates of inflow of sucrose and liquid freon and the rate of outflow of concentrated sucrose plus crystalline hydrate.

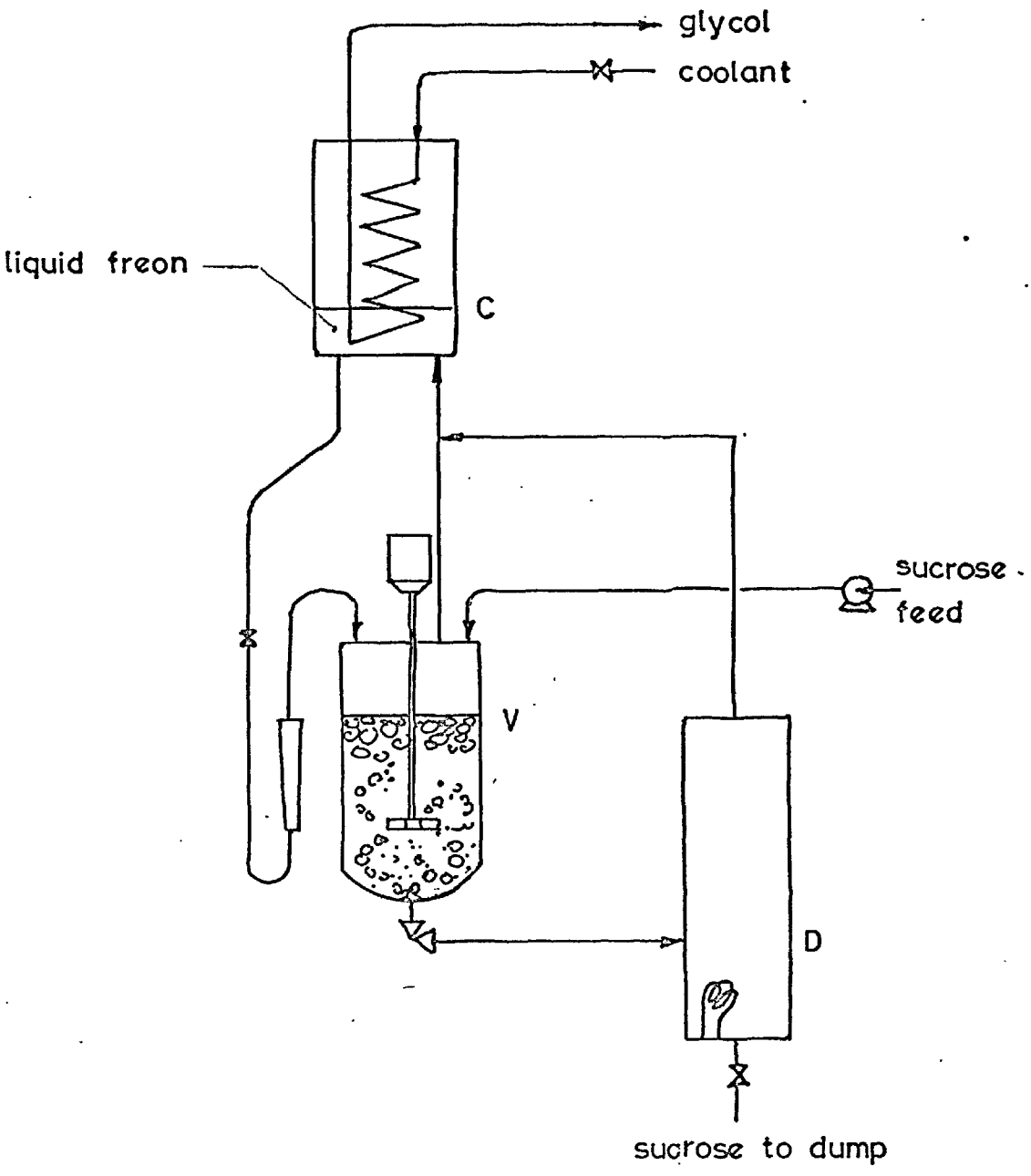


figure 3 Simplified flow sheet

The hydrate slurry was drawn off by gravity from the reactor into a glass vessel D, and was decomposed by an electrical heating element. Reconstituted sucrose was dumped into a vacuum stripping vessel then recycled to the reactor via a storage tank.

Alternatively the reactor could be operated in the manner of a batch process. In this case, while maintaining the freon feed rate constant, hydrate was produced in a fixed volume of sucrose solution. This method was particularly interesting from the standpoint of taking the fraction of crystal hold-up as a variable.

3.11 Selection of Reactor Size and Throughput

A vessel of 5 litres capacity was considered to be a convenient size. This gave a reasonable pilot plant scale of operation; the upper limit was imposed by the availability of glass pressure vessels and the size of the auxiliary refrigeration unit required.

The maximum hydrate production rate for this size of reactor was estimated from the data given by Koppers preliminary study (24). This figure was used as a guide to the design of ancillary equipment. Table 3.1

shows the maximum heat load on the condenser and the precooler, and consequently on the refrigeration plant.

Production rate in 3.5 litre reactor	80 gm water as hydrate/min
Maximum sucrose feed based on minimum residence time of $7\frac{1}{2}$ mins.	460 gm/min sucrose
Heat load on reactor	16 CHU/min
Freon-12 feed rate	205 gm/min
Condenser duty	16 CHU/min
Precooled sucrose feed duty	16 CHU/min
Total duty, including heat leak	38 CHU/min
Rated capacity of 2 stage refrigerator operating $-18^{o}/27^{o}C$, $\frac{1}{2}$HP, 560rpm	40 CHU/min

Table 3.1, Maximum predicted heat load on system

3.2 The Hydrate Reactor

A glass reactor of 6" I.D. and $18\frac{1}{2}$" overall height, with a 1" I.D. bottom exit was available as a standard unit, Q.V.F. (VZ/[illegible]/6), though the manufacturers recommended that adequate safety precautions be taken at pressures in excess of 25 psig. A brass flange lid to the reactor carried eight Simplifix couplings, a pop safety valve and a central stirrer gland housing.

Neoprene gasket material was used for this and all other glass-to-metal or glass-to-glass joints.

The reactor outlet was connected to the decomposition vessel via a right-angled 1" diaphragm valve with a glass body and a one-piece P.T.F.E. diaphragm. In operation the slurry flow was not controlled by this valve, which was subject to blocking when partially closed, but by the decomposed-slurry draw-off valve.

Photographic views of the complete experimental rig and the reactor are shown in figures 4 and 5. The reactor was supported on lengths of 1" angle-iron which were bolted to the major framework of the apparatus, built from $\frac{3}{4}$" I.D. galvanized pipe. A safety screen of $\frac{1}{4}$" thick perspex was secured to the framework to protect the operator in the event of a failure in the glassware. Sheets of expanded polystyrene were moulded to form a 2" thick layer of lagging around the reactor.

3.21 Freon Feed

The rate of addition of liquid freon from the condenser was controlled by a $\frac{1}{4}$" Simplifix valve, type 60, and measured by a G type Rotameter tube with stainless steel float. The Rotameter was designed

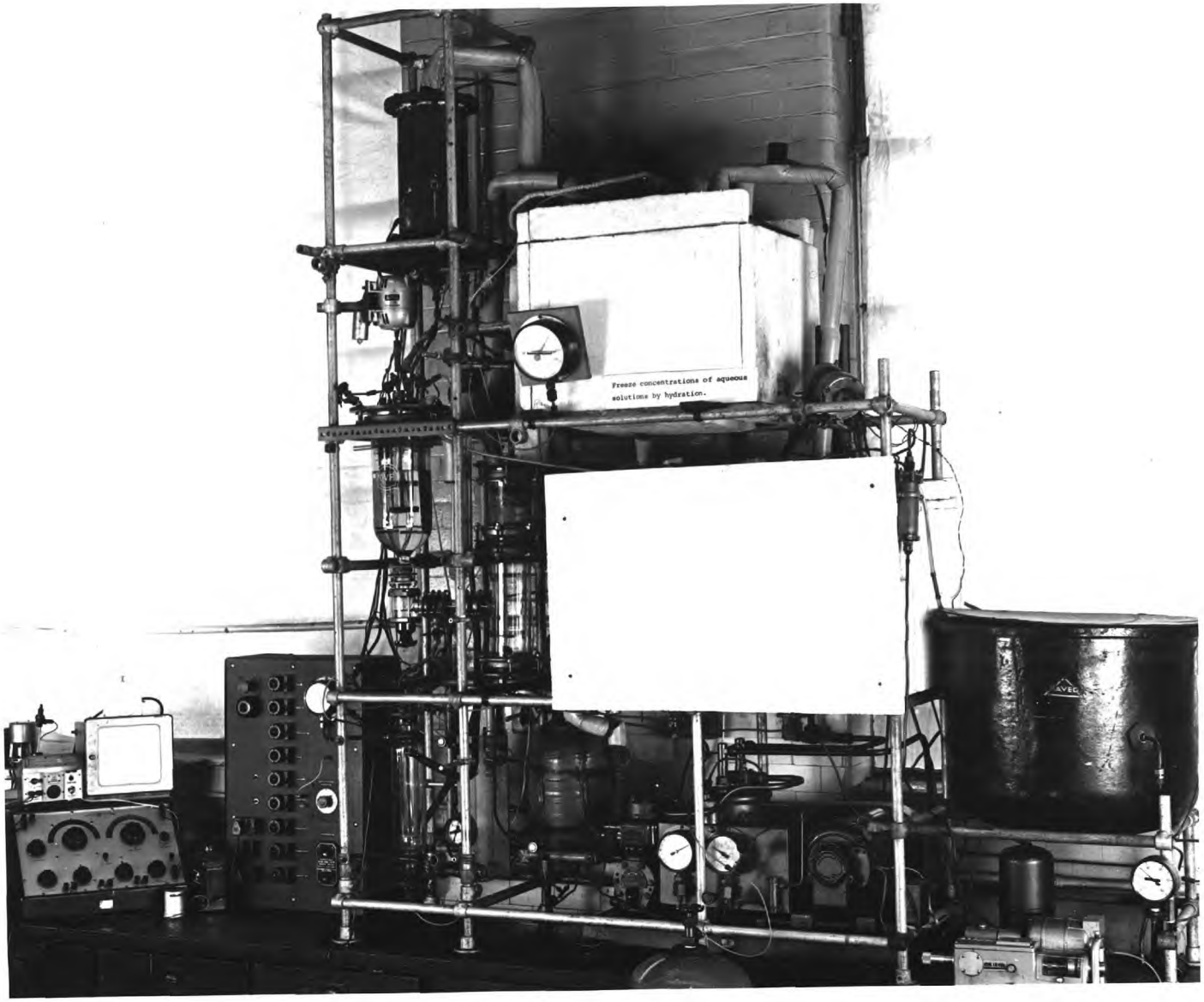


figure 4 Over-all view of apparatus

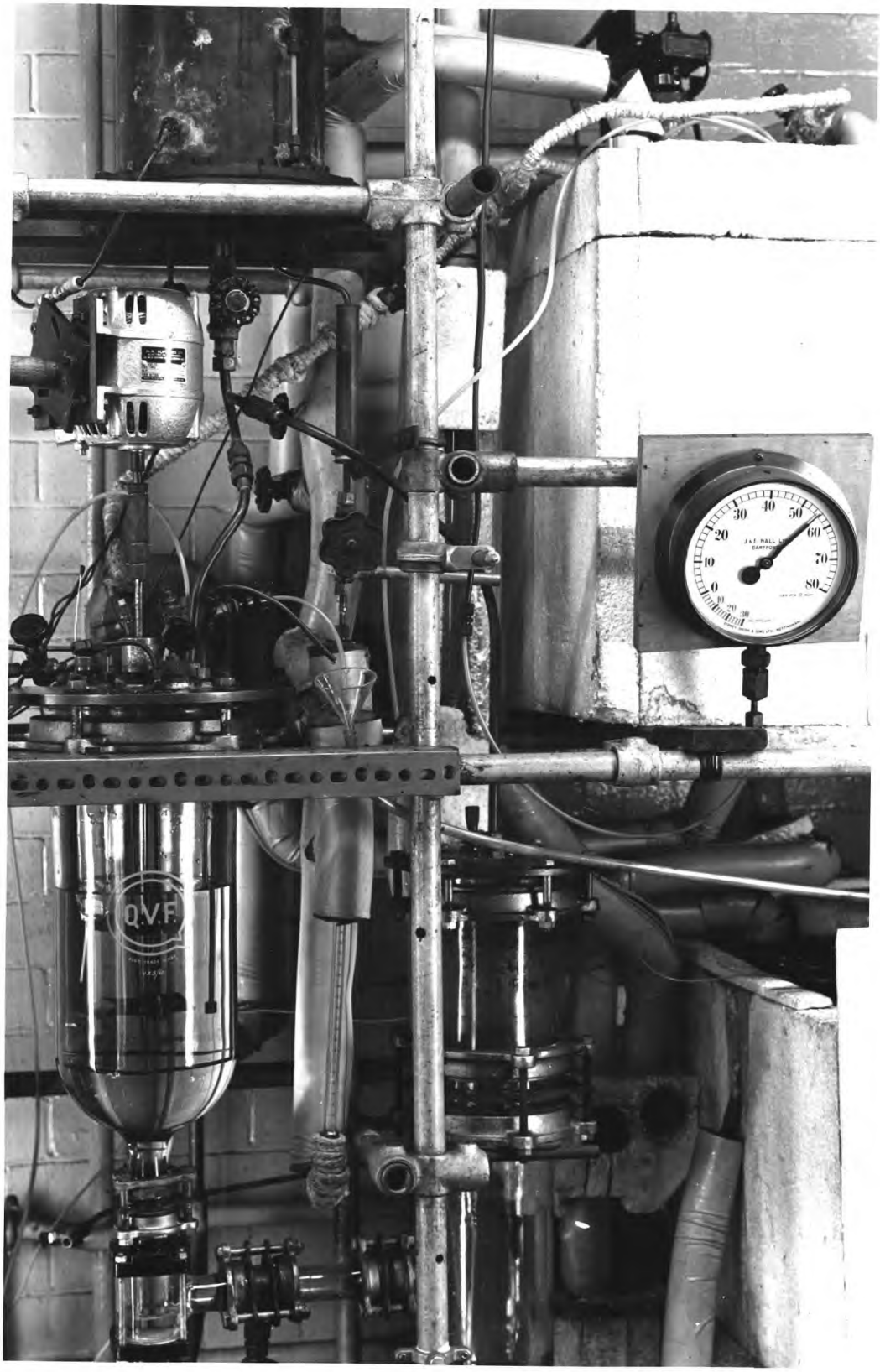


figure 5 Hydrate reactor and auxiliary equipment

for a maximum liquid freon flow rate of 160 cm^3/min at 10°C.

The Rotameter tube was mounted as a part of one limb of a U-tube, see figure 6; the glass tube was secured by Araldite in brass sleeves hard-soldered onto ¼" O.D. copper tube. The unit included a small heat exchanger to insure against flashing in the Rotameter section. Nylon tube was used to connect the U-tube to the feed and delivery lines at the 3/16" Simplifix fittings shown: the flexible coupling prevented strain at the glass-to-metal joints.

This arrangement was adopted for two reasons. In the first case, the construction has a very low heat capacity compared with most tube mountings employed at this pressure range; this low capacity is desirable when dealing with a liquid which boils at a temperature below ambient temperature. Secondly, the U-tube was very easily detached, cleared and cleaned of hydrate which occasionally formed in the feed line or tube section. A rinse with methanol was usually sufficient to re-establish flow through the tube.

Calibration of the Rotameter tube is discussed in sections 3.6 and 6.1.

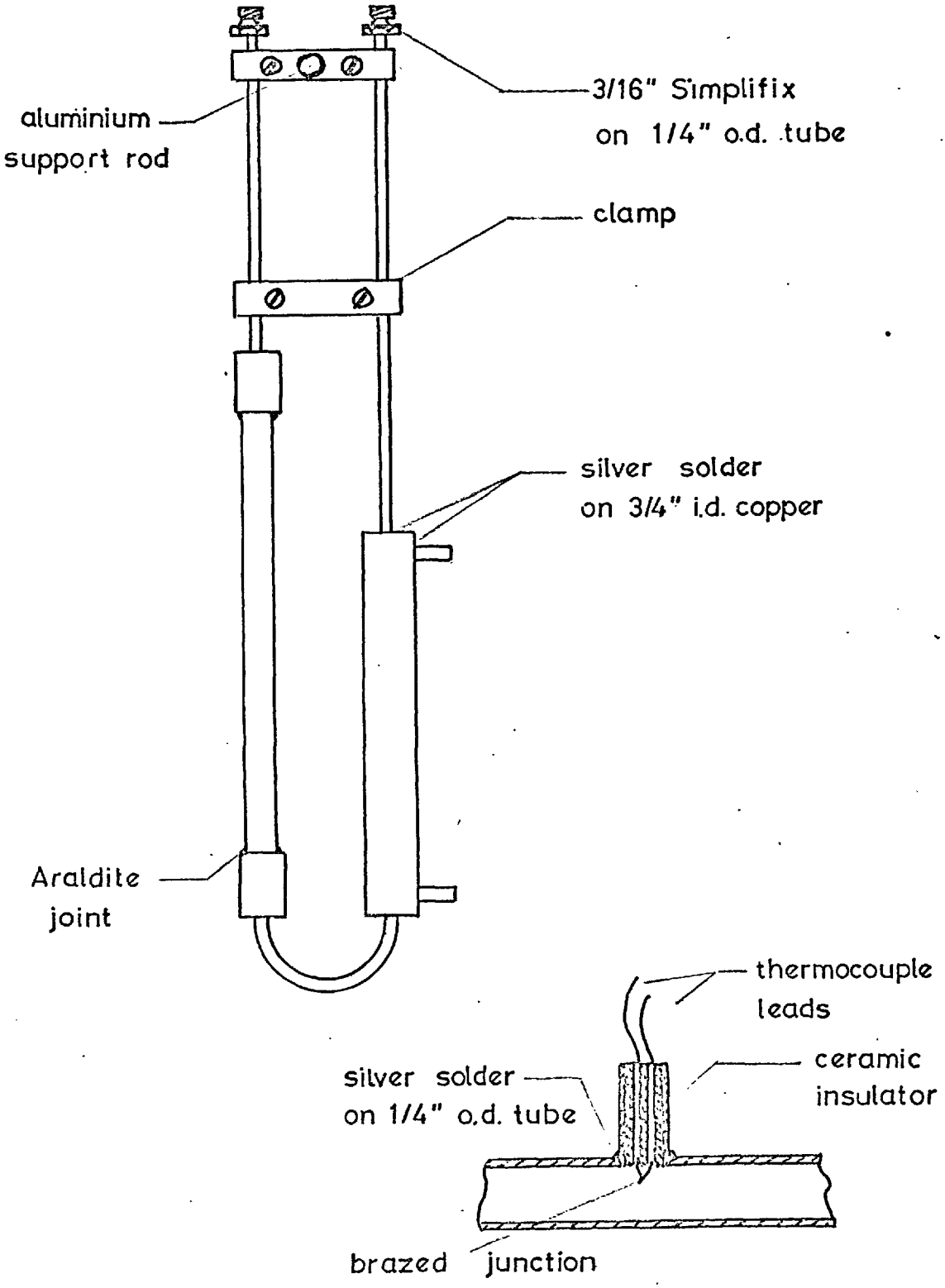


figure 6 Rotameter tube detail (approx. 1/3 scale) and temperature probe in feed line (x2 scale)

3.22 Sucrose Feed

Aqueous sucrose solution was stored in a 30-gallon resin-coated tank. The feed was delivered to the reactor by a D.C.L. metering pump. Dirt was rejected from the solution by a 20-30 micron pore size sintered glass filter, and a small surge tank was used to remove pulses generated by the reciprocating pump action. With a maximum duty of 6.7 gall./hour at 75 psig., the pump delivered a constant rate of supply of liquid, irrespective of pressure. The feed was precooled to the reactor temperature in a 40' length of $\frac{1}{4}$" O.D. copper tube wound as a coil and immersed in a constant temperature bath, see figure 9.

3.23 Stirrer Drive and Agitator Design

A variable speed, series wound motor ($^{1}/_{20}$ HP.) was attached by a flexible coupling of rubber to the brass stirrer shaft ($^{5}/_{16}$" D.) located in the P.T.F.E.-packed gland housing. A second motor, continuous rating a.c. $^{1}/_{10}$ HP, was available to increase the range of stirrer speeds. The motor assembly is shown in figure 5; the support bracket was of welded construction, secured to the main framework with Kee Klamp fittings.

Since geometrical similarity is important in the design of agitation equipment, impeller and baffle dimensions were chosen approximately in accordance with accepted practice, e.g. Westerterp (30). Four baffles $\frac{1}{2}$" wide were positioned against the vessel walls and held in place by the sprung frame on which they were mounted. Preliminary work with a single $2\frac{1}{2}$" diameter 45° pitched four-blade turbine indicated that excessive foaming and nucleation took place at the surface of the four phase mixture. This was assumed to be due to inadequate dispersion of the liquid freon. Departure from the well-stirred condition was corrected by mounting a second impeller on the stirrer shaft; a four- bladed flat paddle which operated nearer the liquid surface, see figure 7. This modification to the standard design was considered justifiable in the light of work published by Bates et al (31) on the power requirements of dual impeller systems in standard vessels.

Operating the reactor at the highest agitation rate and the higher freon feed rate, it was shown that the gas hold-up constituted 30% of the total reactor volume. In view of this the liquid working capacity of the reactor for batch runs with the dual impeller was chosen at 3.35 litres.

No provision was made for measuring the torque of the motor and hence the energy consumption in the gas-liquid dispersion. The principal reason for not taking this measurement was the uncertainty in the fraction of the power wasted at the stirrer gland. Estimates of the power consumed in the aqueous phase were obtained calorimetrically and are given in Appendix G.

3.24 Detailed Flow Sheet

A flow diagram for the reactor and condenser system is shown in figure 8, excluding the arrangement of the glycol bath and constant temperature bath which is presented in figure 9. The configuration of valves was designed for flexible operation with respect to changing the system with freon (F), evacuating the item of equipment (V) or equalizing the pressure between units. Not shown is a storage tank, installed to allow liquid freon to be dumped from the condenser should the need arise. Simplifix valves and fittings were used throughout, mainly for $^{3}/_{16}$" O.D. copper or nylon tube.

3.25 Temperature Measurement in Reactor and Feed-lines

To obtain a temperature distribution of both the liquid and vapour phases in the reactor, probes were

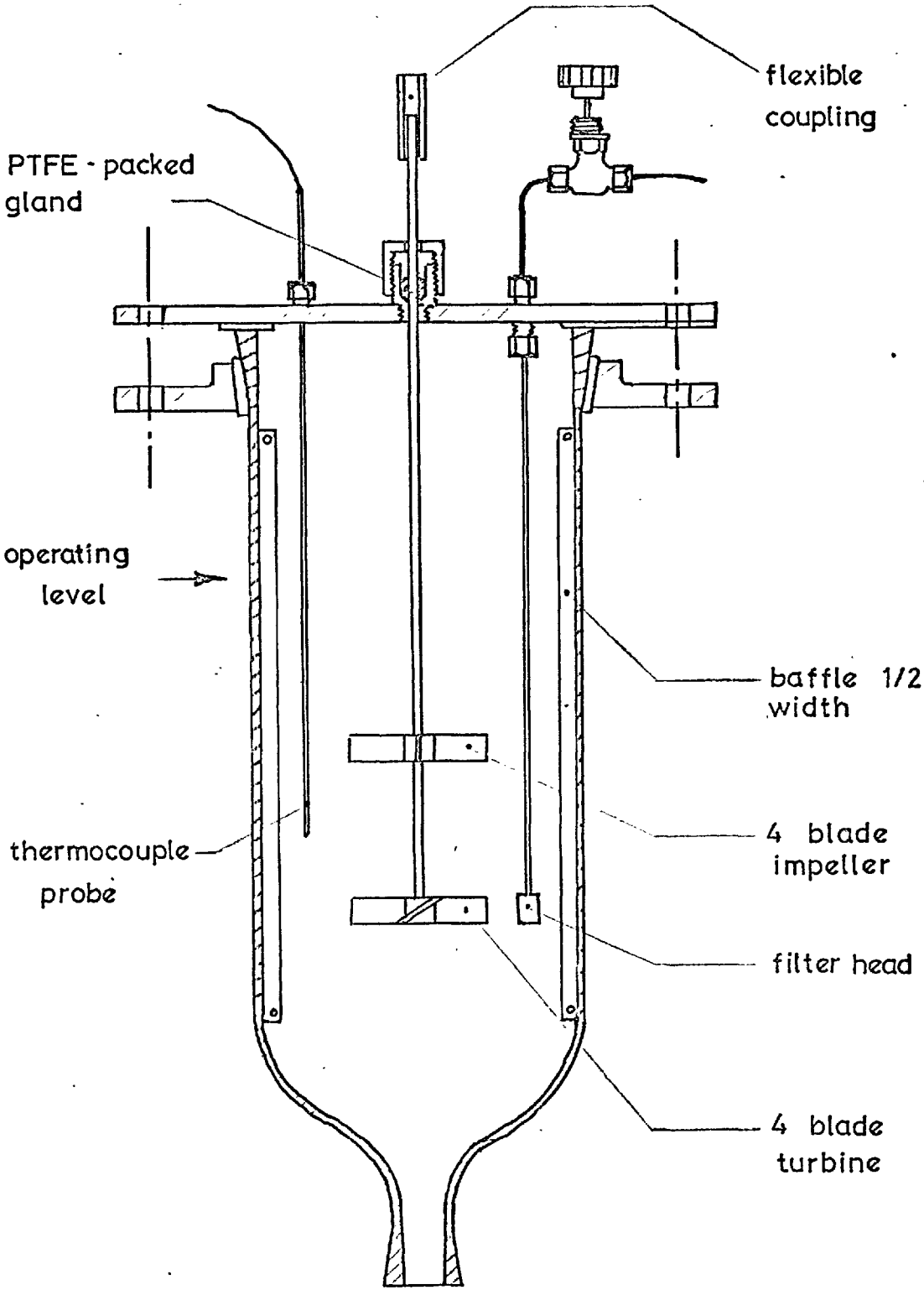
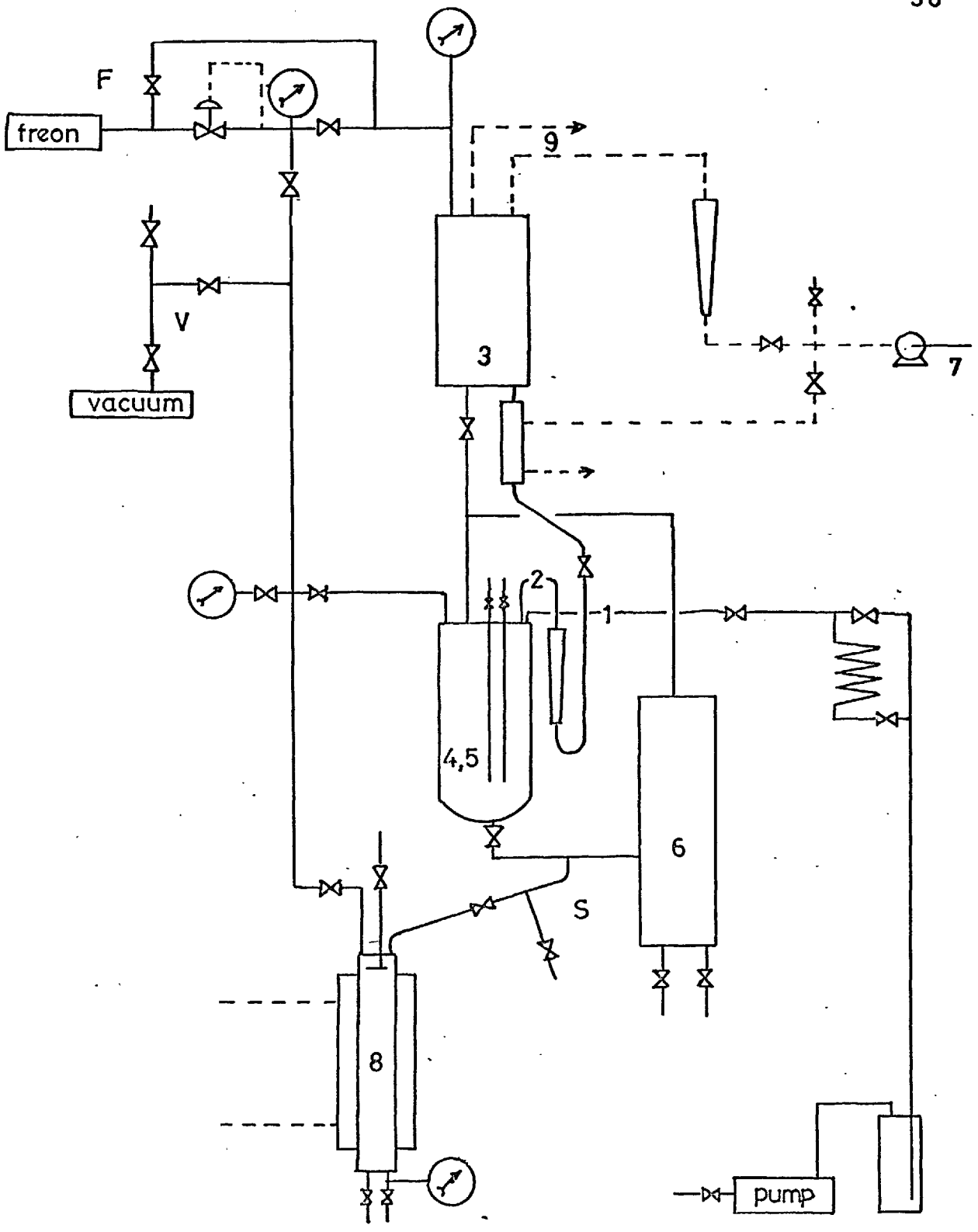


figure 7 Reactor, impeller and baffle arrangement (approx. 1/3 scale)



(numbers correspond to thermocouple sites)

figure 8 Flowsheet for reactor system

installed to measure the temperature at different points. Two thermocouple probes were spaced at different radial distances in the reactor, capable of being adjusted vertically by loosening P.T.F.E.-packed glands in modified Simplifix couplings. Both thermocouples were single junction 32 gauge copper-constantin probes in 15" lengths of 16 gauge hypodermic stainless steel sheath.

Thermocouple probes were sited in both sucrose and freon feed-lines, just prior to the reactor inlets and insulated from them by nylon tube. A detail of the thermocouple installation is shown in figure 6. The wires near the junction were encased in 2mm. twin-bore ceramic insulators and sealed with Araldite into $^{1}/8$" O.D. brass tube, soldered at right-angles to the $\frac{1}{4}$" O.D. feed line. Asbestos string and foam insulation was used on the copper lines. Positions of other thermocouple sites are marked on figure 8.

The e.m.f. was measured accurately on a Pye Universal Precision potentiometer, in conjunction with a Pye 'Scalamp' galvonometer and an ice cold-junction. In addition, a 'Hi-Speed' miniature potentiometric recorder was used to follow the temperature both in the

reactor and at other points in the equipment. This recorder also served to time the point of spontaneous nucleation and subsequent sample withdrawals in batch runs. A 10-way Muirhead switch and an additional double-pole switch were used to select both the thermocouple and the e.m.f. display. A check for heating effects at switch terminals was made regularly by comparing the same e.m.f. source measured both directly and through the switched circuit. The calibration of the thermocouples is given in Appendix G.

3.26 Sucrose Sampling System

Samples of mother liquor were withdrawn from the reactor through a sintered-glass filter. A 10mm. diameter borosilicate glass filter plate was sealed with Araldite into the machined extension of a $^{3}/_{16}$" O.D. by 11" copper tube. This tube was sited in a bulkhead coupling in the reactor lid and connected to a $^{3}/_{16}$" Simplifix shut-off valve. The total capacity of the sample system was approximately 3ml. and enabled a representative sample to be obtained after withdrawing only 0.25% of the reactor volume, allowing for purge. Two such sampling probes were installed, with different sinter porosities, 100-120 and 20-30micron pore size, as supplied by A. Gallenkamp.

Samples were analysed with a high accuracy Abbé '60' refractometer maintained at 20°C and employing a sodium light source. The variation of the refractive index with the concentration of sucrose solutions is shown in Appendix G.

3.3 Freon Cycle Design

The design of an autorefrigerated reactor system called for the selection of a suitable means of pressure control and recycle of the liquid agent. There are basically two possible arrangements for the use of Freon-12 operating in the range 30 to 50 psig, corresponding to saturated liquid temperatures of 0°C to 12.5°C respectively.

(i) The reactor pressure is controlled by a back pressure valve on the vapour line. The vapour generated in the reactor is compressed and then condensed either in an indirect contact exchanger with cooling water or in direct contact heat exchange with melting hydrate cyrstals. In either case there is sufficient excess pressure available to return the liquid agent to the reactor.

(ii) The condenser is cooled by a refrigerated coolant

and operated at the same pressure as the reactor. The condenser pressure is controlled by adjusting either the flow or the temperature of the coolant stream. Flow of liquid agent from the condenser back to the reactor is by gravity, at a temperature roughly corresponding to the saturation temperature of freon. The vapour recompression step required for operation of the process below ambient temperature is incorporated in a secondary refrigeration cycle working against the coolant bath.

Clearly the maximum heat recovery is obtained from process (i), with condensation on melting crystals. This choice would however be difficult to engineer and operate on a small scale. The use of a compressor was avoided and method (ii) chosen for its simplicity. Accurate pressure control was required, particularly during batch runs, and it appeared that a small compressor would not be sufficiently flexible. In addition, contamination of the agent with compressor oil was possible and very undesirable.

3.31 Condenser Design

This unit was designed both as a condenser and as a reservoir for liquid freon. Losses of agent from the

system are incurred by incomplete slurry decomposition, the residue of freon dissolved in solution, and by slight leaks at glands. Rather than add a make-up stream of freon vapour, a measure which complicates pressure control, it was decided to operate with a hold-up of liquid freon in the condenser. For this reason a shell and coil unit was more suitable than a shell and tube condenser.

The condenser coil was manufactured with an O.D. of 6" from 22 feet of $\frac{1}{2}$" O.D. copper pipe. It was arranged in the 8" I.D. shell such that the bottom coil, slightly separated from the other coils, was immersed in liquid freon when the unit was charged with from four to eight pounds of agent. A nylon sight-glass was fitted to facilitate charging; the mid-way position corresponded to about 6 lbs. of freon. Vapour entered the condenser from the reactor through a stand-pipe in the bottom flange cover.

3.32 Condenser Operation

The only disadvantage of the simple gravity flow condenser was that under certain conditions boiling occurred in the feed line to the reactor, resulting in

vapour locks. This problem was solved by using small double-pipe heat exchangers to subcool the feed line.

The condenser could be isolated from the reactor system by closing a ½" globe valve on the vapour line. This prevented exposing the glass reactor to high pressures when the coolant flow was stopped at the conclusion of a series of runs and the condenser warmed up to ambient temperature. Before fitting, a check was made to determine if the pressure drop across the valve would restrict the freon flow in the vapour line. The condenser itself, which was designed to withstand a pressure of 100 psig., was fitted with a Norgren pop safety-valve.

With a steady or slowly changing rate of flow of freon vapour from the reactor, the condenser pressure was controlled adequately, i.e. to the accuracy of the Bourdon gauge, by adjusting the flow of glycol coolant through the condenser coil.

Before the feed subcooler had been incorporated it was not possible to maintain a constant liquid freon feed rate and boiling in the reactor for more than a few minutes. The first modification was to install a temperature controller for the charge of liquid freon

in the condenser. An Airmec N241 controller was used in conjunction with a resistance thermometer sited below the liquid level in the condenser, and a heater tape wrapped around the shell. A magnetic follower was built into the condenser base plate to provide adequate agitation for heat transfer from the walls. This control system was devised to operate at a constant coolant rate, compensating for changes in the freon vapour rate by switching the heater circuit to keep the freon temperature and pressure constant. The response of the heater was unsatisfactory, so the method was rejected. Success was obtained with the second modification, circulating glycol coolant round the freon feed line.

3.4 Glycol Bath and Constant Temperature Bath

A diagrammatic layout of the tanks and circulating pumps is shown in figure 9. Heat was transferred from 20% glycol solution in a well-stirred 50-gallon tank B1, to the evaporation coil of a $\frac{1}{2}$HP. refrigeration unit R. The coil, 90ft. of $\frac{1}{2}$" O.D. copper tube, was designed for a duty of 40 CHU/min. with a minimum temperature differential of 5°C. The refrigerator, a two-stage compressor, was charged with Freon-12. The glycol was

circulated by a No. 12 Stuart Turner pump P1 through a 3-way union to the condenser C, the constant temperature bath B2 and the auxiliary exchangers H on the freon feed line.

Selection of the operating pressure in the condenser dictated the working temperature of the glycol bath. Saturated freon pressures of 46 and 30 psig. required glycol bath temperatures of $-2^{\circ}C$ and $-12^{\circ}C$ respectively. The temperature was maintained by a make-make controller and relay switching the refrigerator. The coolant feed to the condenser was measured and hence controlled by a 18X metric Rotameter tube; the temperature differential across the condenser was measured by thermocouple probes.

The 30-gallon constant temperature bath B2 was equipped with a glycol-cooled coil, stirrer motor and paddle, and thermostatically controlled 500 watt heater. Mercury-toluene switches and Sunvic relays were used for the control both of this bath and the glycol bath. An Ether $\frac{1}{2}$" solenoid valve SV was used to control the glycol feed to the bath B2, operated through the relay on the mercury-toluene switch. Alternatively the bath temperature could be controlled by a heater circuit,

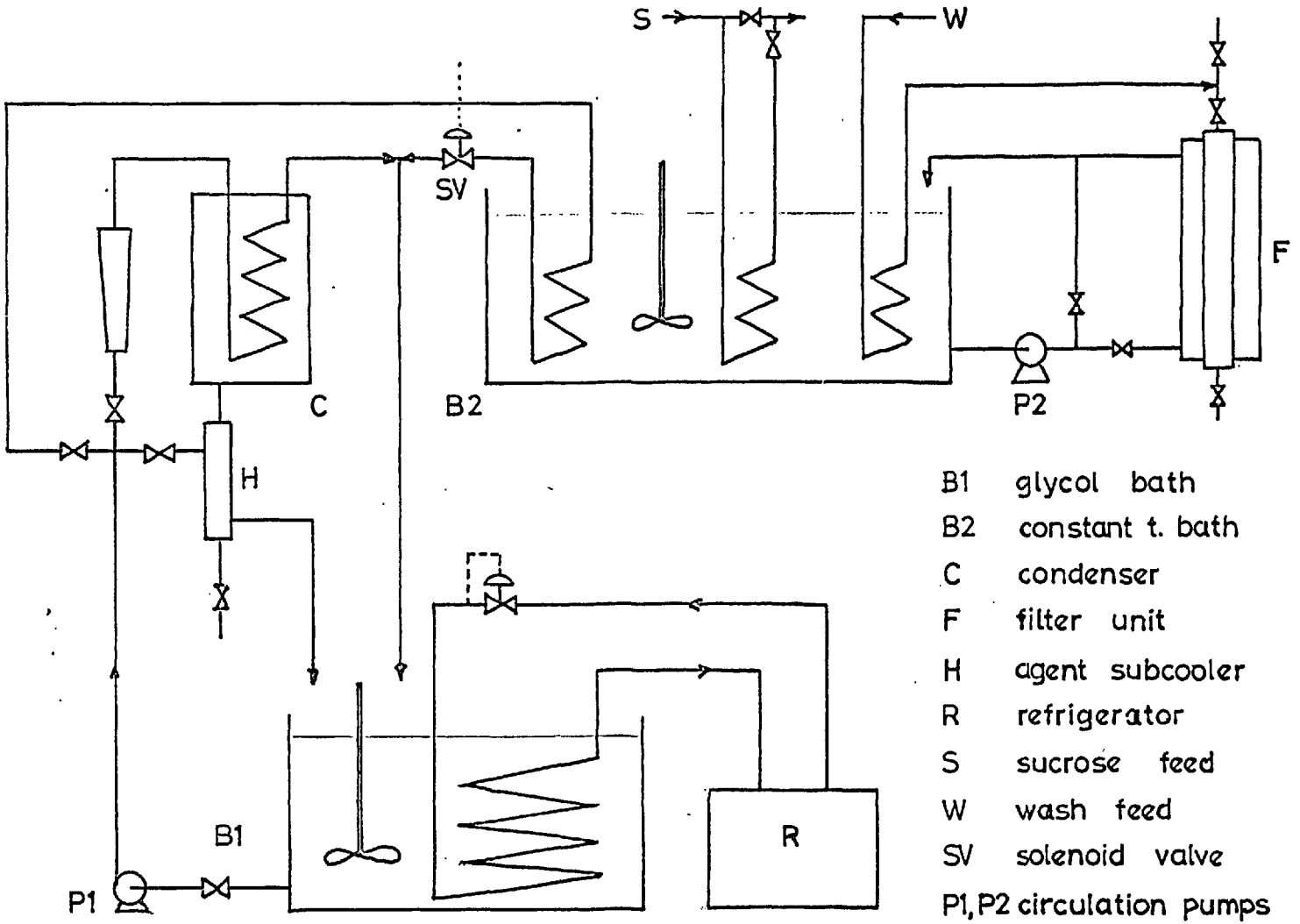


figure 9 Refrigeration and glycol circulation system

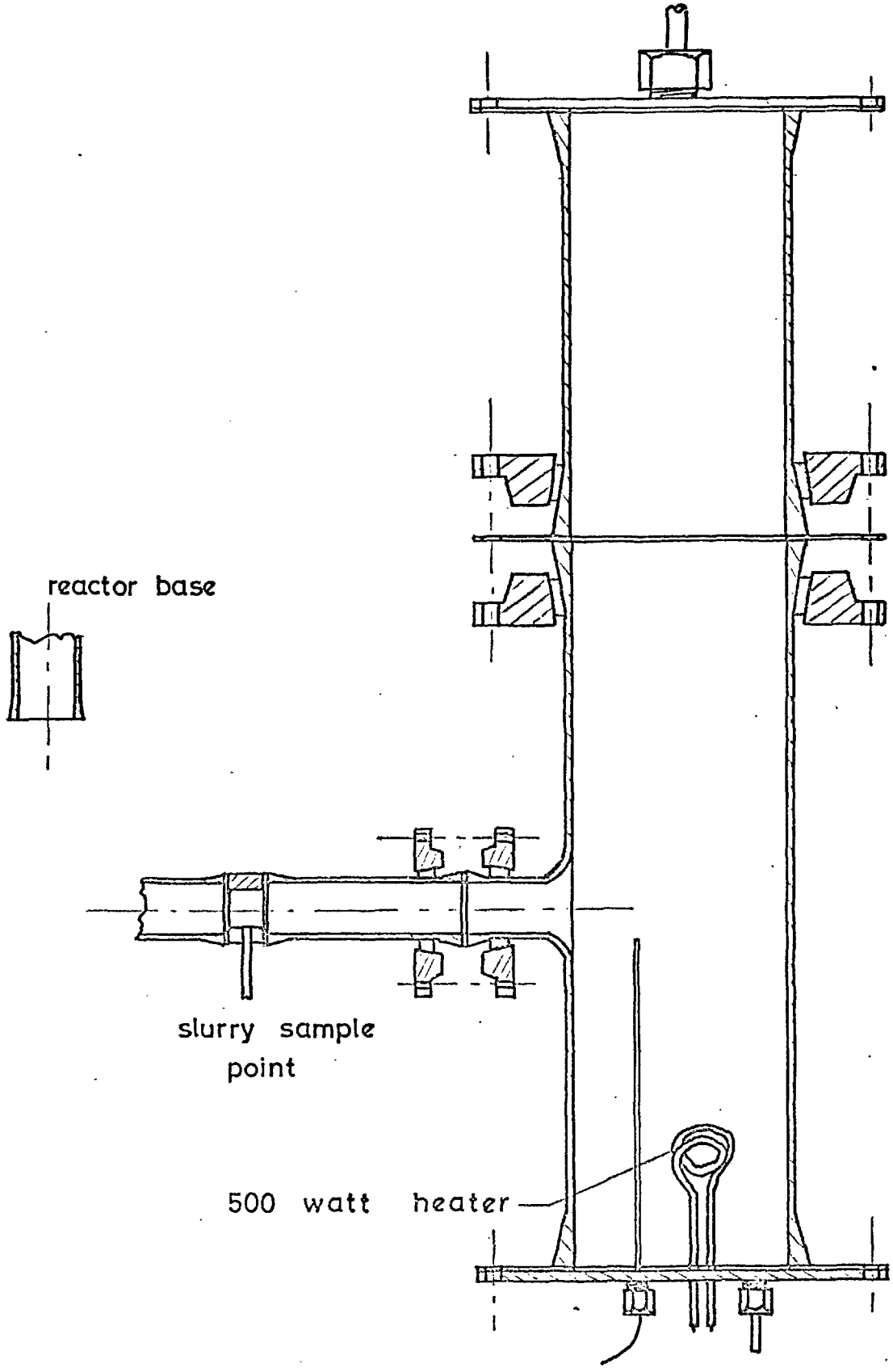


figure 10 Decomposition vessel (approx. 1/3 scale)

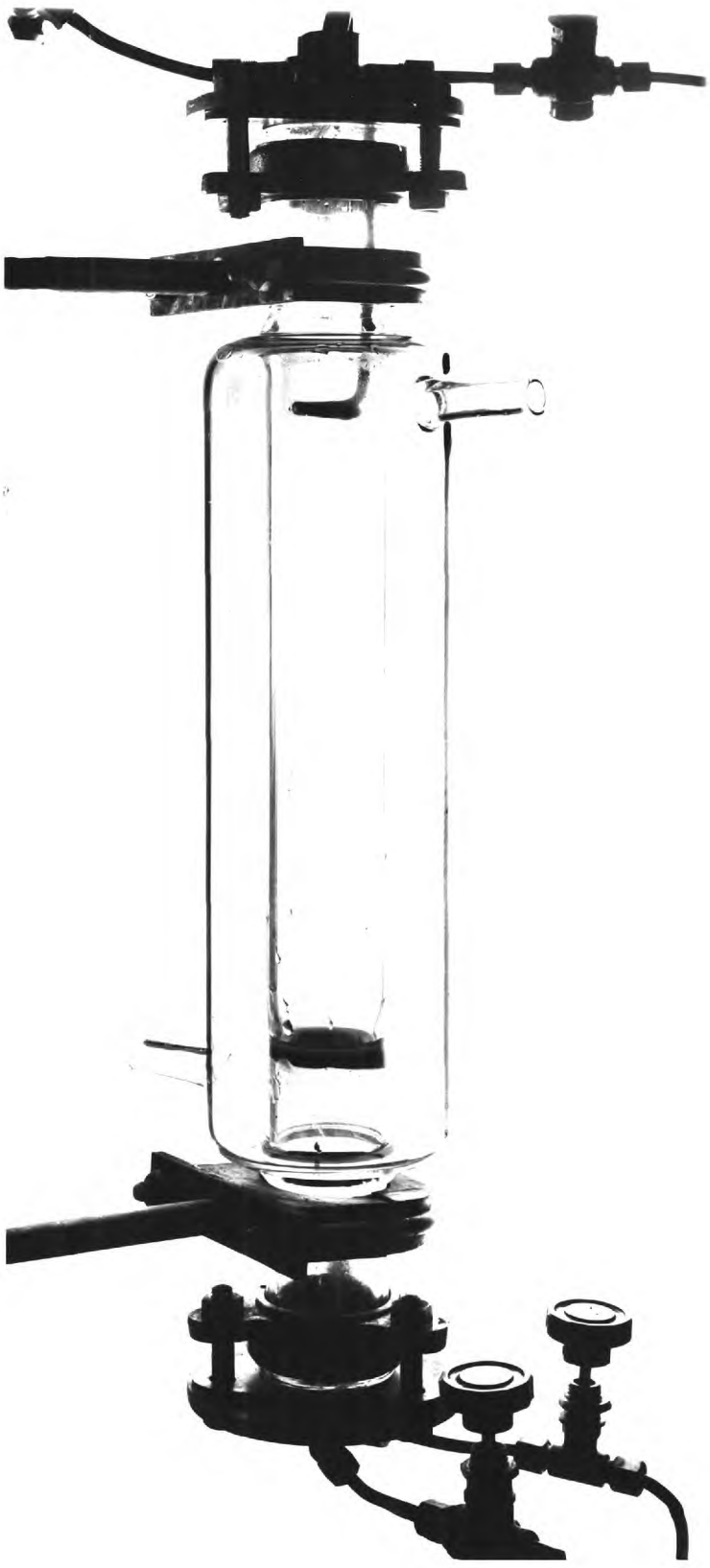


figure 11 Wash column

though adding to the total heat load on the nearly over-stretched refrigerator was not desirable. The temperature variation of the sucrose solution S pre-cooled in E2 was $\pm^{1}/_{6}^{\circ}C$ at the highest sucrose feed rate.

3.5 Decomposition Vessel and Filter Unit

The decomposition vessel, shown in figure 10, was constructed from two standard Q.V.F. 4" diameter glass units, one of which was provided with a 1" diameter side inlet. The upper section was added to provide the correct hydraulic gradient between the reactor contents and the decomposing hydrate slurry for controlling the flow of slurry from the reactor in the course of the steady-state runs.

A variac-controlled 500 watt heater was mounted above the base plate. Two draw-off valves were fitted, a $^{3}/_{8}$" sleeve-packed cock and a $^{3}/_{16}$" needle valve. The former proved to be the more adequate means of control.

The filter and wash column shown in figure 11 was fabricated from a 18" length of 2" diameter Q.V.F. glass pipeline. A 100-120 micron pore size fritted glass filter plate was sealed into the line which was jacketed

by a 4" diameter glass tube. Water from the constant temperature bath B2 was circulated through the jacket by a No. 10 Stuart Turner pump P2, figure 9, to prevent decomposition of the hydrate. Similarly wash water was cooled in a coil W sited in bath B2, before entering the column through a wash distributor. Hydrate slurry was introduced through a slurry sample line into the top of the column.

3.6 Design of Experiments

The discussion in this section is concerned primarily with the design of the batch reactor runs, but it also deals with the experimental variables considered for the steady-state cases. The six variables that can be controlled or measured with comparative ease are; impeller speed, sucrose concentration, residence time, reactor pressure, operating temperature and yield of hydrate. (The hydrate yield is defined as the production rate of water in the form of hydrate, gm/min.). It is necessary to choose an adequate definition of the output or response of the reactor and the best manner of changing the independent variables.

Variable Type	Variable	Control Means	Measuring Means
Dependent Variable, or Response	Operating Temperature (T_r)		Potentiometer
Primary Independent Variables	Stirrer Speed (N)	Rheostat	Stroboscope
	Sucrose Concentration (x_f)	Feedstock	Refractometer
	Reactor Pressure (P)	Temperature and flow of coolant	Bourdon Gauge
	Production Rate (r)	Freon feed rate	Potentiometer
			Refractometer
Secondary Independent Variables	Hydrate Hold-up (ϕ_h)	Batch time	Data-logging system
		Sucrose feed rate (CSTR)	Metering-pump
	Reactor Volume (V_l)	Level of slurry in reactor	

Table 3.6: Experimental Variables

One of the first considerations is the choice of an operating method for the reactor. Either the operating temperature may be chosen and maintained by adjusting the cooling rate and the yield is measured, or the yield may be chosen by fixing the cooling rate and the

operating temperature is measured. The second method is preferable; it involves a fairly constant heat load on the reactor - condenser system, which simplifies control. Hence the reactor operating temperature, rather than the yield, becomes the measured response of the system.

The dependent and primary and secondary independent variables are shown in table 3.6, together with the manner of control of the variable and the measuring means.

The distinction between the two categories of independent variables is solely an experimental one. The effect of the hydrate hold-up fraction ϕ_h was studied separately from the effects of the other independent variables, by analysing the temperature - time response curves, see section 6.1. For this reason ϕ_h is denoted as a secondary variable. Similarly the effect of the volume of hydrate slurry was observed separately, in this case only for the flow reactor runs. The choice of the volume of liquid phase was a special problem since it was shown that the power dissipated in the reactor by the dual impeller agitator depended upon the level of sucrose in the reactor for a given geometry

and speed. No measurements of the stirrer torque were taken so the change in the energy dissipated per unit volume, for a given change in V_l, could not be estimated for reaction conditions.

At the outset of the experimental work there was little to indicate what either the main effect, or the interaction between the effects, of these variables would be. The project is therefore most efficiently planned with the aid of a factorial design, a scheme by which the effects of several factors are studied simultaneously. It is necessary to state the levels of the variables, the experimentally specified conditions at which the independent variable is investigated. These conditions were selected after preliminary experimental work.

The basic choice comprised a $3^2.4.5$ factorial design; three levels each of stirrer speed and pressure, four levels of sucrose concentration and five levels of production rate. In general only a selected fraction of the total 180 experiments would be sufficient to analyse the main effects and interactions. However, in view of the complexity of the reaction mechanism in a four phase reactor, and particularly the work by

de Graauw (26) which showed that the production rate was not a simple function of the driving force for mass transfer, it was considered necessary to conduct all the experiments. Certain modifications to the design were made when experimental difficulties arose. Also certain runs were repeated at random as a check on the reproducibility of the data and the technique. The chosen array does not actually correspond to a true factorial design for one variable, the pressure, is not maintained at the same levels over all levels of the other variables.

The 'high' level of the reactor pressure for a given sucrose solution was chosen such that the reactor temperature at nucleation of the hydrate phase was just greater than the saturated freon temperature (section 2.1). Since the hydrate equilibrium temperature is a function of pressure and sucrose concentration, these 'high' pressure levels vary with concentration and hence the level of another independent variable. To simplify the analysis, equal intervals between pressure levels were chosen, 3 psig., and one level, (37 psig.) was chosen as common to the nine central blocks of runs. The significance of this design modification and possible

alternatives will be discussed with the interpretation of the overall results.

3.61 Design Array for Batch Operation

Table 3.61 shows the levels of three independent variables; stirrer speed N, sucrose concentration x_f and reactor pressure P.

x_f w/w \ N RPM	1420	1140	880	N / P psig
.0	* * * * .10			46 43 40 37
.095	* * * .11	* * * .21	* * * .31	43 40 37
.18	* * * .12	* * * .22	* * * .32	40 37 34
.27	* * * .13	* * * .23	* * * .33	37 34 31
.42	* * * .14		* * * .34	34 31 29

Table 3.61: Levels of the independent variables

In the table each asterisk represents five levels of the production rate, i.e. five levels of r for each

pressure level selected. The underlined numbers in the squares represent experimental blocks, taken as all those runs conducted at constant N and x_f, and are code numbers for handling the subsequent analysis. The first digit shows the level of the stirrer speed and the second represents the sucrose concentration level. Blocks in the overall design were performed in a random order, and the experiments within the block were randomised with respect to the two variables P and r, the production rate.

3.7 Operating Procedure

The system was evacuated by a Speedivac high vacuum pump before the first charge of freon was introduced. Thereafter 6 lb. of freon was maintained in the condenser by periodic topping-up from a 145 lb. cylinder of ICI Arcton-12. Glycol solution was pumped through the condenser coil to cool the contents and reduce the pressure to a little below the required operating pressure. The coolant bath thermostat was adjusted to give a liquid freon subcooling of about $4^{\circ}C$, with respect to the selected pressure, at maximum coolant flow. This condition ensured both the establishment of vapour-free liquid flow through the Rotameter tube and the best degree of condenser control.

3.71 Batch Operation

Sucrose solution at room temperature was pumped into the reactor to the desired level then the feed pump was stopped and the sample probes were purged. The stirrer motor was started with the gland nut slackened off. By tightening the gland to prevent loss of vapour and by adjusting the rheostat in series with the motor, the correct stirrer speed was obtained. The tightness of the gland was checked during runs to maintain a constant agitation speed. Liquid freon was fed into the reactor with glycol circulating through the feed-line cooler. When the reactor pressure and freon feed rate were steady, the reactor temperature was measured at intervals to obtain a cooling curve. This cooling curve constituted a calibration of the Rotameter tube(see section 5.5). The spontaneous nucleation temperature was measured as the minimum reached in the reactor. The transition was usually followed by a rapid rise in temperature, and during this period the glycol coolant flow rate had to be reduced to keep the reactor pressure constant. The temperature of the hydrate slurry was measured at intervals timed from the phase transition point.

Samples of about 3 cc. of mother liquor were withdrawn through the filter probes, after allowing a standard purge volume to pass, and timed by the event-marker facility on the chart recorder. In addition the average level of the contents of the four phase mixture in the reactor was measured at intervals to determine the gas hold-up fraction. The runs lasted from between five to twenty minutes after nucleation of the hydrate phase. A run was stopped either if the reactor temperature had been steady for five minutes or more, or if the temperature had dropped much below the maximum attained.

An E.A.L. MDP-200 data logging system was used to record the reactor temperature for a selection of the batch runs. The thermocouple e.m.f. (0.3 mv.) was pre-amplified to a level acceptable to the data-logger (30 mv.) by a Comark d.c. amplifier type 210. In this way reliable temperature-time data were automatically obtained on punch paper-tape. The accuracy of the data-logger and the potentiometer is very similar; the former was regularly calibrated against the potentiometer to compensate for any drift in the d.c. amplifier. The results of all these experiments are given in Tables I to VII, Appendix A.

3.72 Flow Reactor

From a control aspect, operating the equipment as a flow reactor was complicated by the importance of two further variables, the temperature of the sucrose feed and the flow rate of slurry leaving the reactor.

The initial procedure was identical to that with the batch runs. After a steady slurry temperature had been reached, the sucrose metering pump was started. The feed was precooled in the constant temperature bath to the reactor temperature by adjusting the set-point on the bath thermostat. This controller was also manually assisted by operating the valve on the glycol coolant supply to the bath. The level in the reactor was maintained by adjusting the decomposed-slurry drain valve. Decomposition was controlled by a variac in parallel with the 500 watt heater to give a temperature from 3° to 5°C above the equilibrium decomposition temperature.

Samples of mother liquor were taken after the reactor temperature had become steady. It was assumed that steady-state conditions had been reached when there was no change in either the sucrose concentration or the temperature over a period of ten minutes.

The levels of the independent variables specified for the flow reactor runs correspond approximately to the blocks .11 and .13 in table 5.21. In addition the effects of a change in the slurry volume and a modification to the impeller arrangement were considered.

Experiments were carried out with a single impeller to determine the variation in the reactor performance with power input. The power input is a funtion of both the stirrer speed and geometry: by changing the geometry for a given speed the effect of the power input may be checked independently. A set of runs was repeated without the paddle impeller but with the pitched turbine at the same position as before, figure 7. The results of these experiments are given in tables IX to XIII, with a summary in table VIII, Appendix B.

3.73 Liquid Freon Distributor

Throughout the runs, freon feed was introduced into the top of the reactor as a steady stream of liquid and not through a distributor as a fine spray of droplets. Although a distributor operating below the impeller was specified in the original design, it was found unworkable due to hydrate formation at the outlet holes.

The performance of the reactor with a single turbine impeller, the arrangement which it is assumed exaggerates poor feed distribution, was considerably below that predicted. To test whether the reactor performance could be improved by introducing a fine spray of liquid freon, a simple perforated-pipe distributor was installed in the space above the liquid level. The distributor was fabricated from $^{3}/_{16}$" O.D. copper tube, formed as a 3" diameter ring with 12, $^{1}/_{64}$" holes drilled in the walls of the tube. This device was satisfactory, producing fine jets of freon spraying upon the surface of the reacting mixture, though occasionally holes were blocked with hydrate even with the distributor well clear of the surface. Three sets of runs were repeated with this distributor in the batch and flow reactors. Attention is drawn to these comparisons in the summary tables I and VIII.

3.74 Propane Hydrate Runs

Batch experiments were repeated with propane as the hydrate former for experimental variables corresponding to block .11. No modifications to the apparatus were necessary. The method and results are given in Appendix C.

3.75 Filtration Experiments

Only limited washing experiments were conducted since the main interest was not to investigate wash hydrodynamics but to establish whether mother liquor could easily be recovered from the crystals. To test and investigate the unit a little more thoroughly than these terms of reference suggest, experiments were undertaken with the following variables; bed height, mother liquor concentration, crystal characteristics based on different driving forces, and wash velocity. Only small changes were made in these variables.

The filter unit was evacuated and then filled with freon gas at the reactor pressure. The coolant was circulated from the constant temperature bath and the glassware was cooled to the reactor temperature. A charge of mother liquor and freon hydrate was admitted through sample valve S, figure 8, after purging the line. The bed was drained and the mother liquor passing through the sintered disc was collected in a measuring cylinder. Further additions of slurry were made to form a drained bed of the selected height.

Wash water, precooled to hydrate formation temperature, was pumped through the wash distributor

and hence the hydrate bed at a constant, predetermined rate by a D.C.L. metering pump. The washings were collected in measuring cylinders of 25 ml. and 10 ml. capacities; the smaller size was selected for the sensitive 'breakthrough' area of the washing curve. During the wash period the pressure drop across the column was measured by a pair of pressure gauges. When washing was stopped and the bed was drained, freon hydrate was decomposed in situ and its volume and sucrose content determined. Mother liquor and wash samples were analysed with the Abbe refractometer. The results are given in Appendix F.

4. Equilibrium and Freon Solubility Data

4.1 Phase Diagram for Freon-12 Hydrate in Sucrose Solution

The determination of phase equilibria conditions for the hydrate-freon-sucrose system was necessary in order to describe the departure from equilibrium causing hydrate growth. Equilibrium data for the Freon-12-water system have been published by Wittstruck (32), but the freezing point depression of the hydrate equilibrium by sucrose has not been investigated.

The following study is confined to the solid hydrate-water equilibrium in the presence of the gaseous freon phase; this corresponds to line BC on figure 1.

4.11 Equilibrium Determination in Unstirred Cell

Wittstruck (32) and Wilcox (33) conducted phase equilibrium studies in small unstirred pressure vessels. In each case the pressure cell was placed in a cooled and agitated thermostat bath. The hydrates were formed by flashing off liquid agent from the two phase system which caused cooling and spontaneous nucleation. Pressure measurements were taken for given bath and cell temperatures.

A cell similar to that described by Wittstruck was

used in the present experimental study as a first approach to obtaining phase equilibrium data. The cell was also designed to provide information on spontaneous nucleation in sucrose solutions, solubility and growth of the hydrate. Those observations not related to phase equilibrium are discussed in section 2.4.

The cell used is shown in figure 12, together with a flow diagram. Basically the cell was comprised of a 6" by 3" diameter C.V.F. glass pipe section fitted with base and lid of $\frac{1}{4}$" brass, two $^{3}/16$" Simplifix couplings, two thermocouple probes, a prototype filter tube and a plastic-coated magnetic follower. The cell was mounted above a polythene-jacketed magnetic stirrer motor immersed in a glass water bath. With a solution of about 200 ml. in the cell agitation was effective, but when hydrate was present the stirrer had no effect. The bath was equipped with a stirrer and heater, but no thermostat. Temperature control was by ice addition since a supply of refrigerated glycol was not available.

Hydrate was spontaneously nucleated by condensing freon in the cell and then reducing the pressure. As the freon evaporated, sufficient local subcooling

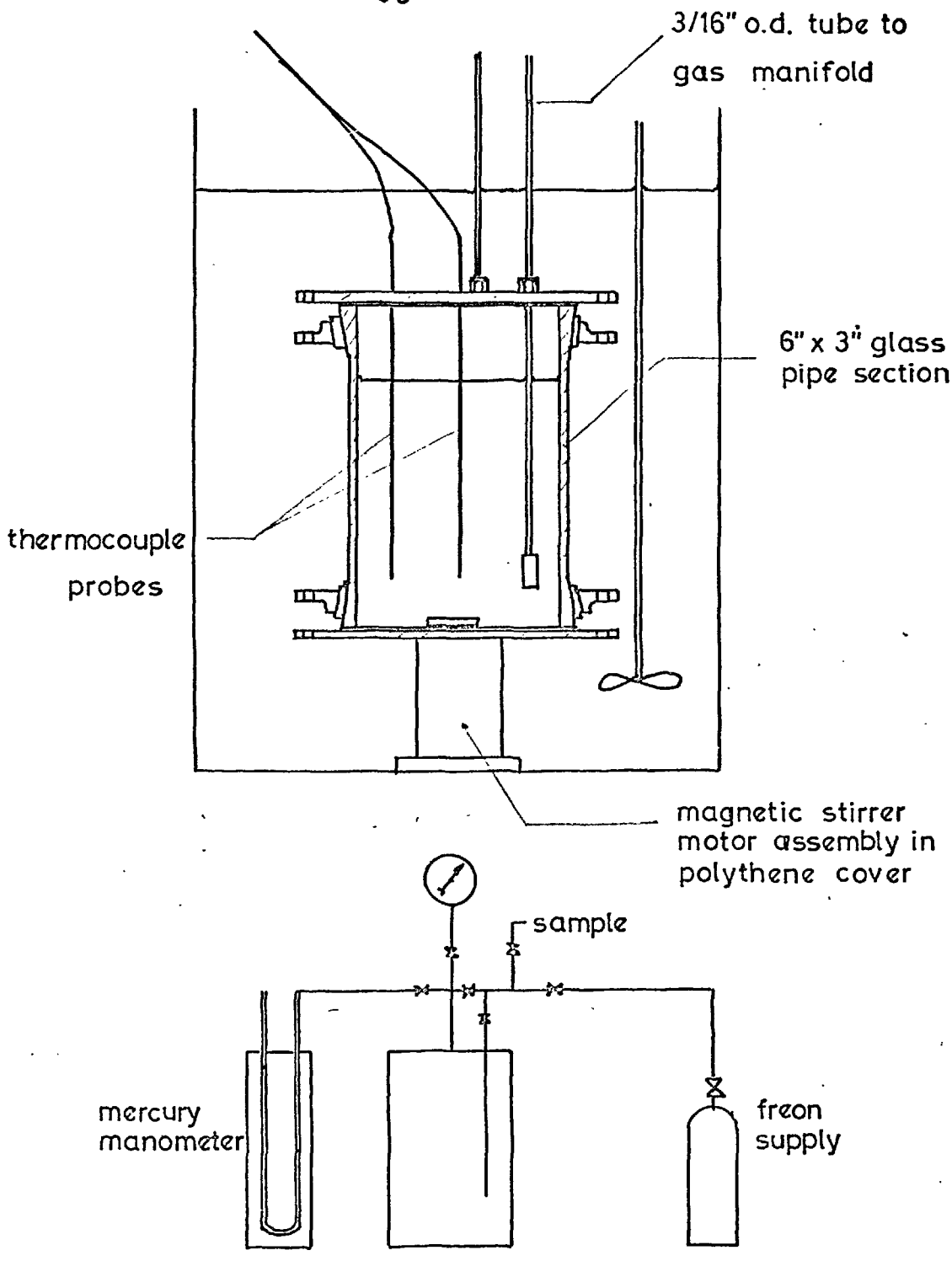


figure 12 Cell for phase equilibrium determination

occurred to cause nucleation and simultaneous rapid growth of hydrate. The cell tended to become a mass of frozen bubbles of gas; that is, hydrate seeming to grow round the evaporating drop, tended to lock the bubble in solution. It was under these conditions that the stirrer failed to be effective.

The bath temperature was adjusted to approximately that of the cell and the steady cell pressure and temperature were recorded. The temperature was considered steady when the readings of the two thermocouples were identical for a period of ten minutes. In this way it was checked that there was no variation in temperature within the cell due to a departure from equilibrium caused by heat conduction across the cell from the bath. The temperature of the bath was then lowered and the cell pressure measured for a new equilibrium. A mercury manometer was employed to measure pressures below atmospheric. The cell was then slowly heated up to the critical decomposition temperature to test whether there was any difference between the data collected from the cooling runs and that collected by heating. A significant difference would have indicated that equilibrium conditions had not been achieved. The results for this section are given in Table XX.

4.12 Freezing Point Depression of Sucrose Solutions

The method of determining the freezing point depression has to take into account the effect of an extra degree of freedom. The quadruple point, previously invariant, becomes univariant in the four phase, three component system and two degrees of freedom are associated with the line B'C'.

The unstirred cell cannot be used to determine the sucrose phase equilibrium in the manner described in the previous section. If the cell is heated, the quantity of hydrate decreases and the sucrose concentration changes. Since mother liquor is trapped in and between hydrate-covered bubbles of gas, it is unlikely that the sucrose concentration will be the same, or change at the same rate, at all points in the unstirred cell. This implies that the measured 'cell' temperature is in fact a local equilibrium temperature in the neighbourhood of the thermocouple probe, at a sucrose concentration probably different from that sampled by the filter tube.

Data for the sucrose system was obtained from the large scale equipment, the well-stirred insulated reactor described in section 3.2. Along line B'C'

there are two degrees of freedom in the 3 phase, 3 component system. Therefore for a given sucrose concentration there is the choice of either pressure or temperature as the single independent variable. With the experimental reactor system it is more convenient to keep the pressure constant and measure the temperature response. In practice it is not possible to maintain a constant mother liquor concentration in a well-stirred reactor; the energy dissipated by the stirrer and the heat leak into the reactor partly decomposes the hydrate, thus diluting the solution. However, a good approximation to constant composition is achieved in the reactor, provided that the power input is not excessive. The temperature and concentration may be taken as uniform throughout the slurry.

Hydrate slurry was formed in the reactor at a low operating pressure; a slurry concentration of about 20% was consistent with an adequate flow of slurry at a stirrer speed of 600 rpm. The pressure was fixed by keeping the condenser pressure constant, adjusting the flow rate and temperature of the glycol coolant as required. The slurry was held at the selected pressure for 15 minutes, then the temperature was noted for the

following 10 minutes. If no change was observed in the second interval the reading was taken to be the equilibrium temperature. At this point a sample of mother liquor was withdrawn and analysed, giving the sucrose concentration in equilibrium with the hydrate at the measured temperature and pressure. If the temperature was not constant, the conditions were maintained for a further interval. The pressure was then altered and a new equilibrium established.

Distilled water and initial sucrose concentrations of 10, 20, 30 and 40% (w/w) were used. The pressure was measured by the same 0-60 psig. Bourdon Tube gauge as was used in the hydrate growth studies. All the results obtained in the stirred reactor are given in Table XXI.

4.2 Hydrate Equilibrium Analysis

The equilibrium along the line BC corresponds to the equation:

$$CF_2Cl_2(g) + 17H_2O(l) \rightleftharpoons CF_2Cl_2.17H_2O(s)^*$$

and the exothermic heat of reaction is λ_{hf} cals/mole.

* The structure of the hydrate crystal and the features of the unit cell are discussed by von Stackelberg (35).

It was shown by Barduhn (34) that the slope of the univariant equilibrium line is governed by the Clausius-Clapeyron equation:

$$\frac{dP}{dT} = \frac{\lambda_{hf}}{T\Delta V} \qquad -- (1)$$

Where $\Delta V = \mathcal{Z}RT/P$

and $\mathcal{Z}$ = compressibility factor for a non-ideal gas

Hence $$\frac{d\ln P}{dT} = \frac{\lambda_{hf}}{\mathcal{Z}RT^2}$$

Integrating this equation assuming that λ_{hf} is independent of temperature:

$$\ln P = -\lambda_{hf}/\mathcal{Z}RT + B \qquad (2)$$

Therefore the equation that may be fitted to the experimental data has the form:

$$\log_{10} P = -A/T + B \qquad (3)$$

4.21 Unstirred Cell

A least squares fit to the cell data, table XX, gave:

$$\log_{10} P = -7521.1/T + 2817.8$$

The data does not deviate significantly from a straight

line on a log P vs. 1/T plot. Comparing A with the constant in equation (2):

$$\lambda_{hf} = \mathfrak{S}R(2.303 \times 7521.1)$$

and since $\mathfrak{S} = 0.905$

$$\lambda_{hf} = 31.15 \text{ K cal/g.mole of hydrate}$$

A correction to this estimate taking into account the heat of solution of freon is considered in Appendix E. Alternatively the data may be fitted to give the equilibrium temperature $t^{o}C$ as a function of pressure:

$$t = 10.46 \log_{10} P - 6.948$$

This form gave a better fit in terms of the sum of squares of errors.

The Wittstruck data agrees very closely with these results, and a least squares fit gave:

$$\log_{10} P = -7274.8/T + 2729.5$$

Hence $\lambda_{hf} = 30.12$ Kcal/grole.

which corresponds to the published data (34), $\lambda_{hf} = 30.14$. If the two sets of data are combined to give a mean effect:

$$t = 10.58 \log_{10} P - 7,094 \qquad (4)$$

the estimated standard deviation of the temperature given by (4) is $0,17^{o}C$.

Source	T_c °C	P_c psia
Unstirred cell	12.03	65.3
Wittstruck (32)	12.29	65.8
Pooled data	12.12	65.4
Koppers	12.11	65.4

Table 4.21: Critical Temperature and Pressure

A comparison of the measured and published values of the temperature and pressure at the critical point is given in table 4.21. The results from the unstirred cell add nothing to the published data: The analysis was useful only as a check on the measurement technique and as a comparison with the subsequent determination, in the stirred reactor, of the effect of sucrose on hydrate equilibrium.

4.22 Freezing Point Depression

It can be shown (83) that the effect of a solute on the freezing point of a pure solvent is related to the activity coefficient of the solute:

$$\Delta T_{fp} = \frac{R(T - \Delta T_{fp})T}{\lambda_{hf}} .\ln a \qquad (5)$$

Where T = Freezing point of pure solvent °K

Although this expression simplifies for the case of dilute solutions to a linear dependence upon the solute mole fraction, it is expected that the expression for concentrated sucrose solutions will be non-linear. The dependence is therefore described as a polynomial:

$$\Delta T_{fp} = c_1 x + c_2 x^2 + c_3 x^3 + \ldots$$

Where x = sucrose concentration (w/w).

Assuming that λ_{hf} is independent of x, it is possible to express the equilibrium temperature as a function of P and x only:

$$t = A' \log_{10} P + B' - c_1 x - c_2 x^2 - c_3 x^3$$

A least squares fit to the well-stirred reactor data, table XXI, with a 4th order polynomial gave:

$$t = 9.41 \log P - 5.009 - 3.407x - 24.61x^2 + 83.68x^3 - 126.8x^4 \quad (6)$$

The estimate of the standard deviation on t is 0.05°C. This corresponds to an error in the measured thermocouple e.m.f. of $\pm 1.6 \mu v$, which is just greater than the potentiometer error ($\pm 1 \mu v$). Several alternative forms were tried, including different orders of polynomial in conjunction with equation (3).

Model in x	Remaining degrees of freedom	Sum of squares of errors	Mean square
Cubic	53	0.13135	0.002478
Quartic	52	0.11161	0.002146
Difference	1	0.01974	0.01974

Ratio of mean square = $\frac{.01974}{.002146}$ = 7.25

F value at 0.01 probability level = 7.20

Table 4.22: Analysis of Variance Test

A model in x^4, equation (6), gave the best fit and is significantly better than a cubic model. This is shown in table 4.22 (after Mandel (36)) by a variance test. The experimental results are plotted together with equation (6) in figure 13.

4.23 Analysis at Constant Sucrose Concentration

The slope of the sucrose equilibrium lines given by equation (6) is greater than the slope given by equation (4) for the pure water phase. This implies that either the heat of formation changes with sucrose concentration, and equation (6) shows the mean effect, or that there is a more basic difference due to the method of measurement.

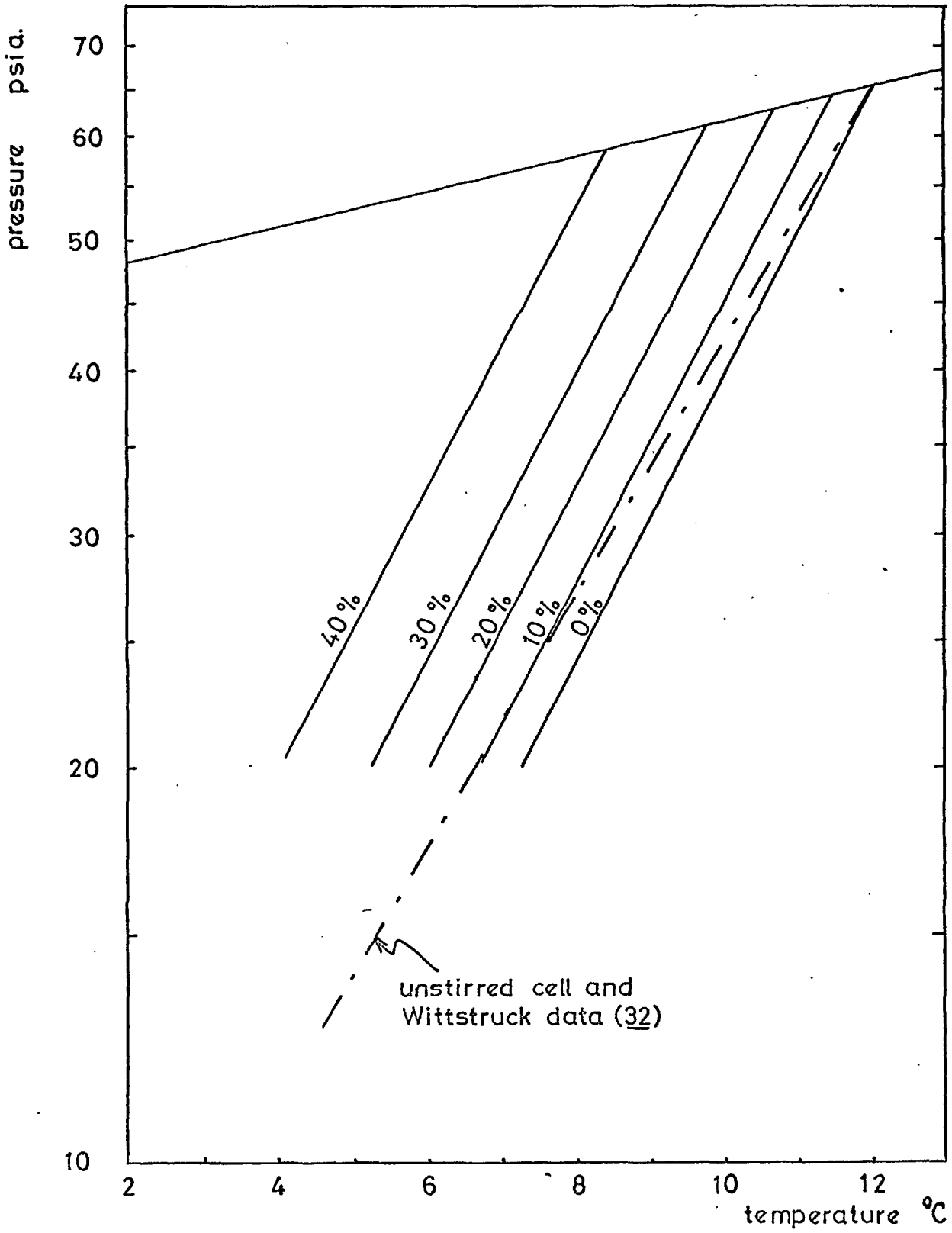


figure 13 Phase diagram: Freon-12/sucrose system

Table 4.23 gives the constants A and B in equation (3) and the calculated heat of formation for a given sucrose concentration. The calculation of these parameters involved correcting the equilibrium data to a mean concentration; the corrections are given in table XXI.

x	A	B	λ_{hf}	T_c	P_c	ΔT_{fp}	ΔT_e
.0	8499.	3161.	35.20	12.08	65.4		
.10	8278.	3088.	34.29	11.53	64.3	0.55	0.55
.20	8210.	3077.	34.01	10.74	62.8	1.34	1.33
.30	8306.	3113.	34.40	9.81	61.0	2.27	2.35
.40	9259.	3466.	38.34	8.33	58.4	3.75	4.08

Table 4.23: Change in estimated λ_{hf} with x

It appears that although the values of T_c and P_c for pure water agree very closely with those calculated from the unstirred cell data, table 4.21, the estimate of the heat of formation is consistently higher for the stirred reactor. The difference cannot be due to an impurity in the freon sample since the same source was used for both determinations, or to any error in the pressure measurements since both gauges were checked against a

standard test gauge. The estimate of λ_{hf} does not vary significantly with x, with the exception of a higher value at 40% (w/w).

The conclusions drawn from this analysis are that the hydrate is not at equilibrium with the sucrose solution in the well-stirred reactor, and that the departure from equilibrium is a function of the reactor pressure. The power dissipated by the turbine impeller together with the heat leak into the reactor causes decomposition of the hydrate. Although the rate of decomposition is very small, a finite driving force is required and hence the measured solution temperature is superheated with respect to the true hydrate equilibrium. This effect can be seen in figure 13; the reactor temperature (0%) is higher for a given pressure than the equilibrium conditions defined by the unstirred cell data.

The difference between the slopes of the equilibrium lines has been assumed to be due to the dependency of the driving force for decomposition upon pressure, though the mechanism involved is not understood. The driving force is a function of the equilibrium solubilities of freon at the phase boundaries and hence by Henry's Law

will be a function of pressure. This effect was shown to be too small to account for the results; further data and discussion are presented in section 7.2.

A comparison is made in table 4.23 of the measured and estimated values of the freezing point depression. Estimates were obtained from equation (5) with activity data for the sucrose-ice system from International Critical Tables. (λ_{hf} was taken as 1.77 Kcal/gmole. water as hydrate). The difference in the freezing point depression values is only significant for 40% sucrose solution, the concentration at which the heat of formation also differs. These discrepancies may be due either to the effect of superheating, exaggerated by the highly viscous liquor, or to some change in the actual composition of the hydrate.

4.24 Summary

Hydrate equilibrium data are best obtained in an unstirred system, though the effect of sucrose on the freezing point may be measured in a stirred reactor. The complications arising from superheating in an agitated reactor cannot easily be avoided. If the heat input is reduced by dissipating less power at the turbine impeller, both the rate of decomposition and the mass

transfer coefficient decrease, and consequently the degree of superheating may stay constant. The problem may possibly be overcome by installing a well-designed cooling coil system to exactly balance the heat input.

The best expression for computing the effect of pressure and sucrose concentration on the equilibrium temperature is based on the slope of the hydrate line given by equation (4), and the freezing point depression given by equation (6). Hence :

$$t = 10.58 \log_{10} P - 7.094 - 3.407x - 24.61x^2 + 83.68x^3 - 126.8x^4 \quad (7)$$

4.3 Solubility of Freon-12 in Sucrose Solutions

The solubility of Freon compounds in water have been determined by E.I. du Pont (37) and Syracuse University (38). Du Pont give solubility isotherms for Freon-12 in water at temperatures above 25°C. The work published by Syracuse does not include Freon-12 but does give the variation of Henry's Law constant with temperature, and the effect of salt on gas solubility for a number of hydrocarbons of the hydrate-forming type.

A set of experiments was carried out to determine the effect of sugar on the solubility of Freon-12 and to

check whether the du Pont data could be satisfactorily extrapolated to hydrate formation temperatures. The experimental techniques used were essentially those described in reference (37), using the reactor as the saturating vessel.

There were two types of experiment to be carried out. Firstly to measure the solubility at atmospheric pressure, the amount of gas dissolved by a given weight of solvent was determined. Secondly, solubility at super-atmospheric pressure was determined by measuring the amount of gas evolved from the solvent when the pressure was reduced to atmospheric. The total solubility was obtained by adding to the measured volume the amount of residual freon in solution at atmospheric pressure.

4.31 Experimental Method

The apparatus shown in figure 14 is the arrangement for measuring the solubility relative to atmospheric pressure. Vessel F was a wide-necked 100 ml. conical glass flask fitted with a B 29/32 cone. A stopper was fabricated in glass with two tubes sealed into the stem of a Quickfit cone. One tube was butt-jointed to the $^{3}/_{16}$" O.D. copper pipe of the sampling system with

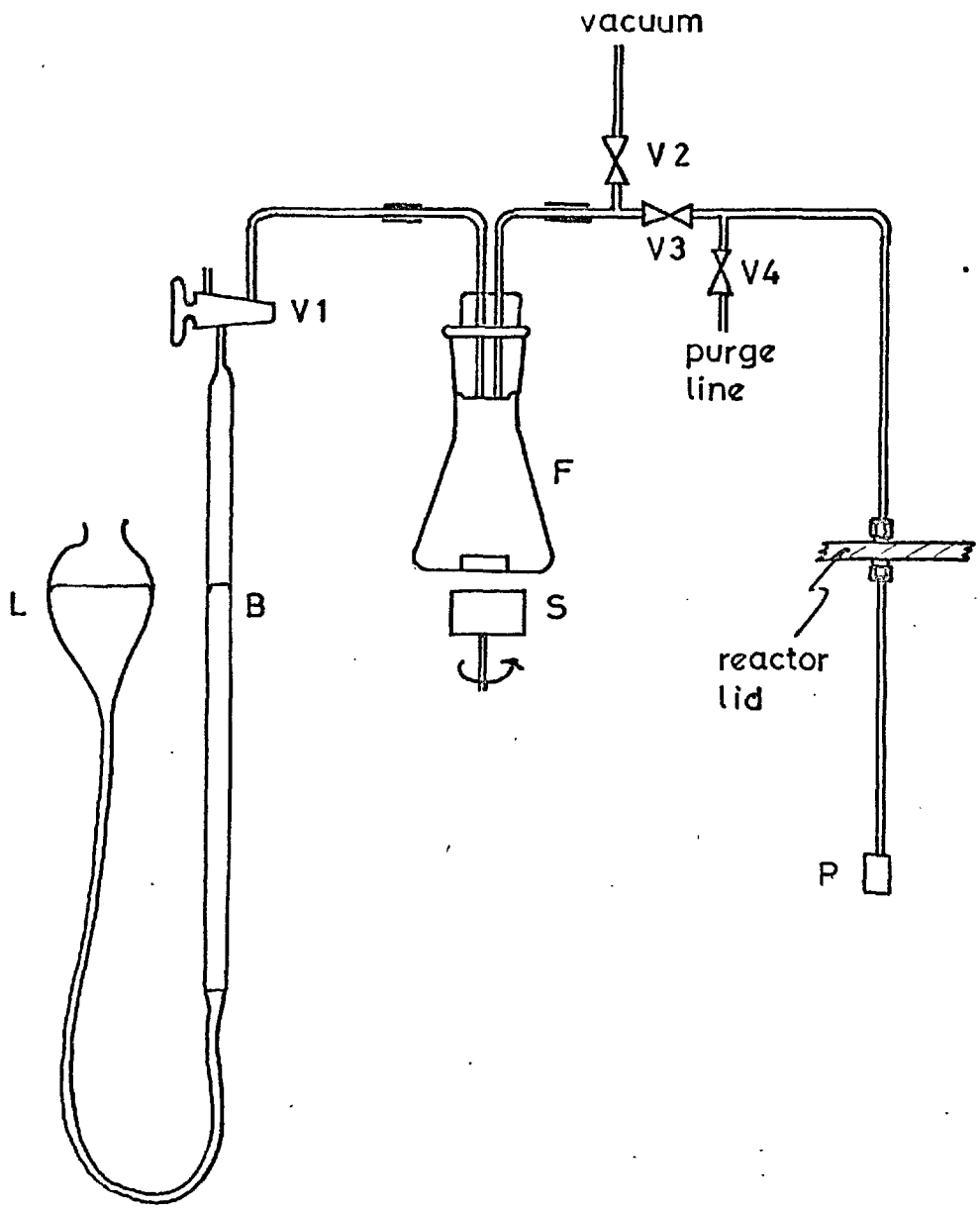


figure 14 Solubility sampling system

P.V.C. tube. The second tube was connected to a 25 ml. burette B incorporating a mercury levelling bulb L, via a three-way glass stop-cock V1. Valves V2, V3 and V4 were $^{3}/_{16}$" Simplifix shut-off valves.

The system was thoroughly tested for leaks under vacuum. The volume between V1, V2 and V3 was calibrated by filling flask F with mercury, evacuating the remaining air and then filling the system with a measured volume of air from the burette. The volume of the burette and valve V1 was calibrated with mercury.

The burette and flask were evacuated with a Speedivac pump with V3 closed, then V2 was shut. A saturated solution of freon in water was removed from the reactor via probe P and purged through the sample line via V4. V3 was then opened and as saturated solution was admitted to the flask, freon flashed out of solution. The flask was filled to the calibrated 130 ml. mark such that a reading could be obtained on the burette when the system pressure was corrected to atmospheric. The contents of the flask and lines were then brought to equilibrium with the ambient temperature and pressure, with the aid of a magnetic stirrer S. Atmospheric pressure was maintained in the flask by adjusting the levelling bulb L.

The steady reading on the burette was taken and the flask contents weighed. The temperature of the saturated solution in the reactor was controlled by the circulation of coolant through a submerged coil.

The solubility of freon in water and sucrose solutions at atmospheric pressure and 12°C was measured after slight alterations had been made to the system described. The capacity of the burette was increased by adding a calibrated glass bulb of approximately 30 ml., and valve V1 was modified to allow the burette to be filled with freon at atmospheric pressure. Flask F was immersed in a constant temperature bath.

The solution was placed in F and deaerated by vacuum applied through valve V2. Freon was introduced from the burette and the pressure in the well-stirred flask was maintained at atmospheric by adjusting L. When equilibrium conditions were reached, the volume of the absorbed freon was measured directly and the flask was weighed.

Solubility measurements were taken with 33 samples and the data, together with a specimen calculation are shown in table XXII, Appendix E.

4.4 Proposed Solubility Model

The solubility of freon in sucrose solution has been measured experimentally with three independent variables; pressure, temperature and sucrose concentration. For the purposes of computation it is necessary to derive a suitable expression relating these three variables which may be expected to give the best fit to the data and which is preferably based on thermodynamic theory. The following sections deal with the effect of each variable.

4.41 Pressure Effect

Du Pont showed clearly that Henry's Law holds for solutions of freon-12 in water at temperatures below 50°C. It can therefore be assumed that at constant temperature:

$$P = Hc$$

P = partial pressure of freon (psia)

c = freon concentration (g.moles/litre)

H = Henry's Law constant.

4.42 Temperature Effect

Glew (39) has shown that the variation of H for

certain methyl halides with temperature may be described by the equation:

$$\ln H = \ln P/c = A + B \log T + C/T \qquad (8)$$

where T is measured in ^{o}K. No theoretical basis was given for the expression but satisfactory fits to equilibrium data for methyl halides were obtained. The three empirical constants were evaluated by the method of least squares.

4.43 Sucrose Concentration Effect

The effect of salt on vapour-liquid equilibrium has been discussed by Johnson and Furter (40). 'Salting-out' is used generally to denote a decrease in the solubility of the non-electrolyte in the solution caused by salt addition. The effect is related to the change in chemical potential of the system, and it is through this relationship that Johnson derived the equation:

$$\ln \frac{\alpha_s}{\alpha} = KN$$

where α = relative volatility

α_s = relative volatility with salt addition

K = 'salting-out' factor

N = mole fraction of salt in 3 component system

The equation was used to fit vapour-liquid equilibrium data of the ethanol-water-salt system type. In terms of solubility of a non-electrolyte (freon) in the aqueous phase, it can be rewritten:

$$\ln \frac{x}{x_s} = KN$$

where x = mole fraction of freon in the aqueous phase.

For dilute solutions the mole fraction x can be replaced by the solubility expressed as g.mole/litre.

$$\ln \frac{c}{c_s} = KN \qquad (9)$$

Combining equations (8) and (9):

$$\log {}^{P}/c_s = A + B \log T + C/T + KN$$

This form will be valid only if there is no interaction between the effects of temperature and sucrose concentration on solubility.

4.44 Experimental Solubility Model

The model which gave the best estimate of the variation of the Henry's Law constant with temperature and sucrose solution was shown to have the form:

$$\ln H = A + C/T + KN$$

The term (B ln T) suggested by Glew was initially included in the analysis but resulted in an increase in the sum of squares of the errors. The best least squares fit for the solubility data from this study and the published data of du Pont, table XXII, gave:

$$\log_{10} H = 9.265 - 1633.2/T + 7.511\ N \qquad (10)$$

The experimental results and the best-fitted lines for constant sucrose solutions are plotted on figure 15.

If the estimate of the standard deviation of the Henry's Law constant given by the fitted data is expressed as the solubility of freon in solution, then the deviation is $\pm$ 0.00045 g.mole/litre. All the data fall within $\pm$ 10% of the value of the concentration calculated from equation (10); this includes the du Pont data for the solubility of freon in pure water.

The tolerance intervals using a 95% confidence coefficient are:

$$9.10 < A < 9.43$$
$$-1681. < C < -1585.$$
$$6.76 < K < 8.26$$

The greatest uncertainty is in the estimate of the effect of sucrose on the Henry's Law constant. The correlation coefficient between parameters C and K was -0.38. This

suggests there is little interaction between the effects of temperature and sucrose concentration.

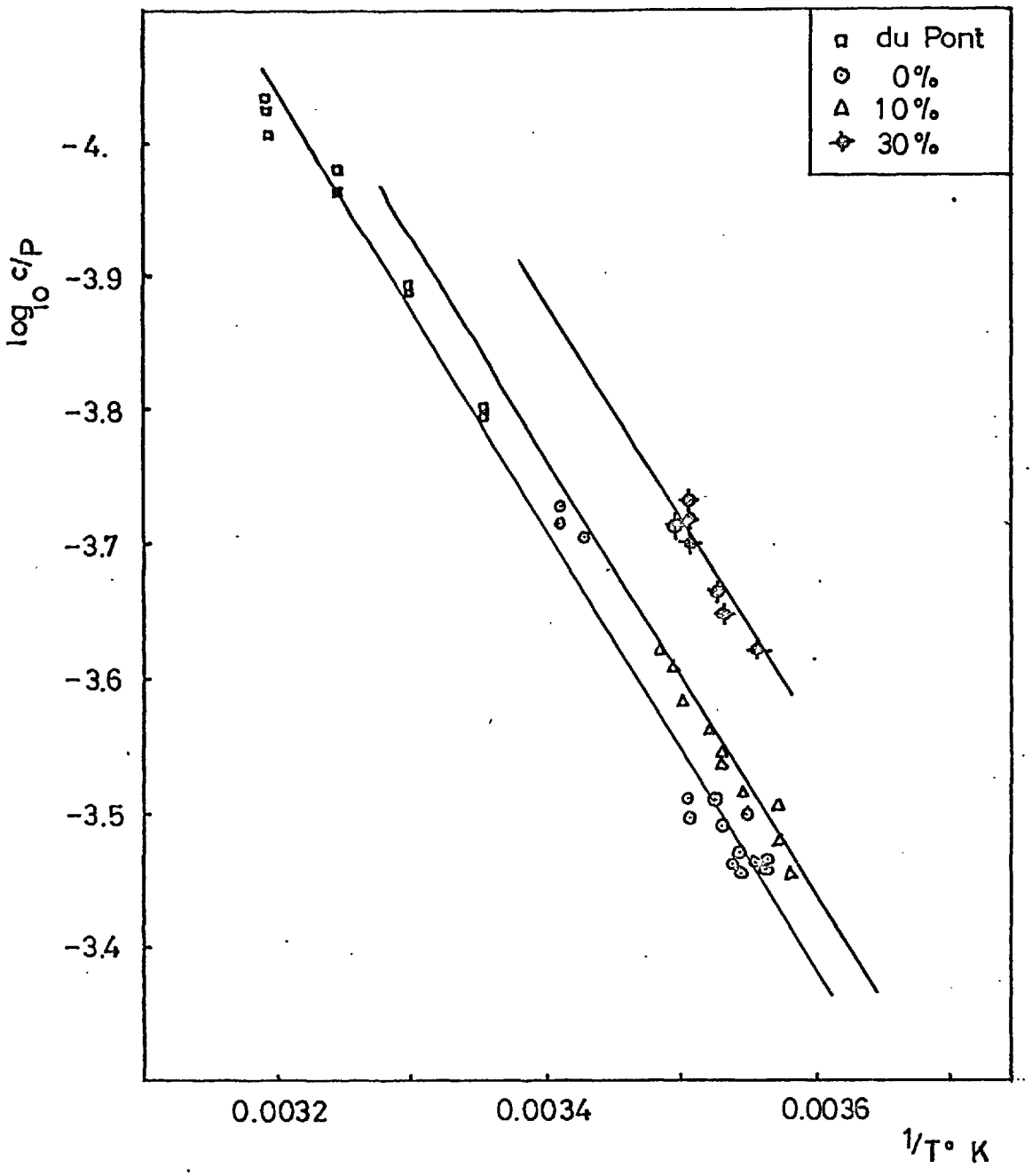


figure 15 Plot of $\log_{10} c/P$ v. $1/T$ with sucrose concentration

5. Theory and Literature Review

The formation of hydrate from sucrose solutions and liquid agent is effected by a series of heat and mass transfer steps. The aims of this chapter are to evaluate the relative importance of the transfer processes involved and, in conjunction with published work on hydrate kinetics, to establish a suitable growth model for the range of experimental conditions. These topics are developed in five sections:

(1) Definition of the heat and mass transfer driving forces in the multiphase system,

(2) Interpretation of published hydrate studies,

(3) Literature survey on effect of power and physical constants on the rate of mass transfer,

(4) Heat transfer characteristics of an auto-refrigerated reactor,

(5) Model for batch hydrate kinetics, simulating reactor start-up.

5.1 Hydrate Growth in Autorefrigerated Reactors

The reactor is considered to be operating under steady-state conditions at pressure P, with the temperature of the aqueous phase T_r such that the heat of formation is transferred to boiling agent at temperature

T_1, figure 16a. T_1 is the condensation temperature of the agent at the pressure of the continuous gas phase, and T_c represents the equilibrium temperature of the hydrate crystals at the operating pressure.

The liquid agent is dispersed throughout the reactor by the turbine impeller and, as heat is transferred into the droplets, the liquid changes to vapour. At the surface of the aqueous phase the vapour detaches itself and passes to the condenser. The history of an individual bubble in the reaction mixture might be expected to depend upon the agitation intensity, the temperature differential (T_r-T_1), the physical properties of the system and the fractional hold-up of the phases present in the reactor. An interesting photographic study of the evaporation of single drops has been made by Sideman and Taitel (41).

Simultaneously with the transfer of heat into the growing bubble, mass transfer of agent is occurring from the bubble into the aqueous phase. Agent diffuses through the boundary layer around the bubble into the solution to a crystal site where it combines with water to form a solid phase. It has been shown that hydrate is never formed in the agent phase, but always in the aqueous phase (26).

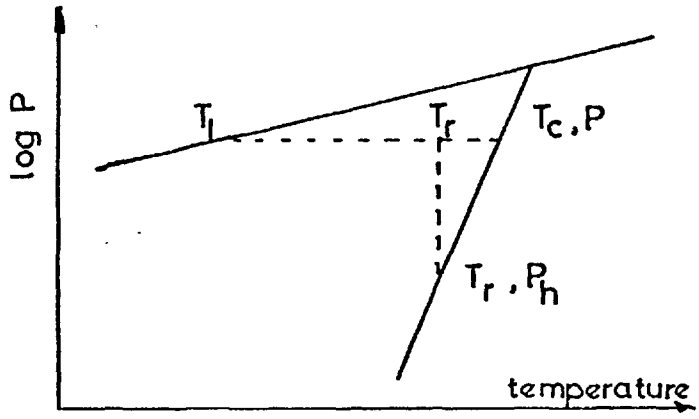


figure 16a Reactor operating conditions

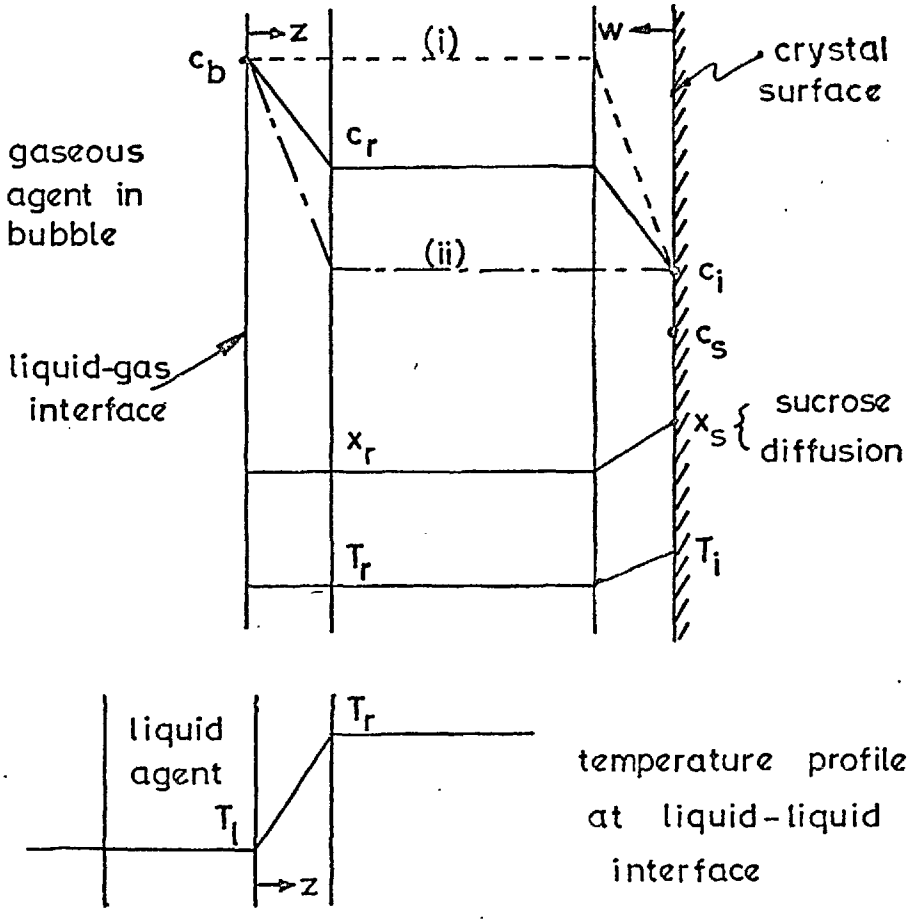


figure 16b Transfer processes at phase boundaries

The crystal growth rate may depend upon both the rate of diffusion of agent to the solid surface and the reaction at the surface. It depends also upon the number of growth sites, which is a function of the nucleation rate and orientation of the crystals. As the crystal grows, the heat of formation is transferred from the crystal surface through a thermal boundary layer to the bulk aqueous solution. The sucrose present in the water which is combining with the agent to form a solid phase accumulates at the hydrate crystal surface and diffuses through the boundary layer into the bulk solution.

The development of the steady-state model is based on the assumption that the agitation is sufficient to make the liquid temperature and concentration essentially uniform around each particle and bubble, and equal to the temperature and concentration in the effluent stream. This assumption of perfect mixing also means that every crystal has an equal probability of leaving the reactor.

The rate of transfer in any exchange process is dependent upon three factors; the effective driving force, the area of contact and the transfer coefficient. These are discussed in turn in the following sections.

5.11 Diffusion from the Hydrating Agent

According to the film theory, the mass transfer of agent from a drop or bubble to the main body of the turbulent liquid is treated as if it occurred by molecular diffusion through a laminar layer of liquid. The applications of the Whitman film theory are discussed by Gordon (42).

For transfer from agent bubbles, the following assumptions may be made:

(i) Each bubble is surrounded by a stagnant film of thickness z, which is small with respect to the bubble diameter.

(ii) A steady state concentration is quickly established in the liquid film after the bubble is formed.

(iii) The concentration of the bulk of the liquid outside the stagnant film is constant and equal to c_r.

(iv) The temperature across the film is uniform and equal to T_r.

(v) The agent is only sparingly soluble in the liquid phase, hence the effect of bulk flow may be neglected.

The mechanism is shown schematically in figure 16b, where concentration c_b is the interfacial concentration of agent in the liquid phase which is assumed to be at equilibrium with the gas phase at the interface. The value of c_b is calculated from Henry's law constant, equation (10) for T_r, P, x_r.

Integration of Fick's first law gives:

$$r_a = \frac{D_{as}}{z} A_b \ (c_b - c_r) \qquad - - (11)$$

where r_a = Rate of mass transfer of agent (g.mol/sec)
D_{as} = Agent diffusivity in sucrose (cm^2/sec)
A_b = Total bubble interfacial area (cm^2)

Equation (11) may be rewritten:

$$r_a = k_l a_b \ (c_b - c_r) \ V_r \qquad - - (12)$$

where k_l = Mass transfer coefficient (cm/sec)
a_b = Specific surface of bubbles (cm^2/cm^3)
V_r = Total reactor volume (cm^3)

Mass transfer from agent droplets may be described by a similar equation, but in this case there is a thermal gradient across the film, and assumption (iv) no longer holds. This point is developed in section 5.41; presently it is sufficient to state that c_b would be given by Henry's law constant for T_l, P, x_r.

5.12 Diffusion to Crystal

Noyes and Whitney (43) have assumed that the diffusion of material to the crystal face is controlled almost entirely by the resistance of the laminar layer near the face. However Cartier (44) has shown that the resistance to mass transfer is comprised of two resistances in series; diffusion across the laminar layer and integration of the

diffused material with the crystal. The boundary layer is assumed to have a constant thickness w from the advancing crystal surface:

$$r_a = \frac{D_{as}}{w} A_c (c_r - c_i)$$

$$r_a = k_c a_c (c_r - c_i) V_r \qquad -- (13)$$

where k_c = Mass transfer coefficient (cm/sec)

a_c = Specific surface of crystals (cm^2/cm^3)

The integration reaction at the surface is given by Cartier as:

$$r_a = KA_c \left[e^{\sigma (c_i - c_s)} - 1 \right]$$

where K = Particle integration factor

σ = Function of the activation energy

Nielson (45) has demonstrated that an alternative form of this expression is:

$$r_a = k_c' a_c (c_i - c_s) V_r \qquad -- (14)$$

where k_c' is a function of the supersaturation, but not dependent upon either the agitation effect or the physical properties of the system.

Equations (13) and (14) can be combined to give:

$$r_a = k_{oc} a_c (c_r - c_s) V_r \qquad -- (15)$$

where $$\frac{1}{k_{oc}} = \frac{1}{k_c} + \frac{1}{k_c'},$$

If $k_c' \gg k_c$, then the process is diffusion controlled. This often occurs when $(c_r - c_s)$ is large: When it is small it has been observed that the surface integration reaction often controls.

5.13 Heat Transfer from Crystal Surface

The heat transfer rate may be expressed in terms of the heat transfer coefficient between the crystal and the bulk solution:

$$q = r_a \lambda_{hf} = hA_c (T_i - T_r) \qquad -- (16)$$

where q = heat flow rate (cals/sec)

λ_{hf} = heat of formation of hydrate (cals/gmole)

$A_c = a_c V_r$ = Total interfacial area (cm^2)

T_i represents the temperature at the crystal surface, figure 16b. The relation between thermal driving force and the concentration is given by the Chilton-Colburn analogy (46), which predicts the ratio of the heat transfer coefficient to the mass transfer coefficient:

$$\frac{k_c}{h} = \frac{1}{\rho_l c_p} \cdot Le^{-2/3}$$

Combining equations (15) and (16), assuming that diffusion controls the crystal growth process:

$$\frac{k_c}{h} = \frac{T_i - T_r}{\lambda_{hf} (c_r - c_s)} \qquad -- (17a)$$

$$\therefore \quad \frac{T_i - T_r}{c_r - c_s} = \frac{\lambda_{hf}}{\rho_l c_p} \cdot Le^{-2/3} \qquad -- (17)$$

Since the value of the Lewis number* varies between 140 and 750 for 0% and 40% sucrose solution, the maximum value of the R.H.S. for Freon-12 is $405^{\circ}C/g.mol.cm^{-3}$.

* Based on D_{as} estimated from equation (43).

The maximum experimental value of $(c_r - c_s)$ is 6×10^{-6} gmol/cm^{-3}, hence:

$$T_i - T_r \not> 2.5 \times 10^{-3} \ ^{\circ}C$$

Hence it may be assumed that diffusion of heat is unimportant and the crystal film is at the bulk temperature T_r.

5.14 Sucrose Diffusion from Crystal Surface

A film model is used in a similar way to show the contribution of the sucrose diffusion to the overall process. The concentration profile in the boundary layer is shown in figure 16b: the flux of sucrose at every point in the w direction is zero since sucrose is not incorporated in the hydrate crystal. Consequently the bulk rate of flow must exactly balance its transfer by diffusion.

The concentration of sucrose at the crystal surface is x_s and in the bulk, x_r. Concentrations are given in weight percentages for consistency with future analysis. By Fick's first law:

$$\text{Sucrose flow rate} = 0 = -\frac{D_{ss}\rho_l A_c}{M_s}\left(\frac{dx}{dz}\right) + \frac{\alpha r_a x M_w}{x_w M_s} \quad - - \quad (18)$$

where α : 1 = Ratio of water to agent in crystal

αr_a = Rate of mass transfer of water (g.mole/sec)

D_{ss} = Diffusivity of sucrose in water (cm^2/sec)

M_w, M_s = Molecular weights of water and sucrose

x_w = Water concentration (w/w)

Integration of equation (18) gives:

$$\ln \frac{x_s}{x_r} = \frac{r_a w}{x_w D_{ss} A_c} \left(\frac{\alpha M_w}{\rho_l}\right)$$

substituting $k_s = D_{ss}/w$

$$\ln \frac{x_s}{x_r} = \frac{r_a}{x_w k_s A_c} \left(\frac{\alpha M_w}{\rho_l}\right) \qquad -- (19)$$

The sucrose concentration x_s given by equation (19) may be used together with the result in 5.13, that the film is at a uniform temperature T_r, to predict the agent concentration at the surface c_s. The equilibrium pressure P_h, figure 16a, is given by equation (7) for T_r, x_s and the agent concentration is then given by equation (10) for T_r, P_h, x_s.

5.15 Summary

The two driving forces for mass transfer have been described, but since the rate is probably determined by only one of the interphase processes, an over-all effective driving force may be defined.

Equations (12) and (15) may be combined to give:

$$r_a = K_o (c_b - c_s) V_r$$

where $$\frac{1}{K_o} = \frac{1}{k_l a_b} + \frac{1}{k_{oc} a_c}$$

If $k_{oc}a_c \gg k_l a_b$, that is the process is controlled by the rate of transfer from the agent, then:

$$r_a = k_l a_b (c_b - c_s) V_r \qquad -- (20)$$

Alternatively if the overall coefficient for transport of agent to the crystal phase is small compared to $k_l a_b$, then:

$$r_a = k_{oc} a_c (c_b - c_s) V_r \qquad -- (21)$$

The two extremes are shown in figure 16b, (i) and (ii), If the crystal resistance determines the rate, the sucrose concentration at the surface given by equation (19) will be substantially different from the bulk concentration, x_r. For gas-phase control, x_s will be approximately equal to x_r.

The magnitude of the individual over-all coefficients depends upon the turbulence created by the stirrer, the crystal size and population, and the proportions and physical properties of the four phases. These aspects will be discussed in section 5.3.

It can be shown that the thermal driving force $(T_c - T_r)$ varies approximately linearly with $(c_b - c_s)$, (Appendix E3) and this has been used as a parameter in

previous hydrate kinetic studies (see section 5.2)

$$r_a = K_c' (T_c - T_r) V_r \qquad - - (22)$$

The over-all transfer coefficient in this case contains the saturation concentration c_b. The main advantage of this form is that it gives the operating temperature T_r for the process directly, and this in turn gives the work required for the refrigeration cycle (see section 6.5).

5.2 Hydrate Kinetic Studies

Previously published experimental investigations have reached conclusions as to the rate determining step in the hydrate process, but many aspects have not been clarified, particularly the effect of the boiling liquid on the rates of mass transfer. Three published studies, Koppers, Pangborn and Williams (24, 27, 28), have dealt with auto-refrigerated reactors and two, Collot d'Escury and de Graauw (25, 26), with a three phase indirectly cooled reactor.

5.21 Autorefrigerated Reactors

Koppers present the most lucid of all hydrate kinetic studies, though insufficient attention was paid to presenting the results in the form of correlations, and the range of the physical variables studies was very small.

The rate of propane hydrate production was shown to vary as the 1.2 power of the stirrer speed and as the 0.5 power of the dispersed liquid phase concentration at a constant thermal driving force ($T_c - T_r$). This suggested that the formation rate was determined by the liquid-liquid interfacial area, since Calderbank and Vermeulen (section 5.34) derived the same exponents in the measurement of the surface area of immiscible liquids. Further, the production rate varied as the propane concentration driving force, so Koppers concluded that the rate determining step was the diffusion from propane drops, equation (20). The hold-up of gaseous propane and transfer from bubbles was not considered.

It was observed that residence times in the reactor, defined as the volume of aqueous charge divided by the feed flow rate, affected the formation rate. At high thermal driving forces the rate of production decreased with increasing residence time, that is with increasing hydrate hold-up. No correlation between the formation rate and the solids hold-up was suggested.

Comparative studies were conducted with Freon-12 and Freon-11, and these showed that the conversion rate of propane : F-12 : F-11 was approximately 3 : 4 : 1. No

conclusion was drawn from this result in terms of the physical constants of the three agents. Mean crystal sizes were given as 25 microns, with a specific surface of 375 cm^2/cm^3.

Pangborn has considered the methyl bromide reaction:

$$CH_3Br\ (l) + 7.9\ H_2O\ (l) \rightleftharpoons CH_3Br\ .\ 7.9\ H_2O\ (S)$$

Experiments were performed under steady state conditions in a vessel of similar size to this work. The effects of agitator speed, residence time, thermal driving force (T_c-T_r) and salt concentration were studied. The published results add little to the Koppers model.

A plot of reaction rate against power input at several salt concentrations is shown in figure 17a. Pangborn concluded that at a low degree of agitation, (1), the dispersion of liquid agent into droplets was the rate controlling factor, and the rate of production varied as the 1.4 to 1.6 power of the thermal driving force (T_c-T_r). Dissolution and diffusion from the drops was important in the second power interval up to 0.03 HP/ft^3. A dense slurry retarded the dissolution process, but this effect was eliminated at power inputs in excess of 0.18 HP/ft^3, where the production rate was linearly dependent on the thermal driving force (3). Pangborn suggests that pure

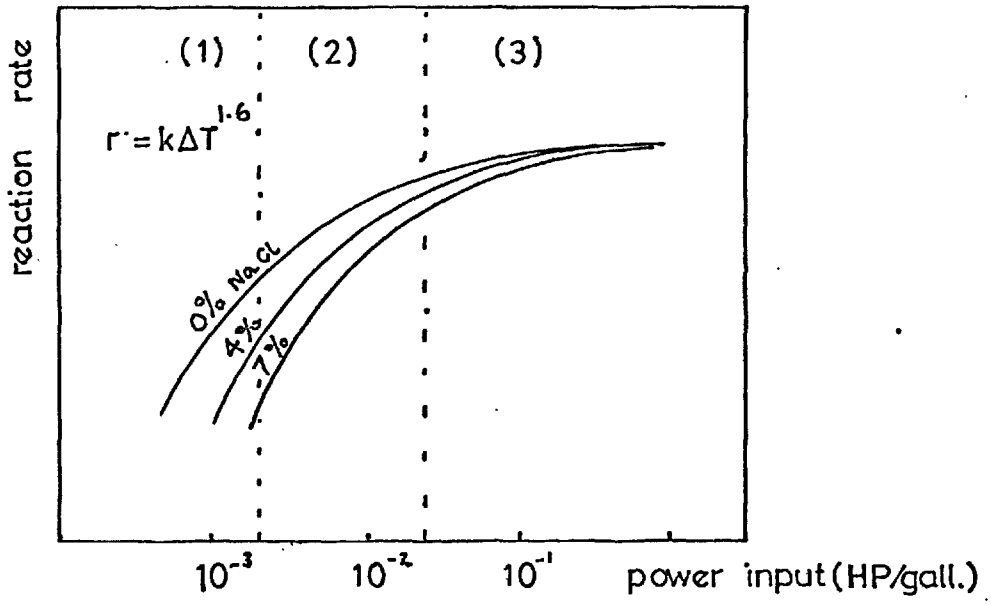


figure 17a Pangborn (27): data for methyl bromide with formation regimes

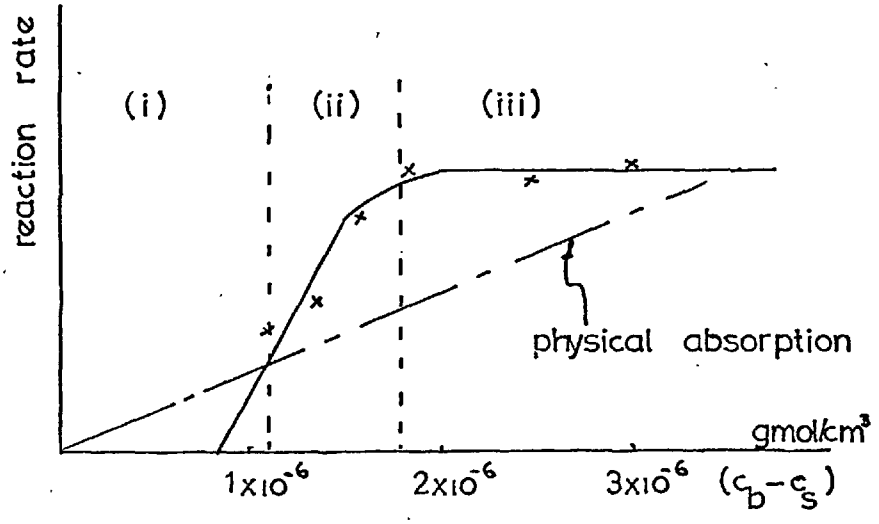


figure 17b de Graauw (26): data for propane showing formation v. concentration driving force.

kinetics can be measured at high power inputs where the rate is independent of the stirring intensity.

A further analysis of Pangborn's data is presented in section 8.2 .

Williams describes a series of experiments with propane hydrate in large scale equipment, solely from the aspect of heat transfer to the boiling drops. He assumed that the transfer of heat to the propane drops limited the amount of heat transferred and hence the amount of hydrate formed in a given volume of vessel, i.e:

$$r_a \sim (T_r - T_l)$$

A model for heat transfer was postulated assuming that the rate of heat transfer was slower than the rate of mass transfer, although Williams showed experimentally that the production rate was only a quarter of that predicted by the heat transfer model, even assuming a very low transfer coefficient. It must therefore be concluded that the Williams model is invalid and that mass transfer is the slowest process. It is worthy of note that the scatter of the results is such that it would be equally possible to state:

$$r_a \sim (T_c - T_r)$$

5.22 Indirectly-cooled Reactors

The hydration of monofluorodichloromethane was studied by Collot d'Escury in a small 5" diameter glass reactor cooled in a thermostat bath. The unsteady-state absorption rate of gaseous agent through the gas-liquid surface of the well-stirred reactor was measured by a soap-bubble technique. The rate was measured with no hydrate present in the aqueous phase and then during the period of nucleation and growth. It was observed that the absorption rate decreased after a time, presumably due to the decrease in the surface area of the interface caused by the crystal hold-up.

The rate determining step was shown to be the absorption process at the liquid surface. By comparing the rate of absorption at different times it was predicted that the concentration of agent in the reactor was greater than that given by the equilibrium concentration at the hydrate surface, c_s. Collot d'Escury suggested that this may indicate the existence of a surface reaction step, equation (14).

The absorption rates of propane and chlorine through the interface were measured by de Graauw, who relied on

vortex formation for gas dispersion. The free area of the gas-liquid interface was measured by observing the reaction rate of air with sodium sulphite solutions.

A typical plot of the formation rate against the concentration driving force $(c_b - c_s)$ is shown in figure 17b. Three regions were defined.

In region (i) the rate was controlled by the physical absorption of propane gas, whereas in the second region hydrate formed in the boundary layer around the bubbles. This accelerated the absorption process, being perhaps a nucleation phenemenon. In the third zone the rate of formation was independent of the concentration driving force. De Graauw suggests that this is due to the boundary layer formation rate being so fast that the bubble is covered with a film of hydrate; hence hydrate production depends only on the rate of supply of new bubbles. The heat transfer characteristics of the cell were not discussed but it may be that this limiting rate depends upon the maximum heat transfer rate through the glass reactor walls.

De Graauw observed that the greatest hydrate production rate occurred at the highest reactor pressure. This was explained by the further observation that the

bubbles at higher pressures tended to be larger and therefore less stable than at lower pressures, consequently giving a larger specific surface. This explanation is not entirely satisfactory, for de Graauw shows the physical absorption rate of oxygen in sulphite solution to be independent of pressure. This point will be discussed in section 6.21.

5.23 Summary

The results of these workers indicate that the rate determining step in the hydrate process is the transfer of agent from drops or bubbles, and that the production rate may therefore be defined by equation (20) or (22). Although the transfer process to the crystals is neglected, the crystal contributes to the model in that the formation rate decreases as the hold-up of crystals increases.

The following section examines the literature available on the variation of over-all mass transfer coefficients in gas-liquid and liquid-liquid agitated systems.

5.3 Effect of Mixing on Over-all Mass Transfer Coefficients

The interfacial area is the main variable determining

the capacity of an agitated two-phase reactor, though the mass transfer coefficient is also a dependent variable. Since both these terms depend upon the power input to the reactor, the first section discusses the change in power consumption with reactor variables.

5.31 Power Requirements in Mixing

The power consumed by a single impeller in a single phase system has been investigated by Rushton (47). The power number $(P_o/\rho_l N^3 D^5)$ which describes the basic flow pattern was plotted against the tank Reynolds number $(ND^2\rho_l/\eta_l)$ in baffled and non-baffled tanks to show the existence of three mixing zones. In the transition region between viscous and turbulent flow, $10^2 < Re < 10^4$, the power number decreases with Reynolds number whereas in turbulent flow the power number is a constant and:

$$P_o = K_{\eta l} N^3 D^5 \qquad -- (23)$$

where K = power number, a function of geometry only. The power required varies systematically with the density of the liquid or liquid pair, Miller (48), but is independent of the viscosity.

The effect of impeller spacing on the power input in dual impeller systems was investigated by Bates (31). The transition region remained unchanged but the power

number is increased depending on the relative spacing of the impellers and their proximity to the tank base. For the arrangement shown in figure 7, the power ratio of the dual to the single impeller system is 1.5 : 1, hence the power number for the agitator is:

$$P_o = 4.5 \rho_l N^3 D^5 \qquad -- (24)$$

5.32 Power Reduction under Gas Load

Although the power dissipated by the impeller in a pure liquid can be represented by equation (24), this does not hold for aerated liquids. The introduction of a gas reduces the density of the agitated mass and hence the power required. Most correlations for gassed systems have used the dimensionless term G/ND^3, which represents the ratio of gas flow to the liquid flow caused by the impeller. Oyama (49) gives:

$$P_g/P_o = 1 - k_g(G/ND^3) \qquad -- (25)$$

where P_g = Power consumption in gassed system
P_o = Power consumption in liquid phase
G = Gas flow rate

Michel & Miller (50) suggest the form:

$$P_g = K_m \left(\frac{ND^3 P_o}{G}\right)^{0.45} \qquad -- (26)$$

Since this correlation is in absolute rather than dimensionless terms it does not hold for all sizes of

equipment. The expression also correlated gas dispersion data in dilute suspensions of solids so the analogy with the hydrate multiphase system may be valid. Friedman (51) has shown that the use of a mean fluid density in equation (23) corrects for the effect of gas hold-up in the reactor. It was shown that the gassed power consumption was proportional to the stirrer speed raised to the 2.1 to 2.4 power.

5.33 Gas-Liquid Interfacial Areas

The effect of mixing on the rates of mass transfer is quite pronounced, for with a high interfacial tension and a large difference in specific gravity considerable energy is required to produce small bubbles and to keep them in suspension. In general terms, a large impeller size is required to create flow and hence a large gas hold-up, while a fast agitation speed is required to produce shear forces.

Calderbank (52) has shown that viscous forces may be ignored in the dispersion of gases in liquids and that the size of a gas bubble is determined by the condition when a balance is reached between surface tension forces and those due to turbulent fluctuations. The mean bubble size is given by:

$$D_b = \text{const.}\left[\frac{\sigma^{0.6}}{E_g^{0.4}\rho_l^{0.2}}\right]$$

where E_g = energy dissipated per unit volume of fluid, equation (39)

Although the right hand side is dimensional, it is one form of the Weber number which characterises the ratio of shear to viscous forces in the system. By measuring the absorption of light through the whole contents of a mixing vessel Calderbank (53) showed:

$$a_b = 230\left[\frac{E_g^{0.4}\rho_l^{0.2}}{\sigma^{0.6}}\right]V_g^{0.5} \qquad -- (27)$$

where a_b = specific bubble surface (cm^{-1})
V_g = superficial gas velocity (ft/sec)

and also that:

$$D_b = 4.14\left[\frac{\sigma^{0.6}}{E_g^{0.4}\rho_l^{0.2}}\right]\phi_g^{0.5} + 0.09 \qquad -- (28)$$

where ϕ_g = volume fraction of gas in dispersion.

Experiments with solutions of electrolytes showed that when a solute was present which inhibited bubble coalescence, the bubble size approaches that of a drop given by equation (35).

Since $$a_b = \frac{6\phi_g}{D_b} \qquad -- (29)$$

if the bubbles are spherical, equations (27) and (28) can be combined to give:

$$\phi_g \sim E_g^{0.4}V_g^{0.5} \qquad -- (30)$$

which is similar to an expression derived by Rushton (54).

Vermeulen (55) measured the interfacial area by means of light transmission probes in the dispersion:

$$a_b = \frac{1400\ N^{1.5} D \rho_l^{0.5} \eta_d^{0.75} \phi_g}{\sigma\ \eta_l^{0.25} f\phi} \qquad -- (31)$$

The mean bubble diameter was shown to depend upon the volume fraction of the dispersed phase. The specific surface area increased with increasing volume fraction but to a much less than proportional extent due to the offsetting influence of increased particle size. The correlation is rather unsatisfactory, since the gas hold-up has to be determined experimentally and a graphical correction, $f\phi$, must be made for the bubble diameter.

Vermeulen did not use the measured power input as the mixing parameter, but preferred a correlation based on the stirrer speed. In some ways this is more suitable than the Calderbank correlation based on the measured power input, since it has been shown that the power term is not an independent function in a gassed reactor, equation (26).

The integral value of the interfacial area was determined by Westerterp (30) by using a fast first order reaction occurring in the boundary layer around the bubbles. Westerterp showed that there was a minimum agitation rate below which the agitator has no effect

on the absorption rate, and criticised the earlier two-phase correlations for not recognising the existence of two regimes. For a turbine impeller:

$$a_b = 0.79\,\eta_l \phi_g (N-N_o)\,\frac{D}{H}\,\left(\frac{\rho_l T}{\sigma}\right)^{0.5} \qquad -- (32)$$

where $N_o D$ = Minimum agitation rate

$$= (1.22 + 1.25\ T/D)\left(\frac{\sigma g}{\rho_l}\right)^{0.25} \qquad -- (33)$$

and T = Tank diameter

H = Liquid height

In the regime with an agitation effect, the gas flow rate was shown to have no effect on the magnitude of the interfacial area. This directly contradicts Calderbank's equation (27). Westerterp reasoned that gas volumes in the dispersion circulate much more rapidly than gas is supplied; hence the circulation rate of gas predominates over the supply rate.

5.34 Liquid-liquid Interfacial Areas

The interfacial area formed by shear stress in a turbulent fluid is related to the equipment size, the turbulence and interfacial tension forces. Rodger (56) measured the drop sizes in oil-water dispersions by photographic and light transmission techniques in a 6" diameter tank:

$$a_d = \frac{K}{T}\left(\frac{N^2 D^3 \rho_l}{\sigma}\right)^{0.36}\left(\frac{\nu_d}{\nu_l}\right)^{\frac{1}{2}} \exp\left(3.6\ (\rho_l-\rho_d)/\rho_l\right) \qquad -- (34)$$

Calderbank (53) gave:

$$D_d = 2.24 \left[\frac{\sigma^{0.6}}{E^{0.4} \rho_1^{0.2}}\right] \phi_1^{0.5} \left(\frac{\eta_d}{\eta_1}\right)^{0.25}$$

hence by equation (29)

$$a_d = 2.58 \left[\frac{E^{0.4} \rho_1^{0.2}}{\sigma^{0.6}}\right] \phi_1^{0.5} \left(\frac{\eta_1}{\eta_d}\right)^{0.25} \quad -- (35)$$

Vermeulen (55) published his results in the form:

$$a_d = \frac{72 N^{1.2} D^{0.8} \rho'^{0.6} \phi_1}{\sigma^{0.6} f\phi} \quad -- (36)$$

where $\rho' = 0.6 \rho_d + 0.4 \rho_1$

5.35 Variation of the Mass Transfer Coefficient with Power Input

Experimental determinations of the effect of power input, geometry and particle size on the transfer coefficient have produced a large number of correlations, mainly for solid-liquid systems. Small drops and bubbles tend to behave as rigid particles so the comparison with gas-liquid and liquid-liquid systems is justified. The main problem is to define a suitable characteristic velocity for the flow relative to the particle, to calculate the Reynolds number. The mass transfer coefficient may then be correlated in terms of the Reynolds and Schmidt numbers:

$$Sh \sim (Re)^a (Sc)^b$$

Hixson and Baum (57) considered dissolution of solids in agitated tanks and proposed:

$$\frac{k_l D_T}{D_{as}} = 0.16 \left(\frac{ND_T^2 \rho_l}{\eta_l}\right)^{0.67} \left(\frac{\eta_l}{\rho_l D_{as}}\right)^{0.5} \quad -- (37)$$

Johnson and Huang (58) gave the correlation:

$$\frac{k_l D_T}{D_{as}} = 0.093 \left(\frac{ND^2 \rho_l}{\eta_l}\right)^{0.71} \left(\frac{\eta_l}{\rho_l D_{as}}\right)^{0.5} \quad -- (38)$$

The dependence on the 0.5 power of the Schmidt number was shown in either case, suggesting the Danckwerts surface - renewal theory was a suitable model for transfer at the interface. The use of the vessel and impeller diameters in the Sherwood and Reynolds numbers indicates that the correlations have no basic significance and are limited to the particular equipment employed.

The application of the Kolmogoroff theory of turbulence to predict the small scale velocity fluctuations in the flow field, and the use of this velocity rather than the impeller tip velocity is discussed by Calderbank and Moo-Young (59). The Kolmogoroff theory shows that in fully developed turbulent flow the energy is dissipated predominantly by small eddies. These are statistically independent of the main flow created by the impeller, with properties determined from the local energy dissipation rate per unit mass of fluid.

The mean square fluctuating velocity of these eddies is given by:

$$\overline{u^2}_d = K(E)^{\frac{2}{3}} (d/\rho_1)^{\frac{2}{3}}$$

where $E = KN^3D^2$ - - (39)

d = diameter of dispersed phase particle

The velocity represents the variation over a distance of the same order as the particle diameter and is therefore used as the characteristic velocity in the Reynolds number.

$$Re = \frac{\rho_1^{\frac{1}{3}} E^{1/6} D_b^{\frac{2}{3}}}{\eta_1^{\frac{1}{3}}}$$

Calderbank and Moo-Young published their results in the form of a general correlation for transfer from gas bubbles, liquid drops and solid particles:

$$k_1 = 0.13 \left(\frac{E\eta_1}{\rho_1}\right)^{\frac{1}{4}} \left(\frac{\eta_1}{D_{as}\rho_1}\right)^{-\frac{2}{3}} \quad - - (40)$$

It was shown to be applicable to small bubbles behaving as rigid spheres and to large bubbles, greater than 2.5 mm., which are affected by form drag resistance. The dependence upon the $\frac{2}{3}$ power of the diffusivity indicates a model for transfer between the Whitman theory and the penetration theory in which the interface is replaced by eddies of the bulk fluid.

Harriott (60) measured the mass transfer coefficients for ion-exchange particles suspended in agitated tanks.

This study has a special interest since it shows that the mass transfer coefficient depends upon the particle size, a conclusion disputed by the Calderbank and Moo-Young correlation. For particles smaller than 0.2 mm. k_l increases with decreasing diameter, whereas particles greater than 0.2 mm. have no effect on the coefficient. As the viscosity increases, so the particles size which affects transfer increases; for example at 16 cp. the critical particle size is 1.0 mm. The coefficient varied as the form:

$$k_l \sim E^{0.12} D_b^{-0.7} D_{as}^{0.8} \eta_l^{0.15} \qquad -- (41)$$

Harriott did not publish a generalised correlation but argued that estimates of the free terminal velocity of the particles could be used to calculate graphically a slip velocity and hence the transfer coefficient. The slip velocity is a function of the fluctuating velocity of the small eddies. Middleman (61) applied Kolmogoroff's theory to Harriott's data and proposed the following correlation:

$$\frac{k_l D_b}{D_{as}} = 2 + 0.55 \left(\frac{ND^2\rho_l}{\eta_l}\right)^{0.5} \left(\frac{D_b}{D}\right)^{0.67} \left(\frac{\eta_l}{\rho_l D_{as}}\right)^{\frac{1}{3}} \qquad -- (42)$$

The Reynolds number is based on the impeller diameter, but the effect of particle size is considered in the Sherwood number and a particle scaling factor.

5.351 Prediction of the Diffusivity of Freon in Sucrose Solutions

Since no experimentally obtained diffusivity data are available for the Freon-12/sucrose system, it is necessary to estimate the effect of sucrose on the diffusivity by means of published correlations.

The agent diffusivity in water at low agent concentrations is given by Wilke and Chang (62) based on the Stokes-Einstein equation:

$$\frac{D_{aw}\eta_w}{T} = 7.4 \times 10^{-8} \frac{(XM)^{0.5}}{V^{0.6}}$$

where D_{aw} = Diffusivity of solute at infinite dilution

η_w = Solution viscosity (cp)

T = Temperature ^{o}K

X = Association parameter

M = Molecular weight of solvent

V = Molecular volume of solute

For CF_2Cl_2 in water this gives:

$$D_{aw} = 3.77 \times 10^{-8} T/\eta_w$$

The diffusivity of gases with respect to a third component in the liquid phase has been investigated by Ratcliffe (63). The systems studied were carbon dioxide absorption in aqueous electrolyte, glycol and glycerol solutions. In general the Stokes-Einstein equation predicted values of the diffusivity that were too low,

and Ratcliffe deduced that the results could be correlated by modifying the dependence upon the solution viscosity. Hence:

$$\frac{D_{aw}}{D_{as}} = \left(\frac{\eta_l}{\eta_w}\right)^{0.637}$$

where D_{as} = Diffusivity of freon in sucrose solution

η_l = Sucrose solution viscosity

Therefore $D_{as} = (3.77 \times 10^{-8} T \eta_w^{-.36}) \eta_l^{-0.637}$ - - (43)

i.e. $D_{as} \sim \eta_l^{-0.64}$

5.36 Summary

The wide range of exponents in the various correlations suggests that it would not be possible to distinguish from the experimentally determined effects of the power input whether, in a three phase system, mass transfer was taking place from drops or from bubbles.

Assuming that transfer takes place from the gas phase:

$$r_a = k_l a_b (c_b - c_s) V_r \qquad - - (20)$$

and that the change in ρ_l, η_d, σ and V_r is small compared to the change in η_l, E and ϕ_g, from equations (31), (40) and (43):

$$r_a \sim E_g^{-.65} \eta_l^{-1.07} \left(\frac{\phi_g}{f\phi}\right)(c_b - c_s) \qquad - - (44)$$

A similar equation can be shown for liquid-liquid interphase transport.

The power consumption is affected by the gas flow rate, which in an autorefrigerated reactor is proportional to the production rate:

$$G = \frac{r_a \lambda_{hf}}{\lambda_l \rho_g} \qquad -- (45)$$

where λ_l = latent heat of agent (cal/g)
ρ_g = density of gaseous agent (g/cm^3)

Since $E_g \sim G^{-0.11} N^{3.15}$ from equation (26), then equation (44) becomes:

$$r_a \sim N^{1.9} \eta_l^{-1.0} \left(\frac{\phi_g}{f\phi}\right)^{0.93} (c_b - c_s)^{0.93} \qquad -- (46)$$

Hence the linear dependence upon the concentration driving force may be concealed by the gas load effect. Yet another dependence upon the driving force is suggested by the Calderbank correlation (27) which simplifies to the form:

$$a_b \sim E_g^{0.4} G^{0.5} \qquad -- (47)$$

Substituting this in equation (21) with (40), (43), (48), (26) gives:

$$r_a \sim N^{3.6} \eta_l^{-1.4} (c_b - c_s)^{1.7} \qquad -- (48)$$

The dependence upon the concentration driving force in equation (48) is similar to that observed by Pangborn (27)

at low stirrer speeds where:

$$r_a \sim (T_c - T_r)^{1.6}$$

Westerterp (30) identified the dependence upon gas flow rate in equation (47) with the region in which the stirrer had no agitation effect. Now Pangborn showed that the above non-linear dependence occurred only at low stirrer speeds and that the dependence changed to a linear one at a higher power input. Hence Pangborn's results might be taken to prove that the Westerterp 'agitation-effect' model is valid. If this is the case then, since the experimental sucrose system was operated entirely in the 'agitation-effect' region, it may be expected that equation (46) represents the transfer process rather than equation (48).

The question of the suitability of literature correlations for the over-all gas-liquid coefficient depends largely upon whether or not the manner in which vapour is introduced to the reactor is important. Clearly the manner of drop formation and of vapour generation during the reaction in the hydrate reactor does not correspond to a standard liquid distributor or gas sparge tube. Although the interfacial area determined from the literature may not be characteristic of the area in the hydrate reactor, it is expected that the liquid-film

transfer coefficient may be predicted fairly accurately.

Sideman (64) showed the effect of the initial bubble size on the over-all transfer coefficient from analysis of single and perforated sparge tube experiments performed by Karwat (65).

$$\frac{k_l a_b \text{ single}}{k_l a_b \text{ dist.}} = 0.5, \text{ at } E = 0.08 \text{ HP/ft}^3$$

$$= 0.8, \text{ at } E = 0.33 \text{ HP/ft}^3$$

The ratio of the over-all coefficients approached the value 1 assymptotically with E. The increase in agitation intensity decreases the difference between the data obtained with a single nozzle and with a distributing grid. In the context of the hydrate reactor, if transfer from the gas phase is important then a distributor would be effective below a power input of 0.4 HP/ft^3.

5.4 Heat Transfer Considerations

The hydrate reaction model is based on the assumption that heat transfer is a much faster process than mass transfer. The rate of production is given by a heat balance on the system (see section 5.51), but the reactor conditions (the degree of subcooling, etc.) are determined by mass transfer considerations. The following section

considers what effect the boiling phase may have on mass transfer.

5.41 Review of Heat Transfer with Change of Phase

The data available on this topic is limited to experimental studies by Sideman (41, 66, 67) and Williams (23).

Sideman conducted a photographic study of single drops evaporating whilst rising in a column of an immiscible liquid. Although a study of free convection is not relevant to this discussion, the characteristics of growing drops is. In evaporating, the vapour formed a spheroid at the upper part of the drop with the volatile liquid concentrated at the base, figure 18a. The liquid phase was considered to be at its boiling temperature T_l, corresponding to the vaporization pressure, and the heat transfer rate was assumed to be controlled by the film resistance in the continuous phase. It was also assumed that there was no heat flux across the film into the gas phase, hence $T = T_r$ at the gas-liquid interface (assumption (iv), section 5.11).

It was shown experimentally that the heat transfer coefficient was independent of the temperature difference

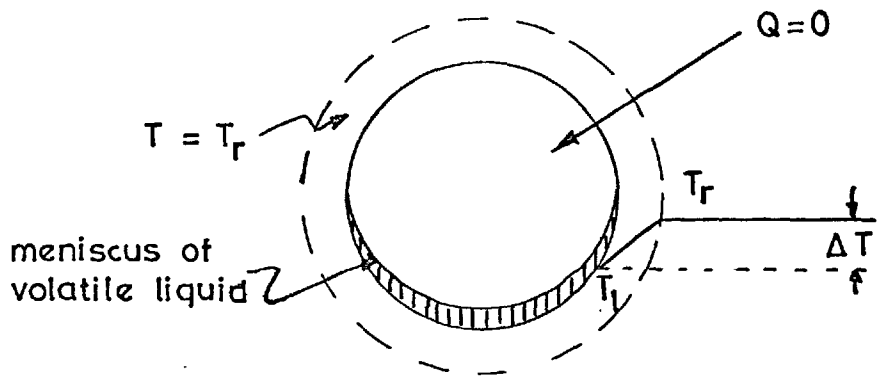


figure 18a Sideman's two phase bubble model (41,66)

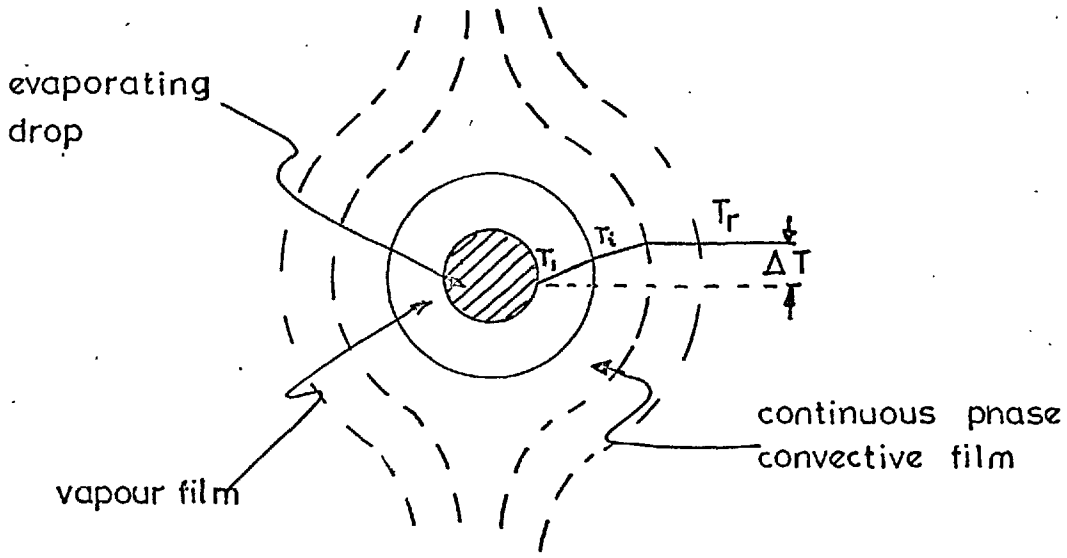


figure 18b William's boiling drop model (27)

(T_r-T_l) and the vapour content of drop and that the internal resistance to heat transfer was negligible compared with the external resistance.

Sideman and Barsky (67) proposed a correlation relating the heat flow rate with the specific power input and temperature driving force in a well-stirred mixing vessel. A model was derived based on the concept of local isothopy, the Kolmogoroff turbulence theory, and the single drop results. The model is discussed in some detail here, partly because the results are of relevance to the hydrate process and partly because Sideman's correlation appears to be at fault.

A droplet enters the agitated fluid fairly close to its boiling point and all the heat transferred to it serves to increase the vapour content. The heat transfer rate is:

$$Q = hA_v (T_r-T_l) \qquad -- (49)$$

Q = Rate of heat transfer (cal/sec)

h = Heat transfer coefficient(cal/sec cm^2 °C)

A_v = Total effective heat transfer area (cm^2)

Sideman assumed that the heat transfer coefficient was a function only of the power dissipation, the equivalent of equation (40), and not dependent on the driving force, (41).

Since the particle size was small, the two phase particle was assumed to remain spherical as in figure 18a. Considering the area as a function of particle size and vapour content:

$$A_v \sim \phi_g^{5/3} E_g^{\frac{1}{2}} \qquad -- (50)$$

and $$h \sim E_g^{\frac{1}{4}}$$

ϕ_g represents the volume fraction of gas hold-up which still contains a fraction of the evaporating liquid phase. Sideman selected the Calderbank correlation, equation (30), to describe the gas hold-up:

$$\phi_g \sim E_g^{0.4} V_g^{0.5}$$

where $V_g \sim Q$ -which is equivalent to equation (45).

Substituting (30) and (50) in (49)

$$\zeta \sim E_g^{17/12} Q^{5/6} (T_r - T_l)$$

Hence $$\zeta^{1/6} \sim E_g^{17/12} (T_r - T_l) \qquad -- (51)$$

Sideman conducted experiments in a five litre well-stirred reactor with n-pentane as the dispersed liquid phase. N-pentane was evaporated by an electrical heater in the tank base plate. From a plot of $\zeta^{1/6}/(T_r - T_l)$ against the gassed power input estimated from a form of equation (25), Sideman showed the exponent of the power input was 2, which agrees fairly well with equation (51).

The correlation was checked because it appeared that the use of the Calderbank gas hold-up function was not justified. There are two reasons for this objection. Firstly, as discussed in 5.33, Westerterp has shown a distinct region in which the gas load has no effect on the interfacial area, and secondly the gas hold-up measured or correlated in simple 2 phase systems may not be the same as the hold-up of gaseous refrigerant containing evaporating liquid. That is, there may be a much larger hold-up of n-pentane gas completely evaporated and taking no part in the heat transfer process. By taking the sixth power of the heat flow rate, Q, Sideman reduces the error and renders insensitive the graphical method.

The method of least sum of squares was used to correlate the data, regressing for the exponents of both (T_r-T_l) and E_g. The data is presented in the Appendix, Table XXVII, and the new correlations are given in Table 5.41.

Heat Transfer Correlations	Sum of Squares	Data Points	df.	Exponent of (T_r-T_l)	Exponent of E
(i) Sideman's Correlation gassed system: $Q^{1/6}/\Delta T$	5.98×10^7	16	14	6.	1.93
(ii) Proposed model, power input as in ungassed system	5.61×10^3	20	17	0.36	0.95
(iii) Model using gassed system (49), $k_g = 12$	14.9×10^3	16	13	0.29	0.48
(iv) Model as in (iii) with $k_g = 6$	8.53×10^3	20	17	0.41	0.97
(v) Model for gassed system, Michel (50)	8.55×10^3	20	17	0.40	1.05
Sum of squares = $\sum_{i=1}^{n} (Q_i - k_1 T_i^{k_2} E_i^{k_3})^2$, Q measured in watts					

Table 5.41 Heat Transfer Models

Clearly the minimum sum of squares is obtained with model (ii):

$$Q \sim E^{0.95}(T_r-T_l)^{0.36} \qquad -- (52)$$

which has a very different form from equation (51), and the sum of squares is very much reduced. Model (iii), which uses the same constant in the Oyama gassed-power equation (49) as Sideman's original correlation, gives a significant increase in the sum of squares of errors compared to the Michel-Miller correlation for the gassed power consumption (50).

If the Calderbank correlation is replaced by equation (82), then equation (51) becomes linearly dependent on (T_r-T_l). This is closer to model (ii) than the original form, but the discrepancy indicates that Sideman was probably wrong in assuming that both h and A_v are independent of (T_r-T_l). It further appears that ϕ_g given by two phase correlations does not represent the evaporating gas phase hold-up, since the high power dependence in (51) is not observed in model (ii). Sideman's data might also be subject to the type of feed distribution effect observed in section 6.31.

Williams (27) postulated a heat transfer model for the boiling drop which considers heat transport across a vapour film, figure 18b. The idealized spherical liquid drop is surrounded by an even gas film of increasing thickness. The over-all temperature difference between the liquid drop boiling at T_l and its surrounding solution is comprised of two parts; (T_r-T_i) due to convective heat transfer to the surface of the vapour, and (T_i-T_l) due to heat conduction through the vapour film to the liquid surface. The convective mechanism may be neglected since it is several orders of magnitude greater than the conduction process, i.e, $T_i=T_r$ at the bubble surface.

This model seems less realistic than that proposed by Sideman, figure 18a. From a consideration of the surface tension forces acting on the liquid it would appear that the liquid would spread inside the bubble to form a thin meniscus in contact with the aqueous phase. The turbulent forces acting on the bubble with a drop at the centre would, by momentum effects, cause the drop to be in contact with the interface. The Williams model seems unstable and consequently the derivation of a heat transfer coefficient based on conduction across a gas film is not pursued.

5.42 Mass Transfer from Liquid Agent

A model is considered which includes transfer both from droplets and from bubbles. The drop area is established to satisfy the heat transfer characteristics of the reactor.

$$r_a = k_l A_v (c_d - c_s) + k_l A_b (c_b - c_s) \qquad -- (53)$$

where c_d = Agent concentration in equilibrium with drop

A_v = Total effective area of liquid freon

Now $$Q = r_a \lambda_{hf} = hA_v (T_r - T_l) \qquad -- (49)$$

From the modified Sideman correlation for heat transfer:

$$Q \sim E^{0.95} (T_r - T_l)^{0.36} \qquad -- (52)$$

Substituting $h \sim E^{0.25}$ and equation (52) in (49):

$$A_v \sim E^{0.7}(T_r-T_l)^{-0.64} \qquad -- (54)$$

Substituting (54) in equation (53):

$$r_a = k_l \left[KE^{0.7}(T_r-T_l)^{-0.64}(c_d-c_s) + A_b(c_b-c_s) \right]$$

This expression depends upon the validity of the Sideman correlation and in particular that the heat transfer coefficient is independent of the temperature driving force. It is unlikely that the expression may be checked in this form, but it may be possible to show that the reaction rate is inversely proportional to some power of the temperature differential (T_r-T_l). Koppers (24) stated that the mass transfer from liquid agent was the rate determining step. If this is the case there will certainly be some interaction between the boiling phase and the reaction rate.

5.43 Effect of Evaporation on Bubble Size

The average size of gas bubbles in a dispersion depends on the equilibrium reached between the break-up by turbulent forces and the coalescence of the bubbles due to surface tension forces. Another factor imposed on this balance in a hydrate reactor is the bubble formed from a boiling drop. The size of a bubble formed by the evaporation of a representative drop is compared with the

size of a bubble calculated from the gas-liquid correlations.

By a mass balance, the initial drop size is equated to the final bubble size:

$$\pi/6\ D_d^3 \rho_l = \pi/6\ D_b^{*3} \rho_g$$

where D_b^* = Diameter of bubble formed from drop size D_d

i.e $$D_b^* = D_d \left(\frac{\rho_l}{\rho_g}\right)^{\frac{1}{3}}$$

For Freon-12, $D_b^* = 3.8\ D_d$

The correlations for liquid-liquid systems in section 5.34 give, for pure water agitated at 1420 RPM, D_d = 0.003 to 0.012 cm., whereas the gas-liquid correlations give D_b = 0.15 to 0.33 cm. The maximum value of D_b^* is thus 0.045 cm. Comparing D_b^* with the smallest bubble size D_b = 0.15 cm., by equation (29), it is seen that the interfacial area for the same gas hold-up has been increased by a factor of 333%.

This increase may not represent the true equilibrium conditions since bubbles will coalesce to give a larger mean size than D_b^*. However the interfacial area given by gas-liquid correlations may well be enhanced by the smaller transient bubbles produced by evaporation.

5.5 Batch Hydrate Kinetics

The principle feature of the batch runs is that the reactor cooling rate is maintained constant while the temperature and sucrose concentration of the slurry are measured from the time at which spontaneous nucleation occurs. The shape of a typical temperature-time plot is shown in figure 19. Analysis of this curve in terms of the hydrate model, equation (20), may lead to a confirmation of the hydrate mechanism and a quantitative estimate of the inhibiting influence of hydrate slurry on the reaction rate.

The analysis may be divided into two parts. In the first case the whole temperature-time curve is considered and the rate of change of the reaction rate with time is related to the change in the concentration driving force and in the hydrate hold-up. In the second case the temperature during the steady unsteady-state period, where the temperature gradient with respect to time is zero, is compared with the steady temperature, T_r, measured for different values of the independent variables given in table 3.61. The distinction is drawn here because for subsequent analysis the cases are treated independently.

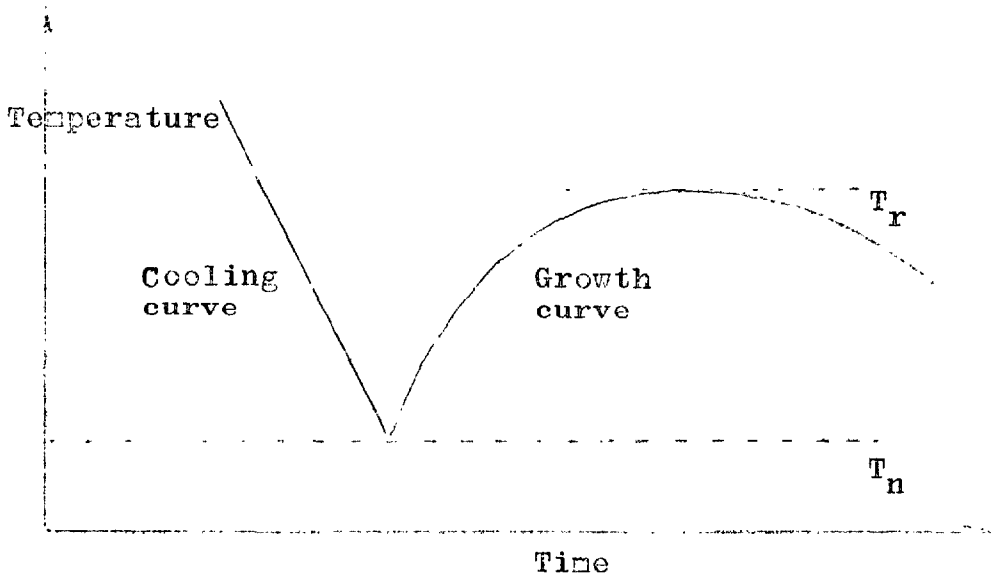


figure 19 Temperature-Time profile

The rate of hydrate production and hold-up of hydrate in the reactor may be estimated from a heat and mass balance. As hydrate is formed, the sucrose concentration of the bulk aqueous phase increases, and this may be taken as a measure of the extent of the reaction. Since this gives the amount of water in the hydrate phase directly, it is more convenient to describe the production rate in terms of a water flow rate , rather than as a flux of agent.

The production rate is defined by:

$$r = \frac{dy}{dt} \qquad -- (55)$$

where r = formation rate of hydrate in (gms. of water/min)

and y = water in the hydrate phase (gms.)

Previously the rate of mass transfer from the agent phase was defined by equation (20):

$$r_a = k_l a_b (c_b - c_s) V_r \qquad -- (20)$$

but since:

$$r_a = \frac{r}{60 M_h}$$

where M_h = molecular weight of water in hydrate

$$r = k_l' a_b (c_b - c_s) V_r \qquad -- (56)$$

where $k_l' = 60 M_h k_l$ (g.cm/g.mole.min)

5.51 Heat and Mass Balance

The net heat release curve, figure 19, can be expressed as the sum of the heat of formation and the heat removed by the evaporating agent.

(i) Consider hydrate formation from the gas phase in which case all liquid agent is evaporated.

$$V_t \rho_t c_{pt} \frac{dT}{dt} = r \lambda_{hfg} - F \lambda_l + K_h$$

where
- T = reactor temperature ^{o}C
- λ_{hfg} = heat of formation from gas phase (cal/g)
- F = agent flow rate (g/min)
- λ_l = latent heat of agent (cal/g)
- K_h = heat leak + power dissipation (cal/min)

(ii) Consider that hydrate formation occurs from the liquid agent phase, hence not all agent is evaporated.

$$V_t \rho_t c_{pt} \frac{dT}{dt} = r \lambda_{hfl} - (F - \frac{r}{\alpha'}) \lambda_l + K_h$$

$$= r (\lambda_{hfl} + \frac{\lambda_l}{\alpha'}) - F \lambda_l + K_h$$

In either case, the heat balance may be expressed:

$$V_t \rho_t c_{pt} \frac{dT}{dt} = r\lambda_{hf} - F\lambda_l + K_h \qquad -- (57)$$

In the cooling curve region, where no hydrate is formed in the reactor:

$$V_t \rho_t c_{pt} \frac{dT}{dt} = -F\lambda_l + K_h = Q \qquad -- (58)$$

where Q = net heat removal rate (cal/min)

Q may be determined calorimetrically by observing the cooling rate at a temperature equivalent to the reaction temperature T_r. This compensates for the heat leak and the power dissipated by the twin impellers.

By a mass balance on the solvent phase:

$$y_t + V_t \rho_t (1-x_t) = V_f \rho_f (1-x_f)$$

where y_t = water in hydrate form at time t (gms.)
x_t = sucrose concentration at time t

A mass balance on the solute, sucrose, phase:

$$V_t \rho_t x_t = V_f \rho_f x_f$$

Hence $$y_t = V_f \rho_f (1-x_f/x_t) \qquad -- (59)$$

5.511 Application of Koppers Model

Consider the simplest model proposed by Koppers and Pangborn, equation (22), with temperature T_r a function of time:

$$r = K_o'(T_c - T)\, V_r \qquad -- (22a)$$

Substituting in (57):

$$V_t \rho_t c_{pt} \frac{dT}{dt} = K_o'(T_c - T)\, V_r \lambda_{hf} - Q \quad -- (60)$$

(i) If $K_o'(T_c - T_n) V_r \lambda_{hf} > Q$, then the temperature will rise from the spontaneous nucleation point.

Integrating equation (60), assuming that:

(a) K_o' is a constant for all T and x,

(b) T_c is a constant.

(c) $V_t \rho_t c_p$ is constant during the reaction.

$$\int_{T_n}^{T} \frac{V_t \rho_t c_{pt}\, dT}{K_o'(T_c - T) V_r \lambda_{hf} - Q} = \int_o^t dt$$

$$T = \left(T_c - \frac{Q}{K_o' V_r \lambda_{hf}}\right) - \left[\left(T_c - \frac{Q}{K_o' V_r \lambda_{hf}}\right) - T_n\right] e^{\frac{-K_o' V_r \lambda_{hf} t}{V_t \rho_t c_{pt}}}$$

This expression gives the growth curve in figure 19 for the simple thermal driving force model. In the actual system it is unlikely that the first two assumptions will hold; both K_o' and T_c will depend upon the extent of the reaction.

(ii) The condition $\frac{dT}{dt} = 0$ is referred to as the steady-state operating criterion of the batch run. In this case (60) simplifies to:

$$K_o'(T_c - T_r)\, V_r \lambda_{hf} = Q$$

Hence $$K_o' = Q / \{(T_c - T_r)\, V_r \lambda_{hf}\}$$

Therefore from an experimental determination of T_r at $dT/dt = o$, an estimate of the reaction constant is obtained.

5.52 Application of Absorption Model

A more realistic approach to simulating the temperature-time curve considers the agent absorption rate given by equation (56) and the variation in the over-all coefficient $k_l'a$ due to the change in the characteristics of the four-phase reaction mixture.

Two-phase correlations were applied in section 5.36 to show the dependence of the over-all transfer coefficient for constant ρ_l, η_d, σ and V_r. These constraints hold for the case of a batch run, hence:

$$k_l'a_b \sim E^{0.65} \eta_l^{-1.07} \left(\frac{\phi_g}{f\phi}\right) \qquad - - (44a)$$

Maude (68) showed that aqueous suspensions of fine emery powders in turbulent flow behave as liquids having the viscosity and density of the suspension, and not as true liquids having the viscosity of water. Although Maude measured the slurry viscosities, Bonilla (69) showed that the Hatschek viscosity correlation may be used for correlating heat transfer data for the flow of slurries through pipes. The Hatschek equation is given by:

$$\eta_h = \eta_l/(1 - \phi_h^{\frac{1}{3}}) \qquad -- (61)$$

where η_h = slurry viscosity

ϕ_h = volume fraction of hydrate

The slurry viscosity η_h should therefore be used in place of the liquid viscosity in equation (44a). It was shown in section 5.31 that for high Reynolds numbers the power consumption was independent of viscosity and, since the slurry density is approximately constant, E may be considered constant. As a first approach, the term $(\phi_g/f\phi)$ will be considered constant too. Hence assume:

$$k_l' a_b \sim (\eta_l/(1-\phi_h^{\frac{1}{3}}))^{-1} \qquad -- (62)$$

Substituting (62) in (56):

$$r = \frac{K_B(1 - \phi_h^{\frac{1}{3}})}{\eta_l} (c_b - c_s) \qquad -- (63)$$

where $K_B = f(E, \phi_g, V_r)$ -- (63a)

hence equation (57) becomes:

$$\frac{dT}{dt} = \frac{1}{V_t \rho_t c_{pt}} \left\{ \frac{K_B(1-\phi_h^{\frac{1}{3}})}{\eta_l} (c_b - c_s) \lambda_{hf} - Q \right\} \qquad -- (64)$$

The hydrate hold-up fraction may be calculated by integrating equation (55):

$$y_t = \int_0^t r \, dt \qquad -- (65)$$

$$x_t = V_f \rho_f x_f / (V_f \rho_f - y_t) \qquad -- (59a)$$

Hence:

$$\phi_h = (1 + \alpha') \frac{\rho_l}{\rho_h} (1 - x_{f/x_t}) \qquad -- (66)$$

The equilibrium concentrations c_b and c_s are functions of variables T and x_t, hence from equation (10):

$$\log c_b = \log P - 9.265 + 1633./T + 273.2 - 7.51\, x_t \quad - (67)$$

$$\log c_s = \log P_h - 9.265 + 1633./T + 273.2 - 7.51\, x_t \quad - (68)$$

where P_h is given by equation (7),

$$\log P_h = 0.0945\,(T + 7.094 + 3.407\, x_t + 24.61\, x_t^2 - 83.68\, x_t^3 + 126.8\, x_t^4) \quad - (69)$$

The change in the values of equations (67) to (69) with the change in sucrose concentration during the course of the reaction is slight, but is included for completeness.

5.521 Solution of Equations to 5.52

To obtain the theoretical temperature and concentration profiles for experimental conditions described completely by P, Q, x_f and V_r, and for the observed boundary conditions T_n and T_r, it was necessary to solve equation (64) iteratively. Equation (64) was integrated in conjunction with (63), (65), (59), (66), (67), (68) and (69) by the method of Runge Kutta, using the IBM 7090 machine and Fortran IV as the programming language.

The initial estimate of K_B was based on the steady-state condition $dT/dt = 0$ at $T = T_r$.

$$K_B = \frac{Q\eta_1}{\lambda_{hf}(c_b - c_s)(1 - \phi_h^{\frac{1}{3}})} \quad - - (70)$$

However the value of ϕ_h at $T = T_r$ is not always experimentally observed. The sucrose concentration x_t was sampled during the course of a batch run, but the particular value at $T = T_r$ was not always obtained. Since the model predicts the sucrose concentration at x_r, it was convenient to solve for x_r iteratively. This approach is particularly useful if no sucrose concentration data is available and only the temperature-time response is known.

If T_{max} is the calculated temperature at $dT/dt = 0$, then if the first estimate of ϕ_h is too large, K_B is too small and $T_{max} < T_r$, hence K_B must be increased. Alternatively if the guess of ϕ_h is too small, the reaction rate is too great and $T_{max} > T_r$.

The iterative procedure was as follows:

(i) Calculate K_B, with ϕ_h estimate, from equation (70).

(ii) Integrate equation (64) from $T = T_n$. Stop at T_{max} when $dT/dt = 0$.

(iii) Compare T_{max} with T_r experimental. If $T_{max} = T_r$ write out all temperature time data. If $T_{max} \neq T_r$ go to (iv).

(iv) Substitute $K_B = K_B + K_B(T_r - T_{max})$. Return to (ii).

By using the substitution in part (iv), the iteration always converges to give $T_{max} = T_r$.

The computer programme was written in a general form such that any model could be examined; in particular a simpler model for comparative purposes based on a concentration driving force but not incorporating the effect of the hydrate slurry viscosity. In addition a more complicated function was introduced, based on the heat transfer consideration in section 5.42. For constant E it was shown, equation (54):

$$A_v \sim (T_r - T_l)^{-0.64}$$

Hence a possible model might be, substituting in (56):

$$r = \frac{K_C(1 - \phi_h^{\frac{1}{3}})(c_b - c_s)}{\eta_l (T - T_l)^{0.64}} \qquad - - (71)$$

Four main models were employed and within these four models various changes were made to the exponents of the viscosity, etc.

$$r = K_A (c_b - c_s) \qquad - (A)$$

$$r = K_B \left(\frac{\eta_l}{1 - \phi_h^{\frac{1}{3}}}\right)^{-1} (c_b - c_s) \qquad (63) - (B)$$

$$r = K_C \left(\frac{\eta_l}{1 - \phi_h^{\frac{1}{3}}}\right)^{-1} \frac{(c_b - c_s)}{(T - T_l)^{0.25}} \qquad (71) - (C)$$

$$r = K_D \left(\frac{\eta_l}{1 - \phi_h^{\frac{1}{3}}}\right)^{-1} (T_c - T) \qquad (22a) - (D)$$

where K_A, K_B, .. are functions of the form (63a), but assumed constant for each run.

The results of these calculated profiles and the adequacy of the models is discussed with the experimental results in section 6.1. Calculated results are presented in Appendix A, Tables III to VII.

5.6 Heat and Mass Balance for Steady-State runs

The steady-state runs, in which the sucrose concentration and temperature in the reactor remains constant, are simpler to analyse but less information is obtained from each run although it takes longer to perform.

Consider a mass balance on the solvent:

$$r + v_r\rho_r(1 - x_r) = v_f\rho_f(1 - x_f)$$

where v_f = feed flow rate of sucrose (cm^3/min)

and subscripts f and r refer to the feed and the reactor conditions respectively.

Also, from a mass balance on the solute:

$$v_f\rho_f x_f = v_r\rho_r x_r$$

hence

$$r = v_f\rho_f(1 - x_f/x_r) \qquad -- (72)$$

A heat balance on the system, assuming that only the latent heat of agent is transferred:

$$v_f\rho_f c_{pf}T_f + K_h = v_r\rho_r c_{pr}T_r - r\lambda_{hf} + (1 + \alpha')r\, c_{ph}T_r + F\lambda_l$$

Assume $v_f \rho_f c_{pf} = v_r \rho_r c_{pr} + (1+\alpha) r\, c_{ph}$

Then $Q' = F\lambda_1 = v_f \rho_f \left\{ c_{pf}(T_f - T_r) + \lambda_{hf}(1 - x_f/x_r) \right\} + K_h$ -- (73)

Hence in the case of steady-state runs it is an easy matter to check the heat balance by calibrating the agent feed rotameter as in section 5.51, and comparing the heat removal rate with the production rate measured by the concentration effect, equation (73).

The conversion in the hydrate reactor is defined as the fraction of water solidified as hydrate from the aqueous feed, hence:

$$\xi = 1 - x_f/x_r$$

For a multistage process with n stages of conversion ξ, it can be shown that the over-all conversion is given by:

$$\xi_o = 1 - (1 - \xi)^n$$

6. Experimental Results

This chapter is concerned with the analysis of all kinetic data, the assessment of postulated models and the development of a general correlation for the over-all transfer coefficient. The analysis is divided into four sections:

(i) The unsteady-state aspect of the batch reactor.

(ii) The batch reactor as an approximation to steady-state conditions.

(iii) The flow reactor.

(iv) Propane hydrate comparative analysis.

To simplify data handling, a generalised least-squares-fit programme was used, based on a standard matrix technique documented in Davies (70).

6.1 Calculation of Temperature-Time Curves

A summary of the batch results is given in Table 1, corresponding to the original design presented in Table 3.61, and all results are given in Table II, Appendix A. Listed are; pressure, nucleation temperature T_n, steady-state temperature T_r, the thermal driving force calculated from equation (7), the concentration driving force calculated from (7) and (10), measured gas hold-up and the

liquid phase viscosity calculated from Appendix G3. The production rate r, at $T = T_r$, was calculated from the agent feed rate, equation (58), and checked by a mass balance, equation (59). An example of this check for a sample run is given in Appendix A1.

The data from Table II was used to solve for the reaction constants K_A, K_B, etc., section 5.21, and hence to derive the temperature-time response predicted by the absorption models. These results together with the experimental temperature-time and concentration-time data, for a representative fraction of the batch runs, are given in Tables III to VII. Tables III to VI show examples of runs at 10 to 40% sucrose with details of the change in hydrate hold-up and estimated slurry viscosities. Other data are given in Table VII, with concise information relating to models A and B only.

A typical temperature-time plot, run 25.13, is shown in figure 20 together with the simulated temperature determined from models A,B,C, and D. Figure 21 shows the calculated values of x and y as a function of time. Further graphs, figure A1 - A12, covering a complete range of sucrose concentration and stirrer speed, are included in Appendix A, and show experimental results compared with

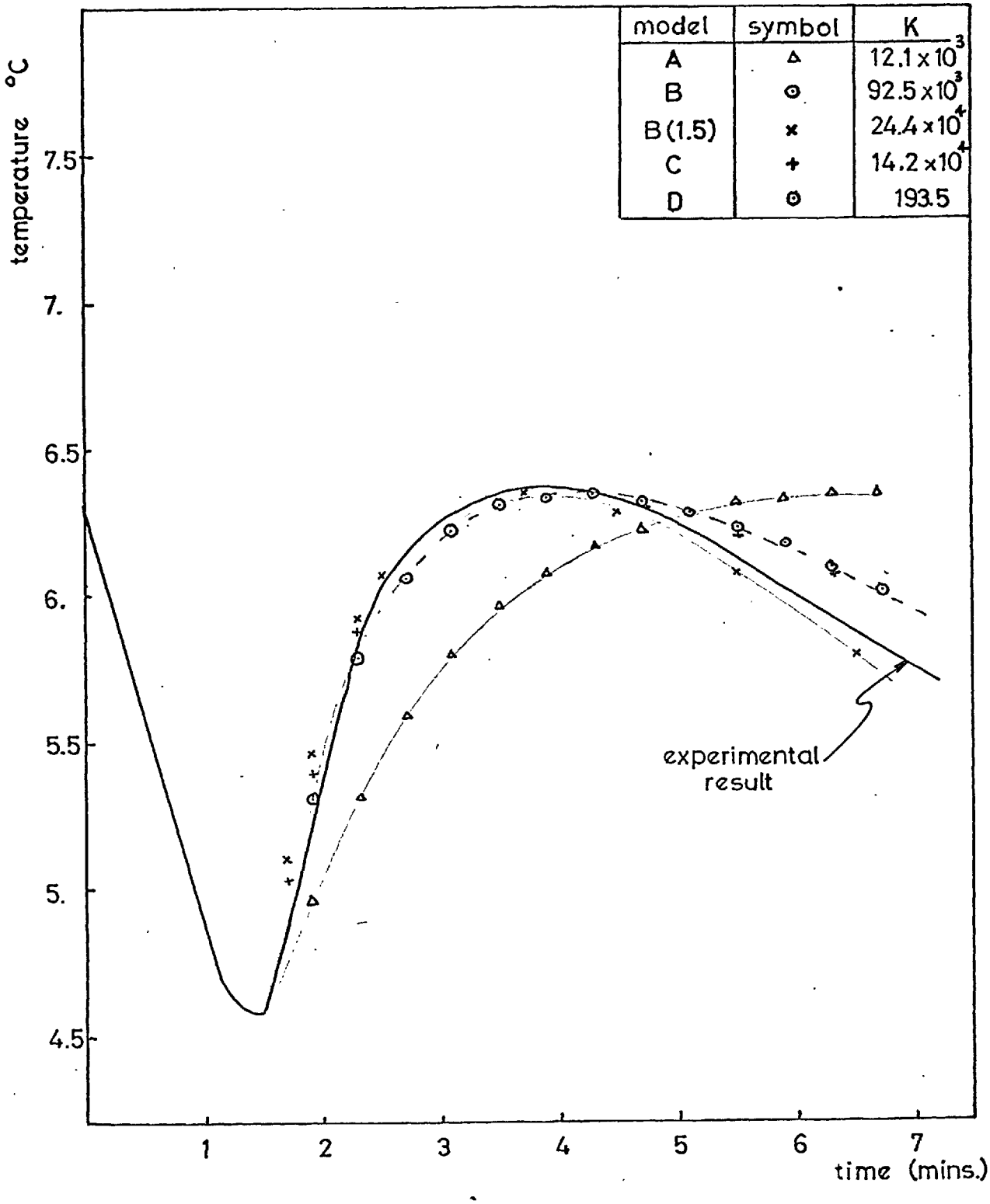


figure 20 Run 25.13 plot of experimental and predicted reactor temperature with time

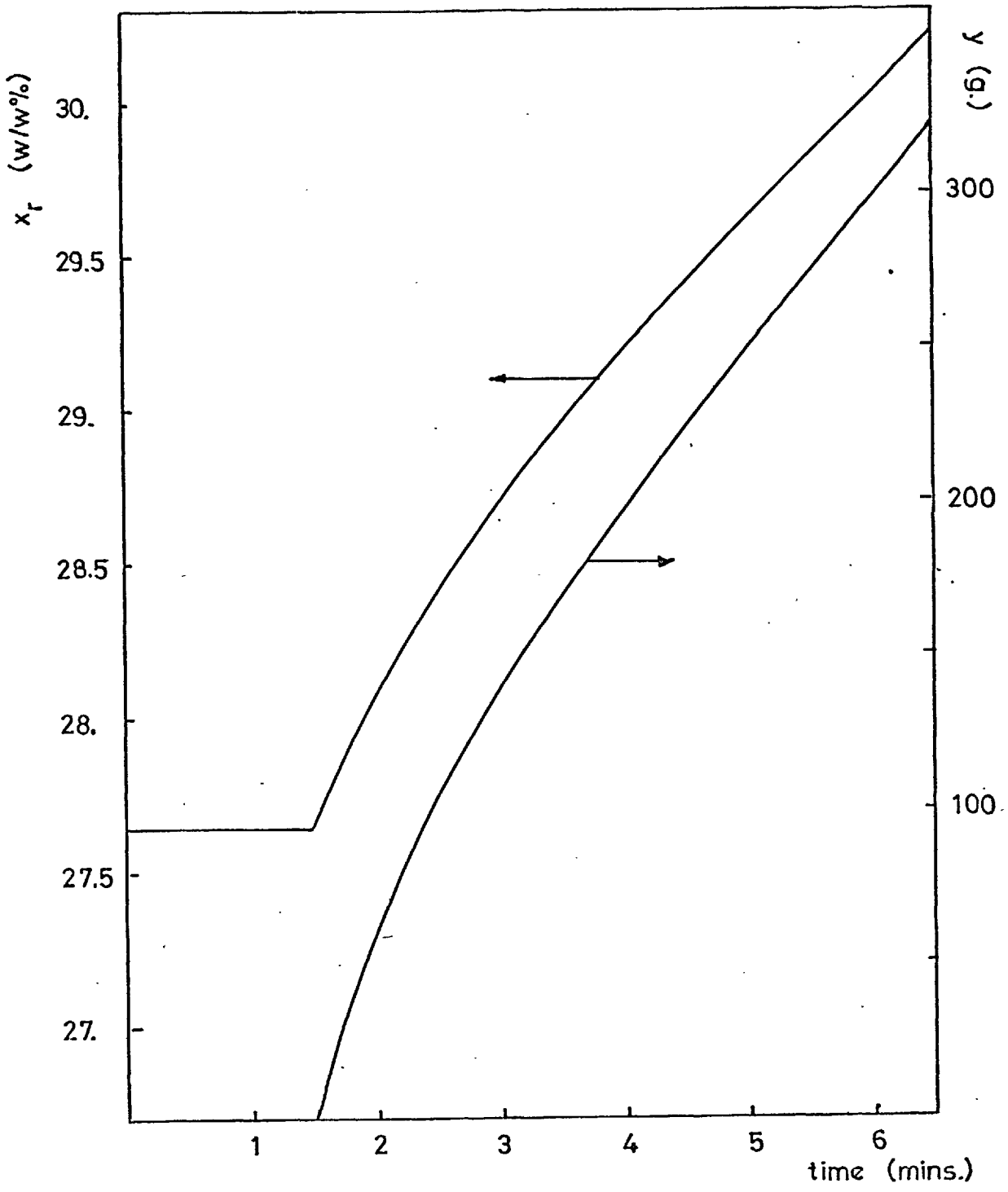


figure 21 Run 25.13 – plot of sucrose concentration and water as hydrate versus run time

models A and B. In some cases model B is modified:

$$r = K_B \left(\frac{\eta_1}{1-\phi_h^{\frac{1}{3}}}\right)^B (c_b - c_s)$$

where $-0.5 > B > -1.5$ and the exponent of the Hatschek viscosity was varied to obtain a better fit to the experimental points.

It was however considered unnecessary to obtain the best value of B for each curve by a numerical technique, e.g. minimising the sum of squares of the differences between experimental and predicted temperatures over the run duration. It was sufficient to check the fit of the curves by eye for an approximate value of B.

6.11 Comparison of Experimental and Theoretical Curves

Model B predicts a temperature profile which fits the experimental results well for a wide range of conditions. This can be seen by comparison with model A which regards K_A as a constant, independent of the liquor viscosity. The shape of the two curves is very different, especially in the example given in figure 20, at 28% sucrose. Model B explains both the rate at which the slurry hinders the reaction and the time at which the maximum temperature occurs. The estimated values of the exponent B, the dependence upon viscosity, vary a little with reactor conditions.

x_f (w/w)% \ N_{rpm}	1420	1140	880
10	-1.2	-1.2	-0.9
18	-1.2	-1.1	-1.2
28	-1.2	-1.0	-1.0
42	-0.7		-0.45

Table 6.11 Variation of B with N and x_f

The mean estimates of B are given in Table 6.11, showing the variation with agitator speed and sucrose concentration. The difference observed in B at different stirrer speeds is as large as the error in the estimate of B, so no conclusion may be drawn as to whether B varies with N. The value of B agrees with the predicted value of -1, equation (44), except for the case of 42% sucrose when the dependence of the transfer coefficient on viscosity does change significantly.

Model C was derived on the assumption that transfer from the liquid agent phase was important. The temperature differential term $(T-T_1)^{0.25}$ in model C, (where the exponent is determined in section 6.2), has only a very slight effect on the shape of the profile. The effect of this extra term is most noticeable at nucleation, but the results are such that it is not possible to distinguish whether the factor is relevant or not.

The temperature driving force (T_c-T) in model D fits the experimental data as well as the concentration driving force model B. This is partially anticipated, Appendix E3.

A second comparison may be made between the models and the experimental results by relating the measured sucrose concentration to the predicted values. Sampling the concentration of the mother liquor is subject to a greater error than sampling the temperature of the slurry, but a fair comparison may be made. Agreement between the concentration history predicted by equations (59a) and (65) in model B, and the measured concentration, are also shown in the Tables III to VII. It was shown that in the case of liquor concentration also, model B provided a better fit to the results than A.

The results suggest that the rate determining step is the absorption of agent from the dispersed agent, in that the rate of formation may be expressed in terms of a linear concentration driving force and an over-all transfer coefficient typically dependent upon the system's viscosity.

6.12 Effect of Slurry Viscosity

Shiloh and Sideman (17) studied the variation in the

heat transfer coefficient with the solids fraction in an aqueous slurry. In their experimental project, the basic factors affecting the rate of evaporation from salt-water ice slurries in a vacuum freezer were investigated. It was observed that the liquid-phase heat transfer coefficient, which governs the process, decreased with increasing ice fraction due to increased viscosity. The hydrodynamic conditions are rather different for the two systems: in the freezer evaporation takes place in the neighbourhood of the interface where the ice concentration is largest, whereas no deviation from the well-stirred condition is considered in the hydrate reactor.

Shiloh (17) indicates that the over-all heat transfer coefficient varies inversely as the square-root of the measured ice slurry viscosity, over the range 0 - 20% solids fraction. His conclusion is thus similar to that reached from the hydrate analysis, in that the slurry viscosity alone may be used as a descriptive parameter for the change in the transfer coefficient with solids hold-up. This is in spite of the inherent differences between the two transfer processes,

The experimentally determined slurry viscosities quoted by Shiloh differ substantially from the Katschek estimates, equation (61). For example at 10% solids fraction Shiloh

gave the value of the fraction (slurry viscosity/true liquid viscosity) as 5.3 compared to a value of 1.9 from the Hatschek equation. If the Hatschek viscosity were used in Shiloh's results, the heat transfer coefficient would vary as the -1.3 power of the viscosity, which compares more favourably with the exponent shown in this work. If however the Shiloh viscosity data is a better estimate of the effect of solids on viscosity then the hydrate transfer coefficient may vary only as the -0.4 power of the viscosity.

The Hatschek equation is only valid when the solids are free flowing when wet: Viscosities tend to be larger when the solids offer resistance to flow. Perry (71) quotes other expressions for the estimated viscosities of suspensions, including that proposed by Ting and Luebbons which incorporates the ratio of liquid and solid densities. This ratio may have special interest in the hydrate system since the crystals are denser than the solution at 10% sucrose and lighter than solution at 30% sucrose. However the quantitative effect is negligible, and none of the expressions predict a slurry viscosity as high as that observed by Shiloh. Maude (68) quotes measured viscosities for aqueous-emery powder suspensions which are just a little greater than the Hatschek expression. It seems possible

therefore that Shiloh's results are incorrect, but some estimates of the true hydrate slurry viscosity may be informative.

6.13 Liquid Agent Hold-up at Nucleation

The models derived in section 5.52 based on equation (57) assume that at the spontaneous nucleation temperature the transition from cooling with no hydrate present to production of hydrate occurs instantaneously. The significance of this is that the net cooling rate must remain constant throughout the transition. An example of a marked deviation from this condition is shown in figure 22.

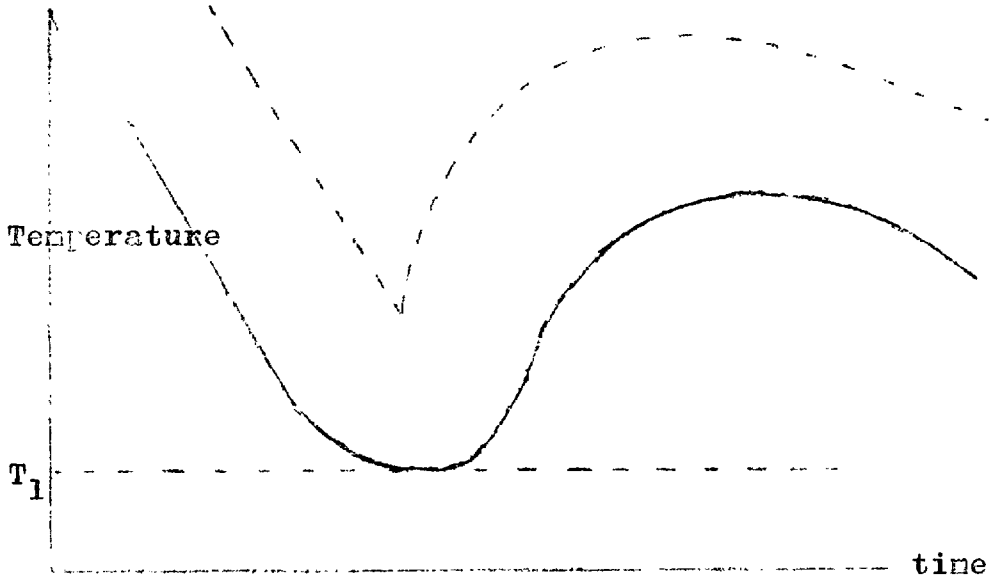


Figure 22 Transition at Nucleation Point

The continuous line shows the cooling curve under reactor conditions which cause the nucleation temperature, T_n, to coincide with the condensation temperature of the agent, T_l. As T approaches T_l the cooling rate decreases since, as the thermal driving force is reduced, the interfacial area of evaporating agent must be increased, causing an accumulation of liquid freon in the reactor. When $T = T_l$, no evaporation takes place and the temperature remains constant until nucleation occurs. Liquid agent accumulates in the reactor during this period, consequently at T_n the liquid agent hold-up is unknown and the heat balance, equation (57) is no longer valid. In addition model C which considers mass transfer from the boiling liquid phase is also invalid.

To avoid this problem, the experimental conditions were chosen such that T_n was always greater than T_l. In general the transition was fairly sharply defined (the broken line in figure 22) but not quite as sharp as the model would indicate. This is recognised as a source of error.

6.2 Batch runs as an approximation to Steady-state Conditions

The following sections deal with the analysis of the observations of the steady unsteady-state temperature in

the reactor. The reaction constant, or over-all coefficient, is determined from the temperature at which the temperature gradient with respect to time is zero. The manner with which this coefficient varies with sucrose concentration, agitator speed, concentration driving force and reactor pressure is determined. This analysis is split into sections which examine where possible the independent effects of the variables. The data in Table II is presented in 14 experimental blocks: A block denotes variables r and P for constant N and x_f. These blocks are examined individually and then the effects of additional parameters are considered.

6.21 Models for Individual Blocks

The conclusion to section 6.1 was that the absorption model B gave close agreement with experimental results, assuming the transfer coefficient to be a simple function of one variable. The model assumed a linear dependence upon the concentration driving force. Any deviation from non-linearity of the form suggested in equation (46), arising from the effect of gas loading on the reactor, could not be distinguished in the unsteady-state profiles. In the individual blocks on the other hand the production rate may be obtained as a function of pressure and (c_b-c_s) only.

Prior to this study, no models incorporating an interaction between the effects of pressure and concentration driving force had been proposed. De Graauw (26) is the only worker to have observed a trend with pressure. Initially it was assumed that pressure had no effect on the system, and that any difference between the results at different pressures occurred as a result of chance.

Since x_f, ℓ_1, N and V_r are constants, equation (46) can be written in the form:

$$r = k_1 (c_b - c_s)^{k_2} \qquad -- (74)$$

where k_1, the over-all mass transfer coefficient, is a constant. Parameters k_1 and k_2 were estimated by the method of least squares, and are shown in Table 6.211 together with other relevant statistical information. A plot of the production rate against concentration driving force at different pressures for a typical block is shown in figure 23. Although the experimental error in measuring the reactor operating temperature is very small, the error in controlling and measuring the variables listed in Table 3.6 may contribute an uncertainty of $\pm 5\%$ in the combined value of the rate coefficient and concentration driving force on the R.H.S. of equation (74).

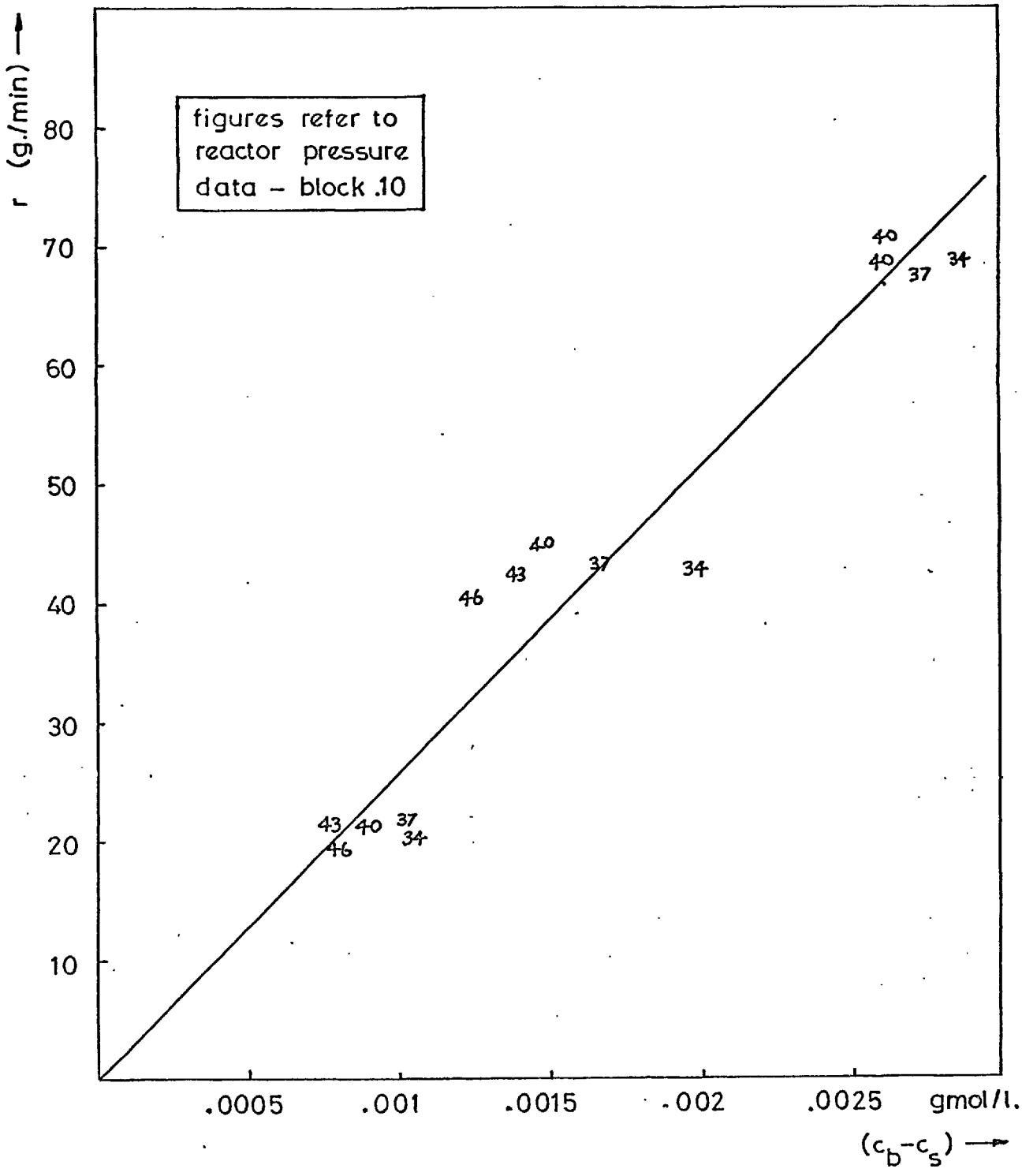


figure 23 Plot of hydrate formation rate versus $(c_b - c_s)$ showing effect of reactor pressure

Block	k_1	k_2	SS	SS_1	d_f	Mean % error	±confidence limits on k_2
.10	2.66	1.01	495.	.0684	14	14.0	.19
.11	3.94	1.06	466.	.0484	18	10.0	.14
.110	87.7	1.54	201.	.0201	10	9.4	.24
.12	0.589	0.80	118.	.0158	15	6.6	.09
.13	0.873	0.95	261.	.0294	18	7.9	.10
.14	0.958	0.58	364.	.0515	13	12.8	.12
.21	0.725	0.83	172.	.0194	18	6.1	.10
.22	0.175	0.65	241.	.0505	16	10.7	.13
.23	0.685	0.96	144.	.0202	21	5.6	.09
.31	0.399	0.83	86.	.0196	13	7.3	.18
.310	2.12	1.06	37.4	.0057	11	4.5	.12
.32	0.402	0.86	129.	.0209	12	9.0	.21
.33	0.800	1.07	62.	.0127	15	5.9	.17
.34	18.75	1.68	156.7	.0315	12	10.1	.56

where: $SS = \sum_{i=1}^{n} (r_i - r_i')^2$ and r_i' is the formation rate predicted by equation (74)

$SS_1 = \sum_{i=1}^{n} (\ln r_i - \ln r_i')^2$

Table 6.211 2 Parameter Model

The average value of k_2 is approximately 1, but the variations between blocks is large and the tolerance limits are rather high. The mean deviation from the model is estimated from the sum of squares of errors quoted in column four. The errors in fitting the data to equation

(74) are greater than the experimental errors involved. It appears too that the errors are biased with pressure. Reference to the phase diagram, figure 24, shows the position of an experimental 'operating-line'* GH with respect to the hydrate equilibrium line BC.

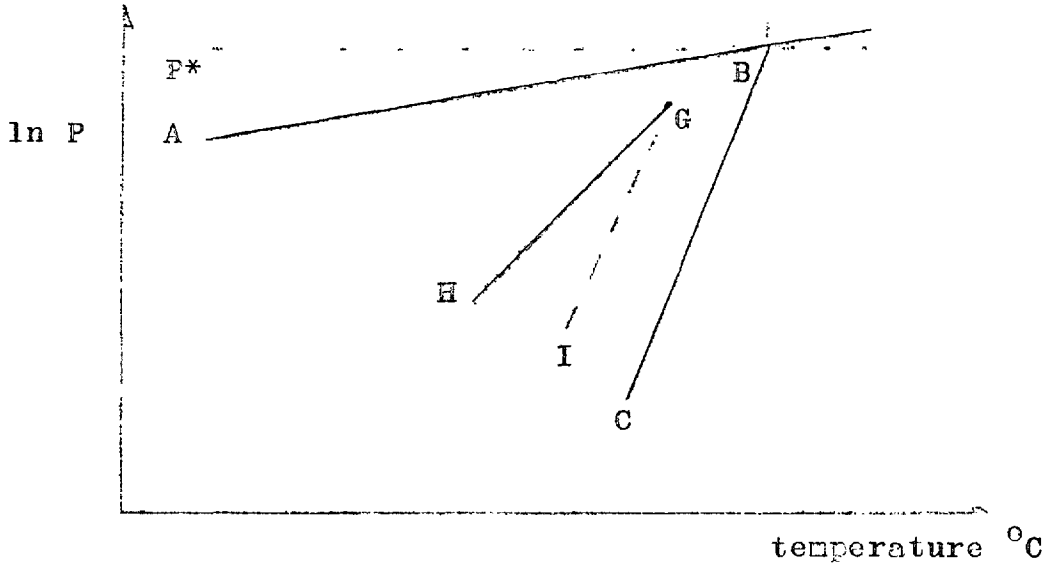


figure 24 Interaction of P and $(c_b - c_s)$

If there was no interaction between the effects of P and $(c_b - c_s)$, the operating line GI would lie roughly parallel to BC after compensating for the effect of pressure on solubility. GH deviates quite markedly from the case GI and from equation (74). It appears therefore that k_1 is a function either of pressure or temperature, or both. An appraisal of the system and the state of knowledge of hydrate kinetics suggested three possibilities, after the accuracy of the equilibrium line and the value

* An operating line refers to a locus of experimental points for which the production at a given N, x_f is constant.

of Henry's law constant had been checked to ascertain whether the equilibrium data were at fault.

(i) Assume that k_1 is a reaction constant and a function of the absolute temperature, as described by the Arrhenius equation:

$$k_1 = Ae^{-E/RT}$$

This is rejected for the following reasons. In the first case it has been shown that model B, independent of the Arrhenius term, fits the experimental results. Secondly the activation energy involved (estimated at about 25 Kcal/g.mole) would render the reaction rates at high sucrose concentrations at least one order of magnitude lower than those observed.

(ii) Assume that the production rate depends upon the liquid freon hold-up, a variable which is determined by the process of heat transfer. This was the basis of model C, and C is modified for the case of constant slurry viscosity to give an expression similar to equation (74)*:

$$r = k_1(c_b-c_s)^{k_2}(T_r-T_l)^{k_3} \qquad -- (75)$$

The values of the three parameters and the confidence intervals for each block are shown in Table 6,212. A weighted mean of the parameters gives a model of the form:

$$r = k_1(c_b-c_s)^{0.97}(T_r-T_l)^{-0.14}$$

* Whereas equation (74) represents the line GI, (75) gives the operating line GH since (T_r-T_l) is a function of pressure.

Table 6.212 Three Parameter Model

Block Number	k_1 x10^{-4}	k_2	k_3	SS	SS_1	d_f	$\mathcal{F}$	F	Mean % error	Confidence Interval ± k_2	Confidence Interval ± k_3
.10	7.74	1.11	-.28	172.2	.0250	13	3.64	24.5	9.1	.12	.12
.11	6.48	1.07	-.26	219.	.0272	17	3.59	19.1	7.6	.11	.15
.110	87.3	1.55	-.08	172.	.0191	9	4.37	1.5	9.8	.24	.22
.12	0.667	0.79	-.12	95.3	.0126	14	2.61	3.33	6.5	.08	.13
.13	0.936	0.93	-.14	218.	.0242	17	3.57	3.33	8.4	.09	.15
.14	0.103	0.55	-.23	288.	.0399	12	4.90	3.16	12.6	.11	.26
.21	0.724	0.84	-.03	170.	.0191	17	3.16	0.20	6.5	.10	.11
.22	0.199	0.62	-.20	272.	.0396	15	4.25	-	10.1	.12	.20
.23	0.688	0.93	-.11	101.	.0171	20	2.24	8.5	5.3	.09	.11
.31	0.398	0.83	-.03	81.8	.0193	12	2.61	0.78	8.2	.19	.14
.310	2.12	1.05	-.09	23.6	.0034	10	1.54	5.85	4.0	.10	.07
.32	0.372	0.80	-.14	94.8	.0159	11	2.94	3.95	7.7	.20	.16
.33	0.760	1.04	-.07	46.7	.0108	14	1.82	4.64	5.8	.17	.09
.34	21.8	1.68	-.22	50.0	.0094	11	2.13	23.5	6.2	.32	.09

To evaluate the improvement in fit due to the third parameter k_3, an analysis of variance test is performed with the 2 and 3 parameter models. The value of F represents the ratio of the improvement of fit arising from the additional parameter to the estimate of the error variance. The F values for each block are shown in the ninth column in Table 6.212. Comparing these F values with a table of the F distribution it is seen that the parameter $(T_r-T_1)^{k_3}$ in equation (75) gives a significant improvement in fit in 6 cases out of 14 at the 5% confidence level and 10 cases out of 14 at the 10% confidence level.

It may be concluded, therefore, that use of the thermal driving force gives a better estimate of the reactor performance than a model which does not take into account the variation with pressure. It cannot definitely be stated, however, that the mass transfer depends upon the boiling liquid transfer surface as postulated in section 5.42.

(iii) Assume that the growth mechanism depends upon the pressure alone, in a similar way to that described in section 7.2 on hydrate decomposition. A model is proposed with a correction factor P/P^*, without any theoretical justification:

$$r = k_1(c_b-c_s)^{k_2} \; P/P^* \qquad -- (76)$$

where P = reactor operating pressure

P* = critical pressure at concentration x_f

P* is shown in figure 24; it may be calculated by solving for the intersection of the saturated liquid line and the phase equilibrium line, equation (7).

The results are shown in Table 6.213. The analysis of the error variance shows that equation (76) gives a better fit to the experimental data than the uncorrected pressure model, equation (74). The F values in the seventh column, which shows the comparison between the correction terms $(T_r-T_l)^{k_2}$, equation (75) and P/P^* in equation (76), indicate that there is little to choose between the two models, though equation (75) provides a significantly better fit in 3 cases out of 14 at the 10% confidence level.

A detailed study of the variables involved failed to pinpoint any physical property of the system which depends upon pressure. The operating pressure is of the order of three to four atmospheres and in this range, there is no significant change in properties such as interfacial surface tension, gas viscosity, etc. No reason for de Graauw's conclusion that gas bubbles were larger and more unstable at the higher pressures could be advanced.

Block No.	k_1 x10^{-4}	k_2	SS	SS_1	d_f	F ratio (ii)/(iii)	± Confidence limits on k_2
.10	5.96	1.10	201.	.0281	14	1.57	.13
.11	6.10	1.10	266.	.0303	18	1.93	.11
.12	0.72	0.81	103.	.0132	15	0.67	.08
.13	1.17	0.97	248.	.0273	18	2.18	.09
.14	0.12	0.60	335.	.0478	13	2.39	.11
.21	0.71	0.81	222.	.0277	18	7.6	.11
.22	0.225	0.67	212.	.0408	16	0.45	.12
.23	0.895	0.96	101.	.0200	21	3.4	.09
.31	0.425	0.82	92.	.0217	13	1.5	.19
.32	0.455	0.85	102.	.0168	11	0.5	.18
.33	1.09	1.05	64.3	.0154	15	6.0	.19
.34	209.	2.06	61.	.0117	12	2.68	.38

Table 6.213 $r = k_1(c_b-c_s)^{k_2} F/P^*$

Block No.	k_1	k_2	k_3	SS	SS_1	d_f	Mean % error	±Confidence limit k_2	±Confidence limit k_3
.10	169.	1.06	-.42	185.	.0294	13	9.4	.14	.15
.11	145.	1.04	-.38	222.	.0277	17	7.6	.10	.16
.12	73.8	0.75	-.23	84.2	.0109	14	6.0	.07	.13
.13	40.1	0.83	-.27	184.	.0204	17	7.7	.08	.14
.14	35.2	0.50	-.29	265.	.0356	12	11.7	.10	.25
.21	63.6	0.81	-.06	170.	.0193	17	6.6	.10	.11
.22	56.1	0.57	-.27	285.	.0425	15	10.6	.11	.21
.23	30.4	0.81	-.23	104.	.0167	20	5.5	.08	.11
.31	36.6	0.77	-.11	76.5	.0180	12	7.9	.17	.14
.32	35.9	0.71	-.23	94.7	.0150	11	7.9	.18	.16
.33	16.8	0.86	-.17	39.2	.0094	14	5.4	.13	.09
.34	7.57	1.27	-.31	48.2	.0090	11	6.0	.24	.09

Table 6.214 $r = k_2(T_c-T_r)^{k_2}(T_r-T_l)^{k_3}$

A further model was evaluated as a consistency check with previous workers. Equation (75) may be rewritten featuring a thermal driving force as in equation (22):

$$r = k_1(T_c-T_r)^{k_2}(T_r-T_1)^{k_3} \qquad -- (77)$$

The values of the parameters k_1, k_2 and k_3 are given in Table 6.214. The residual sums of squares of errors are very similar to those given in Table 6.212. The significant difference is that the dependence upon (T_r-T_1) is much more pronounced. This represents the difference between a model which depends upon a pseudo driving force and equation (75) which depends on solubility and hence pressure.

6.215 Estimate of Error between blocks

An assessment is considered of the variation of the error variances from the estimates given in Table 6.212. The estimate of the error variance is given by:

$$\hat{\sigma}^2 = \frac{SS}{d_f}$$

where d_f = degrees of freedom

From the comparison of error variances between blocks it appears:

(1) The individual block error variances may be pooled for a given stirrer speed: The error involved at one stirrer speed is the same throughout the range of sucrose

solutions considered.

(2) There is no significant difference at the 5% probability level between the errors at 1420 and 1140 rpm, but there is a significant difference at the 1% level in the error of the experiments at these two stirrer speeds and those conducted at 880 rpm. Table 6.215 summarises this information.

Comparison	N rpm	Error variance estimate, $\hat{\sigma}^2$	d_f	F
1	1420	14.19	82	$F_{12} = 1.37$
2	1140	10.38	52	$F_{23} = 2.03$
3	880	5.12	58	$F_{13} = 2.77$

Table 6.215 Summary of error estimates

This pattern may be expected from the manner of the experimental technique. Since the error is largely contained in the estimate of the reactor temperature and the subsequent determination of a temperature difference, the percentage error is greater at the higher agitator speeds. From Table I it can be seen that:

$$(\overline{T_r - T_l})_{880} = 2.5\ (\overline{T_r - T_l})_{1420}$$

and

$$(\overline{T_r - T_l})_{880} = 1.8\ (\overline{T_r - T_l})_{1140}$$

where the bar represents a mean value. If it had been decided to keep the temperature driving force constant,

rather than the production rate (Table 3.6), the error would have been more evenly distributed.

6.216 Temperature Distribution in Reactor

For sample runs the slurry temperature was measured at all points in the reactor by adjusting the thermocouple probes. No variation in temperature was observed at the high agitation rates employed. A probe measuring the gas phase temperature in the free space above the liquid surface showed that the temperature approximated to the condensation temperature of the agent. This confirms that little or no heat is transferred to the gas phase in the boiling reactor. Any variation in the gas phase temperature appeared to be unrelated to $(T-T_1)$ or the production rate, and was presumably due to an absence of mixing in the gas space.

6.22 Distributor Tests

The effect of the initial agent drop size was investigated by modifying the feed inlet with a perforated ring. Blocks .110 and .310 represent repetitions of .11 and .31 repsectively, with a liquid freon distributor in operation. By calculating the mean over-all transfer coefficients from the mean values given in Table 1, it is

seen that the distributor gives a 38% increase in k_l'a at the low stirrer speed and a 7% increase at the high stirrer speed.

To test whether these increases are significant and not due to chance experimental errors, the t test was applied.

Comparison	$\frac{E}{HP/ft^3}$	S^2_{pool}	$\hat{\sigma}$	$\bar{x}_1-\bar{x}_2$	d_f	t	t_c
.110/.11	0.56	.00178	.0420	.03	26	1.73	2.0 @5%
.310/.31	0.134	.00103	.0321	.14	22	9.7	2.8 @1%

Table 6.22 Distributor Significance Test

where $\bar{x}_1-\bar{x}_2 = \ln\left(\frac{\bar{r}}{\overline{c_b-c_s}}\right)_1 - \ln\left(\frac{\bar{r}}{\overline{c_b-c_s}}\right)_2$

$$S^2_{pool} = \frac{1}{n-3}\sum_{i=1}^{n}(\ln r_i - \ln r_i')^2$$

where r_i' = 3 parameter predicted production rate the i th case.

and $$t = \frac{\bar{x}_1 - \bar{x}_2}{\hat{\sigma}}\sqrt{\frac{n_1 n_2}{n_1+n_2}}$$

where subscripts 1 and 2 refer to the distributed and non-distributed systems respectively.

The improvement is significant at 886 rpm since t is greater than the critical value, t_c, but not at 1420 rpm.

The increase in the transfer coefficient suggests that the initial drop size is an important factor in the mechanism of hydrate formation below a certain power input. It does not however indicate that mass transfer takes place necessarily from the liquid droplets, though this could be one interpretation. The alternative explanation is that smaller agent drops give rise to smaller bubbles and consequently the interfacial area of the gas phase is increased.

The order of the effect on the over-all coefficient is the same as that observed by Karwat (65) in the comparative study of single and sparge tubes in gas-liquid contacting, with change in power input (section 5.36). Karwat showed similarly that the distributor had a reduced effect at high power inputs.

The results do indicate that a real process must incorporate an effective distribution system to save on power requirements.

6.23 Effect of Power on the Over-all Coefficient

Figure 25 shows the effect of the power input on the hydrate transfer coefficient at different sucrose concentrations. The power input was taken to be the power

consumed in a non-gassed system. In this way it is possible to describe the power effect in terms of an independent parameter, the stirrer speed, rather than as a complicated function of the gas flow rate (equations (25) or (26)). For the same reason the reactor volume V_r, a dependent variable, is not considered as a separate term. The gas hold-up term is included in the over-all coefficient, hence equation (56) becomes:

$$r = k_l' A (c_b - c_s) \qquad -- (78)$$

where A = total interfacial area

The relation between a and A will be shown in section 6.261.

It can be seen from figure 25 that the dependence upon E is approximately constant over the sucrose range. The actual dependence was determined from least-square fits at each sucrose concentration:

$$r_{10\%} = 1.76 \times 10^4 \, E^{0.57} \, \Delta T^{-0.05} \, \Delta C^{0.87}$$

$$r_{18\%} = 5.36 \times 10^3 \, E^{0.45} \, \Delta T^{-0.16} \, \Delta C^{0.71}$$

$$r_{28\%} = 1.21 \times 10^4 \, E^{0.44} \, \Delta T^{-0.04} \, \Delta C^{0.94}$$

$$r_{42\%} = 1.59 \times 10^3 \, E^{0.42} \, \Delta T^{-0.21} \, \Delta C^{0.58}$$

where $\Delta T = T_r - T_l$

$\Delta C = c_b - c_s$

and $E = 0.70 \times 10^{-9} \, N^3/V_l$ (H.P./ft^3)

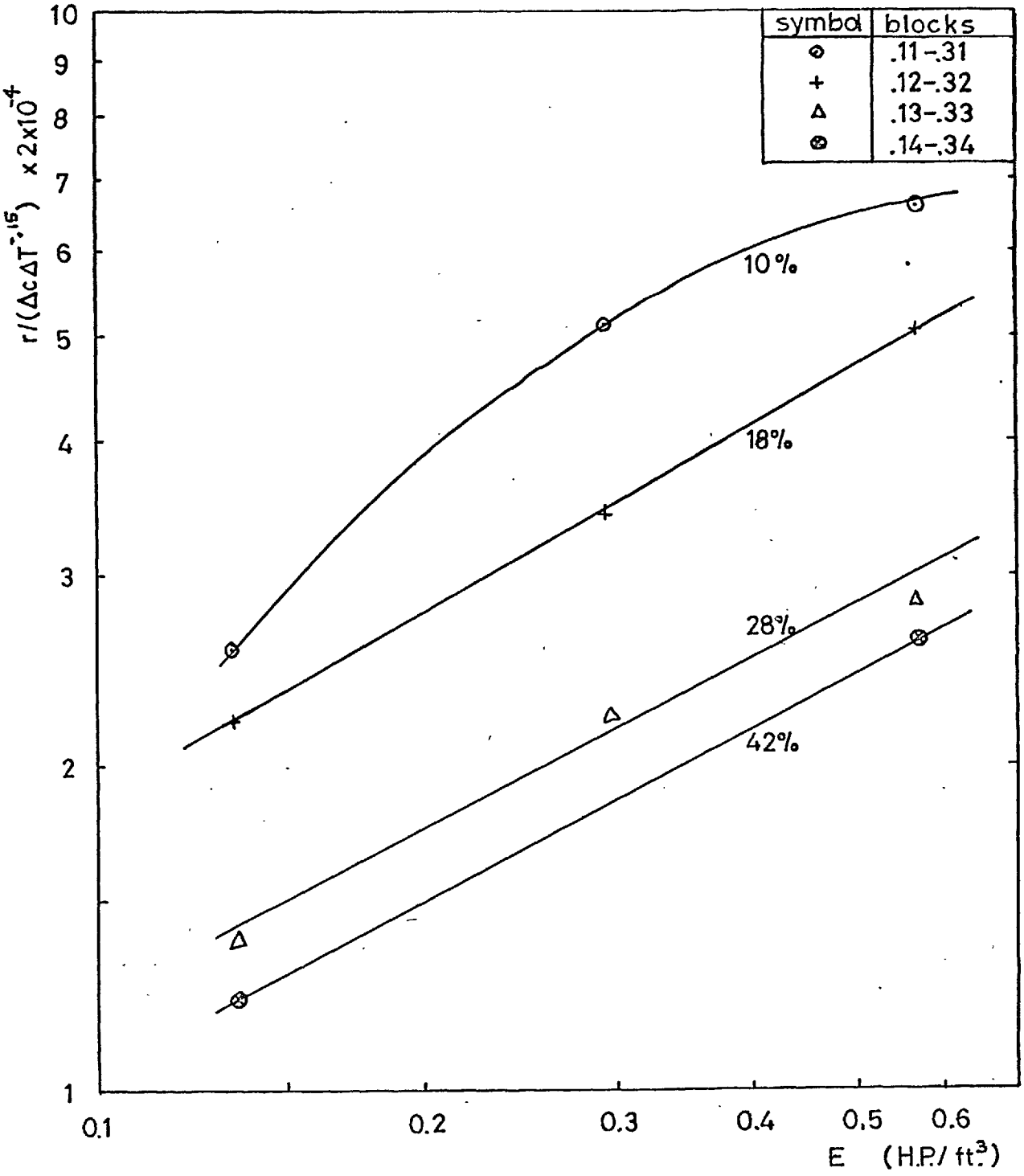


figure 25 Over-all transfer coefficient versus power input for all sucrose solutions

The error variance and tolerance limits on the estimates of the power exponents are shown in Table 6.23.

x_f %	SS	Data points	σ^2	Mean % deviation	Tolerance on E exponent
10.	1067	55	20.9	11.5	$\pm$ 0.08
18.	551	49	12.2	7.3	$\pm$ 0.06
28.	502	60	8.9	6.8	$\pm$ 0.05
42.	517	29	20.7	11.2	$\pm$ 0.10

Table 6.23 Tolerance intervals on power exponent

From the error variance column it is seen that for 18 and 28% sucrose, the error variance is similar to the experimental error variance given in Table 6.215. At 10% and 42% however, the error is larger and the exponent at 10% differs considerably from the other estimates.

It appears that the power dependence agrees fairly well with the exponent predicted by equation (46), or variations of this equation depending on the literature correlations selected. The differences might be explained by the absence of gas hold-up as a variable. The pressure correction term ΔT provides a better fit than the three parameter model, but the exponent varies substantially.

6.24 Effect of Sucrose Concentration in the Over-all Coefficient

The effect of sucrose on the system has already been partially accounted for in model (75) etc., since the concentration driving force depends on the freezing point depression and on the salting-out effect of sucrose on freon solubility. In addition to these corrections, the over-all transfer coefficient clearly depends upon the sucrose concentration, as seen from the curves at constant sucrose in figure 25. The only variables that change markedly with concentration are viscosity and density. The interfacial surface tension, a factor which is of great importance in establishing the balance between coalescence and shear in a two phase system, changes only a few percent over the entire range considered. The variation of viscosity and surface tension with temperature and sucrose concentration is considered in the Appendix, section G3.

A graph of the pressure-corrected over-all transfer coefficient against viscosity is shown in figure 26. It appears that the coefficient is nearly inversely proportional to the liquid viscosity up to 28% sucrose, after which the dependence changes significantly. It is clearly inadequate to treat the data at constant stirrer speed in

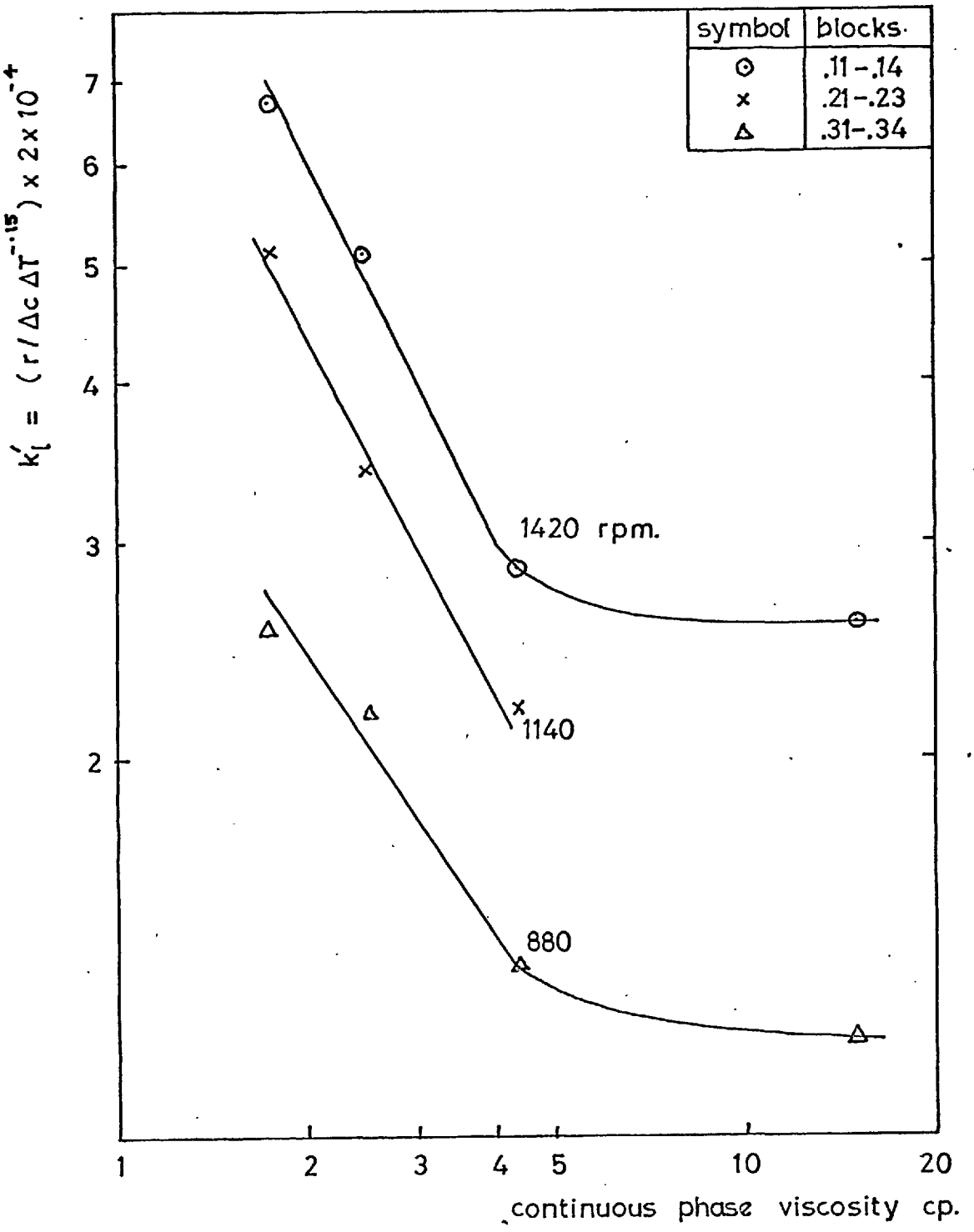


figure 26 Over-all transfer coefficient versus viscosity for all stirrer speeds

one group. For example at 1420 rpm, the best fit for all sucrose concentrations gives:

$$r_{1420} = 6.55 \times 10^{3} \eta_l^{-0.32} \Delta T^{-0.25} \Delta C^{0.72}$$

This gives an error variance of 55, far greater than the experimental error involved, so the sucrose range 10 - 28% is considered separately:

$$r_{1420} = 3.65 \times 10^{4} \eta_l^{-0.88} \Delta T^{-0.11} \Delta C^{0.95}$$

$$r_{1140} = 9.16 \times 10^{3} \eta_l^{-0.76} \Delta T^{-0.07} \Delta C^{0.79}$$

$$r_{880} = 9.70 \times 10^{3} \eta_l^{-0.66} \Delta T^{-0.05} \Delta C^{0.90}$$

The error variance in each case is close to the error variance stated in section 6.215, a mean deviation from the model of 7.7%.

If the non-linear dependence on $(c_b - c_s)$ were replaced by a linear model, to compare with model C in the unsteady-state section, the exponents of the viscosity would become -0.93, -0.98 and -0.72 in order of the equations given above. These values compare favourably with the values of B shown in Table 6.11. Since the effects of the slurry viscosity and the liquid phase viscosity are similar, the case for using the former to simulate the temperature-time curves is strengthened. It is interesting to note too that the change in the dependence on viscosity at the higher level of the sucrose solution was observed in the

unsteady-state runs. Clearly the method of approach in section 6.11 is justified.

The change in the dependence upon viscosity above 30% sucrose was not expected since the Calderbank correlation for the mass transfer coefficient, equation (40), was stated to be valid up to a viscosity of 80 cp. It does not appear, however, that the rate determining step changes at the higher viscosity range, since the over-all coefficient is dependent upon the same power exponent as at the lower viscosities. Rather it may be concluded that the mass transfer coefficient has a different dependence on the viscosity due to some interaction with the bubble or droplet sizes. As the viscosity increases both Calderbank and Westerterp (53, 30) have shown that the bubble size is decreased. Harriott (60) has shown that the effect of viscosity on the mass transfer coefficient is reduced as the particle size is reduced. Taking the case where the mass transfer coefficient is dependent on the viscosity only as it affects the diffusivity, the coefficient becomes dependent on the -.41 to -.30 power of the viscosity. It is probable that this type of effect may be the explanation for the observed experimental trend.

6.25 Reaction Rate at Constant Pressure

Since it appeared that the distinction between the pressure correction terms in equations (75) and (76) was imprecise, a further test was carried out on the experimental data.

The interaction between the effects of pressure and yield is due to the change in the total differential (T_c-T_l) with pressure. Because this total differential also changes with the change in sucrose concentration, analysis of constant pressure data may be informative. The experimental work was arranged to provide 54 data points at constant pressure and varying sucrose concentration in the design table 3.61. Three forms were considered, equivalent to equations (74), (75) and (76):

$$r_1 \sim E^{0.45}\eta_l^{-0.63}\Delta C^{0.82} \qquad 1237.$$

$$r_2 \sim E^{0.45}\eta_l^{-0.73}\Delta T^{-0.15}\Delta C^{0.79} \qquad .1235.$$

$$r_3 \sim E^{0.45}\eta_l^{-0.55}(P/P^*)^{-1.5}\ C^{0.82} \qquad 1394.$$

The sum of squares of errors are quoted for each expression. The exponent of (T_r-T_l) in the second expression is of the order expected from the parameters given in Table 6.212, but the decrease in sum of squares arising from this extra parameter is insufficient to justify its use at constant pressure. The exponent of

the correction term ($^{P}/P^{*}$) is very different from that considered in equation (76), and the increase in the sum of squares renders it unsuitable. It appears therefore that the rate is perhaps dependent upon the absolute pressure.

6.26 Correlation for Over-all Transfer Coefficient

The effects of the variables were combined in a single expression for the rate equation. Initially all the batch data, with the exception of the distribution runs, were shown to give the expression:

$$r = 8.10 \times 10^{3} E^{0.45} \eta_{l}^{-.36} \Delta T^{-.23} \Delta C^{0.71}$$

The mean deviation from this equation was $\pm$ 13.4% with 209 data points. The model is unsatisfactory since the dependence upon the liquid viscosity has been shown to change with sucrose concentration. Several alternative forms were tested, incorporating the concepts presented in section 5.3: In particular the Michel-Miller correlation for gassed power input, equation (26); a bulk density term, equation (24); a gas hold-up correction, equation (46); and the liquid phase density. Each of these additional parameters caused the error variance to increase.

The over-all coefficient was established for the range 10 to 30% sucrose with greater certainty. The best rate expression for 164 data points was:

$$r = 2.3 \times 10^4 \; E^{0.50} \eta_1^{-.76} \Delta T^{-.08} \Delta C^{0.85} \qquad -(79)$$
$$\pm.04 \quad \pm.07 \quad \pm.06 \quad \pm.05$$

The estimate of the error variance was 16.5 and the mean deviation $\pm 9.2\%$. The 5% probability tolerance intervals are given below the parameters. The rate equation is valid for Reynolds numbers in the range 1.5×10^4 to 5.7×10^4.

To obtain the relation for the over-all coefficient stated in equation (78) an equivalent expression to (79) was derived, linearly dependent upon $(c_b - c_s)$:

$$r = 6.57 \times 10^4 \; E^{0.56} \eta_1^{-.89} \Delta T^{-.04} \Delta C \qquad - (80)$$

The precision of the experimental fit to this equation (deviation $\pm 10.1\%$) is shown in figure 27 for nine data blocks. Comparing with equation (78):

$$k_1'A \sim E^{0.56} \eta_1^{-.89} \Delta T^{-.04}$$

now $k_1'A = k_1'aV_r$

and $V_r = V_1 \phi_1^{-1}$, where V_1 is constant

hence: $k_1'a \sim E^{0.56} \eta_1^{-.89} \Delta T^{-.04} \phi_1$

To evaluate the manner in which ϕ_1 depends upon the system variables, the data was fitted to the original equation

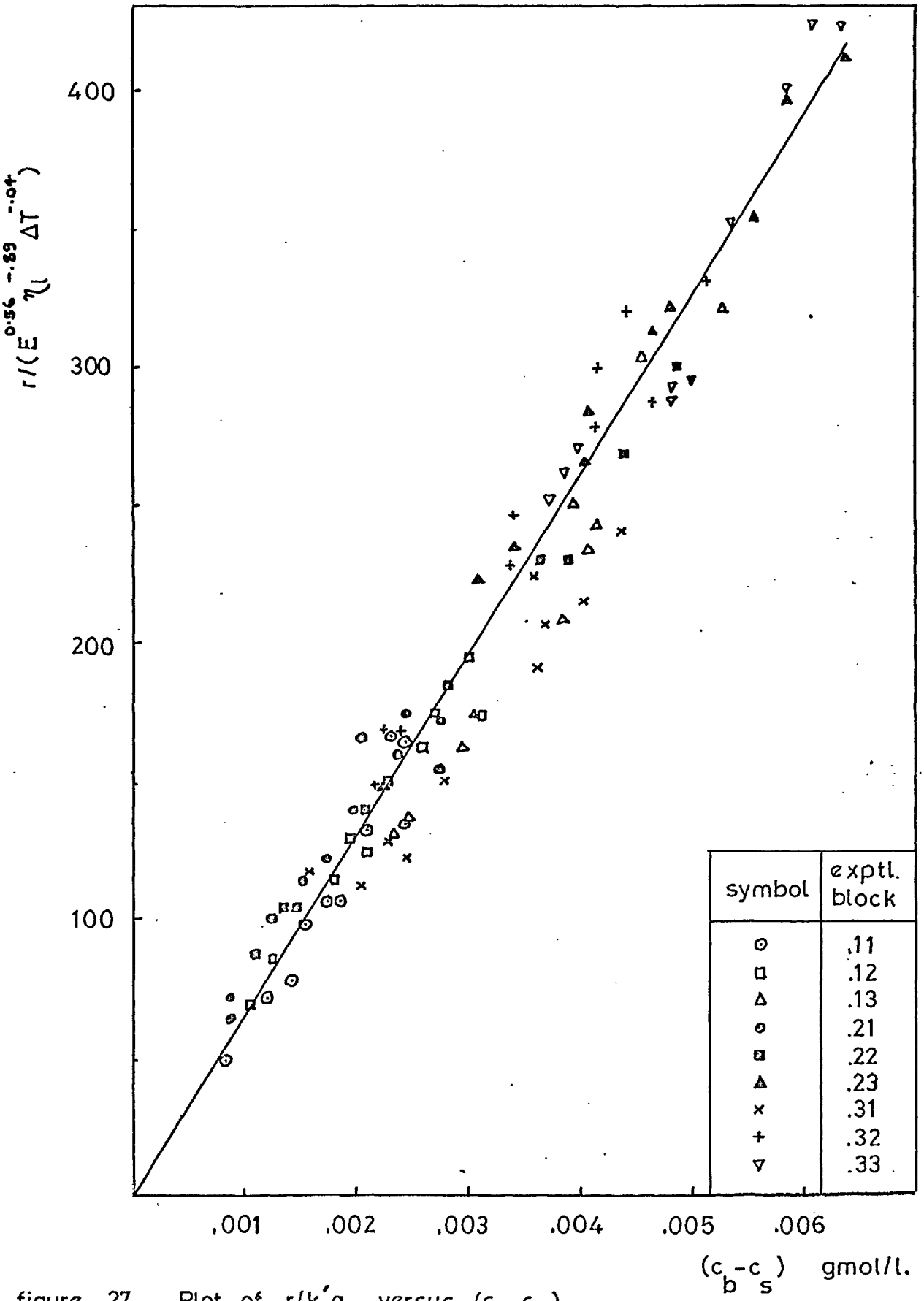


figure 27 Plot of $r/k'_l a_b$ versus $(c_b - c_s)$

(56), hence:

$$k_l'a \sim E^{0.48} \eta_l^{-.85} \Delta T^{-.03}$$

and $$\phi_l \sim E^{-0.08} \eta_l^{0.04} \qquad - - (81)$$

The total errors arising from a fit to equation (56), which requires an experimentally measured value of V_r, were identical with the errors based on (78) which is independent of V_r. Consequently the use of equation (78), which is preferable, is justified.

From the correlations in section 5.3 it can be shown that the over-all coefficient is linearly dependent upon the liquid phase density. This could not be demonstrated with the experimental results. Substitution of the continuous phase density gave:

$$k_l'a \sim E^{0.47} \eta_l^{-.93} \rho_l \Delta T^{-.03}$$

with an increase in the sum of squares of errors. Neither could the dependence upon the gas phase hold-up be shown to agree with the expected trend, equation (46). A least-squares fit gave:

$$k_l'a \sim E^{0.62} \eta_l^{-.81} \phi_g^{-.45} \Delta T^{-.08}$$

with a similar error as given by equation (80), whereas the study by Vermeulen (55) showed that the over-all coefficient was proportional to the square-root of the dispersed phase hold-up. This unexpected trend may be due to the insensitivity of the method of least-squares

with a large number of parameters. When the equations are linearised in logarithmic terms the errors become ratios rather than true differences.

6.261 Gas Hold-up

The dependence of the hold-up on the gas load was given by Calderbank (53) in equation (30), and disputed by Westerterp (30). In the hydrate reactor the gas hold-up was shown to be independent of the gas flow rate, thus agreeing with Westerterp's conclusion for the regime with an agitation effect. From the results in Table II it is shown:

$$\phi_g \sim E^{0.45} \eta_l^{-.22} \qquad -- (82)$$

The exponent of the power input agrees fairly well with the Calderbank equation (30), though Calderbank employed the measured gassed power input.

6.262 Fractional Factorial Design

The original design envisaged in section 3.6 stipulated that all the experiments in the factorial design were to be performed. The subsequent analysis has shown the only interactions to be between the effects of pressure and $(c_b - c_s)$ and between x_f and η_l, so the number of experiments might have been reduced substantially. In

the case of a future application, which involved a different agent and a different aqueous solution, a fractional factorial design would be adequate.

As a comparative test a group of 24 data, equivalent to a fractional design of a 4 variable problem, was selected from 164 items in Table II with the aid of random number tables. The selected data were then fitted to a similar form of equation (79):

$$r \sim E^{0.48}\eta_1^{-.81}\Delta T^{-.20}\Delta C^{0.92}$$
$$\pm.12 \quad \pm.19 \quad \pm.23 \quad \pm.15$$

The estimate of error variance was 18 and the mean deviation 10%. The tolerance intervals on the parameters are considerably greater than those given by equation (78) which used nearly seven times as much information, but the form closely resembles (79). It may therefore be concluded that a fractional design would show clearly the main effects of the variables.

6.3 Analysis of Steady-state Data

The results of the steady-state runs are given in Appendix B, headed by a summary table (VIII) which gives the main variables and the code for the sets of runs presented in Tables IX to XIII. The five sets were designed to: (i) check whether the models derived in

section 6.2 were representative of steady-state operation, (ii) test the effect of V_r as a parameter, (iii) evaluate the performance of the reactor with a single rather than dual impeller. Variables r, P and ϕ_h were considered for each set.

The tabulated data include the sucrose feed rate and feed temperature, the steady-state sucrose conversion, and the temperature and concentration driving forces. The production rate, column 12, was determined from the sucrose mass balance, equation (72), which also gives the estimated reactor heat load in column 14. The net cooling rate Q' was calculated from equation (73); the freon feed rate was estimated from the Rotameter calibration cruve, figure A13, and the total heat leak K_h was given in Table VIII. Thus the comparison of columns 13 and 14 gives the agreement between the net heat absorbed and heat released; on average the figures agree to $\pm$5%.

The analysis is divided into two parts. Firstly the study of the individual sets, and secondly the effect of the special variables. The flow reactor experiments were carried out at constant sucrose concentrations.

6.31 Individual Sets of Data

The five sets of results in Table IX to XIII were

fitted to the rate equation (74) which assumes the over-all coefficient to be independent of P and ϕ_h. The analysis is shown in Table 6.311: The errors and tolerance intervals are large and the rate is clearly dependent upon pressure. The data were therefore fitted to equation (75) and the values of the three parameters are shown together with the respective errors in Table 6.312. The analysis of variance test was performed with these results and the F value is given in column 8 of Table 6.311: In four cases the improvement of fit due to the parameter $(T_r-T_l)^{k_3}$ was significant at the 1% probability level. Both the improvement of fit and the dependence upon (T_r-T_l) is greater than in the batch runs; this may be due to the difference in experimental technique.

The single impeller runs (S4) were compared with the dual system (S2), operating at the same impeller speed. The ratio of the power input for the two cases was 1 : 2.9, see Table XXVI Appendix G, although Bates et al (31) predicted a ratio of 1 : 1.5. The effect of power on the over-all coefficient was demonstrated in a similar way to section 6.23:

$$r \sim E^{0.82} \Delta T^{-.16} \Delta C^{0.69}$$

The higher dependence upon E compared with equation

Run Code	k_1 x10^3	k_2	SS	SS_1	d_f	Mean % error	F	Confidence interval on k_2
S1	12.0	0.96	174.	.0167	8	7.6	44.	.47
S2	5.86	0.84	494.	.0475	12	12.0	49.	.37
S3	2.51	0.75	1001.	.0989	12	16.6	48.	.64
S4	1.03	0.64	326.	.0408	5	14.4	62.	.73
S5	0.22	0.32	466.	.0625	6	17.0	0.3	.65

Table 6.311 $r = k_1(c_b-c_s)^{k_2}$

Run Code	k_1 x10^3	k_2	k_3	SS	SS_1	d_f	Mean % error	Confidence interval k_2	Confidence interval k_3
S1	36.7	1.10	-.27	24.4	.0027	7	3.2	.21	.11
S2	19.8	0.97	-.38	109.	.0092	11	4.8	.18	.12
S3	13.5	0.98	-.48	186.	.0194	11	7.5	.31	.16
S4	0.545	0.53	-.16	19.5	.0025	4	3.8	.22	.05
S5	0.310	0.37	-.08	443.	.0595	5	17.4	.77	.44

Table 6.312 $r = k_1(c_b-c_s)^{k_2}(T_r-T_1)^{k_3}$

(79) confirmed that the excessive foaming which was observed at the surface of the reaction mixture with the single impeller was indeed causing bad distribution of the liquid agent and a low value of $k_l'a$. It was this effect that first indicated the need for a freon distributor; S5 represents the repetition of runs S4 with a perforated ring distributor.

Comparing the mean values of $k_l'a$ for S4 and S5 in the manner of the significance test in section 6.22, the runs with a feed distributor were shown to give a significant 25% improvement in $k_l'a$ at a power input of 0.192 HP/ft^3. This compares with a 38% improvement at 0.134 HP/ft^3 in the batch runs; the extent of the improvement is dependent upon the power level. It appears that at the low power inputs the turbulent flow field fails to shear the agent feed stream into droplets of the equilibrium size predicted by Weber number correlations. The equilibrium drop size is only approached with prior break-up of the feed by a distributor.

The dependence upon (c_b-c_s) appears to be non-linear for both S4 and S5. This is again due to the foaming conditions at the gas-liquid surface. As the total differential (T_c-T_l) is increased the surface offers greater resistance to the agent feed, since solid hydrate

is plainly visible on 'frozen' bubbles of gas undisturbed by the action of the impeller. This effect causes a decrease in the value of k_l'a as (T_c-T_l) is increased and results in the non-linear dependence on (c_b-c_s).

Sets S1 and S2 represent a change of 10% in the height of slurry in the reactor; the stirrer speed and gas hold-up were the same in each case. Although the value of k_l'a was shown to be 3% greater for the smaller reactor volume (S2), the difference was not significant. It is shown in Appendix G and figure A 23 that the power consumed in the dual impeller system is a function of the height of liquid in the reactor; hence for the two cases considered here the power dissipated per unit volume is approximately the same. It would therefore be expected that the over-all coefficient would not change.

The change in power input with liquid height is considered to be due to the proximity of the upper impeller to the liquid surface, a factor which was not taken into account at the design stage. With the single lower impeller operating, the effect is not apparent.

6.32 Effect of Power on Over-all Transfer Coefficient

The best-fit equation for all runs, excluding S4, is given by:

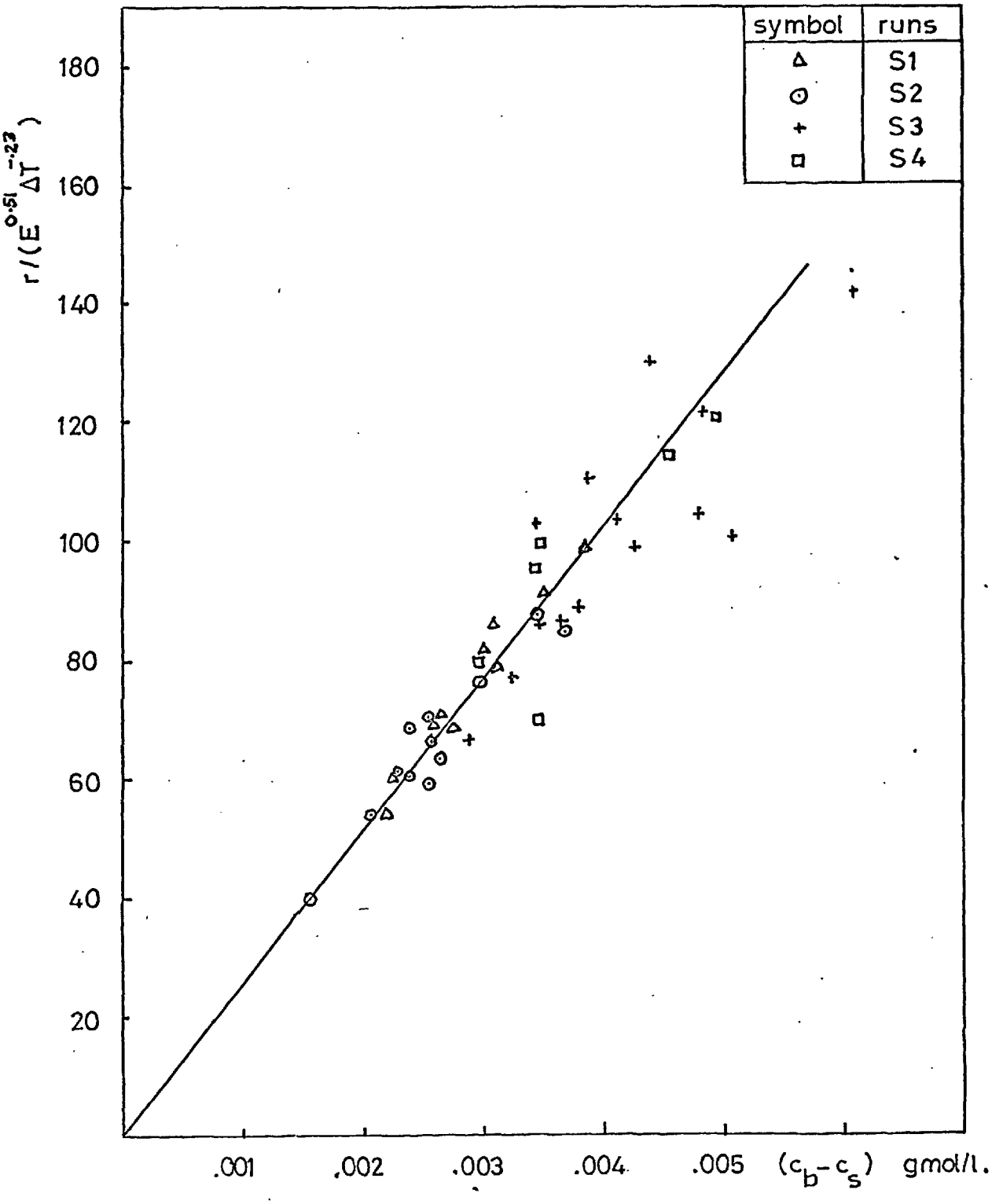


figure 28 Plot of $r/k_l' a_b$ versus (c_b-c_s) for flow reactor

$$r = 7.0 \times 10^{3} \; E^{0.51} \Delta T^{-.22} \Delta C^{0.78} \qquad -- (83)$$

$$\pm.25 \quad \pm.10 \quad \pm.21$$

The 44 data points and the best-fit line are plotted on figure 28. The mean deviation from the model is $\pm 9.4\%$, and the model itself bears a close resemblance to equation (78) derived from the batch results. Upon substitution of the Michel-Miller correlation for gassed power, equation (26), the expression becomes:

$$r \sim E_g^{0.42} \Delta T^{-.15} \Delta C^{0.72}$$

with a mean deviation of $\pm 12.3\%$. The factor P/P^* gives a significantly poorer fit than equation (83).

6.33 Effect of Solids Hold-up

Throughout the sets of experiments, the residence time was varied to obtain the reaction rate for different values of the steady-state hold-up of hydrate crystals. The solids fraction was actually varied from 9 to 27% (see column 8, Table IX). The reaction rate varied very little with ϕ_h and it was not possible to correlate the small change in terms of the Hatschek viscosity, as was done in section 6.1. This was unexpected both because of the batch results and the results of previous workers, Koppers and Fangborn (24, 27), who noticed a significant change in reactor performance with a change in the residence time.

The absence of an effect in this work is considered to be due to the change in the gas phase hold-up with solids fraction. As the hydrate hold-up is increased the viscosity increases and therefore by equation (82) the gas hold-up decreases. Since the power input is a function of the bulk fluid density (equation (24)) which incorporates the gas hold-up, the power input per unit volume increases with solids fraction. The net result being that the reaction rate stays approximately constant even though the solids hold-up may have changed substantially. It is thought the problem may be exaggerated in this system by the manner in which power depends on liquid height. The above argument is not relevant to the batch runs in which V_l is clearly defined.

6.34 Effect of Sucrose Feed Temperature

The basis for equation (75) is that the term (T_r-T_l) explains the observed variation with pressure and is theoretically proposed on the grounds that the reaction rate may depend upon the area of liquid freon in the system. Since the latter is dependent upon the heat transfer characteristics of the stirred reactor, a method of testing the model was devised which varied the heat load independently of the freon flow rate by adjusting the

sucrose feed temperature. If the sucrose feed temperature T_f is increased at a constant agent feed then, by equation (73), the reaction rate is decreased. However the overall coefficient should be increased since the hold-up of agent per unit reaction rate has increased. Runs 12-14, Table XI, considered a change in T_f, but the resultant change in $k_1'a$ was not significant.

Together with the result in section 6.25, this new information suggests that perhaps the term (T_r-T_l) is simply a convenient pressure correction parameter and that the reaction rate is independent of the liquid agent phase hold-up.

6.35 Comparison of Batch and Flow Reactors

It has been demonstrated that the effects of the parameters are approximately the same for batch and steady-state operation. A comparison of the relative magnitude of the results was made with the Hatschek viscosity as a variable. A least squares fit gave:

$$r = 1.30 \times 10^4 \eta_h^{-0.67} \Delta T^{-.15} \Delta C^{0.75}$$
$$\pm 0.42 \quad \pm 0.20 \quad \pm 0.18$$

This result for sets S1 and S2, and batch results .11 is shown in figure 29. The agreement is fairly satisfactory but the magnitude of $k_1'A$ appears to be slightly greater

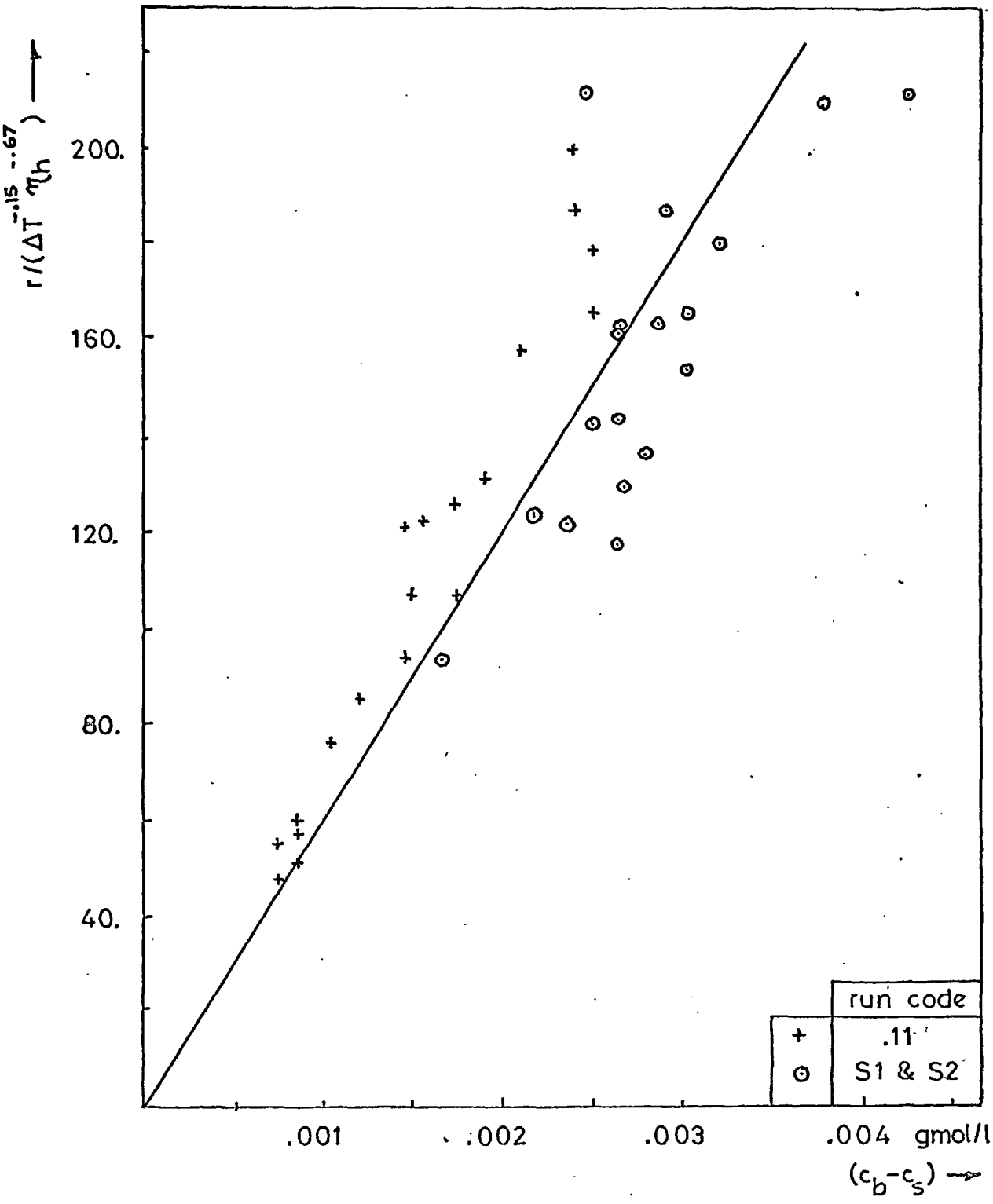


figure 29 Comparison of batch and flow reactor results

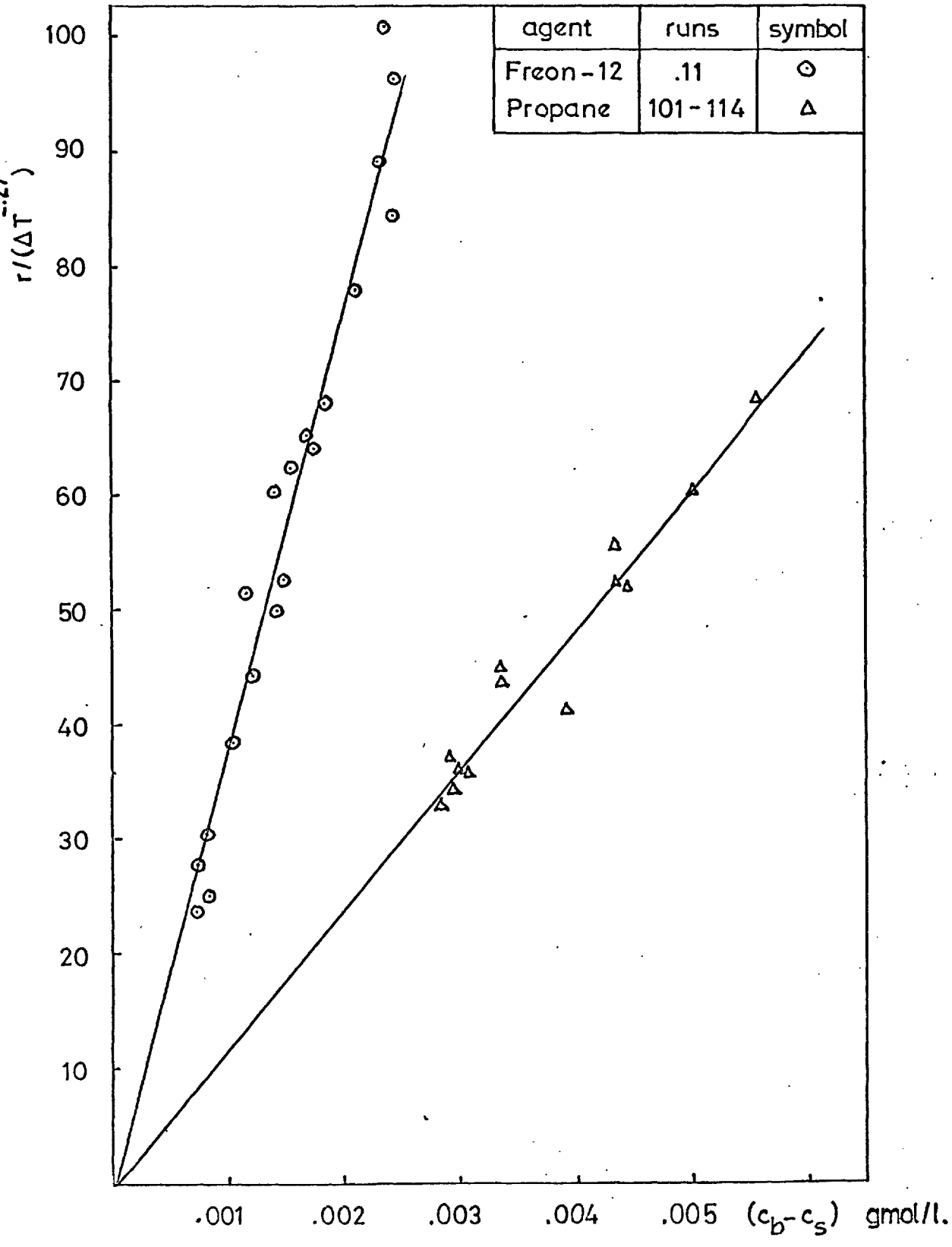


figure 30 Comparison of freon and propane hydrate formation rates at 1420 rpm.

for the batch runs.

6.4 Propane Hydrate Experiments

The detail of the experimental work is given in Appendix C together with the method, equilibrium and solubility data. A heat and mass balance and reactor operating conditions are presented in Table XV. The set of runs corresponds exactly to batch block .11 with the dual impeller agitator, and the experiments were scaled to give approximately the same production rates as for the freon runs. The mean operating data are:

$$\bar{r} = 38.2 \qquad (g/min)$$

$$\overline{c_b - c_s} = 3.74 \times 10^{-3} \qquad (g.mol/l)$$

$$\overline{T_r - T_l} = 2.02\ ^{\circ}C$$

The analysis was performed with equations (74) to (77) and the results are presented in Table 6.4. Clearly equation (75) gives the best fit to the data, significantly so when compared to (74) and (76). The expression:

$$r = 10. \times 10^{3}(c_b - c_s)^{0.96}(T_r - T_l)^{-.28} \quad - - (84)$$

is plotted in figure 30 together with the freon results, block .11. Two conclusions are drawn. Firstly, the rate expression is very similar to that predicted in the freon experiments and, secondly, the mean over-all transfer coefficient for the freon system is a factor of 3.1 times larger than for the propane system. The significance of this difference will be discussed in Chapter 8.

Table 6.4 Propane Hydrate Analysis

Model	Best-fit Parameters	Data Points	d_f	Sum of Squares (SS)	SS_1	Standard deviation	Mean % deviation	Confidence intervals k_2, k_3	Correlation Coefficient k_2 & k_3
(74)	$2.8\times10^{3}(c_b-c_s)^{0.77}$	14	12	388.6	.0548	5.68	11.86	0.38 to 1.16	
(75)	$10.0\times10^{3}(c_b-c_s)^{0.96}(T_r-T_l)^{-.28}$	14	11	77.6	.0115	2.67	5.35	0.78 to 1.14 -.36 to -.20	-0.31
(76)	$5.5\times10^{3}(c_b-c_s)^{0.87}\ P/P^*$	14	12	345.	.0384	5.35	9.73	0.54 to 1.18	
(77)	$33.4(T_c-T_r)^{0.82}(T_r-T_l)^{-.32}$	14	11	88.8	.0128	2.84	5.47	0.64 to 1.00 -.42 to -.23	-0.39

7. Nucleation, Decomposition and Filtration Results

Three additional topics were investigated which, though relevant to the hydrate process, are not directly concerned with the subject of hydrate kinetics. The aspect of nucleation considered here is the variation of the spontaneous nucleation temperature with reactor conditions. No data on the rate of nucleation is presented for it was considered that measurements of the crystal size distribution was beyond the scope of this work. The decomposition study was undertaken to verify conclusions reached in section 4.22 and the filtration experiments were conducted to determine whether hydrate crystals could be washed free of mother liquor.

7.1 The Onset of Spontaneous Nucleation

The spontaneous nucleation temperature T_n shown in the temperature-time curve in figure 19 is the temperature at which the initiation of the transformation of an unstable phase to a more stable phase occurs. This temperature was measured during each batch run (column 6, Table II), consequently the analysis presented here is a by-product of the batch experiments. The sucrose solutions were unseeded but, although a 20 micron pore size filter was used on the sucrose feed line, this did

not exclude all foreign matter.

It was observed that an increase in the cooling rate (the rate of addition of liquid freon) caused the spontaneous nucleation temperature to decrease. This is shown in figure 31; the subcooling, T_c-T_n, is plotted against the cooling rate, Q, for different sucrose concentrations at a constant agitation rate. The subcooling required for nucleation is shown to increase with increasing sucrose concentration though the effect of cooling rate remains constant.

The effect of stirrer speed on subcooling for 10% sucrose solution is shown in figure 32; increasing the stirrer speed decreases the required subcooling. Since the nucleation temperature was reproducible and its dependence upon the cooling rate was quite pronounced, a model was devised to correlate the subcooling in terms of the reactor variables. The following equation appeared the most satisfactory:

$$T_c-T_n = a_1 f(N, \eta_l, \rho_l) + a_2 Q + a_3 Q^2$$

where a_1, a_2 and a_3 are numerical constants.

This expression conforms to Ting and McCabe's (85) interpretation of the Ostwald concept of a metastable limit. Ostwald defined two areas of the supersaturated

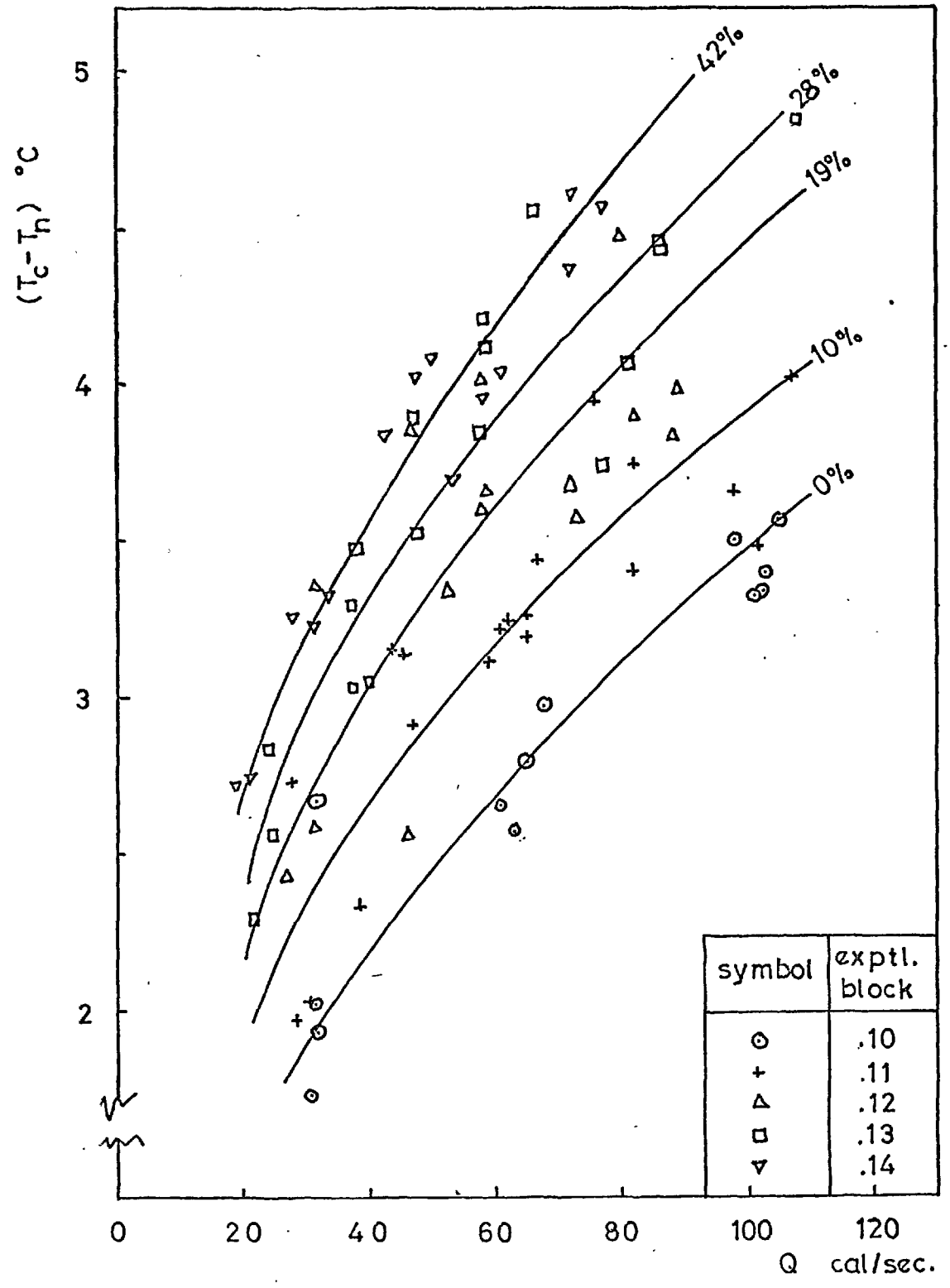


figure 31 Plots of subcooling at nucleation versus cooling rate with variable sucrose composition

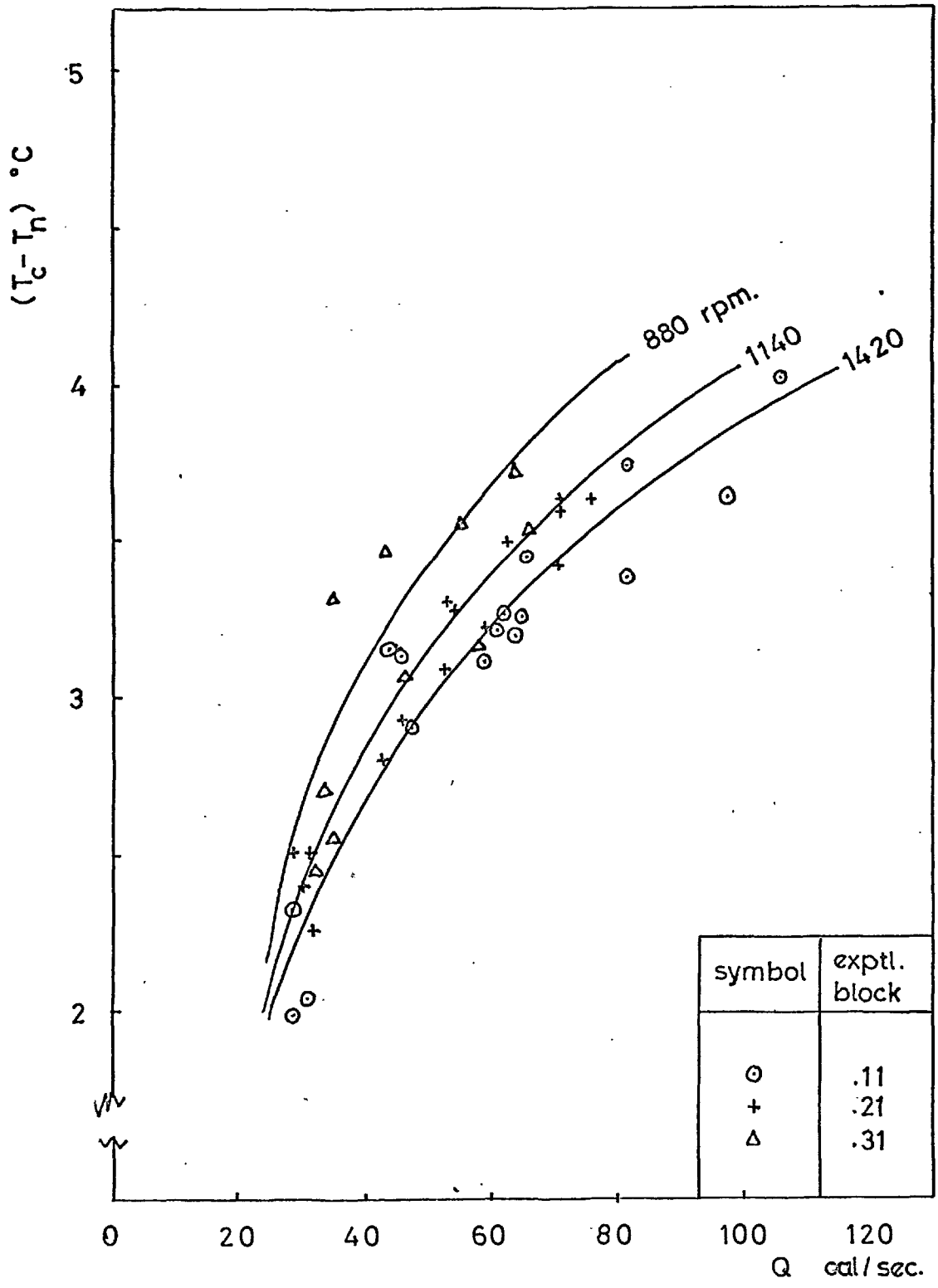


figure 32 Plots of subcooling at nucleation versus cooling rate with variable stirrer speed

state: The metastable region in which inoculation was necessary to start the crystallization process, and the labile region in which the solution was capable of crystallizing spontaneously. The line of demarcation between the two states was called the metastable limit. Ting and McCabe showed that there was no unique metastable or supersolubility limit, but that the transition state was a function of factors such as the mechanical stimulus to crystallization. The true metastable limit in the above expression occurs at $Q = 0$ and at a stirrer speed beyond which mechanical stimulus has no effect.

Initially the results at constant sucrose concentration were fitted to the expression:

$$T_c - T_n = a_1 N^{a_o} + a_2 Q + a_3 Q^2 \qquad (N_1 \text{ constant})$$

A computer programme based on a hill-climbing technique was used to regress for the parameters a_o to a_3. The results for each sucrose level are shown in Table 7.1; where Q is measured in cal/sec., N in rev/sec. and a_1 is a function of the sucrose concentration, viscosity, etc.

x_f w/w%	a_o	a_1	a_2	a_3	data points	Mean % deviation
10	-.19	2.1	2.88	-.106	55	7.2
18	0.58	0.17	3.63	-.151	49	6.8
28	4.32	-0.61×10^{-7}	6.75	-.325	60	8.0
42	-.34	5.68	2.80	-.083	29	5.6

Table 7.1 Best-fit parameters for subcooling correlation

There is an order of magnitude agreement between the parameters for 10 and 42% sucrose, but the change in the value of a_o suggests that the effect of stirrer speed is not the same for each concentration. If all the data are fitted to one correlation with viscosity as a variable, the expression becomes:

$$T_c - T_n = 2.2N^{-.24}\eta_l^{0.29} + 8.80\ Q - 0.106\ Q^2 \quad -- (85)$$

The mean deviation from the model for 209 data points is $\pm 8.1\%$. Several other forms of equation (85) were considered, including the substitution of other parameters such as the mean density of the three phase system, but no significant improvement in fit could be achieved.

No particular importance is attached to the numerical constants in equation (85); the expression is simply used to provide an estimate of the effects of the main variables. The first term resembles a function of the Reynolds number, indicating that the degree of subcooling required is high when the ratio of shear to flow is large.

The model suggested in equation (85) was completely upset when the spontaneous nucleation temperature was measured with the freon feed distribution in operation (runs .110 and .310). The distributor, sited in the gas space above the aqueous phase, was splashed with aqueous

solution as freon bubbles left the surface. Droplets of solution encountering cold liquid freon on the copper distributor tube, at a temperature far below the nucleation temperature, formed stable hydrate nuclei. Hydrate crystals dropped back into the reactor to nucleate the bulk phase at a higher temperature than before. This is effectively a seeding process; the hydrate nuclei behave as more active sites than the foreign particles.

7.11 Interpretation of the Nucleation Results

Heterogeneous nucleation is initiated by foreign nuclei and is due to the catalytic effect of their surfaces as well as the walls and surfaces of the reactor. If the variability of the spontaneous nucleation temperature is caused by chance, then at a slower cooling rate one would predict a higher nucleation temperature than at a faster cooling rate: The probability of inducing a phase transition should increase with time. This is just what has been observed experimentally, so it is concluded that the nucleation mechanism involves the chance simultaneous occurrence of site and environment.

This mechanism is contradicted, however, in the results published by Sherwood et al (72) for a similar three phase system. Here the spontaneous nucleation

temperature of ice, in the system iso-butylene evaporating in salt solutions, was shown to be independent of the cooling rate. The nucleation temperature was regarded as a fixed temperature, independent of chance, to which the active sites had to be cooled to initiate nucleation. From experiments in which potassium chloride was deposited from solution at various cooling rates, Melia and Moffitt (73) confirmed the basis of equation (85). Melia showed that the induction period decreased with increasing cooling rate and that the required supersaturation for nucleation increased with cooling rate. Further evidence for the dependence of nucleation on the rate of cooling is given by Ting and McCabe (85) from experiments with magnesium sulphate.

The process of nucleation is visualised as the result of foreign matter contacting cold spots in the reactor to provide active nucleation sites. The effect of the stirrer speed in equation (85) may be explained by the increase in the circulation rate in the reactor with an increase in N. The increase in circulating fluid increases the probability of meeting an active cold site. Alternatively the explanation for the change in the value of a_o shown in Table 7.1 might be that a decrease in stirrer speed increases the size of cold eddies of fluid

or area of cold freon, and hence increases the probability of nucleation.

7.2 Decomposition Studies

The purpose of this section is twofold: Firstly, to examine briefly the mechanism of dissolution as opposed to growth of hydrate and, secondly, to confirm the reasoning given for the differing results obtained in the phase diagram studies.

7.21 Experimental Procedure

A 500 watt heater was installed in the 5 litre reactor, with the element in the neighbourhood of the impeller. Hydrate was produced in the reactor under normal batch conditions to give an approximately 15% slurry in 10% sucrose solution. A particular stirrer speed and heat load were selected and the pressure was maintained constant at the chosen level. A variac and wattmeter were used to control and measure respectively the heat input.

The reactor temperature was measured with the thermocouple probes and the steady temperature was recorded. Samples of mother liquor were withdrawn at timed intervals and analysed (Table XIX). Each run was checked by

comparing the heat input, corrected for the heat leak and power dissipation terms, with the rate of decomposition as measured by the change in sucrose concentration. A specimen calculation is given in Appendix D together with a summary of the 15 decomposition runs, Table XVIII. The experimental study was not extensive, being limited to two stirrer speeds, 880 and 1420 rpm, and 10% sucrose solutions.

7.22 Comparison of Mass Transfer in Decomposition and Growth

A preliminary analysis of the runs at 880 rpm for 100 and 200 watts heat input, Table XVIII, showed that at constant pressure the decomposition rate was linearly dependent on the superheating $(T_d - T_c)$. This suggested that the process of decomposition might be analogous to the mechanism of dissolution of crystals in solution. Initially, therefore, the rate of decomposition is considered to be limited by the transfer of agent from the crystals which are supersaturated with respect to the bulk solution. The decomposition rate from hydrate crystals may be expressed:

$$r_d = k_d A_c (c_s - c_r) \qquad - - (86)$$

r_d = rate of decomposition (g. of water/min.)

k_d = mass transfer coefficient (units as eq.(56))

c_r = concentration of agent in equilibrium with aqueous phase at T_d, P (g.mol/l)

It is assumed that since heat transfer is a much faster process than mass transfer, c_s is the concentration of agent in equilibrium with the hydrate crystals at the decomposition temperature T_d, and the equilibrium pressure P_h (see figure 35). Since there is no counterpart of the surface reaction step in dissolution and the process is controlled only by diffusion, k_d is a true mass transfer coefficient. This was confirmed by Lal (75) in experiments on the dissolution and growth of potassium chloride crystals from solution. Under certain agitation conditions the deposition of potassium chloride is a surface reaction controlled process but the rate of dissolution under the same conditions was shown to be faster and independent of the surface concentration effect.

The use of a combined diagram to represent growth and evaporation rates from melts was suggested by Kitchener and Strickland-Constable (74): Such diagrams have also been used to relate growth and dissolution rates in solution. If the hydrate growth rate was limited by a diffusion process at the crystal surface, then the growth and decomposition plots would be mirror images. Although this possibility has already been rejected by the analysis in chapter 6, the results are conveniently compared on a growth-dissolution plot.

Figures 33 and 34 show the two sets of curves for the two stirrer speeds considered. For the case of constant pressure the graphs verify the linear dependence upon concentration driving force indicated in equation (86). The over-all transfer coefficient for decomposition appears to be a factor of 2.5 times greater than that for growth at each speed. This confirms the hypothesis that during growth the rate controlling step, a slower process than the integration of freon into the hydrate crystal, is the rate of transfer of agent from suspended drops or bubbles. The alternative explanation for the difference between the two curves, that the slower growth process entails a surface reaction mechanism, is not valid. The growth rate has been clearly shown to be a diffusional mechanism in chapter 6.

7.23 The effect of Pressure on Decomposition

The rate of decomposition is shown in figure 33 to depend upon pressure: As the decomposition pressure is increased the driving force required for a given dissolution rate is decreased. The interaction of P $(c_s - c_r)$ is shown in figure 35 (cf. figure 24).

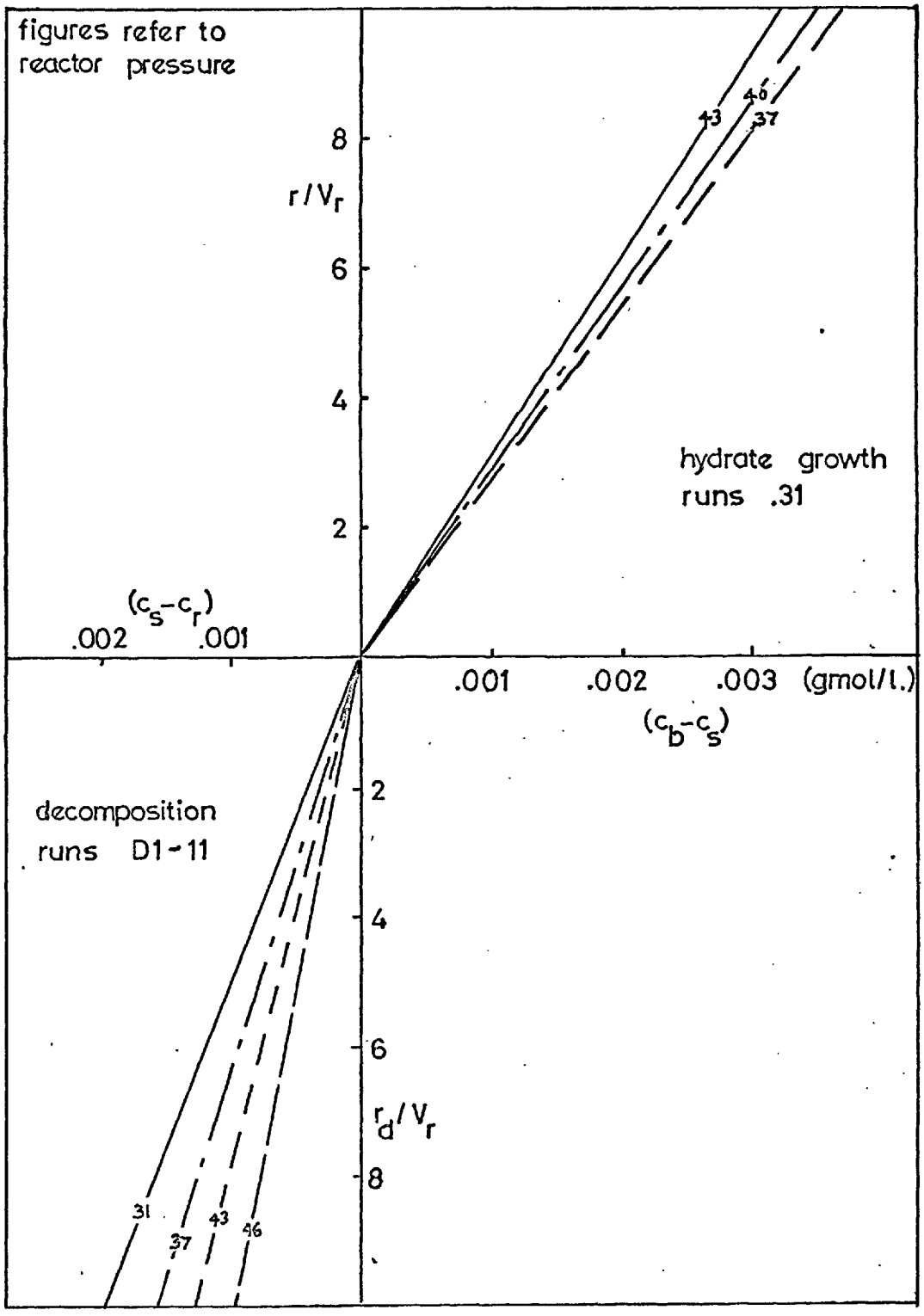


figure 33 Comparison of growth and decomposition rates at 880 rpm.

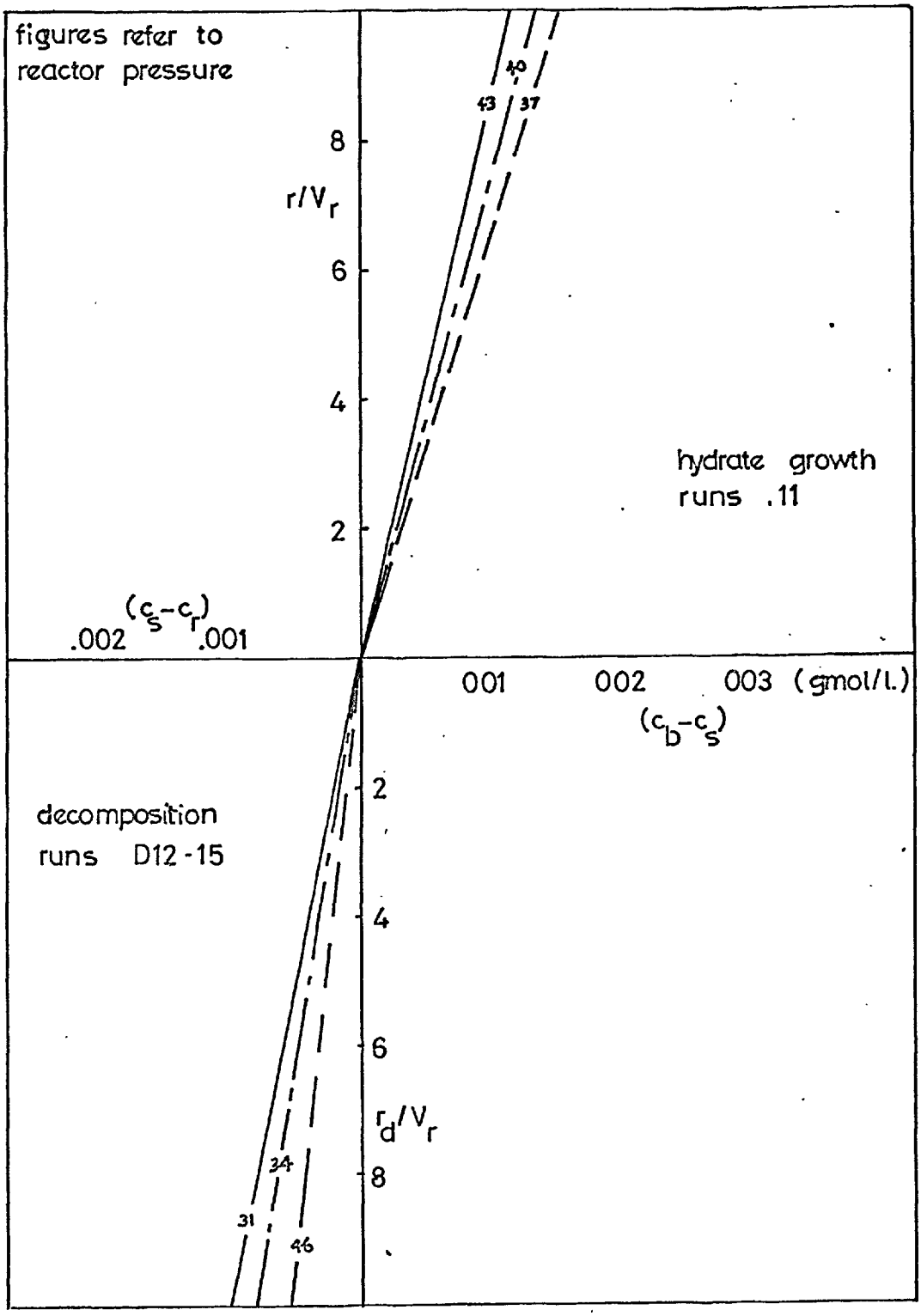


figure 34 Comparison of growth and decomposition rates at 1420 rpm.

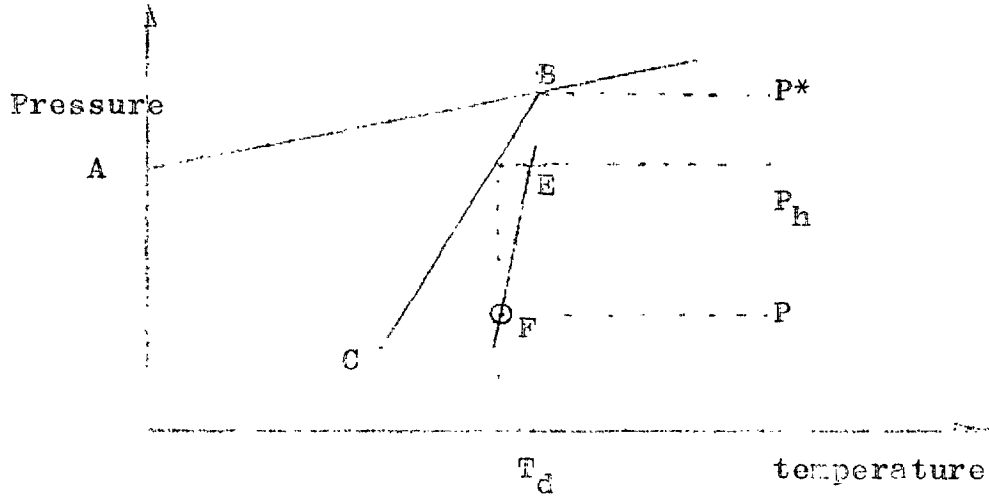


figure 35 Interaction of P and (c_s-c_r)

The conditions during a typical run are shown as the circled point at F, with a slurry temperature T_d and reactor pressure P. The line EF is an operating line, representing a constant rate of decomposition. Clearly equation (86) is not an adequate description of the decomposition process.

The classical approach to crystallization sometimes makes use of a supersaturation term which is defined as the ratio, s, of the concentration in solution to the saturated concentration at the same temperature. In the case of decomposition, the saturated concentration is equivalent to the agent concentration in the continuous phase and equation (86) becomes:

$$r_d = k_d' A_c (s-1)$$

where $s = c_s/c_r$

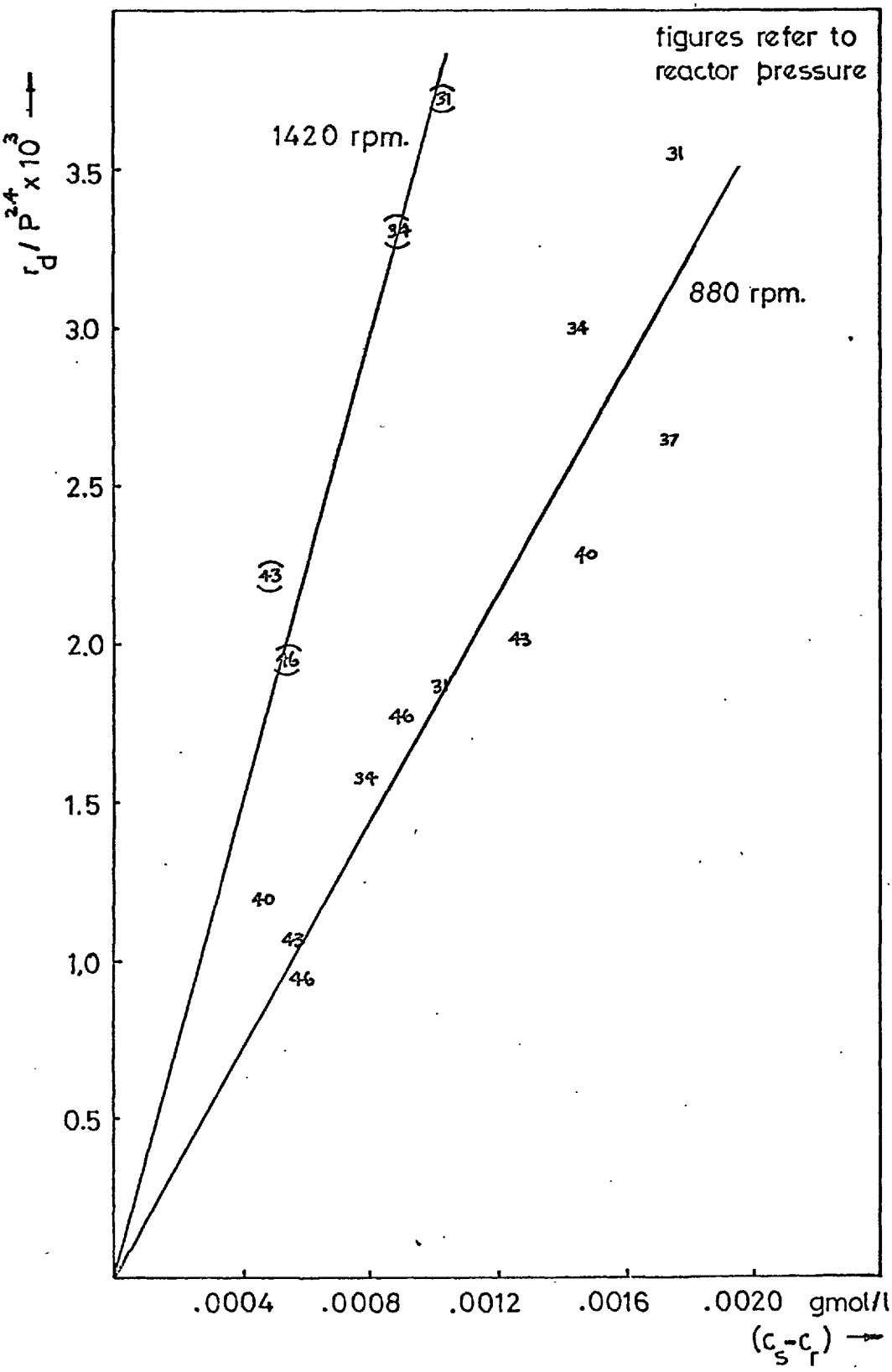


figure 36 Plot of pressure-corrected decomposition rate versus driving force

Although this suggests that $(c_s-c_r)/c_r$ or $(P_h-P)/P$ may be a better parameter to use in equation (86), both these terms tend to exaggerate the pressure dependence shown in figure 35, rather than correct it.

One method of 'normalizing' the concentration driving force is to introduce the ratio P/P^*, where P^* is the equilibrium pressure at the invariant point. This is the form used in equation (76) to describe the variability of growth rate with pressure. The factor P/P^*, tabulated in column 11 Table XVIII, improves the fit relative to equation (86) though the errors are still greater than expected, even when handling such small driving forces. The alternative is that the decomposition process depends on a higher power of the pressure. On the basis of the conclusion to section 6.25, an absolute pressure term rather than a pressure ratio was employed, and a least squares fit gave:

$$r_d \sim (c_s-c_r)\, P^{2.4} \qquad -- (87)$$

The corrected decomposition data are shown in figure 36.

This conclusion is important since it infers that both decomposition and growth processes are a function of pressure. Hence the term (T_r-T_1), whilst being a satisfactory correction for the pressure dependence in hydrate growth, can no longer be justified in terms of

the heat transfer model originally proposed. A summary of the growth models corresponding to equation (87) is presented in section 8.1.

Experimentally it was shown that the supersaturation required for decomposition did not vary with the crystal hold-up; as the hydrate was decomposed during a run the slurry temperature remained constant. Two explanations are possible.

(1) As the slurry hold-up and area decreases, so the mass transfer coefficient increases due to the decrease in viscosity (model B), with the result that the product, $k_d A_c$, remains constant.

(2) The decomposition rate is independent of the hydrate hold-up and depends upon the mechanism of the escape and coalescence of bubbles from the hydrate crystals and bulk solution.

It may be that the process of stripping gaseous agent from the slurry is a reasonable alternative to the postulated dissolution process. Rather than the transfer of dissolved freon through a boundary layer around the crystal, decomposition could be envisaged as the removal of gas bubbles formed at the crystal surface. For example, crystals may be effectively insulated by a layer

of gas bubbles, in which case the transfer of heat to the particles may be the limiting step. However, insufficient information is available to deduce the decomposition mechanism or to clarify the significance of the pressure dependence.

7.3 Results of Wash Studies

The wash experiments were performed to test whether a bed of hydrate crystals behaves as a normal packed bed, and to establish the fraction of voids. A series of runs was carried out to determine the effect of hydrate formation conditions on these two criteria. The results are summarised in Table XXIII, Appendix F, for the wash and hydrate growth conditions specified in Table XXIV.

The volume fraction of crystals in the bed was estimated from a mass balance on the slurry and a measurement of the melted volume of the hydrate crystals. A typical calculation is shown in Appendix F1. The solid fraction varied between 25 and 40%, but the error involved was too large to conclude whether there was a significant change with formation conditions.

The ratio of the sucrose concentration in the wash effluent to the concentration in the original filtrate,

x_F/x_o, was plotted against the accumulated wash volume. If the bed had behaved ideally, a step change in x_F/x_o would have been observed as the residual sucrose was displaced from the voids by plug flow. Rather the bed behaves as other packed beds in that longitudinal mixing occurs due to viscous effects and to molecular diffusion. Figure 37 shows a typical set of 'breakthrough' curves for a set of runs (l = 22 cm., x_f = 10%). The theory for longitudinal mixing, characterized by a dispersion coefficient and a Fick's law expression, is given by Danckwerts (76). The approximate solution for the displacement curve presented by Danckwerts is given in Appendix F2, together with a specimen calculation of the dispersion coefficient. Two values of the dispersion coefficient, calculated from different points on the curve, are shown in columns 6 and 7 of Table XXIII. Although there is a substantial discrepancy between these two estimates of the Danckwerts' dispersion coefficient, there is also a large difference between estimates for different runs under similar wash conditions, indicating that the experimental error is fairly high. Apart from the error involved in actual sampling, the breakthrough curve is affected by poor wash distribution and bypassing caused by hydrate plugging.

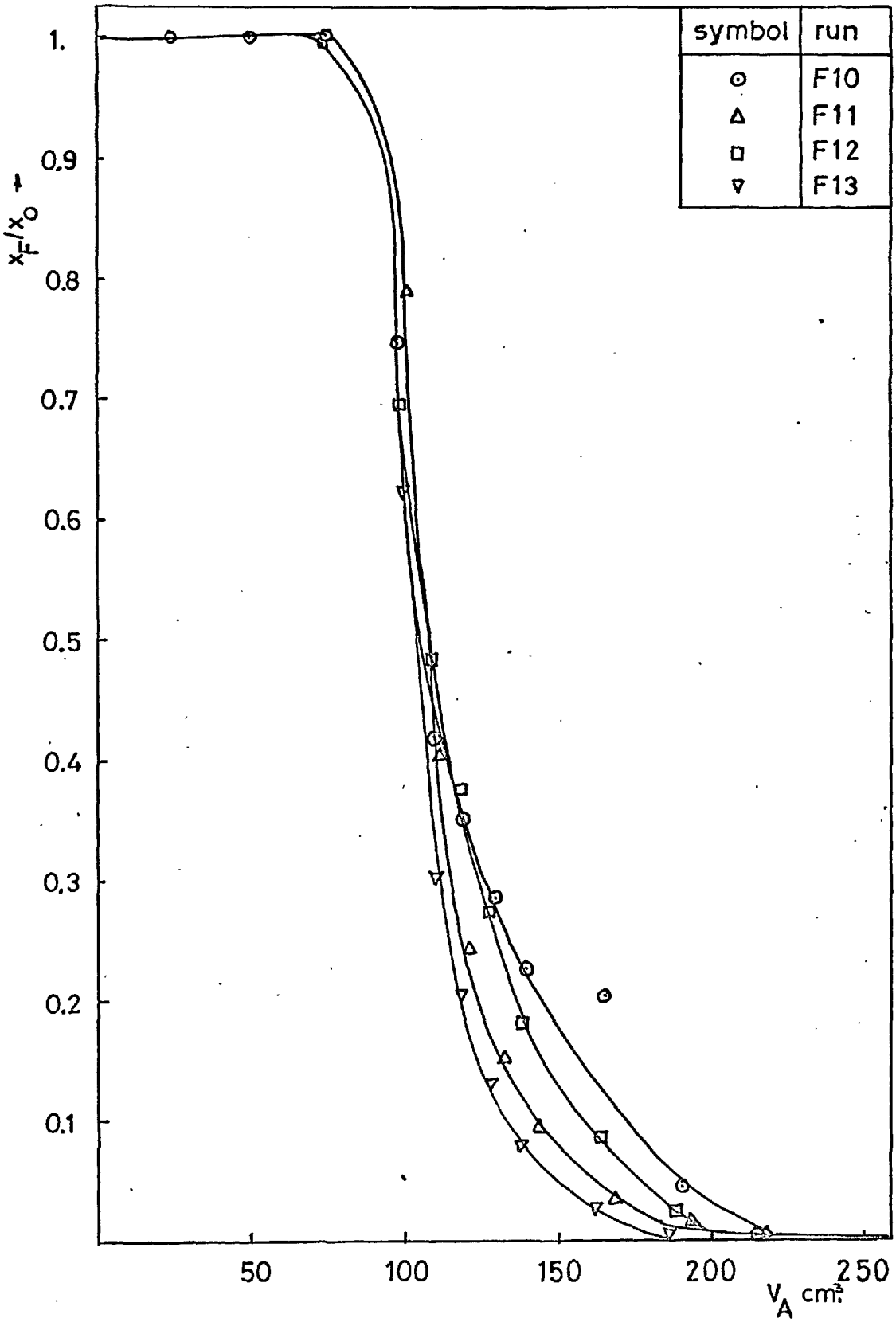


figure 37 Concentration profile in wash effluent – 22 cm. bed

The mean dispersion coefficient with runs at 10% sucrose is 7.4 x 10^{-3} cm^2/sec., and the effects of bed height and wash velocity conform to the Danckwerts model. Variations in the hydrate formation conditions appear to have no effect on the value of the dispersion coefficient, indicating that perhaps the size and shape of crystals are independent of the concentration driving force. The mean dispersion coefficient at 25% sucrose is 25 x 10^{-3} cm^2/sec.

The results in Table XXV show that the concentration has been reduced to about 0.4% of the original mother liquor concentration after the residual sucrose has been displaced by three times its own volume. It is expected that as high a recovery of mother liquor should be achieved in a commercial centrifuge (section 2.3).

The effective crystal size was calculated from pressure drop measurements across the bed. The mean diameter of the crystals appeared to be in the range 20 to 35 microns, (Appendix F3). Observations of the packed hydrate indicated that the crystals tended to compact together and form a rather rigid or integrated structure allowing bypassing of the bed, particularly in the neighbourhood of the walls. Such bypassing would throw doubt

on the significance of the pressure drop measurements and estimates of the crystal size. Further evidence for bypassing is the high concentration of sucrose, x_m, in the melted slurry (column 6, Table XXIV). This figure is far in excess of the final effluent concentration, suggesting that some sucrose is trapped in inaccessible pockets.

8. Discussion of Results and Design Criteria

This chapter considers the mass transfer rate of freon in the hydrate reactor compared to the rate predicted by established correlations for gas-liquid systems, and to the rate of transfer of other hydrating agents. The performance of the reactor as a typical concentration stage is discussed together with some aspects of scale-up procedure.

8.1 The Hydrate Growth model

The rate of hydrate formation has been shown to depend on the rate of supply of hydrating agent by diffusion from the dispersed gas phase. Hydrate crystals take no part in the mechanism, which may be considered as an instantaneous reaction in the turbulent aqueous phase, but the presence of hydrate does affect the rate of formation by thickening the aqueous slurry. This effect has been related to a dependency of the transfer coefficient on the slurry viscosity, similar to the dependency on the liquor viscosity derived separately.

Although the transfer process resembles typical gas-liquid agitated systems in that the over-all mass transfer coefficient is characteristically dependent on the power

input and viscosity, the hydrate production rate cannot be completely described in terms of a rate coefficient and an effective concentration driving force. The diffusion process depends upon the system pressure in a way which has been quantitatively determined, but not theoretically interpreted. In the primary analysis of the results, the pressure effect was related to the evaporation of liquid agent by the temperature differential $T_r - T_l$. Although this correlated the results satisfactorily, the model is not valid when considered in the light of the decomposition studies in which a similar pressure effect was observed. The results in terms of the absolute pressure are summarised below: Apart from the flow reactor results, the fit was not improved by the use of the parameter P rather than $T_r - T_l$.

(i) Batch results, equation (79) becomes:

$$r \sim E^{0.5} \eta_l^{-.74} P^{0.40} \Delta C^{0.87}$$

The individual results in section 6.21 show a dependency on P ranging from 0.3 to 2.5

(ii) Steady-state conditions, equation (83) becomes:

$$r \sim E^{0.51} P^{2.7} \Delta C^{0.93}$$

Apart from a significant improvement in fit, this dependence on the concentration driving force conforms better to equation (46).

(iii) Propane batch results, equation (84) becomes:

$$r \sim P^{3.4} \Delta C^{0.96}$$

(iv) Decomposition results:

$$r \sim P^{2.4} \Delta C \qquad -- (87)$$

Three suggestions are put forward to explain the dependence on pressure of the hydrate growth process.

(a) The mechanism depends on some pressure-sensitive property of the gas phase which affects the interfacial area, e.g. de Graauw (26) suggested that bubbles at a higher pressure were less stable than those at a lower pressure.

(b) The process involves a reaction constant rather than a mass transfer coefficient.

(c) The equilibrium agent concentrations c_b and c_s are not realised in the reactor. The approach to the effective concentration driving force is pressure dependent and given by $(c_b - c_s)P^{2.5}$.

Possibility (a) is discounted since both decomposition and formation processes are dependent upon the same function of pressure. Arguments put forward in section 6.21, and the further evidence that the rate coefficient is typically dependent on the sucrose viscosity, indicate that the rate is limited by diffusion and not a reaction

constant as in (b). The third possibility is only conjecture. The linear dependence on $(c_b - c_s)$ holds for a wide range of pressures, and there is no experimental method of checking the value of c_s under formation conditions. The propane results suggest that the pressure effect is independent of the agent composition.

It has been demonstrated the the batch runs provide a useful and valid method for determining the reactor performance. The agreement of the steady-flow results with the batch results is a significant conclusion, since the batch system involves less equipment and generates more information per run than the flow reactor.

8.2 Comparison of the Over-all Mass Transfer Coefficient with Published Data

The over-all coefficient defined in equation (20) may be expressed in terms of the agent diffusivity and other variables by:

$$k_l a_b = 32.6\, E^{0.46} \eta_l^{-0.55}\, Das^{0.5}\, \rho_l\, (P^{0.47})_{sec^{-1}} \quad --(88)$$

This relation was derived from the pressure-corrected form of equation (80) using the diffusivity correlation, equation (43), and the assumption that transfer at the interface conforms with Danckwert's surface renewal theory. Equation (88) does not hold for 40% sucrose; for this

concentration the coefficient was shown to depend upon only the -0.15 power of the viscosity, see figure 26. This deviation may be due to an interaction between the bubble size and the mass transfer coefficient: Calderbank (59) has shown that in aerated systems the transfer coefficient changes rapidly as the bubbles pass through a transition size region. Alternatively, the slope of the curve in figure 26 above a viscosity of 5 cp. may be explained by the linear dependence of the interfacial area on μ_l as shown by Westerterp (30) for glycerol solutions.

The value of $k_l a_b$ varies between 0.07 and 0.40 sec^{-1} for the experimental conditions and, although the form of equation (88) resembles that of the two-phase correlations presented in section 5.3, the magnitude of the experimental coefficients is somewhat larger than predicted. Table 8.2 summarises the comparison between the measured and predicted coefficients for four runs chosen at the extreme values of the operating levels. The Middleman correlation for the transfer coefficient, equation (42), was used in conjunction with equation (29), relating specific surface to bubble size, to estimate the mean bubble size associated with the measured value of $k_l a_b$. The specific surface thus varies from 16.3 to 37.5 cm^{-1} and differs considerably from the estimates given by Calderbank, Westerterp and

Vermeulen. The Westerterp correlation predicts reasonable values of a_b at the high viscosity, the effect of viscosity is to prevent bubble coalescence, but at 10% sucrose the estimates are very low.

These discrepancies may be due to the choice of the Middleman transfer correlation which is based on mass transfer studies in solid-liquid rather than gas-liquid systems, although for small bubbles the two processes are usually regarded as analogous. The Calderbank and Moo-Young correlation, equation (40), gives much smaller values of k_l than predicted by Middleman, but the transfer coefficients given by Yoshida and Miura (78) are much larger and the resultant bubble sizes are much closer to the predicted values. The Yoshida correlation was derived for the absorption of oxygen in sulphite solutions.

These comparisons must, however, be qualified by the context of the original experimentation. Calderbank's work on interfacial areas is based on power input, whereas Westerterp and Vermeulen's work is based on impeller speed and is therefore dependent on equipment geometry. With a dual impeller the power consumption is about three times that of a single turbine, hence the estimates of a_b from equations (31) and (32) should be multiplied by a factor

Run		1.11	1.31	4.14	4.34
x_f		0.093	0.095	0.42	0.42
ϕ_g		0.24	0.12	0.15	0.08
E		0.56	0.13	0.56	0.13
Re $(ND^2\rho_l/\eta_l)$		61,000	37,800	7,500	4,650
Sc $(\eta_l/\rho_l D_{as})$		2,280	2,280	77,200	77,200
$k_l a_b$ experimental (sec^{-1}) defined by equation (20)		0.289	0.129	0.126	0.069
D_b estimated from equations (42), (29). Middleman (61)	D_b	0.050	0.044	0.024	0.021
	a_b	29.	16.3	37.5	23.
	k_l	0.01	0.008	0.0034	0.0028
D_b estimated from equations (89), (29) Yoshida (78)	D_b	0.24	0.21	0.16	0.12
	a_b	6.1	3.45	5.6	3.87
	k_l	0.0455	0.0375	0.0220	0.0180
D_b Calderbank, eqn. (28)		0.30	0.34	0.25	0.29
a_b Calderbank, eqn. (28)		4.80	2.1	3.6	1.65
a_b Westerterp, eqn. (32) (brackets refer to E)		2.4 (3.7)	0.96 (1.5)	23.7 (36.7)	8.9 (13.8)
a_b Vermeulen, eqn. (31)		10.7	2.6	4.5	1.5)
k_l Calderbank, eqn. (40)		.0051	.0036	.00083	.00062

Table 8.2 Experimental and predicted bubble characteristics

of $3^{0.4}$. A further consideration is the effect of initial gas distribution on the over-all coefficient and the problem of relating the correlations to a system in which vapour is generated in the agitated dispersion.

It has been demonstrated that the over-all coefficient is dependent on the initial drop size of the liquid agent. This suggests that bubble size is related to drop diameter, perhaps in the way put forward in section 5.43, and explains why predicted bubble sizes in simple gas-liquid systems are larger than those obtained when bubbles are generated from drops. The discrepancy between the predicted values of the mass transfer coefficient makes it impossible to determine the precise effect of this process, but one interpretation is considered based on the Westerterp and Middleman results in Table 8.2. At low viscosities the difference between predicted bubble and drop sizes is large; consequently the effect of the generated bubble, D_b^*, is large and the true a_b is much larger than given by Westerterp. At high viscosities the bubble size approaches the drop diameter, as shown by Westerterp and Calderbank (30, 53), since coalescence is inhibited, and therefore D_b^* differs little from the bubble diameter. This mechanism explains the differences and agreements in Table 8.2 and the changing effect of viscosity on the over-all coefficient.

The mass transfer from liquid freon in the dispersed phase given by equations (53) and (49) was shown by equation (17a) to account for only 1% of the total absorption rate.

8.3 Comparison with Propane and Methyl Bromide as Hydrate formers

The batch hydrate runs using propane under identical conditions to freon showed that the over-all coefficient was 3.1 times greater for the freon system. This result provides a means for testing the generality of equation (88), and for examining the effects of other variables as listed in Table 8.3. When corrections are made for the liquid viscosity, equation (88), and the dependence on the dispersed phase viscosity and interfacial tension given by Vermeulen, equation (31), the freon coefficient is reduced to twice that of the propane coefficient. The several possible explanations for this difference are reviewed here.

Agent	η_1	η_d	σ	$(\rho_1/\rho_v)^{\frac{1}{3}}$	$D_{as} \times 10^5$	E	$\rho_v \lambda_1$	λ_1
Freon-12	1.7	.012	63	3.8	0.69	0.56	0.78	35
Propane	2.08	.0075	63	3.75	0.69	0.56	0.84	90
CH_3Br	1.34	.010	48.5	6.6	1.0	0.214	0.31	60

Table 8.3 Physical constants for hydrating agents

The effect of gas loading on the power dissipated in the reactor has been discussed previously in section 5.36, and the experimental evidence of its effect in the reactor is seen as the dependence of the hydrate formation rate on

the approximately 0.9 power of the driving force. However, the power term used in equation (88) is the power consumed in a single phase rather than a gassed system, since gassed power is a dependent function. The power input is given by the Oyama correlation, equation (25), and when this is expressed in terms of the production rate, equation (45),:

$$P_g = P_o \left(1 - k_g\left(\frac{r_a \lambda_{hf}}{\lambda_1 \rho_g N D^3}\right)\right)$$

Consequently for a constant production rate, with λ_{hf} nearly constant for all hydrate formers, the relevant variable is $\lambda_1 \rho_g$, which is shown to be nearly equal for the two systems. The effect of the generated vapour on the power does not therefore explain the difference in coefficients.

In the previous section it was suggested that the transient bubble size, D_b^*, might well be significant at low viscosities. In which case, from the considerations in section 5.43, the factor $(1/\rho_g)^{\frac{1}{3}}$ may be important; for small values the effect of bubble generation is enhanced. Although the values for propane and freon are nearly equal, another physical constant which may have an effect of D_b^*, the latent heat, is markedly different. Unfortunately, the literature on heat transfer to drops evaporating while in dispersion is very limited and latent heat has not been

considered as a variable. However Sideman (67) showed the area for heat transfer was a function of the vapour content and, since for a given heat input the vapour content of the drop is inversely proportional to the latent heat, it may be expected that the area and hold-up of liquid agent is latent heat dependent. A higher latent heat results in less liquid agent in suspension and a consequent reduction in the number of bubbles generated with a size D_b^*. Although this model may explain the difference in the hydrate coefficients, the presentation is a major simplification especially in view of the pressure effect on the diffusion process.

The results for methyl bromide hydrate formation in salt solutions were published by Pangborn (27) in the form of equation (22) for individual stirrer speeds and concentrations. To compare the Pangborn data with the present work, his results were fitted to a rate expression including the concentration driving force and the effect of viscosity:

$$r = 2.69 \times 10^2 E^{0.12} \eta_l^{-.80} \Delta C^{0.92} V_r$$

The mean deviation is $\pm 25\%$ and the dependency on η_l and ΔC is very similar to the freon model. The experimentation was largely at constant pressure (19 psia. for 4% NaCl) so the effect of pressure could not be established.

With the higher solubility of methyl bromide, the concentration driving force was nearly ten times greater than that for freon, and the reactor was operated closer to the condensation line with $T_r - T_l$ generally less than $1^{\circ}C$. No success was achieved when the Hatschek term was introduced to explain the effect of residence time.

In terms of the over-all coefficient:

$$k_l a_b = 0.0316\ E^{0.12} \eta_l^{-.80} \qquad sec^{-1}$$

and for a typical run (no. 62) with r = 22.7 g. of water solidified/min., $T_c - T_r = 1.12^{\circ}C$ and $c_b - c_s = 0.0235$ gmol/l., the value of $k_l a_b$ is 0.02 sec^{-1}. Substituting the values of the variables for methyl bromide listed in Table 8.3 into equation (88), together with the corrections due to Vermeulen and the gassed power relationship of Oyama, the value of $k_l a_b$ predicted from the freon analysis is 0.15 sec^{-1}. While this coefficient is intended to predict the methyl bromide formation rate at 57 psia., the Pangborn reactor was actually operated at 19 psia. and the measured coefficient was seven times less. If the observed effect of pressure on formation rate is independent of the nature of the hydrating agent, then a more realistic prediction of the coefficient is a factor of $(19/57)^{2.5}$ smaller, i.e. 0.010 sec^{-1}. It appears, however, that there are too many unknowns to drawn a meaningful comparison between the freon results and Pangborn's study.

It may be possible to derive a general correlation for the over-all coefficient in hydrate systems based on the variables considered here, but equation (88) has been shown to hold for the hydrate of freon-12 only. One reason for this appears to be the pronounced effect of the evaporation of the immiscible liquid phase on bubble sizes, and it is this same effect which makes the familiar gas-liquid correlations inapplicable.

8.4 Reactor Performance as a Concentration Stage

The real performance of the reactor is measured as the conversion and throughput of the equipment rather than in terms of an over-all mass transfer coefficient. The maximum yield of a steady-state run in the experimental system is presented here.

Considering the sucrose throughput with run 50, Table IX, 6.3 gph. of 9.69% sucrose was concentrated to 5.53 gph. of 11.03% sucrose, which represents a stage conversion of 12.1%. The removal of 7.66 lbs. of water per hour as hydrate nearly corresponds to the maximum working capacity of this equipment. The limit is imposed by the concentration of hydrate which flows freely through the exit line and the duty of the auxiliary equipment, rather than the reactor size. The maximum conversion achieved was

21% at a hydrate volume fraction of 0.27, but a reasonable design conversion is considered to be 15%. The yield of the 5 litre reactor could be doubled by doubling both refrigeration duty and sucrose feed pump capacity.

8.5 Scale-up Considerations

The emphasis of this work has been placed on the derivation of a model for the mechanism of hydrate formation in an autorefrigerated reactor; the actual design of a commercial plant for the concentration of a liquid foodstuff has not been undertaken. The results are, however, presented in a form which enable the best operating conditions and performance of possible reactor types to be predicted. Several aspects of the design are considered here, pertinent to both concentration and desalination processes.

Briggs and Barduhn (20) have compared the energy requirements in saline water conversion for six hydrating agents and shown that the energy consumption of the plants decreases with increasing heat of formation. The basis of this comparison is the minimum work requirement for the concentration process (the work for the two-stage compression system described in section 2.31) given by Dodge and Eshaya (77) as:

$$W = Q \left(\frac{T_1 - T_2}{T_2}\right)\left(\frac{T_o}{T_1}\right)$$

where Q = heat taken up at T_2
T_1 = condenser/melter temperature ^oK
T_2 = reactor operating temperature ^oK
T_o = heat sink temperature ^oK

The first bracketed term represents the primary compression duty. The total differential (T_1-T_2) is made up of four major terms; the temperature differential in the decomposer (T_d-T_c), the freezing point depression of the solution, the temperature driving force for hydrate formation (T_c-T_r) and the temperature differential for evaporation of the refrigerant (T_r-T_1). Of these four a little work has been done on the decomposition process with emphasis on (T_c-T_r) and an evaluation of the freezing point depression. Although the value of (T_r-T_1) has generally exceeded 2^oC in the hydrate runs, a commercial reactor may be operated with only a fraction of this differential, since the heat transfer area varies with operating conditions.

Briggs and Barduhn assumed that with a 5% hold-up of hydrate in saline solution a driving force of 3^oF for growth would be adequate for all hydrate formers. Hence by assuming (T_1-T_2) is constant, the main variable is the work required of the secondary compressor, $Q\ (T_o/T_1)$,

which decreases regularly with increasing formation temperature. The hydrate formers are therefore economically placed in ascending order according to the critical decomposition temperature. The Briggs assumption is, however, disputed on the evidence of section 8.3: The concentration driving force appears to be dependent on the nature of the agent. Apart from th differences due to solubility, the physical constants of the system and the effect of pressure must be accounted for.

For a given hydrate it is clear that a reactor must be operated at the highest temperature that is consistent with a realistic conversion. This involves operating at the highest pressure that allows agent evaporation, and by consequence the pressure effect on the absorption rate is maximised. The stirrer, scaled on the criterion of power per unit volume, should be designed to give a high dissipation of power, preferably in a reactor design that utilises the turbulence generated by the vapour phase. Such a design may comprise a draught tube baffle which increases the flow rate and hence hold-up in such a system. Also the initial distribution of liquid agent as a fine spray will improve the reactor efficiency.

The hold-up of hydrate imposes a limit on the conversion of a single stage reactor. For a given hydrate concentration in the reactor exit line, the conversion may be increased by recycling mother liquor from the separator. Figure 38 shows a recycle system in which the mother liquor is split into a recycle and product stream.

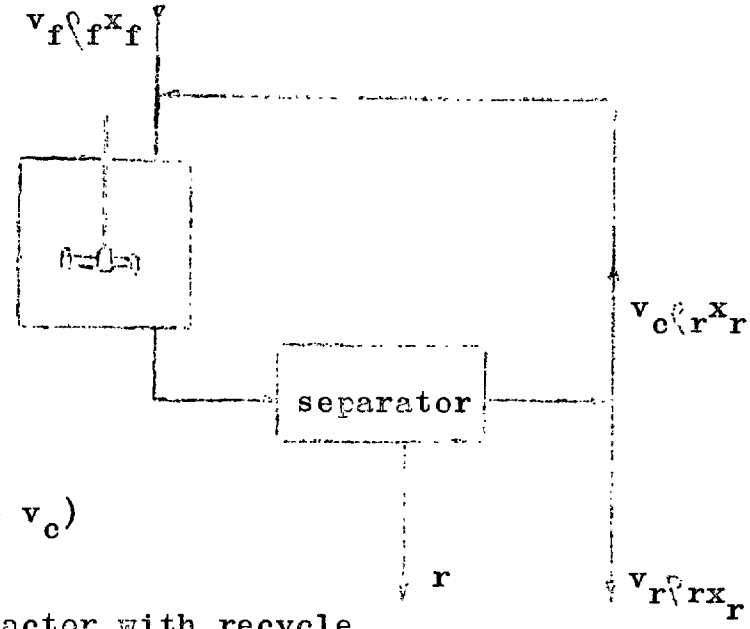


figure 38 Reactor with recycle

As an example, assume that a feedstock containing 4% dissolved solids is to be concentrated to 40% solids. Since the probable limit on hydrate hold-up is 20%, this would require a 14 stage process without liquor recycle (see section 5.6 for definition of over-all conversion). Alternatively, with the same hydrate hold-up and a recycle

of about 2.5 times the feed rate, this concentration effect could be achieved in a 4 stage process with stage conversions of 43%. The optimisation problem is twofold. Firstly, the number of stages is optimised by considering the difference between operating a large number of reactors under progressively lower temperatures (a differential process) and a small number of stages operated with recycle costs at high concentrations in each reactor. Secondly, the best value of ϕ_h and recycle rate must be selected for each reactor: As ϕ_h is increased the operating costs increase since the operating temperature is dependent on the slurry viscosity, but the recycle and separator costs decrease. This optimisation procedure must conform with the policy of separation and subsequent decomposition of the hydrate.

8.6 Recommendations for further work

The future for the hydrate process using Freon-12 rests largely on the evaluation of the effect of the agent on liquid foodstuffs and the human system. Clayton (79) has reviewed the toxicity of members of the fluorocarbon family and, from inhalation tests, it would appear that Freon-12 was the least toxic and least hazard to health of the hydrate formers. There is, however, some dispute

as to its use in aerosol sprays containing foodstuffs, but this may well be due to the possibility of hydrolysis on long term contact or at elevated temperatures, with the unwelcome appearance of phosgene. What is required is a full toxicity test on concentrates stripped of agent to the order of p.p.m.

The construction of a larger plant, scaled by the experimental correlation for the over-all transfer coefficient, and its operation as a single or multistage process with liquor recycle should be the next stage in assessing the feasibility of the hydrate process for concentrating liquid foods.

The basis of the model, the interfacial area of gaseous agent in suspension, is largely dependent upon the effects of agitation and vapour generation within the reactor. Little is known of the relation between turbulence and heat transfer in direct contact systems and a study of this process on a small scale with different refrigerants may give a better indication of the contact areas relevant to the hydrate process. On the other hand, the discrepancies observed with the simpler two phase systems point pessimistically to difficulties with the development of sufficiently general a correlation. The effect of pressure on hydrate formation is certainly one factor which invites further study.

Appendix A Batch hydrate results

A1 Heat and Mass Balance: Sample Calculation

The production rate at T_r quoted in Table II is that estimated from the net cooling rate, equations (57) and (58):

$$r = \frac{Q}{\lambda_{hf}} = \frac{V_t \rho_t c_p}{\lambda_{hf}} \left(\frac{dT}{dt}\right)_{T=T_r}$$

An alternative estimate of the production rate may be derived from the rate of change of the sucrose concentration at the steady temperature T_r. Substituting equation (59) in (55):

$$r = \frac{dy}{dt} = \frac{d}{dt}\left[V_f \rho_f (1 - x_{f/x_t})\right]_{T=T_r}$$

The advantage of calculating the mass transfer from the gradient of the production curve, rather than integrating equation (57) over the total run time, is that any error involved at nucleation, see section 6.13, is discounted.

Example: Run 5.22

Reactor liquid capacity = 3.35 l.

Sucrose concentration = 18.34 w/w %

ρ_l = 1.074 g/cm^3)
c_p = 0.880 cal/g) See G3
λ_{hf} = 90. cal/g. of water as hydrate

Net cooling rate = 1.132 °C/min

$\therefore \dot{Q}$ = 3340 cal/min

$\therefore \dot{r}$ = 37.1 g/min

The value of x_t is given in Table VII, and y_t is calculated from equation (59):

Time mins.	$1 - x_{f/x_t}$	y_t g.
0	0	0
2.	.0389	140.
3.6	.0561	202.
6.0	.0820	294.

The slope of y_t against time at t = 3.2, corresponding to $T=T_r$ is 39.4 g/min.

$\therefore$ by mass balance $\underline{r = 39.4 \text{ g/min.}}$

This checks within 5% of the heat balance estimate. In general the agreement was as good as $\pm 5\%$; if the discrepancy was greater than 10%, the run was rejected from the data analysis. The heat balance figures are not tabulated in Table II, though each run was checked for consistency. A further example of this calculation is shown in Table XVI, Appendix C, which considers a smaller number of runs with propane hydrate.

A2 Condenser Heat Load

During a batch run the heat load on the condenser changed considerably over the period from nucleation of the hydrate phase to the steady operating temperature T_r. Experimentally it was necessary to arrest the flow of

glycol coolant at the onset of nucleation to prevent the reactor pressure falling. The feed was recommenced some thirty seconds afterwards, and adjusted to maintain a constant pressure in the system. The actual variation in the heat load is examined here.

A heat balance on the refrigerating agent may be drawn up on the reactor-condenser cycle. The flow rate of gaseous agent from the reactor is given in equation 5.51 (ii):

$$\text{Return flow rate} = F - r/\alpha'$$

where the same nomenclature is used as before. The heat load on the condenser, Q_c is the sum of the heat required to condense this return flow rate and the heat leak into the system.

$$Q_c = (F - r/\alpha')\lambda_l + K_h$$

For comparative purposes, the heat load is calculated at nucleation and at the condition $T=T_r$.

Run 3.11

$T_c = 10.78$, $T_r = 10.11$, $T_n = 7.43\ ^oC$

$r_r = 54.8$, $r_n = 274$ g/min.

and $F = 170.4$ g/min.

Hence $(Q_c)_n = 2.18$ Kcal/min.

and $(Q_c)_r = 5.20$ Kcal/min.

This magnitude of change in Q_c explains why the condenser coolant flow rate required careful control.

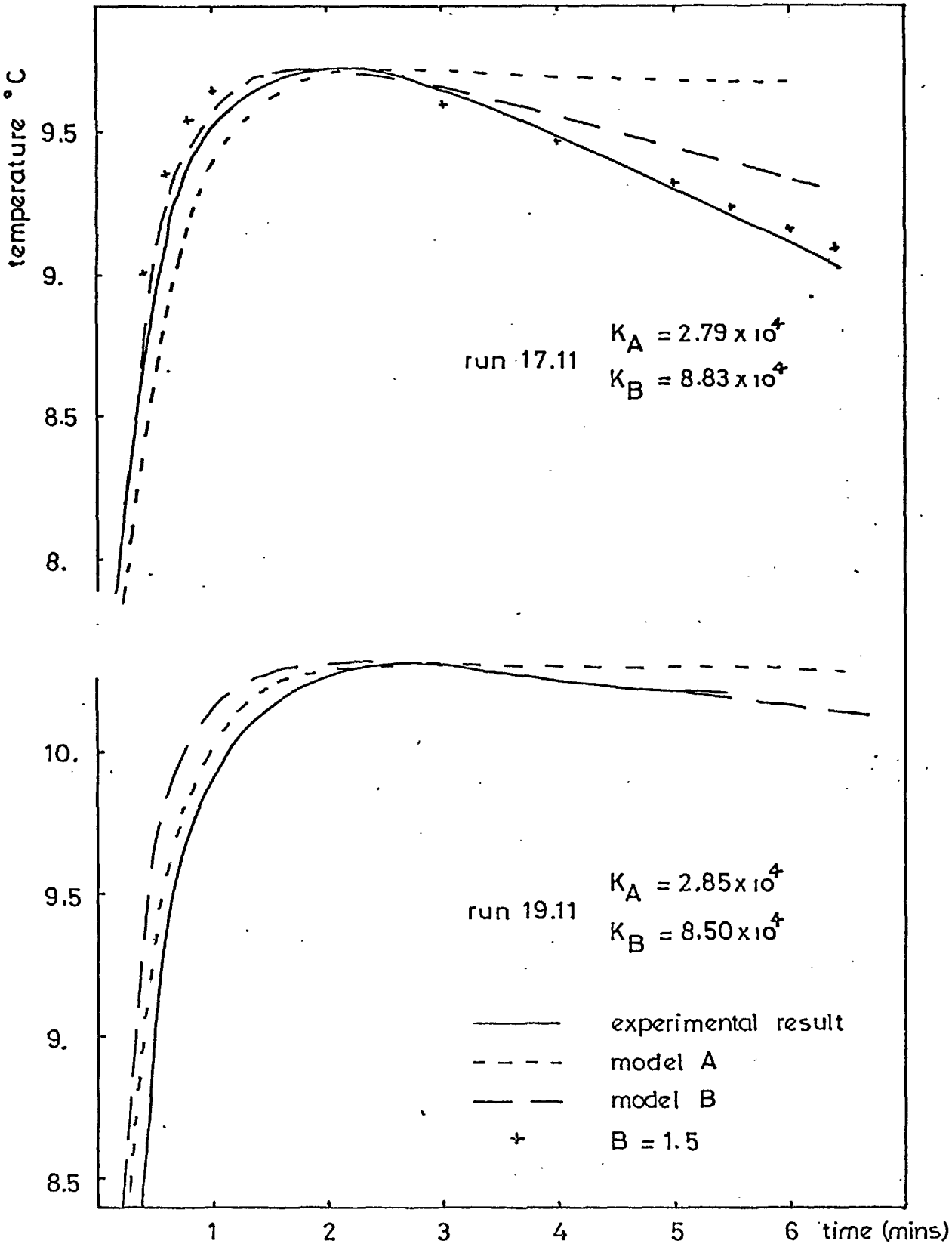


figure A1 Experimental and theoretical temperature profiles

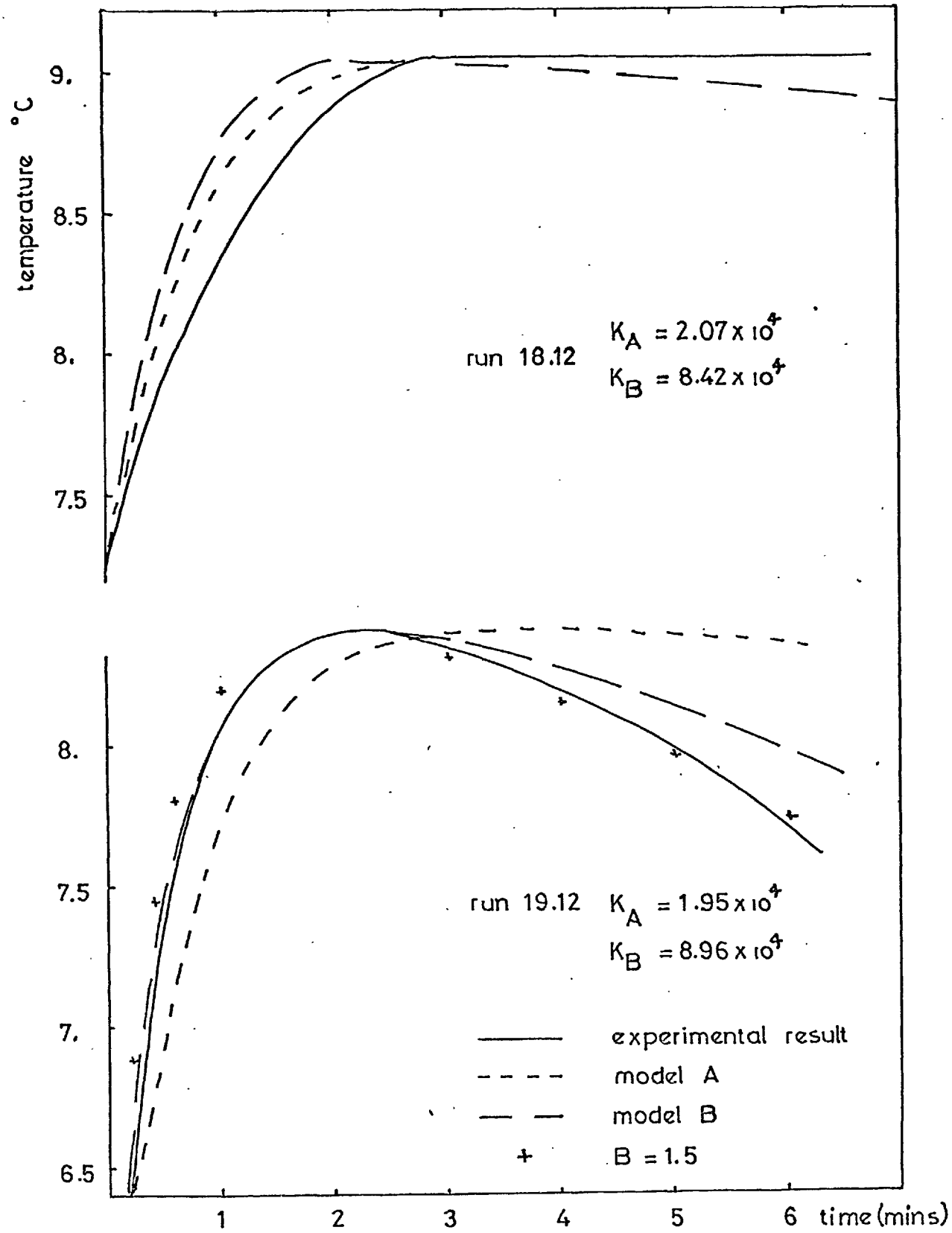


figure A2 Experimental and theoretical temperature profiles

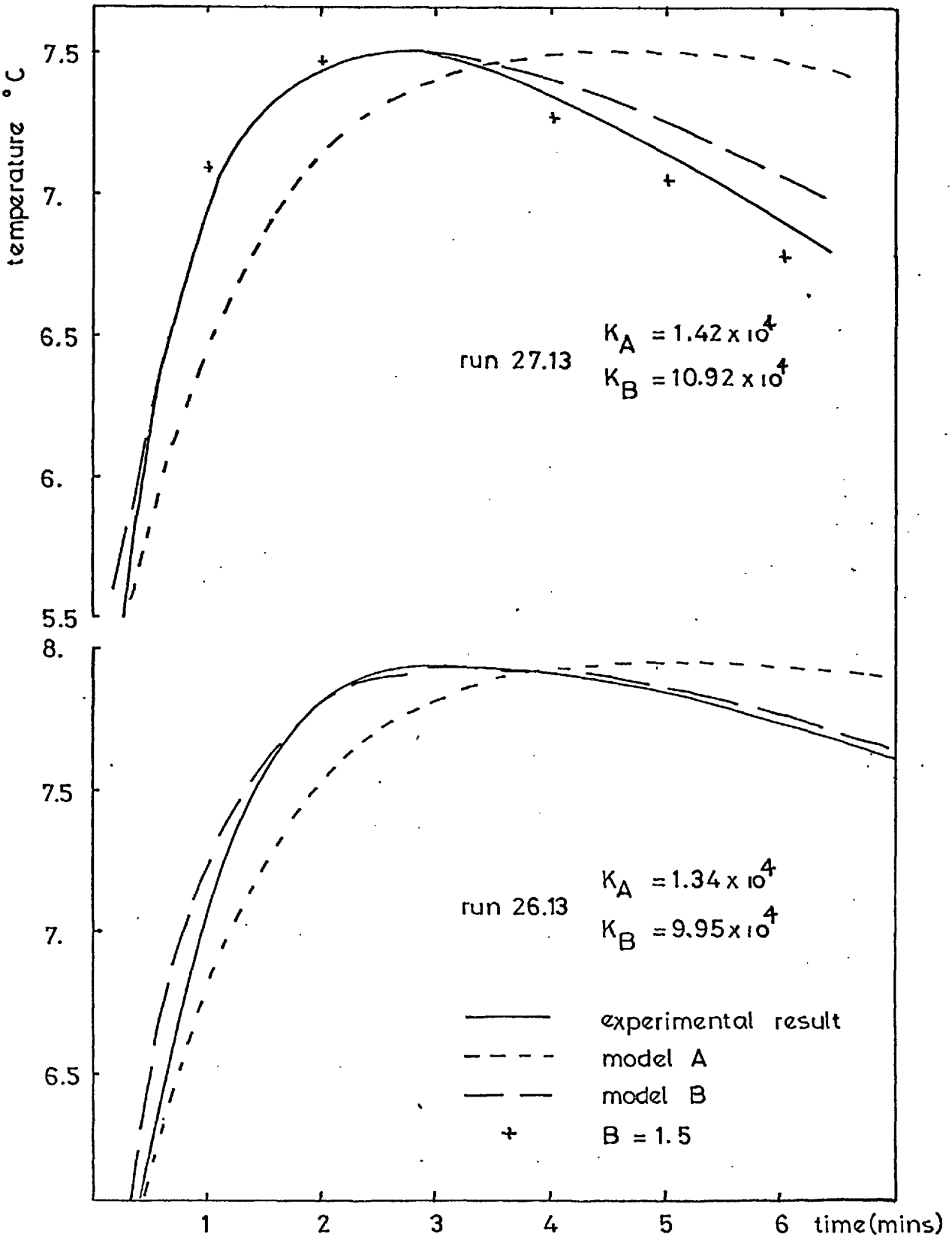


figure A3 Experimental and theoretical temperature profiles

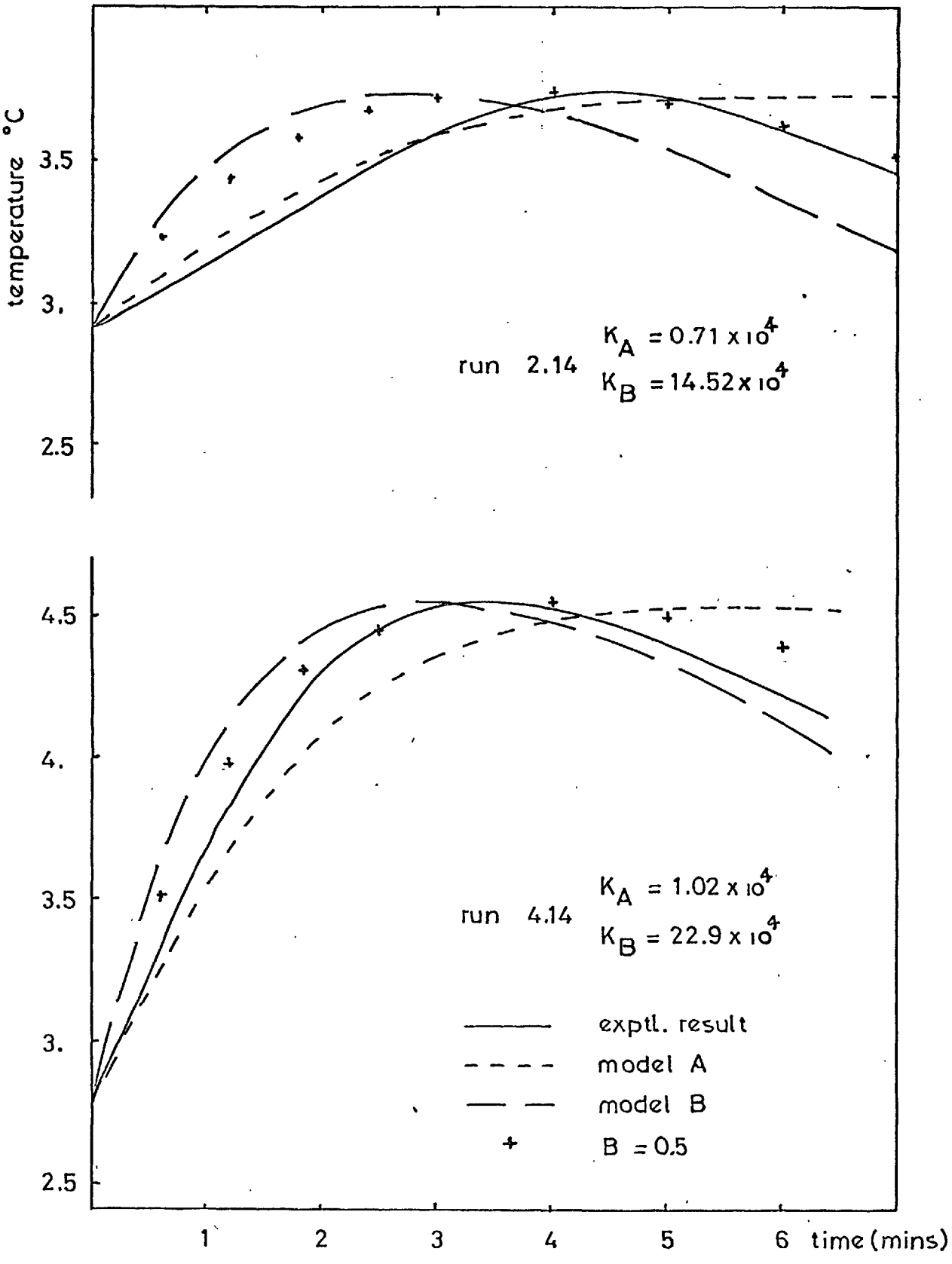


figure A4 Experimental and theoretical temperature profiles

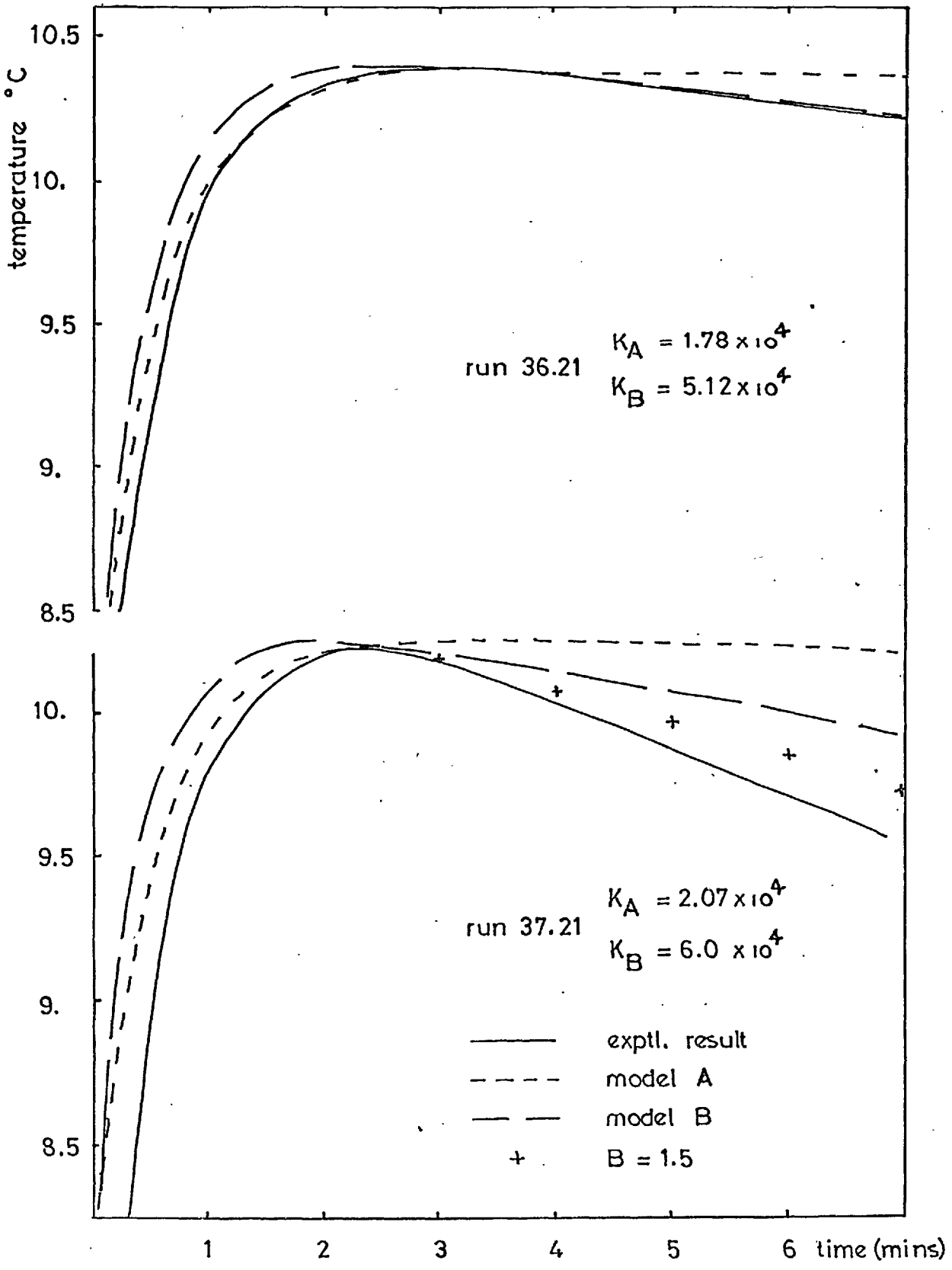


figure A5 Experimental and theoretical temperature profiles

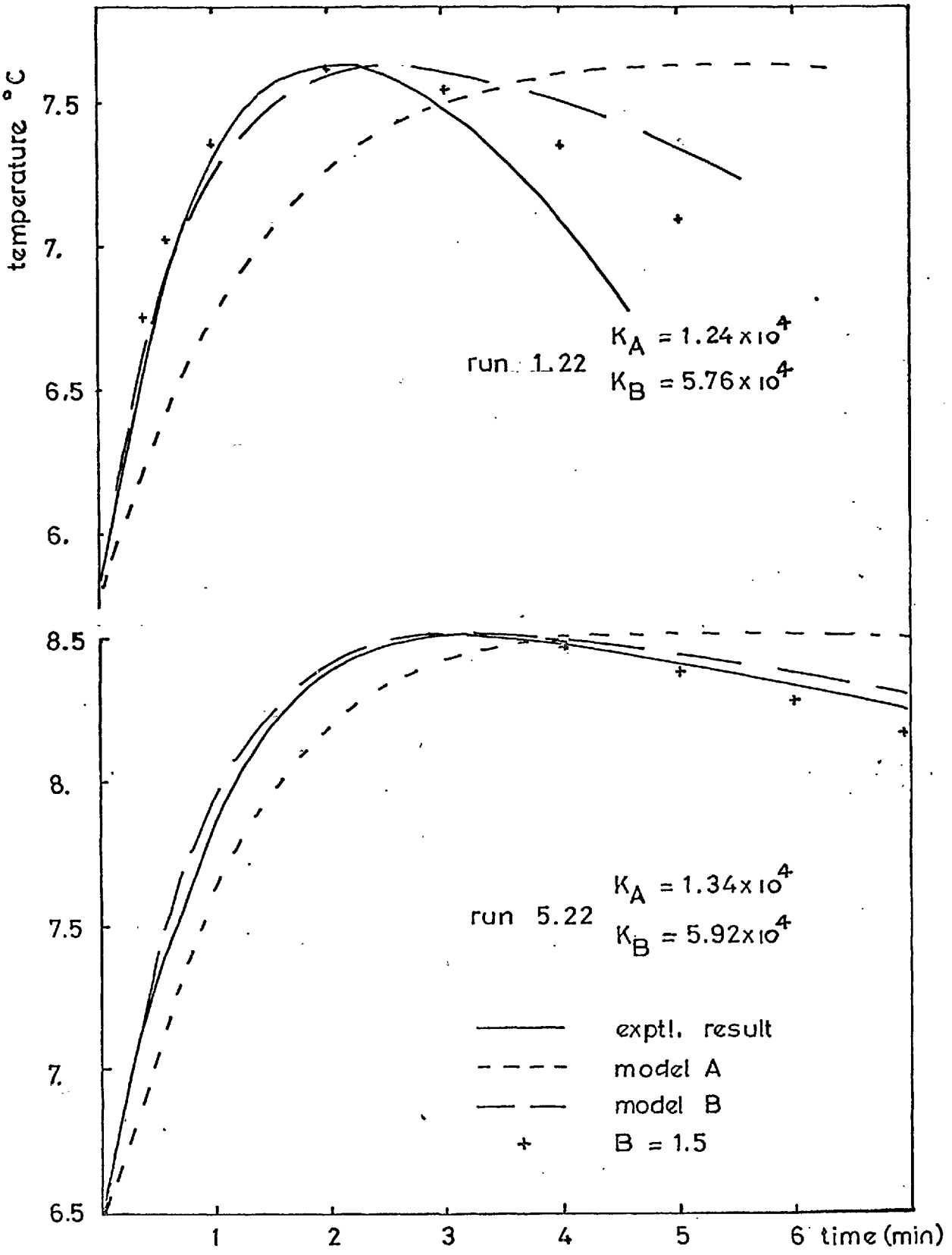


figure A6 Experimental and theoretical temperature profiles

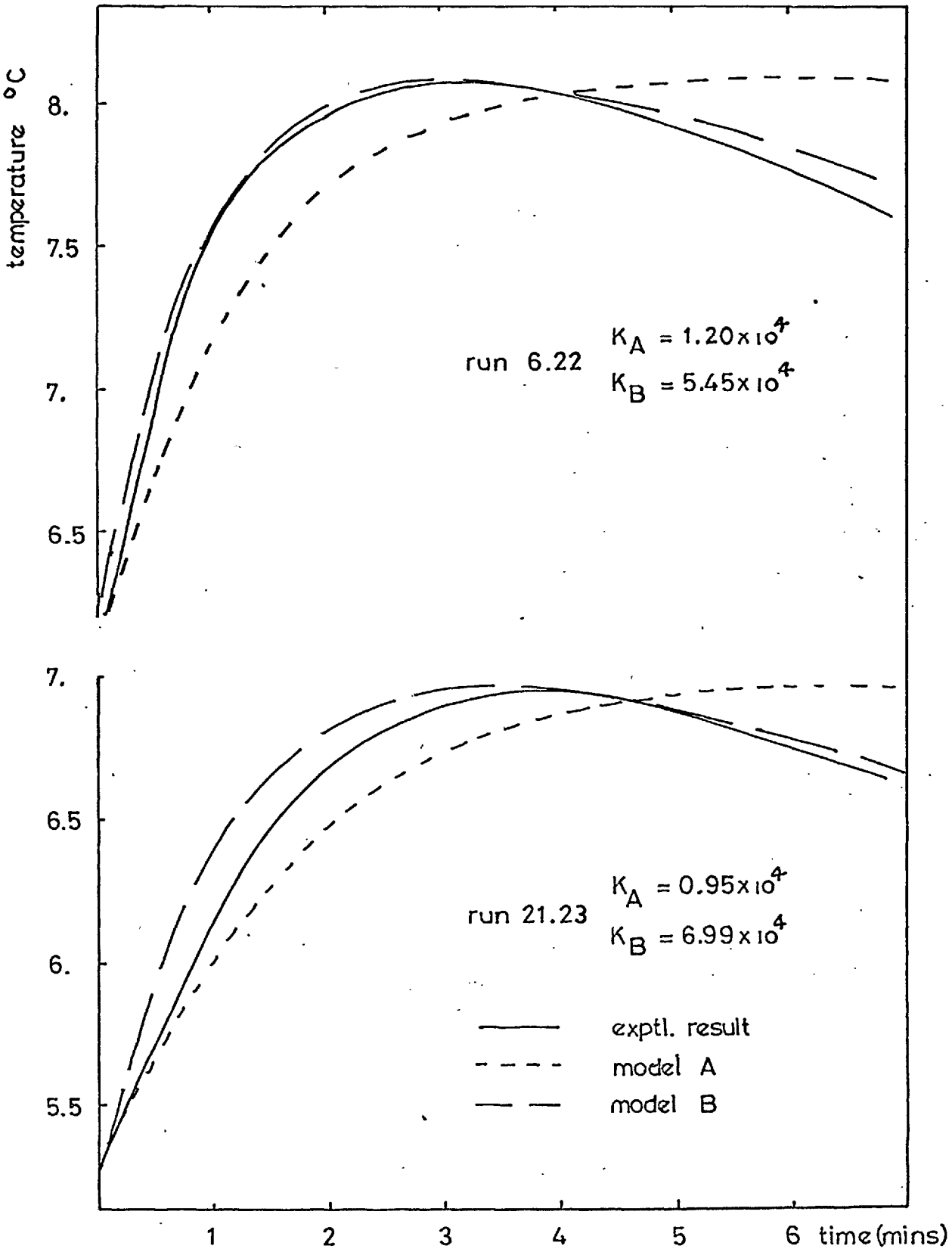


figure A7 Experimental and theoretical temperature profiles

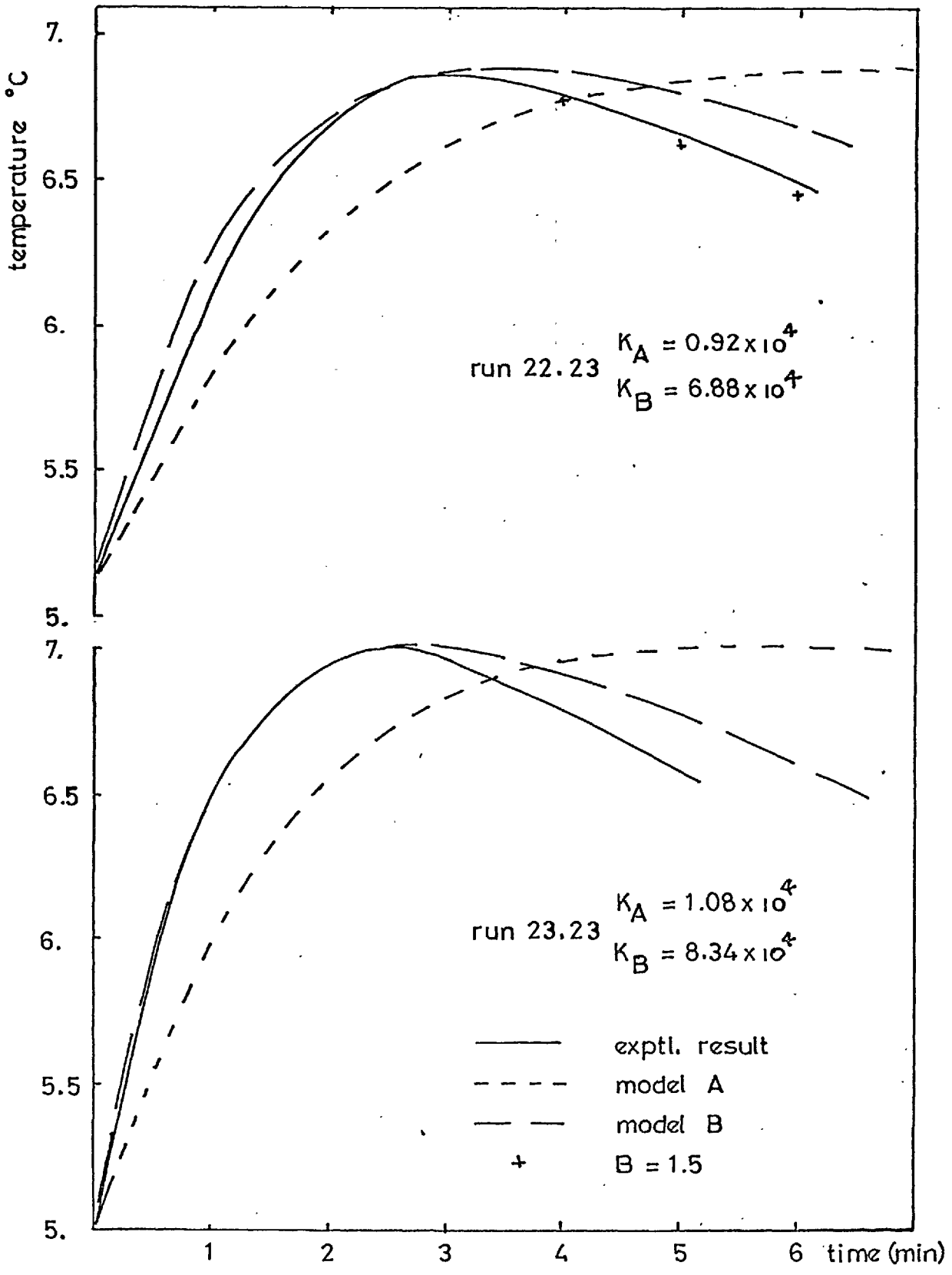


figure A8 Experimental and theoretical temperature profiles

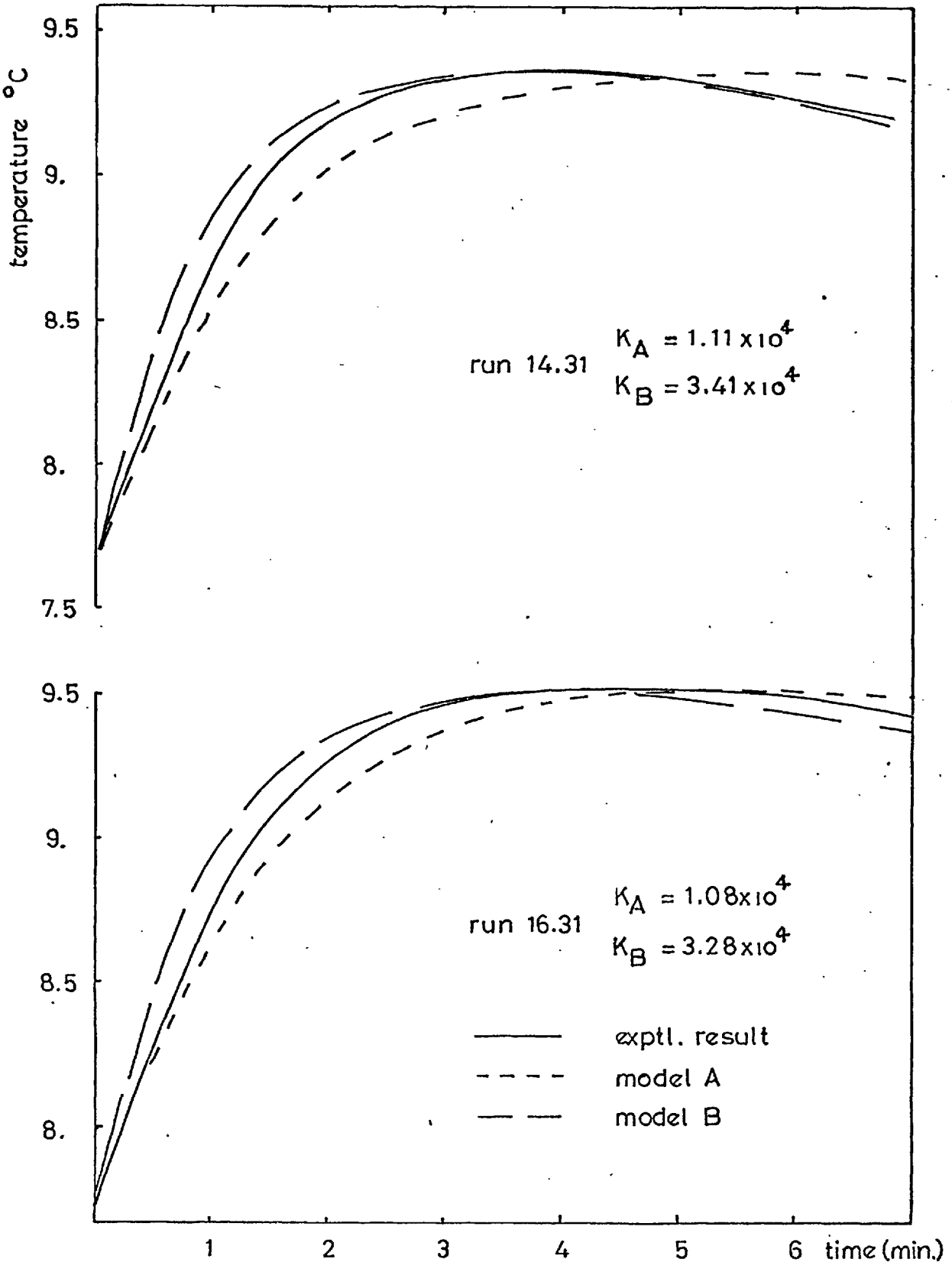


figure A9 Experimental and theoretical temperature profiles

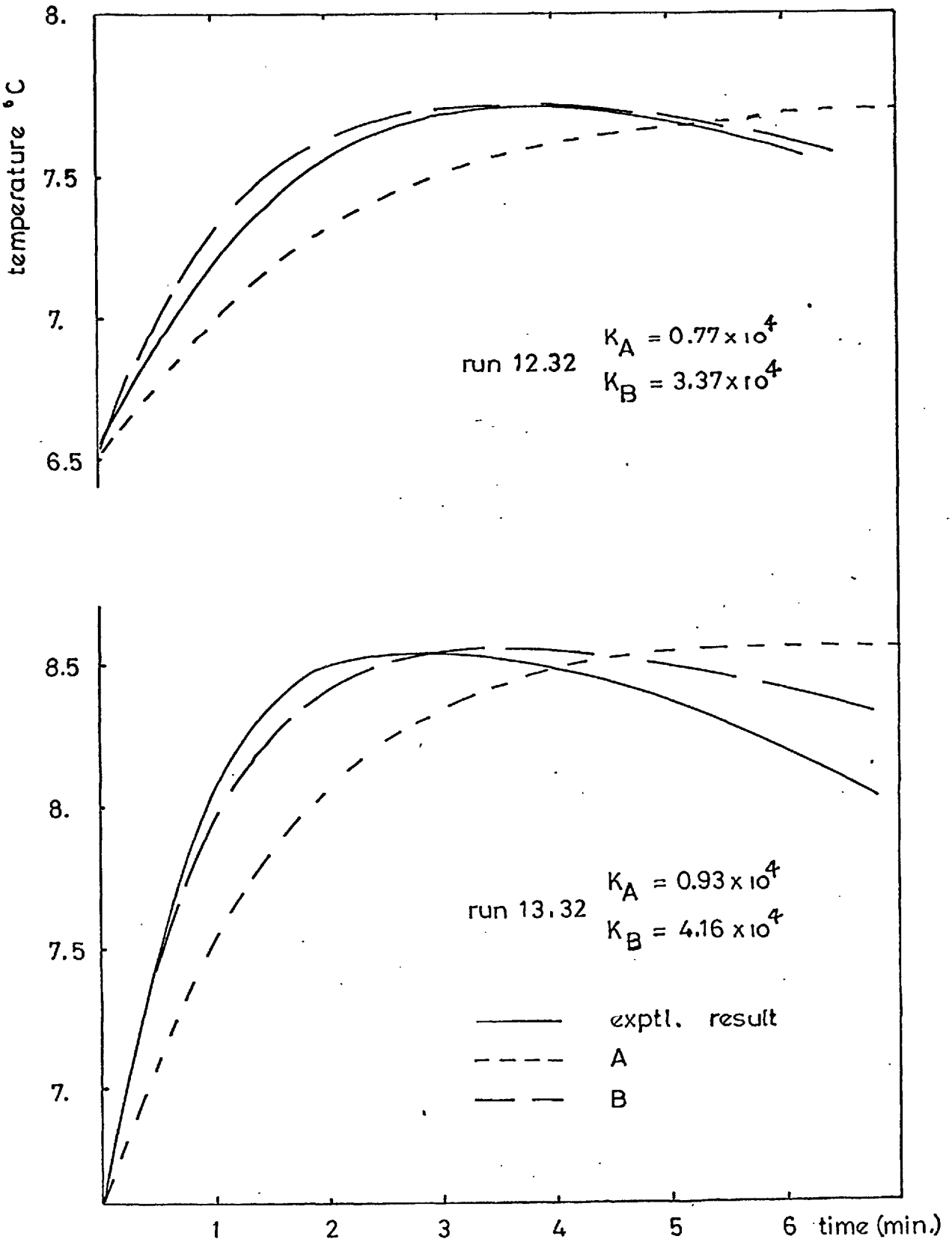


figure A10 Experimental and theoretical temperature profiles

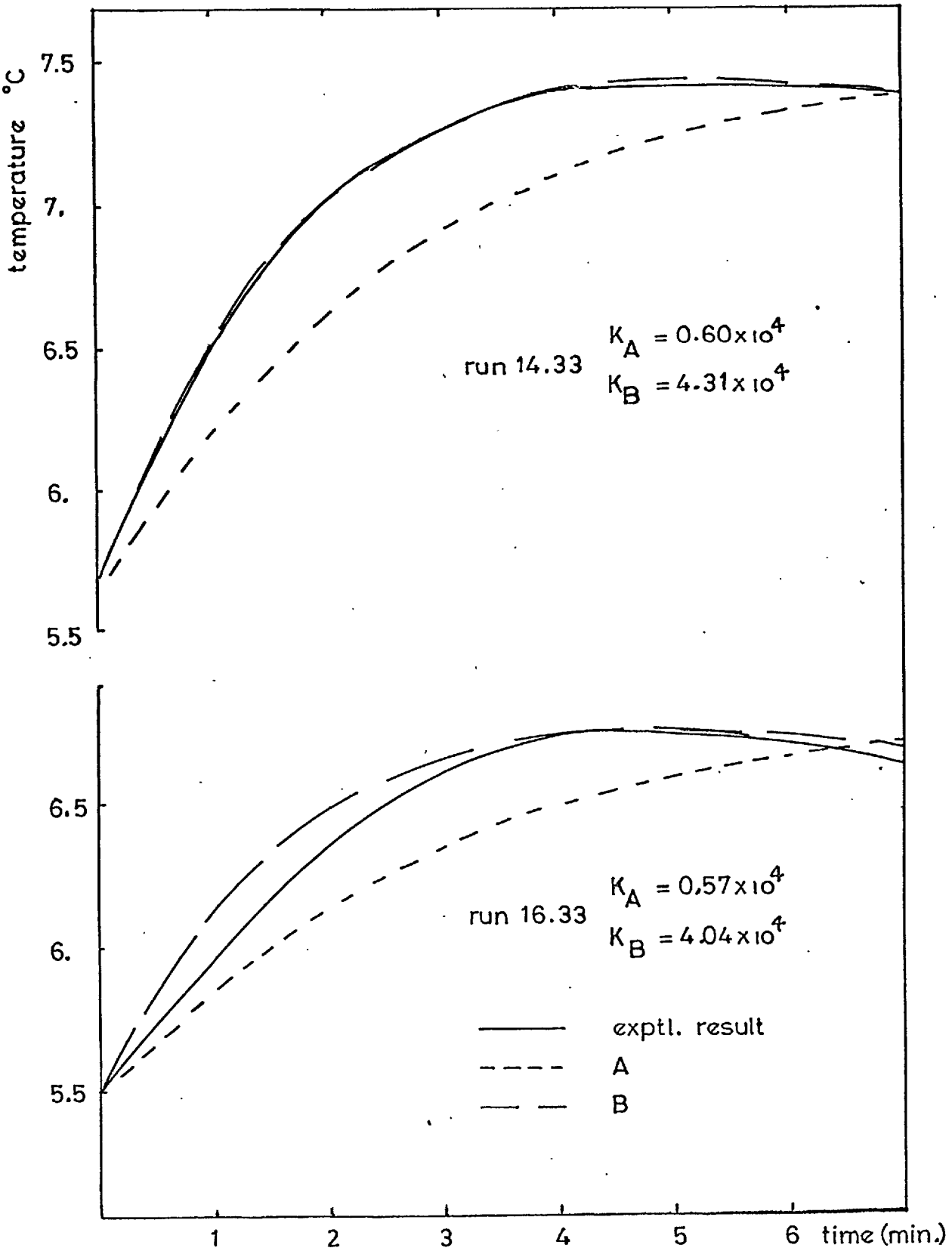


figure A11 Experimental and theoretical temperature profiles

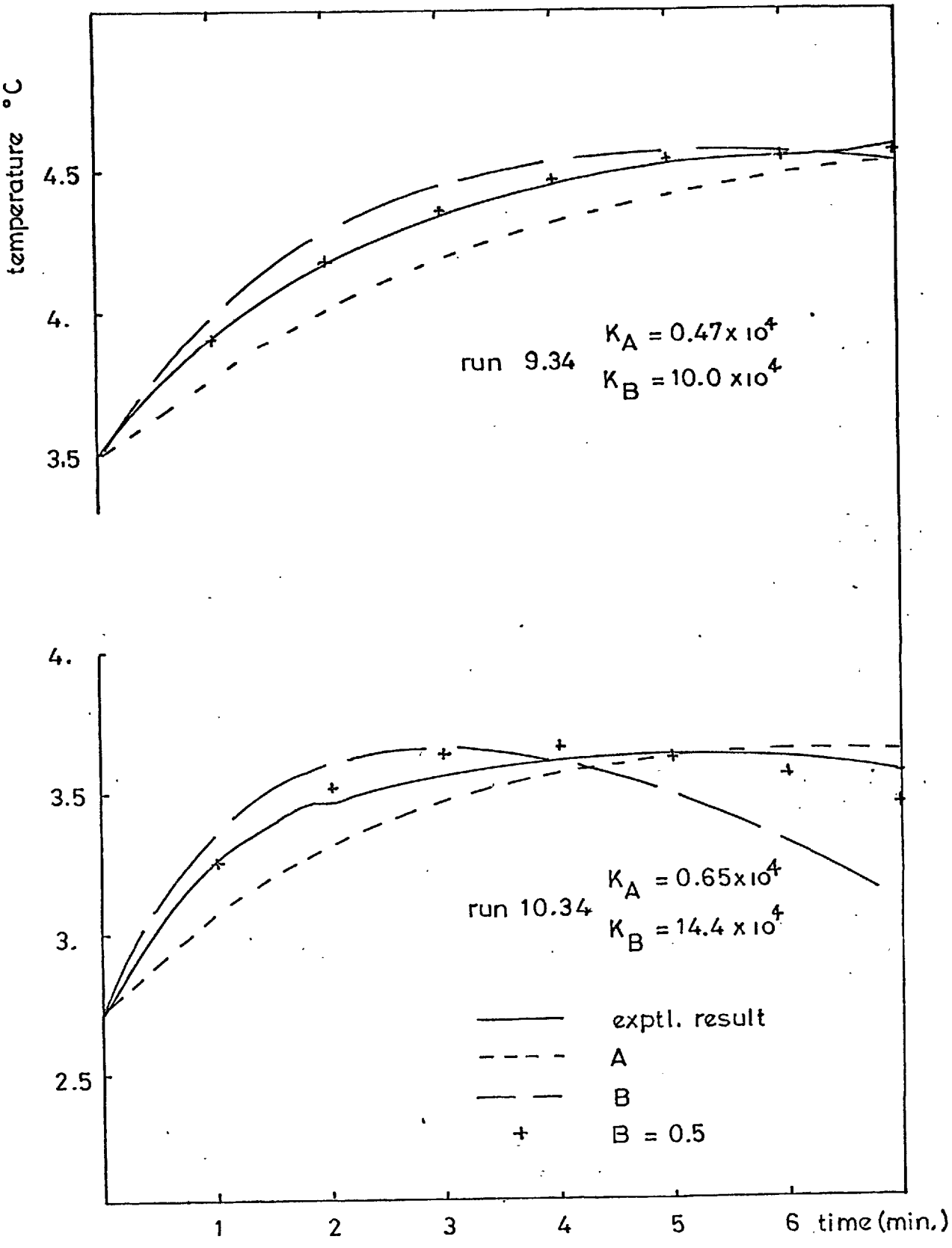


figure A12 Experimental and theoretical temperature profiles

TAPLE I

Summary of batch runs, showing block code and mean production rates

BLOCK NUMBER	N RPM	x_f% (w/w)	SPECIAL FEATURE	$\bar{r}$ g/min	$(\overline{C_b - C_s})$ g.mol/l	$(\overline{T_c - T_r})$ °C	$(\overline{T_r - T_l})$ °C
.10	1420.	0.		43.8	.00172	0.51	4.97
.11	1420.	9.4		40.3	.00151	0.47	3.91
.110	1420.	9.4	Distributor	45.2	.00158	0.50	4.05
.12	1420.	17.5		38.9	.00193	0.69	4.72
.13	1420.	27.5		38.2	.00341	1.54	4.88
.14	1420.	42.0		32.4	.00301	1.84	3.68
.21	1140.	9.4		35.3	.00170	0.54	3.93
.22	1140.	17.5		38.4	.00280	1.04	4.36
.23	1140.	27.0		34.5	.00392	1.80	4.76
.31	880.	9.4		31.7	.00304	1.00	3.75
.310	880.	9.4	Distributor	36.1	.00251	0.80	3.63
.32	880.	17.5		33.6	.00375	1.40	3.98
.33	880.	27.5		29.5	.00530	2.48	3.77
.34	880.	42.5		29.3	.00542	3.43	2.15

V_1 = 3.55 l., initial volume of sucrose = 3.35 l.

TABLE II

Batch runs. 'Steady unsteady-state' data

Run	r	P	N	x_f	T_m	T_r	T_c-T_r	C_b	C_b-C_s	T_r-T_l	ϕ_g	μ_l
	gm/min	psig	rpm	w/w%	°C	°C	°C	x10^3 g.mol/l	x10^3 g.mol/l	°C		cp
1.10	42.9	34.	1420.	0.	8.20	10.11	0.65	15.36	2.02	7.57	0.24	1.31
2.10	42.7	34.	1420.	0.	8.20	10.12	0.64	15.36	1.99	7.58	0.24	1.31
3.10	20.3	34.	1420.	0.	9.04	10.48	0.33	15.13	1.04	7.89	0.24	1.30
4.10	68.8	34.	1420.	0.	7.36	9.83	0.93	15.57	2.85	7.29	0.24	1.32
5.10	20.8	37.	1420.	0.	9.01	10.72	0.31	15.85	1.05	6.26	0.24	1.29
6.10	43.1	37.	1420.	0.	8.23	10.53	0.51	15.99	1.67	6.07	0.24	1.30
7.10	67.6	37.	1420.	0.	7.71	10.18	0.85	16.26	2.76	5.72	0.24	1.31
8.10	70.1	40.	1420.	0.	7.73	10.49	0.80	16.95	2.72	4.23	0.24	1.30
9.10	21.4	40.	1420.	0.	9.37	11.04	0.25	16.52	0.89	4.78	0.24	1.28
10.10	45.1	40.	1420.	0.	8.32	10.87	0.43	16.66	1.48	4.60	0.24	1.29
11.10	21.6	43.	1420.	0.	8.87	11.23	0.21	17.20	0.77	3.36	0.24	1.27
12.10	42.5	43.	1420.	0.	8.14	11.16	0.38	17.34	1.39	3.18	0.24	1.28
13.10	68.6	40.	1420.	0.	7.97	10.53	0.77	16.92	2.61	4.27	0.24	1.30
14.10	65.3	43.	1420.	0.	8.06	10.91	0.63	17.54	2.23	2.93	0.24	1.29
16.10	19.8	46.	1420.	0.	9.33	11.56	0.21	17.90	0.80	1.97	0.24	1.27
17.10	40.6	46.	1420.	0.	9.13	11.45	0.33	17.99	1.23	1.85	0.24	1.27
1.11	38.3	40.	1420.	9.37	7.68	10.40	0.38	15.40	1.22	4.14	0.24	1.74
2.11	43.2	40.	1420.	9.40	7.62	10.30	0.48	15.47	1.54	4.03	0.24	1.75
3.11	54.8	40.	1420.	9.40	7.43	10.11	0.67	15.60	2.10	3.85	0.24	1.76
4.11	21.4	40.	1420.	9.44	8.78	10.52	0.26	15.31	0.84	4.26	0.24	1.74
5.11	68.1	40.	1420.	9.40	7.33	10.00	0.78	15.69	2.45	3.73	0.24	1.76
6.11	44.4	40.	1420.	9.43	7.36	10.23	0.55	15.52	1.75	3.97	0.24	1.75
7.11	31.7	37.	1420.	9.43	7.65	10.06	0.46	14.79	1.43	5.30	0.24	1.76
8.11	54.5	37.	1420.	9.41	6.81	9.71	0.91	15.03	2.44	5.25	0.24	1.78

.../

TABLE II (continued)

Run	r	P	N	x_f	T_L	T_r	$T_c - T_r$	C_b	$C_b - C_s$	$T_r - T_l$	ϕ_g	ϕ_l
	cm/min	psig	rpm	m/m	°C	°C	°C	x10^3 g.mol/l	x10^3 g.mol/l	°C		°C
10.11	43.5	37.	1420.	9.40	7.20	9.81	0.61	14.89	1.85	5.45	0.24	1.77
11.11	71.1	43.	1420.	9.42	7.04	10.82	0.71	16.20	2.32	5.34	0.24	1.75
12.11	28.3	43.	1420.	9.42	7.91	10.72	0.30	16.00	1.02	2.75	0.24	1.73
13.11	50.7	43.	1420.	9.41	7.10	10.59	0.51	16.15	1.68	2.55	0.24	1.74
14.11	19.0	43.	1420.	9.46	8.32	10.78	0.25	15.96	0.83	2.81	0.24	1.72
15.11	40.0	43.	1420.	9.42	7.85	10.58	0.45	16.11	1.49	2.61	0.24	1.73
16.11	10.3	37.	1420.	9.64	8.21	10.23	0.27	14.62	0.84	5.77	0.24	1.77
17.11	65.2	37.	1420.	9.66	6.91	9.72	0.72	14.97	2.35	5.26	0.24	1.79
18.11	19.1	40.	1420.	9.67	8.81	10.53	0.28	15.25	0.75	4.27	0.24	1.75
19.11	41.6	40.	1420.	9.66	7.57	10.32	0.44	15.41	1.42	4.05	0.24	1.76
20.11	18.1	43.	1420.	9.68	8.18	10.79	0.22	15.89	0.78	2.82	0.24	1.74
21.11	39.8	43.	1420.	9.66	7.94	10.66	0.34	15.99	1.14	2.69	0.24	1.75
1.110	20.7	37.	1420.	9.37	9.19	10.21	0.81	14.68	0.96	5.75	0.24	1.75
2.110	68.1	37.	1420.	9.34	8.17	9.82	0.70	14.95	2.10	5.37	0.24	1.77
3.110	55.0	37.	1420.	9.37	8.29	9.97	0.55	14.85	1.38	5.51	0.24	1.76
4.110	36.7	37.	1420.	9.38	8.72	10.09	0.44	14.77	1.34	5.39	0.24	1.76
5.110	69.1	40.	1420.	9.47	8.11	10.09	0.69	15.69	2.19	3.82	0.24	1.76
6.110	36.7	40.	1420.	9.47	8.69	10.33	0.45	15.45	1.45	4.06	0.24	1.75
7.110	52.9	40.	1420.	9.47	8.20	10.21	0.57	15.53	1.81	3.95	0.24	1.75
8.110	21.6	40.	1420.	9.47	9.32	10.48	0.35	15.37	1.12	4.17	0.24	1.74
9.110	37.8	43.	1420.	9.37	8.29	10.64	0.39	16.06	1.31	2.66	0.24	1.73
10.110	54.0	43.	1420.	9.35	8.23	10.50	0.52	16.17	1.74	2.53	0.24	1.74
11.110	69.1	43.	1420.	9.37	8.00	10.33	0.70	16.30	2.30	2.35	0.24	1.75
12.110	20.5	43.	1420.	9.37	9.16	10.72	0.30	16.00	1.02	2.75	0.24	1.73

.../

TABLE II (continued)

Run	r	P	N	x_f	T_n	T_r	T_c-T_r	C_b	C_b-C_s	T_r-T_l	ϕ_g	η_l
	gm/min	psig	rpm	w/w%	°C	°C	°C	x10^3 g.mol/l	x10^3 g.mol/l	°C		cp
1.12	38.3	37.	1420.	17.48	6.67	9.30	0.64	13.81	1.80	4.84	0.19	2.44
2.12	53.2	37.	1420.	17.48	5.54	8.81	1.14	14.16	3.12	4.35	0.19	2.47
3.12	59.8	37.	1420.	17.44	6.11	8.84	1.11	14.13	3.08	4.38	0.19	2.47
4.12	38.3	37.	1420.	17.48	6.30	9.19	0.76	13.90	2.13	4.73	0.19	2.44
5.12	48.9	34.	1420.	17.43	6.17	8.69	0.98	13.41	2.58	6.15	0.19	2.48
6.12	38.8	34.	1420.	17.45	6.14	8.94	0.73	13.24	1.95	6.39	0.19	2.47
8.12	21.2	34.	1420.	17.53	7.16	9.30	0.38	13.05	1.05	6.76	0.19	2.42
9.12	23.7	37.	1420.	17.53	6.96	9.52	0.44	13.71	1.26	5.06	0.19	2.40
10.12	55.0	40.	1420.	17.50	6.38	9.27	0.93	14.60	2.68	3.01	0.19	2.44
11.12	47.4	40.	1420.	17.48	6.61	9.48	0.78	14.54	2.28	3.16	0.19	2.42
12.12	38.5	40.	1420.	17.50	6.15	9.59	0.62	14.43	1.89	3.38	0.19	2.41
13.12	29.3	40.	1420.	17.55	6.41	9.75	0.47	14.34	1.38	3.48	0.19	2.39
14.12	21.2	40.	1420.	17.47	6.98	9.91	0.31	14.24	0.92	3.35	0.19	2.37
15.12	38.8	40.	1420.	17.46	6.64	9.65	0.54	14.35	1.60	3.39	0.19	2.42
18.12	31.0	34.	1420.	18.49	7.10	9.05	0.55	13.99	1.46	6.51	0.19	2.56
19.12	58.6	34.	1420.	18.38	5.85	8.40	1.19	13.39	3.07	5.86	0.19	2.61
20.12	18.0	37.	1420.	18.37	7.53	9.65	0.92	13.41	0.64	5.19	0.19	2.51
7.13	30.9	34.	1420.	27.52	4.78	7.16	1.71	12.33	3.83	4.61	0.19	4.29
8.13	25.1	34.	1420.	27.52	5.68	7.78	1.06	11.89	2.45	5.23	0.19	4.28
10.13	44.5	34.	1420.	27.52	4.41	6.96	1.88	12.38	4.16	4.41	0.19	4.40
11.13	44.6	37.	1420.	27.52	4.35	7.39	1.75	12.92	4.08	2.93	0.19	4.27
12.13	31.3	37.	1420.	27.52	5.39	7.91	1.22	12.60	2.94	3.45	0.19	4.19
14.13	25.2	37.	1420.	27.52	5.77	8.18	0.96	12.45	2.34	3.72	0.19	4.14
15.13	58.0	34.	1420.	27.47	4.55	6.38	2.47	12.73	5.39	3.83	0.19	4.49
16.13	44.8	31.	1420.	27.49	4.93	6.67	1.88	11.77	3.95	6.16	0.19	4.46
17.13	31.8	31.	1420.	27.60	5.16	7.10	1.45	11.55	3.13	6.59	0.19	4.36

.../

TABLE II (continued)

Run	r	P	n	x_f	T_f	T_r	T_e-T_r	C_b x10^2	C_c-C_s x10^3	T_r-T_l	ϕ_s	μ_l
	gr/min	psig	rpm	w/w%	°C	°C	°C	g.mol/l	g.mol/l	°C		cp
18.13	25.1	31.	1420.	27.59	5.65	7.41	1.14	11.40	2.51	6.92	0.19	4.26
19.13	38.3	31.	1420.	27.64	4.81	6.96	1.59	11.60	3.39	6.45	0.19	4.41
20.13	72.1	34.	1420.	27.64	4.12	6.03	2.83	12.98	5.97	3.48	0.19	4.50
21.13	57.5	31.	1420.	27.64	4.23	5.86	2.70	12.27	5.45	5.35	0.19	4.55
22.13	35.3	34.	1420.	27.64	5.33	7.24	1.62	12.28	3.35	4.70	0.19	4.27
23.13	16.8	31.	1420.	27.74	6.10	7.89	0.66	11.11	1.48	7.38	0.19	4.25
24.13	14.3	34.	1420.	27.64	6.67	8.36	0.48	11.58	1.16	8.81	0.19	4.18
25.13	58.8	31.	1420.	27.64	4.59	6.35	2.20	11.96	4.55	5.84	0.19	4.50
26.13	38.4	37.	1420.	27.74	5.23	7.94	1.17	12.54	2.83	3.48	0.19	4.24
27.13	51.8	37.	1420.	27.67	4.88	7.49	1.63	12.81	3.82	3.03	0.19	4.31
28.13	16.1	34.	1420.	27.70	6.40	8.61	0.51	12.15	1.27	4.15	0.19	4.14
1.14	46.2	31.	1420.	41.78	2.96	4.09	2.40	9.55	3.88	3.58	0.15	15.59
2.14	33.0	31.	1420.	41.89	2.90	3.74	2.74	9.71	4.37	3.23	0.15	15.86
3.14	29.1	34.	1420.	41.89	3.42	5.19	1.59	9.65	2.82	2.64	0.15	14.78
4.14	39.3	34.	1420.	42.01	2.75	4.55	2.23	9.95	3.82	2.01	0.15	15.25
5.14	18.9	34.	1420.	42.01	3.97	6.17	0.60	9.20	1.13	3.63	0.15	14.09
6.14	40.4	28.	1420.	42.65	2.26	3.08	3.20	9.59	4.81	4.00	0.15	16.38
7.14	32.4	28.	1420.	42.75	2.59	4.09	2.19	9.13	3.46	5.01	0.15	15.59
8.14	14.3	31.	1420.	42.59	4.09	6.03	0.46	8.69	1.82	5.52	0.15	14.19
9.14	48.4	31.	1420.	42.52	2.26	3.68	2.80	9.74	4.45	3.17	0.15	15.91
10.14	35.8	28.	1420.	42.67	2.96	3.83	2.45	9.25	3.82	4.75	0.15	15.79
11.14	28.8	31.	1420.	42.64	3.51	5.28	1.20	9.31	2.07	4.77	0.15	14.71
12.14	51.3	34.	1420.	42.81	2.52	4.52	2.25	9.96	3.86	1.98	0.15	15.27
13.14	12.6	34.	1420.	42.84	4.38	6.56	0.22	9.03	0.41	4.01	0.15	15.82
14.14	21.1	34.	1420.	42.79	3.88	5.88	0.89	9.33	1.65	3.34	0.15	14.29
15.14	38.7	31.	1420.	42.58	2.90	4.14	2.34	9.58	3.80	3.63	0.15	15.55

.../

TABLE II (continued)

Run	F	P	N	x_f	T_p	T_r	T_c-T_r	C_b	C_k-C_s	T_r-T_l	ϕ_g	η_l
	g./min	psig	rpm	%/%	°C	°C	°C	x10^3 g.mol/l	x10^3 g.mol/l	°C		cp
5.21	47.4	43.	1140.	9.14	7.48	10.29	0.73	16.31	2.40	2.32	0.18	1.75
6.21	33.3	42.	1140.	9.14	7.80	10.52	0.52	16.19	1.73	2.55	0.18	1.73
9.21	47.2	37.	1140.	9.14	7.16	9.85	0.68	14.96	2.08	5.40	0.18	1.76
10.21	36.3	31.	1140.	9.14	7.51	10.00	0.53	14.85	1.32	5.54	0.18	1.76
11.21	33.2	40.	1140.	9.14	8.04	10.40	0.40	15.46	1.29	4.14	0.18	1.72
15.21	47.4	40.	1140.	9.25	7.20	10.03	0.77	15.70	2.41	3.76	0.18	1.75
18.21	41.9	37.	1140.	9.20	7.30	9.89	0.63	14.91	1.92	5.43	0.18	1.77
21.21	40.6	4 .	1140.	9.21	7.33	10.09	0.68	15.60	2.14	3.83	0.18	1.76
22.21	35.8	40.	1140.	9.19	7.07	10.27	0.51	15.50	1.64	4.01	0.18	1.75
23.21	30.8	43.	1140.	9.20	8.15	10.64	0.38	16.04	1.27	2.66	0.18	1.74
25.21	33.5	43.	1140.	9.22	7.30	10.56	0.46	16.09	1.52	2.59	0.18	1.74
26.21	44.4	47.	1140.	9.20	6.75	9.89	0.88	15.75	2.75	3.63	0.18	1.77
28.21	33.3	37.	1140.	9.22	7.36	9.85	0.66	14.91	2.00	5.40	0.18	1.78
31.21	18.4	31.	1140.	9.67	8.30	10.49	0.27	15.28	0.87	4.23	0.18	1.76
32.21	21.0	37.	1140.	9.68	8.29	10.20	0.80	14.64	0.93	5.74	0.18	1.77
33.21	20.6	40.	1140.	9.65	8.40	10.49	0.27	15.28	0.87	4.23	0.18	1.76
34.21	28.0	37.	1140.	9.65	8.07	10.09	0.41	14.71	1.25	5.64	0.18	1.78
35.21	20.2	43.	1140.	9.67	8.55	10.73	0.27	15.94	0.92	2.76	0.18	1.74
36.21	36.3	43.	1140.	9.67	7.73	10.40	0.60	16.18	1.99	2.43	0.18	1.76
37.21	51.2	43.	1140.	9.69	7.42	10.26	0.75	16.29	2.45	2.29	0.18	1.77

.../

TABLE II (continued)

Run	r	P	N	x_f	T_c	T_r	T_c-T_r	C_b	C_b-C_s	T_r-T_l	ϕ_g	η_l
	gm/min	psig	rpm	w/w%	°C	°C	°C	x10^3 g.mol/l	x10^3 g.mol/l	°C		cp
1.22	58.3	34.	1140.	18.36	5.74	7.62	1.98	13.92	4.88	5.68	0.14	2.67
2.22	28.1	34.	1140.	18.35	8.87	9.64	0.77	13.14	2.09	6.29	0.14	2.57
3.22	21.4	37.	1140.	18.33	7.45	9.40	0.48	13.58	1.35	4.94	0.14	2.52
4.22	20.8	34.	1140.	18.34	7.74	9.07	0.54	13.00	1.43	6.53	0.14	2.55
5.22	37.1	34.	1140.	18.34	6.35	8.52	1.09	13.34	2.81	5.98	0.14	2.59
6.22	45.7	34.	1140.	18.35	6.14	8.07	1.54	10.63	3.88	5.52	0.14	2.63
7.22	35.1	37.	1140.	18.33	6.55	8.87	1.01	13.92	2.76	4.41	0.14	2.56
8.22	43.8	37.	1140.	18.33	6.32	8.52	1.36	14.18	3.63	4.08	0.14	2.59
9.22	18.5	40.	1140.	18.36	7.43	9.78	0.36	14.12	1.08	3.51	0.14	2.49
10.22	45.3	40.	1140.	18.34	6.58	9.04	1.10	14.62	3.11	2.78	0.14	2.55
21.22	23.8	40.	1140.	16.82	6.96	9.65	0.59	14.47	1.74	3.39	0.14	2.36
25.22	58.0	40.	1140.	18.97	6.26	8.26	1.98	15.45	5.41	2.00	0.14	2.47
30.22	29.8	40.	1140.	16.97	7.56	9.85	0.37	14.30	1.11	3.59	0.14	2.37
31.22	29.3	40.	1140.	16.99	6.96	9.43	0.81	14.61	2.36	3.15	0.14	2.39
34.22	56.5	37.	1140.	17.11	6.40	8.32	1.65	14.52	4.37	3.86	0.14	2.49
37.22	47.4	37.	1140.	16.98	6.29	8.38	1.58	14.47	4.22	3.92	0.14	2.49
38.22	25.5	37.	1140.	16.96	7.07	9.48	0.51	13.81	1.45	5.02	0.14	2.37
39.22	41.8	37.	1140.	16.96	6.40	8.88	1.10	14.17	3.01	4.42	0.14	2.43
2.23	45.4	34.	1140.	26.96	4.64	6.30	2.59	12.91	5.57	3.75	0.14	4.36
3.23	40.6	34.	1140.	26.96	5.22	6.78	2.11	12.61	4.65	4.24	0.14	4.28
4.23	50.7	34.	1140.	26.96	4.46	6.14	2.75	13.00	5.85	3.60	0.14	4.38
5.23	34.6	34.	1140.	26.96	5.27	7.10	1.79	12.42	4.01	4.56	0.14	4.23
6.23	28.5	34.	1140.	26.96	5.82	7.54	1.35	12.16	3.09	5.00	0.14	4.16
7.23	28.5	32.	1140.	26.96	5.51	7.28	1.44	11.86	3.18	5.94	0.14	4.20
8.23	36.2	31.	1140.	26.96	5.11	6.67	1.94	11.90	4.09	6.16	0.14	4.30
9.23	40.6	31.	1140.	26.96	4.93	6.29	2.31	12.12	4.79	5.78	0.14	4.26

.../

TABLE II (continued)

Run	F	P	N	x_f	T_n	T_r	T_c-T_r	C_b	C_b-C_s	T_r-T_l	ϕ_g	η_l
	gm/min	psig	rpm	w/w%	oC	oC	oC	x10^3 g.mol/l	x10^3 g.mol/l	oC		cp
11.23	50.7	31.	1140.	28.96	4.23	5.39	3.21	12.65	6.36	4.88	0.14	4.51
12.23	19.4	31.	1140.	28.96	5.65	7.59	1.01	11.38	2.24	7.08	0.14	4.15
13.23	39.6	31.	1140.	26.96	5.01	6.46	2.14	12.02	4.47	5.95	0.14	4.33
14.23	41.7	37.	1140.	28.96	4.58	7.22	1.95	13.11	4.54	2.76	0.14	4.21
15.23	31.8	37.	1140.	28.96	4.87	7.74	1.43	12.79	3.42	3.28	0.14	4.13
16.23	24.2	34.	1140.	28.96	5.80	7.51	1.39	12.18	3.17	4.96	0.14	4.17
17.23	24.2	34.	1140.	28.96	5.77	7.53	1.36	12.16	3.11	4.99	0.14	4.16
18.23	48.1	31.	1140.	27.68	4.69	6.01	2.55	12.18	5.18	5.50	0.14	4.53
19.23	28.1	34.	1140.	27.67	5.56	7.75	1.10	11.94	2.54	5.20	0.14	4.25
20.23	17.9	31.	1140.	27.61	5.88	7.72	0.84	11.22	1.87	7.21	0.14	4.25
21.23	38.0	34.	1140.	27.87	5.25	6.96	1.89	12.40	4.19	4.41	0.14	4.37
22.23	38.4	34.	1140.	27.77	5.07	6.88	1.97	12.44	4.34	4.38	0.14	4.39
23.23	50.4	37.	1140.	27.77	4.98	7.01	2.11	13.13	4.82	2.56	0.14	4.36
24.23	26.5	37.	1140.	27.64	5.46	7.84	1.18	12.56	2.85	3.48	0.14	4.22
25.23	16.5	37.	1140.	27.75	6.17	8.36	0.77	12.31	1.89	3.90	0.14	4.15
1.31	38.1	43.	880.	9.47	7.62	9.56	1.22	16.01	3.72	3.30	0.12	1.78
2.31	20.6	43.	880.	9.48	7.59	10.17	0.85	16.42	2.78	2.20	0.12	1.75
3.31	21.3	43.	880.	9.46	7.74	10.40	0.62	16.24	2.05	2.43	0.12	1.74
4.31	36.3	43.	880.	9.46	7.51	9.98	1.14	16.64	3.66	1.91	0.12	1.77
5.31	22.7	40.	880.	9.43	8.11	10.00	0.72	15.71	2.47	3.73	0.12	1.76
6.31	30.5	40.	880.	9.46	7.77	9.80	0.98	15.84	3.05	3.53	0.12	1.77
7.31	31.3	37.	880.	9.41	7.62	9.45	1.07	15.21	3.16	4.99	0.12	1.79
8.31	38.8	37.	880.	9.46	7.40	9.13	1.39	15.45	4.04	4.67	0.12	1.80
9.31	23.4	37.	880.	9.43	8.03	9.75	0.78	15.01	2.33	5.29	0.12	1.77
10.31	44.3	40.	880.	9.41	7.39	9.33	1.45	16.19	4.38	3.07	0.12	1.80
12.31	42.4	43.	880.	9.67	7.30	9.88	1.12	16.58	3.60	1.91	0.12	1.78

.../

TABLE II (continued)

Run	r	P	N	x_f	T_n	T_r	T_c-T_r	C_b	C_b-C_s	T_r-T_l	ϕ_g	η_l
	gm/min	psig	rpm	w/w%	°C	°C	°C	x10^3 g.mol/l	x10^3 g.mol/l	°C		cp
13.31	21.7	40.	880.	9.65	8.38	10.27	0.49	15.74	1.57	4.01	0.12	1.77
14.31	37.5	37.	880.	9.65	7.57	9.34	1.16	15.24	3.40	4.88	0.12	1.81
15.31	26.0	37.	880.	9.65	7.91	9.71	0.79	14.38	2.38	5.25	0.12	1.79
16.31	32.3	37.	880.	9.68	7.65	9.48	1.03	15.15	3.03	5.02	0.12	1.81
1.310	42.4	43.	880.	9.34	7.88	10.17	0.85	16.42	2.78	2.20	0.12	1.75
2.310	26.4	43.	880.	9.35	8.23	10.46	0.56	16.19	1.87	2.49	0.12	1.74
3.310	30.3	40.	880.	9.35	8.11	10.11	0.67	15.60	2.10	3.85	0.12	1.76
4.310	51.8	43.	880.	9.36	7.82	9.91	1.11	16.62	3.58	1.94	0.12	1.77
5.310	28.7	40.	880.	9.35	8.46	10.20	0.58	15.54	1.84	3.94	0.12	1.75
6.310	48.5	40.	880.	9.35	7.56	9.71	1.07	15.90	3.31	[illegible]	[illegible]	1.78
7.310	24.8	43.	880.	9.35	8.32	10.52	0.51	16.15	1.68	2.55	0.12	1.74
8.310	39.9	40.	880.	9.35	7.88	9.91	0.87	15.75	2.71	3.65	0.12	1.77
9.310	39.9	37.	880.	9.35	7.77	9.54	0.98	15.15	2.90	5.09	0.12	1.79
10.310	47.4	37.	880.	9.37	7.59	9.36	1.16	15.28	3.41	4.90	0.12	1.80
11.310	31.3	37.	880.	9.32	7.82	9.80	0.73	14.97	2.19	5.34	0.12	1.77
12.310	23.2	37.	880.	9.32	8.40	9.95	0.57	14.86	1.74	5.49	0.12	1.77
13.310	41.0	43.	880.	9.32	8.00	10.23	0.80	16.37	2.80	2.26	0.12	1.75
1.32	39.6	34.	880.	17.62	6.78	8.03	1.64	13.82	4.15	5.48	0.10	2.54
2.32	32.8	34.	880.	17.59	7.07	8.30	1.37	13.64	3.52	5.75	0.10	2.52
3.32	23.3	37.	880.	17.61	7.36	[illegible]	[illegible]	13.93	2.27	4.67	0.10	2.45
4.32	28.2	37.	880.	17.59	6.78	8.52	1.43	14.33	3.82	4.06	0.10	2.50
5.32	38.8	37.	880.	17.55	6.61	8.17	1.77	14.57	4.66	3.71	0.10	2.53
6.32	32.0	40.	880.	17.56	6.98	9.01	1.19	14.82	3.38	2.75	0.10	2.46
7.32	23.7	40.	880.	17.55	7.34	9.40	0.81	14.55	2.34	3.14	0.10	2.43
8.32	38.8	40.	880.	17.54	6.69	8.72	1.48	15.02	4.14	2.46	0.10	2.48

.../

TABLE II (continued)

Run	r	P	N	x_f	T_n	T_r	T_c-T_r	C_b	C_b-C_s	T_r-T_l	ϕ_g	η_l
	gm/min	psig	rpm	w/w%	°C	°C	°C	x10^3 g.mol/l	x10^3 g.mol/l	°C		cp
9.32	14.6	40.	880.	17.55	6.69	8.62	1.59	15.10	4.41	2.35	0.10	2.49
10.32	44.6	37.	880.	17.56	6.55	7.98	1.97	14.71	5.12	3.52	0.10	2.54
11.32	19.4	34.	880.	18.34	7.17	8.76	0.84	13.19	2.21	6.22	0.10	2.57
12.32	35.3	34.	880.	18.34	6.49	7.75	1.86	13.84	4.60	5.20	0.10	2.66
13.32	39.7	40.	880.	18.34	6.58	8.56	1.58	14.95	4.35	2.30	0.10	2.59
14.32	29.8	37.	880.	18.36	6.96	8.55	1.33	14.14	3.56	4.09	0.10	2.59
1.33	38.3	31.	880.	27.64	4.73	5.07	3.53	12.86	6.90	4.56	0.10	4.55
2.33	32.6	34.	880.	27.64	5.19	6.11	2.76	12.97	5.85	3.57	0.10	4.44
3.33	24.2	34.	880.	27.62	5.51	6.56	2.31	12.68	5.01	4.01	0.10	4.39
4.33	28.0	31.	880.	27.58	5.19	5.92	2.65	12.27	5.38	5.41	0.10	4.50
5.33	34.3	31.	880.	27.64	4.84	5.33	3.27	12.69	6.46	4.82	0.10	4.52
6.33	35.0	34.	880.	27.58	4.93	5.88	3.02	13.20	6.36	3.34	0.10	4.39
7.33	24.6	37.	880.	27.64	4.83	7.01	2.11	13.11	4.82	2.56	0.10	4.38
8.33	24.6	37.	880.	27.64	5.51	7.04	2.10	13.17	4.84	2.58	0.10	4.30
9.33	35.8	37.	880.	27.64	4.98	6.41	2.73	13.57	6.08	1.96	0.10	4.40
10.33	22.7	37.	880.	27.64	5.27	7.39	1.72	12.85	4.00	2.93	0.10	4.35
11.33	40.9	37.	880.	27.64	4.20	6.20	2.94	13.70	6.48	1.74	0.10	4.44
12.33	21.1	31.	880.	27.61	5.42	6.73	1.83	11.77	3.86	6.22	0.10	4.40
13.33	20.9	34.	880.	27.61	6.00	7.20	1.66	12.27	3.71	4.65	0.10	4.32
14.33	23.2	37.	880.	27.67	5.60	7.43	1.70	12.88	3.98	2.97	0.10	4.29
15.33	38.8	34.	880.	27.65	4.76	5.74	3.11	13.16	6.48	3.19	0.10	4.56
16.33	25.6	34.	880.	27.65	5.45	6.75	2.10	12.53	4.60	4.21	0.10	4.39
17.33	29.2	31.	880.	27.72	4.81	5.89	2.67	12.26	5.40	5.38	0.10	4.54

.../

TABLE II (continued)

Run	n	P	N	x_f	T_n	T_r	T_c-T_r	C_b	C_b-C_s	T_r-T_l	ϕ_g	μ_l
	gm/min	psig	rpm	w/w%	°C	°C	°C	$x10^3$ g.mol/l	$x10^3$ g.mol/l	°C		cp
1.34	31.9	34.	880.	42.60	3.01	3.55	3.41	10.71	5.61	1.00	0.08	14.72
2.34	39.1	34.	880.	42.45	2.64	3.56	3.39	10.70	5.58	1.02	0.08	14.71
3.34	28.0	34.	880.	42.45	3.30	3.85	3.10	10.54	5.17	1.31	0.08	14.50
4.34	23.9	34.	880.	42.39	3.30	4.24	2.71	10.35	4.61	1.70	0.08	14.24
5.34	27.0	31.	880.	42.37	2.78	2.97	3.70	10.84	5.71	2.46	0.08	15.14
6.34	39.6	31.	880.	42.34	2.20	2.41	4.25	10.62	6.41	1.91	0.08	15.55
7.34	32.9	31.	880.	42.40	2.72	2.87	3.79	10.39	5.84	2.36	0.08	15.21
8.34	23.2	31.	880.	42.50	2.98	3.37	3.29	10.13	5.18	2.86	0.08	14.85
9.34	18.4	34.	880.	42.38	3.49	4.58	2.37	10.18	4.11	2.03	0.08	14.01
10.34	33.5	34.	880.	42.51	2.75	3.66	3.29	10.64	5.44	1.12	0.08	14.64
11.34	19.3	31.	880.	42.38	3.42	3.81	2.85	9.92	4.59	3.30	0.08	14.54
12.34	28.0	29.	880.	42.55	2.98	2.72	3.73	10.00	5.56	3.65	0.08	15.32
13.34	36.2	29.	880.	42.40	2.44	1.98	4.47	10.38	6.48	2.90	0.08	15.89
14.34	29.8	31.	880.	42.54	2.96	3.01	3.65	10.31	5.65	2.50	0.08	15.11

TABLE III

RUN 14.31: Experimental and predicted response in batch reactor, Hatschek viscosity

TIME	T_r EXPT.	T_r MODEL B	x_r EXPT.	x_r MODEL B	T_c	ϕ_h	η_h	$C_b \times 10^2$	$C_s \times 10^2$	T_r MODEL C	T_r MODEL A
mins	°C	°C	w/w%	w/w%	°C		cp	g.mol/l	g.mol/l		
0.	7.70	7.70	9.65	9.65	10.54	.0		1.65	0.88	7.70	7.70
0.4	8.13	8.32		9.77	10.54	.016	2.45	1.61	0.99	8.39	8.06
0.8	8.55	8.74		9.85	10.53	.028	2.61	1.58	1.07	8.81	8.42
1.2	8.87	9.00		9.93	10.53	.037	2.72	1.56	1.12	9.06	8.69
1.6	9.07	9.16		9.99	10.52	.046	2.81	1.55	1.15	9.20	8.89
2.0	9.19	9.25		10.04	10.52	.053	2.89	1.54	1.17	9.28	9.03
2.4	9.27	9.30		10.09	10.51	.060	2.97	1.54	1.18	9.32	9.13
2.8	9.31	9.33		10.14	10.51	.067	3.04	1.54	1.19	9.34	9.20
3.2	9.34	9.34		10.19	10.51	.073	3.11	1.54	1.19	9.35	9.25
3.6	9.34	9.34		10.24	10.51	.080	3.18	1.54	1.19	9.35	9.28
4.0	9.34	9.33	10.31	10.28	10.50	.086	3.25	1.54	1.19	9.33	9.31
4.4	9.34	9.32		10.33	10.50	.092	3.32	1.54	1.19	9.30	9.33
5.2	9.32	9.28		10.42	10.49	.105	3.45	1.54	1.19	9.28	9.34
5.6	9.29	9.25		10.46	10.49	.111	3.52	1.54	1.19	9.25	9.34
6.0	9.25	9.23		10.51	10.49	.117	3.59	1.54	1.19	9.23	9.35
6.4	9.22	9.20		10.56	10.49	.123	3.66	1.54	1.19	9.20	9.35
6.8	9.17	9.18		10.60	10.48	.130	3.73	1.54	1.19	9.18	9.35
7.2	9.13	9.15	10.70	10.65	10.48	.137	3.80	1.54	1.19	9.15	9.34
7.6	9.10	9.12		10.70	10.48	.143	3.88	1.54	1.19	9.13	9.34

Note: the subscript r in Tables III to VII refers to the time dependent reactor temperature.

TABLE IV

RUN 19.12: Experimental and predicted response in batch reactor, Ratschek viscosity

TIME	T_r EXPT.	T_r MODEL B	x_r EXPT.	x_r MODEL B	T_c	ϕ_h	η_h	$C_b \times 10^2$	$C_s \times 10^2$	T_r MODEL C	T_r MODEL A
mins	°C	°C	w/w%	w/w%	°C		cp	g.mol/l	g.mol/l	°C	°C
.0	5.85	5.85	18.38	18.38	9.68	.0		1.43	0.73	5.85	5.85
0.4	7.16	7.29		18.76	9.65	.028	3.78	1.39	0.86	7.40	6.86
0.8	7.88	7.92		19.01	9.64	.049	4.07	1.37	0.96	8.00	7.51
1.2	8.18	8.22		19.20	9.62	.061	4.28	1.36	1.01	8.26	7.90
1.6	8.32	8.35		19.36	9.61	.072	4.46	1.36	1.03	8.38	8.13
2.0	8.39	9.40		19.50	9.60	.083	4.64	1.36	1.05	8.41	8.27
2.4	8.40	8.40		19.64	9.59	.093	4.81	1.36	1.05	8.41	8.34
2.8	8.37	8.38	19.77	19.77	9.58	.103	4.98	1.36	1.05	8.38	8.38
3.2	8.32	8.35		19.90	9.57	.113	5.16	1.37	1.05	8.35	8.40
3.6	8.26	8.31		20.04	9.56	.123	5.33	1.37	1.04	8.31	8.41
4.0	8.20	8.27		20.17	9.55	.133	5.51	1.37	1.03	8.26	8.41
4.4	8.13	8.22		20.30	9.54	.143	5.70	1.37	1.03	8.22	8.40
4.8	8.06	8.16	20.22	20.44	9.53	.153	5.89	1.38	1.02	8.17	8.40
5.2	7.93	8.11		20.58	9.52	.163	6.09	1.38	1.01	8.12	8.39
5.6	7.82	8.05		20.71	9.51	.173	6.29	1.38	1.01	8.06	8.38
6.0	7.72	8.00		20.85	9.50	.184	6.51	1.38	1.00	8.01	8.37
6.4		7.94	20.83	21.00	9.49	.194	6.72	1.39	0.99	7.95	8.36
6.8		7.88		21.14	9.48	.205	6.95	1.39	0.99	7.89	8.35
7.2		7.81		21.28	9.47	.215	7.18	1.40	0.98	7.83	8.34
7.6		7.75		21.43	9.46	.226	7.43	1.40	0.98	7.77	8.33

TABLE V

RUN 26.13: Experimental and predicted response in batch reactor, Hatschek viscosity

TIME	T_r EXPT.	T_r MODEL B	x_r EXPT.	x_r MODEL B	T_c	ϕ_h	μ_h	$C_b \times 10^2$	$C_s \times 10^2$	T_r MODEL C	T_r MODEL A
mins	°C	°C	w/w%	w/w%	°C		cp	g.mol/l	g.mol/l		
.0	5.23	5.23	27.74	27.74	9.23	.0		1.42	0.65	5.23	5.23
0.4	6.01	6.39		28.15	9.20	.021	5.87	1.38	0.75	6.62	6.01
0.8	6.80	7.04		28.43	9.18	.035	6.29	1.34	0.84	7.24	6.60
1.2	7.32	7.43		28.65	9.16	.046	6.59	1.31	0.90	7.58	7.02
1.6	7.64	7.67		28.83	9.14	.056	6.84	1.30	0.94	7.76	7.33
2.0	7.81	7.81		28.99	9.13	.064	7.06	1.29	0.97	7.87	7.54
2.4	7.89	7.89		29.13	9.11	.071	7.27	1.28	0.98	7.92	7.69
2.8	7.90	7.93		29.26	9.10	.078	7.47	1.28	0.99	7.94	7.79
3.2	7.93	7.94	29.36	29.39	9.09	.084	7.68	1.28	1.00	7.95	7.85
3.6	7.93	7.94		29.51	9.08	.090	7.88	1.28	1.00	7.93	7.89
4.0	7.90	7.93		29.63	9.07	.096	8.08	1.28	1.00	7.92	7.92
4.4	7.87	7.90		29.74	9.06	.102	8.28	1.29	1.00	7.89	7.93
4.8	7.84	7.88		29.86	9.05	.108	8.49	1.29	1.00	7.86	7.94
5.2	7.80	7.85		29.98	9.03	.114	8.70	1.29	0.99	7.83	7.94
5.6	7.76	7.81		30.09	9.02	.120	8.91	1.29	0.99	7.80	7.94
6.0	7.73	7.78		30.21	9.01	.126	9.13	1.29	0.99	7.76	7.94
6.4	7.70	7.74	30.25	30.33	9.00	.132	9.36	1.29	0.98	7.73	7.93
6.8	7.67	7.70		30.45	8.99	.138	9.58	1.30	0.98	7.69	7.92
7.2	7.59	7.66		30.57	8.98	.144	9.82	1.30	0.98	7.65	7.91
7.6	7.54	7.62		30.69	8.91	.150	10.06	1.30	0.97	7.62	7.90

TABLE VI

RUN 4.14: Experimental and predicted response in batch reactor, Katschek viscosity

TIME	T_r	T_r	T_r	x_r	T_c	ϕ_h	η_h	$C_b x10^2$	$C_s x10^2$	T_r	T_r
	EXPT.	MODEL B	MO.B*	MODEL B						MODEL C	MODEL A
mins	°C	°C	°C	w/w%	°C		cp	g.mol/l	g.mol/l	°C	°C
0.0	2.75	2.75	2.75	42.01	7.24	.0		1.15	0.43	2.75	2.75
0.4	3.13	3.45	3.30	42.42	7.18	.014	17.59	1.12	0.50	3.68	3.13
0.8	3.50	3.88	3.70	42.74	7.12	.026	19.06	1.10	0.54	4.09	3.44
1.2	3.82	4.16	3.98	42.89	7.07	.036	20.24	1.08	0.57	4.32	3.70
1.6	4.06	4.34	4.19	43.02	7.02	.045	21.30	1.07	0.60	4.45	3.91
2.0	4.29	4.46	4.34	43.26	6.98	.052	22.29	1.07	0.62	4.53	4.08
2.4	4.42	4.52	4.44	43.48	6.94	.059	23.26	1.06	0.63	4.56	4.21
2.8	4.50	4.55	4.50	43.69	6.90	.067	24.21	1.06	0.64	4.55	4.31
3.2	4.54	4.55	4.54	43.88	6.87	.073	25.17	1.06	0.64	4.53	4.39
3.6	4.55	4.53	4.53	44.06	6.83	.079	26.14	1.06	0.64	4.50	4.45
4.0	4.52	4.49	4.55	44.24	6.80	.085	27.12	1.06	0.64	4.45	4.49
4.4	4.47	4.43	4.54	44.41	6.76	.091	28.13	1.06	0.64	4.39	4.52
4.8	4.42	4.37	4.51	44.58	6.73	.097	29.15	1.07	0.64	4.33	4.54
5.2	4.37	4.30	4.48	44.74	6.69	.103	30.21	1.07	0.64	4.26	4.54
5.6	4.30	4.22	4.44	44.91	6.66	.109	31.30	1.08	0.63	4.18	4.54
6.0		4.13	4.39	45.23	6.63	.114	32.41	1.08	0.62	4.11	4.53

MODEL B* refers to MODEL B with B = -0.5

TABLE VII

Experimental and predicted temperature and concentration data

Run	Time (mins)	T_r EXPT. °C	T_r MODEL B °C	T_r MODEL A °C	x_r EXPT. w/w%	x_r MODEL B w/w%	C_b-C_s x10^3 g.mol /l
17.11	0.	6.91	6.91	6.91	9.66	9.66	
	0.4	8.64	8.86	8.46		9.94	5.73
	0.8	9.34	9.46	9.19		10.08	3.13
	1.2	9.58	9.66	9.51		10.18	2.56
	1.6	9.67	9.71	9.64		10.27	2.40
	2.0	9.70	9.71	9.69		10.35	2.39
	2.4	9.69	9.69	9.71		10.43	2.43
	2.8	9.66	9.66	9.71		10.51	2.49
	3.2	9.61	9.63	9.71	10.67	10.60	2.58
	3.6	9.54	9.59	9.71		10.68	2.66
	4.0	9.47	9.56	9.70		10.76	2.75
	4.4	9.40	9.52	9.70		10.85	2.83
	4.8	9.34	9.48	9.69	10.92	10.94	2.92
	5.2	9.26	9.45	9.69		11.03	3.02
	5.6	9.19	9.41	9.68		11.12	3.11
	6.0	9.12	9.36	9.67		11.21	3.20
	6.4	9.04	9.32	9.67	11.30	11.30	3.31
	6.8		9.28	9.66		11.40	3.42
	7.2		9.23	9.66		11.49	3.53
19.11	0.	7.57	7.57	7.57	9.66	9.66	
	0.4	9.64	9.49	9.18		9.90	3.98
	0.8	9.65	10.07	9.88		10.01	2.26
	1.2	10.02	10.25	10.16		10.08	1.69
	1.6	10.17	10.30	10.26		10.14	1.51
	2.0	10.26	10.31	10.29		10.19	1.47
	2.4	10.30	10.30	10.30		10.24	1.48
	2.8	10.29	10.29	10.31	10.30	10.30	1.50
	3.2	10.27	10.28	10.31		10.35	1.53
	3.6	10.25	10.27	10.30		10.40	1.57
	4.0	10.23	10.25	10.30		10.45	1.60
	4.4	10.21	10.24	10.30		10.50	1.64
	4.8	10.20	10.22	10.29		10.56	1.67
	5.2	10.18	10.21	10.29		10.61	1.71
	5.6	10.15	10.19	10.29		10.66	1.75
	6.0		10.18	10.28	10.74	10.72	1.79
	6.4		10.16	10.28		10.77	1.82
	6.8		10.15	10.28		10.83	1.86
	7.2		10.13	10.27		10.89	1.90

.../

TABLE VII (continued)

Run	Time (mins)	T_r EXPT. °C	T_r MODEL B °C	T_r MODEL A °C	x_r EXPT. w/w%	x_r MODEL B w/w%	$C_b - C_s$ x10^3 g.mol/l
18.12	0.	7.10	7.10	7.10	18.49	18.49	
	0.4	7.75	8.18	7.95		18.75	3.77
	0.8	8.14	8.66	8.45		18.91	2.60
	1.2	8.46	8.88	8.73		19.02	2.01
	1.6	8.70	8.98	8.89		19.10	1.83
	2.0	8.89	9.03	8.97	19.17	19.18	1.59
	2.4	8.99	9.04	9.01		19.25	1.54
	2.8	9.04	9.04	9.03		19.32	1.53
	3.2	9.05	9.04	9.04		19.39	1.54
	3.6	9.04	9.02	9.04		19.46	1.56
	4.0	9.04	9.01	9.04		19.53	1.58
	4.4	9.04	9.00	9.04		19.60	1.60
	4.8	9.04	8.98	9.04		19.66	1.63
	5.2	9.04	8.96	9.03	19.63	19.73	1.66
	5.6	9.03	8.95	9.03		19.80	1.69
	6.0		8.93	9.02		19.87	1.72
	6.4		8.91	9.02		19.94	1.75
	6.8		8.90	9.01		20.01	1.78
	7.2		8.88	9.01	19.97	20.09	1.82
25.13	0.	4.52	4.52	4.52	27.64	27.64	
	0.4	5.18	5.33	4.96		28.01	6.62
	0.8	5.78	5.78	5.31		28.29	5.61
	1.2	6.12	6.06	5.59		28.53	5.28
	1.6	6.27	6.22	5.80		28.75	4.96
	2.0	6.33	6.31	5.96		28.95	4.76
	2.4	6.34	6.34	6.08		29.13	4.67
	2.8	6.33	6.35	6.17		29.31	4.64
	3.2	6.27	6.32	6.23	29.45	29.49	4.65
	3.6	6.21	6.28	6.28		29.66	4.70
	4.0	6.12	6.23	6.31		29.83	4.78
	4.4	6.02	6.17	6.33		29.99	4.87
	4.8	5.91	6.10	6.34		30.16	4.98
	5.2	5.72	6.02	6.35	30.23	30.33	5.10
	5.6		5.93	6.35		30.49	5.23
	6.0		5.84	6.35		30.66	5.37
	6.4		5.75	6.34		30.83	5.52

.../

TABLE VII (continued)

Run	Time (mins)	T_r EXPT. °C	T_r MODEL B °C	T_r MODEL A °C	x_r EXPT. w/w%	x_r MODEL w/w%	$C_b - C_a$ 3×10^3 g.mol/l
27.13	0.	4.88	4.88	4.88	27.67	27.67	
	0.4	5.90	6.10	5.65		28.14	6.87
	0.8	6.72	6.75	6.23		28.47	5.56
	1.2	7.13	7.12	6.64		28.74	4.77
	1.6	7.34	7.33	6.94		28.96	4.28
	2.0	7.44	7.44	7.14		29.16	4.01
	2.4	7.48	7.49	7.28		29.35	3.88
	2.8	7.49	7.50	7.37		29.52	3.82
	3.2	7.47	7.48	7.43		29.69	3.83
	3.6	7.40	7.45	7.47	29.73	29.86	3.87
	4.0	7.33	7.40	7.49		30.03	3.94
	4.4	7.25	7.35	7.49		30.19	4.02
	4.8	7.18	7.29	7.50		30.36	4.12
	5.2	7.10	7.22	7.49		30.53	4.23
	5.6	7.02	7.16	7.48		30.69	4.35
	6.0	6.92	7.08	7.47		30.86	4.47
	6.4		7.01	7.46		31.03	4.60
	6.8		6.93	7.45	30.46	31.11	4.74
28.13	0.	6.40	6.40	6.40	27.70	27.70	
	0.4	6.67	7.22	7.01		27.96	5.69
	0.8	6.98	7.72	7.48		28.14	3.58
	1.2	7.36	8.04	7.81		28.27	2.83
	1.6	7.72	8.25	8.06		28.37	2.32
	2.0	8.00	8.39	8.23		28.46	1.97
	2.4	8.17	8.47	8.35		28.54	1.75
	2.8	8.32	8.53	8.44		28.60	1.59
	3.2	8.43	8.57	8.50		28.66	1.49
	3.6	8.49	8.59	8.54		28.72	1.43
	4.0	8.53	8.60	8.56	28.70	28.77	1.39
	4.4	8.56	8.61	8.58		28.82	1.37
	4.8	8.59	8.60	8.59		28.88	1.36
	5.2	8.62	8.60	8.60		28.93	1.37
	5.6	8.62	8.59	8.60		28.98	1.37
	6.0	8.62	8.58	8.61		29.03	1.38
	6.4	8.61	8.57	8.60		29.08	1.39
	6.8	8.60	8.57	8.60	29.27	29.13	1.39

.../

TABLE VII (continued)

Run	Time (mins)	T_r EXPT. °C	T_r MODEL B °C	T_r MODEL A °C	x_r EXPT. w/w%	x_r MODEL B w/w%	C_b-C_s x10^3 g.mol/l
36.21	0.	7.73	7.73	7.73	9.67	9.67	
	0.4	9.00	9.57	9.32		9.82	4.63
	0.8	9.72	10.04	9.82		9.91	3.22
	1.2	10.10	10.25	10.10		9.98	2.54
	1.6	10.25	10.35	10.24		10.03	2.24
	2.0	10.32	10.38	10.32		10.08	2.11
	2.4	10.37	10.40	10.36		10.13	2.06
	2.8	10.39	10.39	10.38	10.35	10.17	2.07
	3.2	10.38	10.38	10.39		10.21	2.08
	3.6	10.37	10.37	10.39		10.26	2.11
	4.0	10.35	10.36	10.39		10.30	2.15
	4.4	10.33	10.34	10.39		10.35	2.19
	4.8	10.32	10.33	10.39	10.57	10.39	2.23
	5.2	10.30	10.31	10.39		10.44	2.27
	5.6	10.29	10.29	10.39		10.48	2.32
	6.0	10.27	10.28	10.38		10.53	2.36
	6.4	10.25	10.26	10.38		10.57	2.41
	6.8	10.24	10.24	10.38		10.62	2.45
37.21	0.	7.42	7.42	7.42	9.69	9.69	
	0.4	8.80	9.61	9.35		9.86	4.51
	0.8	9.58	10.02	9.82		9.97	3.26
	1.2	9.92	10.18	10.05		10.05	2.74
	1.6	10.11	10.24	10.16		10.11	2.56
	2.0	10.20	10.25	10.22		10.18	2.51
	2.4	10.22	10.24	10.24		10.24	2.53
	2.8	10.18	10.22	10.25	10.42	10.30	2.58
	3.2	10.13	10.20	10.25		10.36	2.64
	3.6	10.08	10.17	10.25		10.43	2.71
	4.0	10.02	10.15	10.25		10.49	2.78
	4.4	9.97	10.12	10.24	10.71	10.55	2.85
	4.8	9.90	10.09	10.24		10.62	2.92
	5.2	9.83	10.06	10.24		10.69	3.00
	5.6	9.76	10.03	10.23		10.75	3.08
	6.0	9.69	10.00	10.23		10.82	3.15
	6.4	9.64	9.97	10.22	11.01	10.89	3.23
	6.8		9.94	10.22		10.96	3.32

.../

TABLE VII (continued)

Run	Time (mins)	T_r EXPT. °C	T_r MODEL B °C	T_r MODEL A °C	x_r EXPT. w/w%	x_r MODEL B w/w%	$C_b - C_s$ $\times 10^3$ g.mol/l
1.22	0.	5.74	5.74	5.74	18.36	18.36	
	0.4	6.62	6.62	6.24		18.64	7.17
	0.8	7.15	7.09	6.63		18.86	6.18
	1.2	7.46	7.36	6.92		19.04	5.57
	1.6	7.58	7.51	7.13		19.20	5.22
	2.0	7.63	7.59	7.28		19.34	5.03
	2.4	7.61	7.62	7.40		19.48	4.94
	2.8	7.51	7.62	7.48		19.62	4.93
	3.2	7.40	7.60	7.53	19.57	19.75	4.95
	3.6	7.25	7.56	7.57		19.89	5.03
	4.0	7.11	7.51	7.60		20.02	5.13
	4.4	6.88	7.45	7.61	19.97	20.15	5.24
	4.8		7.38	7.62		20.28	5.36
	5.2		7.31	7.63		20.41	5.50
	5.6		7.24	7.63		20.54	5.64
	6.0		7.16	7.63		20.68	5.79
5.22	0.	6.35	6.35	6.35	18.34	18.34	
	0.4	7.14	7.30	6.99		18.59	5.77
	0.8	7.67	7.82	7.47		18.77	4.60
	1.2	8.03	8.13	7.81		18.90	3.86
	1.6	8.26	8.32	8.04		19.02	3.40
	2.0	8.39	8.43	8.21	19.08	19.12	3.12
	2.4	8.46	8.49	8.32		19.22	2.96
	2.8	8.50	8.51	8.40		19.31	2.88
	3.2	8.51	8.52	8.45		19.39	2.85
	3.6	8.49	8.52	8.48	19.43	19.48	2.84
	4.0	8.47	8.51	8.50		19.56	2.86
	4.4	8.44	8.49	8.51		19.64	2.89
	4.8	8.41	8.47	8.52		19.72	2.93
	5.2	8.39	8.44	8.52		19.81	2.97
	5.6	8.37	8.41	8.52		19.89	3.03
	6.0	8.33	8.39	8.52	19.97	19.97	3.09
	6.4	8.29	8.36	8.52		20.06	3.14
	6.8	8.25	8.33	8.51		20.14	3.20
	7.2	8.21	8.29	8.51		20.23	3.27

.../

TABLE VII (continued)

Run	Time (mins)	T_r EXPT. °C	T_r MODEL B °C	T_r MODEL A °C	x_r EXPT. w/w%	x_r MODEL B w/w%	C_b-C_s x10^3 g.mol/l
21.23	0.	5.25	5.25	5.25	27.87	27.87	
	0.4	5.63	5.88	5.60		28.15	6.44
	0.8	6.00	6.28	5.89		28.37	5.69
	1.2	6.30	6.54	6.13		28.56	5.16
	1.6	6.51	6.71	6.32		28.72	4.80
	2.0	6.67	6.83	6.48		28.88	4.55
	2.4	6.78	6.90	6.60		29.02	4.37
	2.8	6.86	6.94	6.69		29.15	4.27
	3.2	6.90	6.96	6.77	29.38	29.28	4.21
	3.6	6.93	6.96	6.83		29.41	4.19
	4.0	6.95	6.95	6.87		29.53	4.19
	4.4	6.92	6.93	6.90		29.65	4.22
	4.8	6.89	6.90	6.93		29.77	4.25
	5.2	6.83	6.86	6.94		29.89	4.31
	5.6	6.78	6.82	6.95	29.98	30.01	4.37
	6.0	6.75	6.78	6.96		30.13	4.45
	6.4	6.72	6.73	6.96		30.25	4.53
	6.8		6.68	6.96		30.37	4.61
	7.2		6.62	6.96		30.49	4.69
22.23	0.	5.07	5.07	5.07	27.77	27.77	
	0.4	5.53	5.73	5.43		28.05	6.74
	0.8	5.91	6.14	5.73		28.28	5.97
	1.2	6.29	6.42	5.98		28.47	5.42
	1.6	6.53	6.60	6.18		28.64	5.04
	2.0	6.70	6.73	6.34		28.80	4.76
	2.4	6.80	6.81	6.47		28.94	4.58
	2.8	6.85	6.86	6.57		29.08	4.46
	3.2	6.86	6.88	6.65		29.21	4.40
	3.6	6.82	6.88	6.72		29.34	4.36
	4.0	6.78	6.87	6.77		29.47	4.36
	4.4	6.74	6.85	6.80		29.59	4.38
	4.8	6.69	6.83	6.83		29.71	4.42
	5.2	6.64	6.79	6.85		29.83	4.47
	5.6	6.57	6.75	6.87		29.96	4.54
	6.0	6.50	6.70	6.87		30.08	4.60
	6.4		6.65	6.88	30.18	30.19	4.68

.../

TABLE VII (continued)

Run	Time (mins)	T_r EXPT. °C	T_r MODEL B °C	T_r MODEL A °C	x_r EXPT. w/w%	x_r MODEL B w/w%	C_b-C_s $\times 10^3$ g.mol/l
16.31	0.	7.65	7.65	7.65	9.68	9.68	
	0.4	8.17	8.39	8.14		9.79	5.98
	0.8	8.59	8.82	8.51		9.87	4.89
	1.2	8.89	9.08	8.79		9.94	4.19
	1.6	9.10	9.25	8.99		9.99	3.72
	2.0	9.25	9.36	9.14		10.04	3.43
	2.4	9.37	9.42	9.24		10.09	3.24
	2.8	9.44	9.46	9.32	10.15	10.13	3.14
	3.2	9.47	9.47	9.37		10.18	3.08
	3.6	9.49	9.48	9.41		10.22	3.06
	4.0	9.50	9.48	9.43		10.26	3.06
	4.4	9.50	9.47	9.45		10.30	3.08
	4.8	9.50	9.46	9.46		10.34	3.09
	5.2	9.49	9.44	9.47		10.37	3.14
	5.6	9.49	9.43	9.48		10.41	3.18
	6.0	9.48	9.41	9.48		10.45	3.22
	6.4	9.46	9.39	9.48	10.52	10.49	3.26
	6.8	9.44	9.37	9.48		10.53	3.31
	7.2	9.40	9.35	9.48		10.57	3.36
	7.6	9.37	9.33	9.48		10.62	3.43
12.32	0.	6.49	6.49	6.49	18.34	18.34	
	0.4	6.83	6.94	6.72		18.49	6.54
	0.8	7.09	7.22	6.91		18.62	5.94
	1.2	7.30	7.41	7.07		18.73	5.51
	1.6	7.46	7.54	7.21		18.83	5.20
	2.0	7.56	7.63	7.32		18.92	4.99
	2.4	7.64	7.69	7.41		19.01	4.85
	2.8	7.70	7.73	7.48		19.10	4.76
	3.2	7.73	7.75	7.54	19.16	19.18	4.71
	3.6	7.74	7.75	7.59		19.26	4.68
	4.0	7.74	7.75	7.62		19.34	4.68
	4.4	7.73	7.73	7.65		19.41	4.69
	4.8	7.71	7.72	7.68		19.49	4.73
	5.2	7.68	7.69	7.70		19.57	4.77
	5.6	7.63	7.66	7.71		19.64	4.82
	6.0		7.63	7.72		19.72	4.89
	6.4		7.60	7.73	19.72	19.80	4.96
	6.8		7.56	7.74		19.87	5.02

.../

TABLE VII (continued)

Run	Time (mins)	T_r EXPT. °C	T_r MODEL B °C	T_r MODEL A °C	x_r EXPT. w/w%	x_r MODEL B w/w%	C_b-C_s $\times 10^3$ g.mol/l
13.32	0.	6.58	6.58	6.58	18.34	18.34	
	0.4	7.35	7.34	7.03		18.56	7.46
	0.8	7.88	7.79	7.39		18.73	6.39
	1.2	8.22	8.09	7.67		18.87	5.67
	1.6	8.39	8.28	7.90		18.99	5.18
	2.0	8.50	8.41	8.07		19.10	4.85
	2.4	8.53	8.48	8.20		19.21	4.64
	2.8	8.53	8.53	8.30		19.30	4.51
	3.2	8.52	8.55	8.37	19.52	19.40	4.45
	3.6	8.50	8.55	8.43		19.49	4.41
	4.0	8.47	8.55	8.47		19.58	4.42
	4.4	8.43	8.53	8.50		19.67	4.45
	4.8	8.39	8.51	8.52		19.76	4.49
	5.2	8.33	8.48	8.54		19.85	4.55
	5.6	8.27	8.45	8.55		19.94	4.61
	6.0	8.20	8.41	8.55	20.06	20.02	4.69
	6.4	8.11	8.37	8.55		20.11	4.77
14.33	0.	5.60	5.60	5.60	27.67	27.67	
	0.4	6.03	6.07	5.86		27.86	6.98
	0.8	6.36	6.41	6.09		28.01	6.31
	1.2	6.64	6.66	6.29		28.15	5.80
	1.6	6.85	6.85	6.46		28.27	5.39
	2.0	7.02	7.00	6.61		28.39	5.06
	2.4	7.14	7.12	6.74		28.49	4.80
	2.8	7.22	7.21	6.85		28.59	4.60
	3.2	7.29	7.28	6.95	28.66	28.68	4.44
	3.6	7.36	7.33	7.03		28.77	4.31
	4.0	7.40	7.37	7.10		28.85	4.22
	4.4	7.41	7.39	7.16		28.94	4.14
	4.8	7.41	7.41	7.21		29.02	4.09
	5.2	7.41	7.42	7.25		29.09	4.07
	5.6	7.40	7.42	7.28		29.17	4.05
	6.0	7.40	7.42	7.31		29.25	4.04
	6.4	7.39	7.41	7.34		29.32	4.04
	6.8	7.38	7.40	7.36		29.39	4.06
	7.2	7.37	7.38	7.37		29.47	4.08
	7.6	7.36	7.36	7.39	29.49	29.54	4.10

.../

TABLE VII (continued)

Run	Time (mins)	T_r EXPT. °C	T_r MODEL B °C	T_r MODEL A °C	x_r EXPT. w/w%	x_r MODEL B w/w%	$C_b - C_c$ $\times 10^3$ g.mol/l
16.33	0.	5.45	5.45	5.45	27.65	27.65	
	0.4	5.67	5.80	5.62		27.82	6.65
	0.8	5.88	6.05	5.78		27.96	6.18
	1.2	6.06	6.24	5.91		28.08	5.82
	1.6	6.24	6.38	6.03		28.20	5.53
	2.0	6.36	6.49	6.14		28.31	5.30
	2.4	6.47	6.58	6.23	28.52	28.41	5.13
	2.8	6.56	6.64	6.31		28.51	4.99
	3.2	6.65	6.69	6.38		28.60	4.88
	3.6	6.71	6.72	6.44		28.69	4.80
	4.0	6.73	6.74	6.49		28.78	4.75
	4.4	6.74	6.75	6.54	28.90	28.87	4.71
	4.8	6.73	6.76	6.58		28.95	4.69
	5.2	6.73	6.75	6.61		29.03	4.69
	5.6	6.72	6.74	6.64		29.11	4.69
	6.0	6.70	6.73	6.66		29.19	4.70
	6.4	6.68	6.71	6.68	29.35	29.27	4.72
	6.8	6.65	6.69	6.70		29.35	4.76
	7.2	6.61	6.67	6.72		29.43	4.79
9.34	0.	3.49	3.49	3.49	42.38	42.38	
	0.4	3.70	3.74	3.61		42.55	5.73
	0.8	3.86	3.93	3.73		42.69	5.43
	1.2	3.99	4.08	3.83		42.83	5.18
	1.6	4.10	4.20	3.92		42.95	4.98
	2.0	4.17	4.29	4.01	42.99	43.06	4.81
	2.4	4.24	4.37	4.09		43.17	4.67
	2.8	4.30	4.43	4.16		43.28	4.55
	3.2	4.36	4.48	4.22		43.38	4.46
	3.6	4.40	4.51	4.27	43.43	43.47	4.38
	4.0	4.43	4.54	4.32		43.56	4.32
	4.4	4.47	4.56	4.36		43.65	4.26
	4.8	4.50	4.57	4.40		43.74	4.22
	5.2	4.51	4.57	4.44		43.83	4.19
	5.6	4.53	4.57	4.47		43.91	4.17
	6.0	4.55	4.56	4.49		43.99	4.16
	6.4	4.56	4.55	4.51	44.00	44.07	4.17
	6.8	4.58	4.51	4.53		44.23	4.18
	7.2	4.59	4.51	4.55		44.31	4.19

TABLE VIII

Summary of Steady-state runs, showing block code and mean production rates

BLOCK CODE	STIRRER SPEED N RPM	x_f %w/w	V_r l	V_l l	ϕ_g %	Impeller Type	Power HP.	Special Feature	$\bar{r}$ gm/min	$(\overline{C_b - C_s})$ g.mol/l	K_h Kcal/min
S1	1420	9.69	4.40	3.50	20.5	Dual	.070		44.5	.00299	1.03
S2	1420	9.65	4.02	3.16	21.4	Dual	.070		43.5	.00284	1.03
S3	950	9.65	4.05	3.70	8.6	Dual	.033		42.1	.00420	0.658
S4	1420	9.80	3.35	3.25	3.0	Single	.024		35.3	.00489	0.608
S5	1420	9.37	3.35	3.25	3.0	Single	.024	Distributor	39.4	.00440	0.608

TABLE IX

Steady-state runs: S1 1420 RPM, Dual Impeller

RUN	P	v_f	T_r	T_f	x_f	x_r	ξ *	$(T_c-T_r)(T_r-T_l)(C_b-C_s)$		r	$\dot{q}'$	Reactor Heat Load
	psig	cm^3/min	°C	°C	w/w%	w/w%	%	°C	°C	g.mol/l x10^3	g/min	Kcal/min	Kcal/min
44.	43.	460.	10.29	10.03	9.69	10.43	7.1	0.71	2.32	2.21	33.8	4.09	3.96
45.	43.	460.	10.13	10.03	9.69	10.68	9.4	0.85	2.16	2.66	45.0	5.15	5.04
46.	43.	460.	9.97	9.94	9.69	10.97	11.7	1.00	2.00	3.09	55.6	6.19	6.03
47.	43.	293.	10.11	9.94	9.69	11.33	14.5	0.83	2.14	2.56	44.0	5.15	4.94
48.	40.	460.	9.94	9.45	9.69	10.73	9.7	1.00	3.48	2.98	46.2	5.15	5.06
49.	40.	293.	9.97	9.39	9.69	10.89	11.2	0.75	3.71	2.25	34.0	4.09	3.93
50.	40.	460.	9.42	9.04	9.69	11.03	12.1	1.30	3.16	3.83	58.0	6.19	6.07
51.	40.	293.	9.64	9.33	9.69	11.38	14.8	1.06	3.38	3.13	45.1	5.15	5.00
52.	37.	460.	9.24	8.95	9.69	10.78	10.1	1.23	4.78	3.49	48.2	5.15	5.24
53.	37.	293.	9.51	8.90	9.69	10.97	11.7	0.95	5.05	2.73	35.4	4.09	4.05

* hydrate hold-up, ϕ_h = 1.3 %

TABLE X

Steady-state runs: S2 1420 RPM, Dual Impeller

RUN	P	v_f	T_r	T_f	x_f	x_r	ξ	$(T_c-T_r)(T_r-T_l)(C_b-C_s)$		r	Q'	Reactor Heat Load
	psig	cm^3/min	°C	°C	w/w%	w/w%	%	°C	°C	$g.mol/l \times 10^3$	g/min	Kcal/min	Kcal/min
1.	43.	335.	10.14	9.91	9.60	11.08	13.4	0.81	2.17	2.53	46.4	5.15	5.13
3.	43.	460.	10.17	9.74	9.60	10.64	9.7	0.81	2.20	2.53	46.6	5.15	5.03
4.	43.	210.	10.11	9.82	9.60	12.15	21.0	0.77	2.14	2.38	45.7	5.15	5.08
5.	43.	460.	10.05	9.85	9.60	10.91	12.0	0.91	2.08	2.83	57.2	6.14	6.09
7.	43.	460.	10.34	9.79	9.60	10.36	7.3	0.66	2.37	2.04	34.9	4.09	3.93
19.	40.	460.	9.27	9.16	9.63	10.99	12.4	1.44	3.01	4.25	59.0	6.19	6.29
24.	40.	460.	9.95	9.51	9.68	10.46	7.5	0.80	3.69	2.39	35.6	4.09	4.03
26.	37.	293.	9.13	9.38	9.67	11.46	15.6	1.30	4.67	3.67	47.4	5.15	5.09
27.	37.	460.	9.59	9.21	9.67	10.47	7.4	0.90	5.13	2.58	36.4	4.09	4.14
28.	37.	293.	9.53	9.21	9.68	10.93	11.4	0.93	5.07	2.65	34.7	4.09	4.06
37.	40.	335.	9.88	9.51	9.67	10.75	10.0	0.85	3.62	2.54	34.9	4.09	4.05
38.	40.	460.	9.56	9.42	9.67	10.88	11.1	1.16	3.30	3.45	53.0	5.57	5.74
39.	43.	335.	10.50	9.80	9.67	10.44	7.4	0.51	2.53	1.56	25.6	3.17	3.11
41.	43.	460.	10.03	10.03	9.68	10.86	10.9	0.94	2.06	2.93	51.8	5.57	5.74

TABLE XI

Steady-state runs: S3 950 RPM, Dual Impeller

RUN	P	v_f	T_r	T_f	x_f	x_r	ξ	$(T_c-T_r)(T_r-T_l)(C_b-C_s)$		r	Q'	Reactor Heat Load
	psig	cm^3/min	°C	°C	w/w%	w/w%	%	°C	°C	g.mol/l x10^3	g/min	Kcal/min	Kcal/min
9.	43.	460.	9.53	9.79	9.60	10.95	12.3	1.43	1.56	4.39	58.8	6.19	6.06
10.	43.	293.	9.68	9.77	9.60	11.44	16.1	1.25	1.71	3.85	48.8	5.15	5.08
12.	43.	460.	9.65	7.59	9.60	10.90	11.9	1.32	1.68	4.15	57.2	5.15	4.87
13.	43.	460.	9.88	12.52	9.60	10.41	7.8	1.12	1.91	3.48	37.1	5.15	5.17
14.	43.	460.	9.88	13.33	9.60	10.59	9.3	1.10	1.91	3.44	44.5	6.19	6.20
16.	40.	293.	9.04	9.27	9.60	11.41	15.8	1.65	2.78	4.80	47.9	5.15	5.03
18.	40.	460.	8.60	9.16	9.63	10.97	12.2	2.13	2.34	6.08	58.2	6.19	6.16
29.	37.	460.	8.78	8.69	9.68	10.50	7.8	1.71	4.32	4.78	37.2	4.09	3.97
30.	37.	293.	8.62	8.64	9.68	10.98	11.8	1.84	4.16	5.10	36.0	4.09	3.90
33.	37.	335.	9.16	8.52	9.67	10.62	8.9	1.32	4.70	3.76	31.0	3.17	3.25
34.	40.	335.	9.66	9.21	9.87	10.55	8.3	1.08	3.40	3.23	29.0	3.17	3.11
35.	40.	335.	9.27	9.24	9.67	10.87	11.0	1.45	3.01	4.27	38.3	4.09	4.10
2.	43.	335.	9.79	9.77	9.68	10.85	10.8	1.18	1.82	3.64	37.4	4.09	4.02
3.	43.	335.	10.08	9.77	9.68	10.54	8.2	0.91	2.11	2.83	28.3	3.17	3.10

TABLE XII

Steady-state runs: S4 1420 RPM, Single Impeller

RUN	P	v_f	T_r	T_f	x_f	x_r	ξ	$(T_c-T_r)(T_r-T_l)(C_b-C_s)$		r	Q'	Reactor Heat load
	psig	cm^3/min	°C	°C	w/w%	w/w%	%	°C	°C	g.mol/l $\times 10^3$	g/min	Kcal/min	Kcal/min
30.	43.	460.	8.46	8.81	9.77	10.73	8.9	2.52	0.49	7.39	42.7	5.15	4.60
32.	43.	460.	8.93	8.43	9.80	10.66	8.1	2.06	0.96	6.17	38.5	4.09	3.85
33.	46.	460.	9.94	9.85	9.80	10.59	7.5	1.28	0.35	4.12	35.6	4.09	3.77
64.	46.	460.	9.68	9.04	9.80	10.97	10.7	1.52	0.09	4.82	50.9	4.09	4.90
65.	43.	293.	9.68	8.93	9.80	10.81	9.3	1.29	1.71	4.00	28.4	3.17	2.95
66.	46.	293.	10.32	10.14	9.80	10.68	8.2	0.90	0.73	2.91	25.0	3.17	2.81
68.	40.	293.	9.29	8.87	9.81	10.73	8.6	1.45	3.03	4.26	26.1	3.17	2.83

TABLE XIII

Steady-state runs: S5 1420 RPM, Single Impeller with freon distributor

RUN	P	v_f	T_r	T_f	x_f	x_r	ξ	$(T_c-T_r)(T_r-T_l)(C_b-C_s)$		r	Q'	Reactor Heat load
	psig	cm^3/min	°C	°C	w/w%	w/w%	%	°C	°C	g.mol/l x10^3	g/min	Kcal/min	Kcal/min
70.	43.	460.	9.36	8.72	9.37	10.49	10.7	1.63	1.39	4.99	50.8	5.15	4.90
71.	46.	460.	10.34	10.08	9.37	10.19	8.0	0.90	0.75	2.98	38.3	4.09	3.94
72.	43.	460.	9.90	9.71	9.37	10.20	8.1	1.12	1.93	3.48	38.8	4.09	4.01
73.	46.	460.	10.17	9.97	9.37	10.45	10.3	1.06	0.58	3.42	49.2	5.15	4.95
74.	40.	460.	7.71	7.91	9.37	10.32	9.2	3.05	1.45	8.41	43.8	5.15	4.64
75.	40.	460.	9.21	8.78	9.37	10.24	8.5	1.55	2.95	4.57	40.5	4.09	4.06
76.	43.	293.	9.90	9.60	9.37	10.28	8.8	1.11	1.93	3.46	26.8	3.17	2.94
77.	46.	293.	10.24	10.11	9.37	10.29	8.9	1.00	0.65	3.23	27.1	3.17	3.01

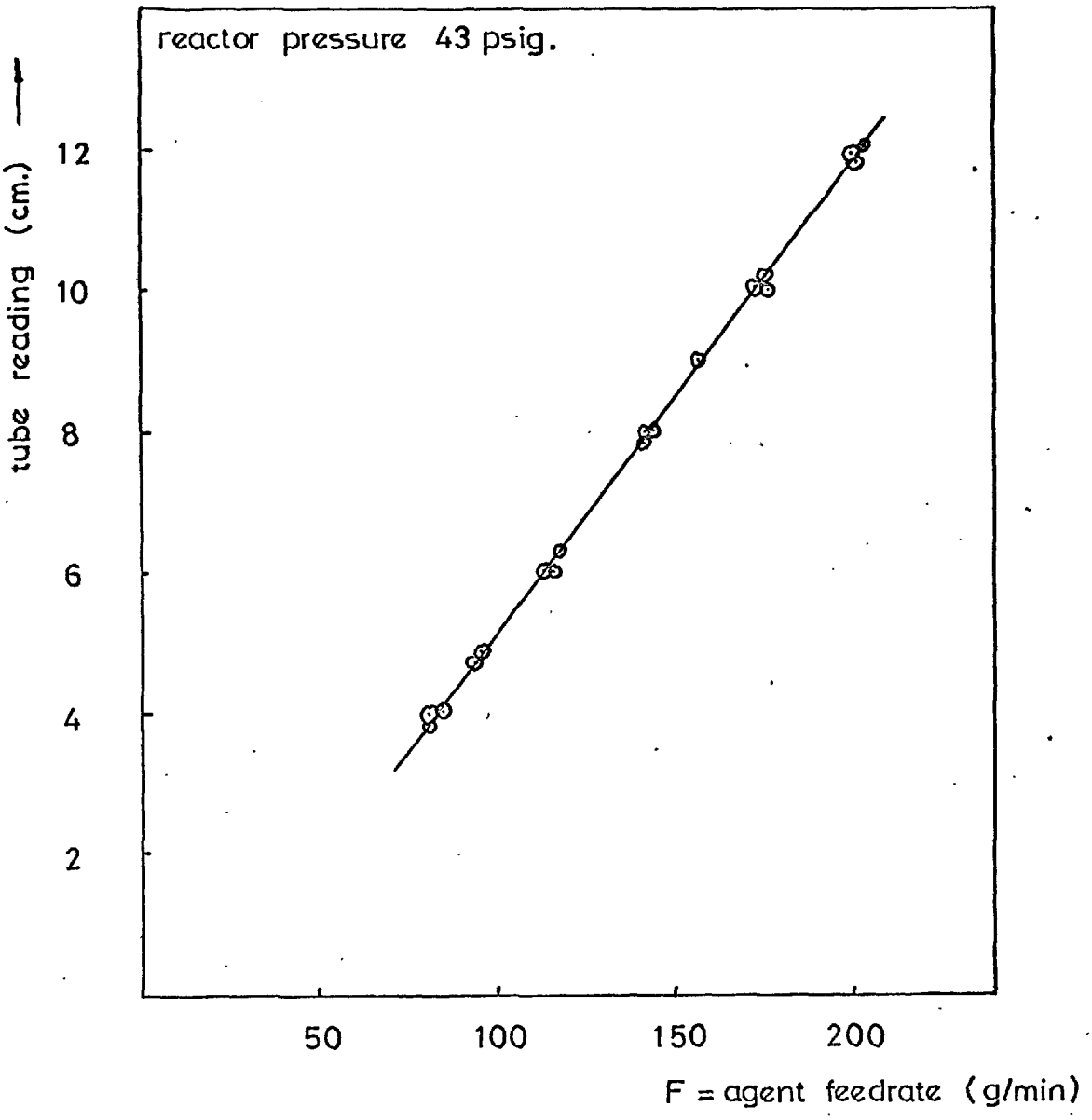


figure A13 Calibration of Freon-12 feed Rotameter

Appendix C Propane hydrate data

C1 Introduction to Propane Hydrate Experiments

A comparison of the formation rates of propane and freon hydrate by Koppers (24) shows that the freon hydrate formation rate is just the larger of the two for a given thermal differential. There is insufficient data available to make a comparison in terms of the concentration driving force or to draw any conclusion as to the effect of the operating pressure on the propane hydrate formation rate. In order to make this comparison and perhaps strengthen the case for the postulated models, section 6.2, experiments were carried out with propane in the five litre reactor.

The experiments were conducted batchwise in a similar fashion to the earlier freon runs. The analysis was restricted to measurement of the steady, unsteady-state temperature T_r, and to a heat balance check by sampling the concentration of the mother liquor. Only one agitation rate, 1420 RPM, and one sucrose concentration, 10% was considered, corresponding to experimental block .11. The operating conditions were chosen by the same criterion as was used for the inter-block comparisons in the freon runs. The mean propane hydrate production rate was chosen to correspond

approximately to the formation rate of freon hydrate in block .11, such that the hydrate hold-up and heat load on the system are equivalent.

The critical decomposition temperature and pressure for 10% sucrose is approximately 4.9°C and 78.5 psia. respectively, hence it was necessary to maintain the glycol bath at -12°C and the reactor at 50-60 psig. The glass reactor was considerably outside its safety limit in this range, so the number of experiments was kept to a minimum.

The same rotameter as was used for liquid freon was used for liquid propane feed to the reactor. Since the latent heat of propane (90 cal/g.) is rather larger than for freon-12 (35 cal/g.), the flow rate of propane was considerably reduced to satisfy the criterion of equivalent production rates. The feed rotameter was dealing with a very small flow rate (maximum 50 g/min., see figure A15) at approximately 0°C, hence the feed tended to boil unless both feed subcoolers were working efficiently. The only operational difficulty arose from the fact that propane, unlike freon, is lighter than water. Any water vapour condensed in the condenser tended to collect near the liquid propane outlet in the condenser base. As a result, the feed line was

frequently blocked with hydrate.

The subcooling required for spontaneous nucleation to occur was of the same order, i.e. 2° to $3^{\circ}C$, as in the equivalent freon hydrate runs. No nucleation results are given in this section, since the spontaneous nucleation temperature was in the region of $0^{\circ}C$ and was consequently difficult to measure with the potentiometer.

C2 Experimental Results

Table XV shows details of the reactor conditions and production rate, the same nomenclature being used for the propane and freon systems. A heat balance is given; the net cooling rate Q was measured at T_r with no hydrate present, and the reactor heat load was determined from a mass balance. Samples of mother liquor were withdrawn and analysed during the course of the reaction. From this data, Table XVI, the rate of hydrate formation at T_r was estimated, see section 6.4. A comparison of the measured rates of heat and mass transfer is shown in figure A14.

C3 Phase Diagram for Propane Hydrate

The data presented by Williams (23) for the system

water-propane-hydrate can be fitted to the same model as that described in section 4.22.

$$T_c = 10.528 \log_{10} \cdot P_a - 14.50$$

The analysis of the propane hydrate runs required the evaluation of the freezing point depression on the hydrate equilibrium by 10% sucrose solution. The phase diagram was experimentally determined by the method described in 4.12. Although this method is not completely satisfactory, the error is negligible over the small range of temperature considered.

The slope of the above expression was quite representative of the sucrose results, hence for the range of 10% sucrose:

$$T_c = 10.528 \log_{10} \cdot P_a - 14.50 - 6.67x_r$$

The results are shown in Table XIV and the complete phase diagram is given by figure A16. Vapour pressure data was obtained from the Refrigeration Handbook. The saturation temperature $T_1\,^{\circ}C$ corresponding to P_a psia. can be expressed:

$$T_1 = 77.37 \ (\log_{10} \cdot P_a + 1.8357)$$

Pressure psig.	Temperature °C	Concentration w/w%
50.	3.81	11.14
54.	4.08	10.98
58.	4.30	10.75
60.	4.40	10.60
48.	3.82	11.03
52.	4.08	10.77
56.	4.33	10.43
60.	4.53	10.17
48.	3.72	11.04
52.	4.02	10.82
56.	4.26	10.52
58.	4.38	10.43
48.	3.71	9.88
50.	3.91	9.82
52.	4.07	9.76

TABLE XIV: Experimental Phase Equilibrium

C4 Propane Solubility in Sucrose Solutions

The solubility of propane in brine solutions was published by Umano (80); it was shown that Henry's Law holds for this system. The solubility model discussed in section 4.4 is used therefore to describe the solubility of propane in sucrose solutions. The 'salting-out' constant K was assumed to be the same for propane in sucrose as for freon in sucrose; the Henry's Law constant has the same order of magnitude in each case. A correlation for the constant is given by:

$$\log_{10} H = 8.25 - 1262.5/T + 7.51N$$

Umano's data and this expression is shown in figure A17.

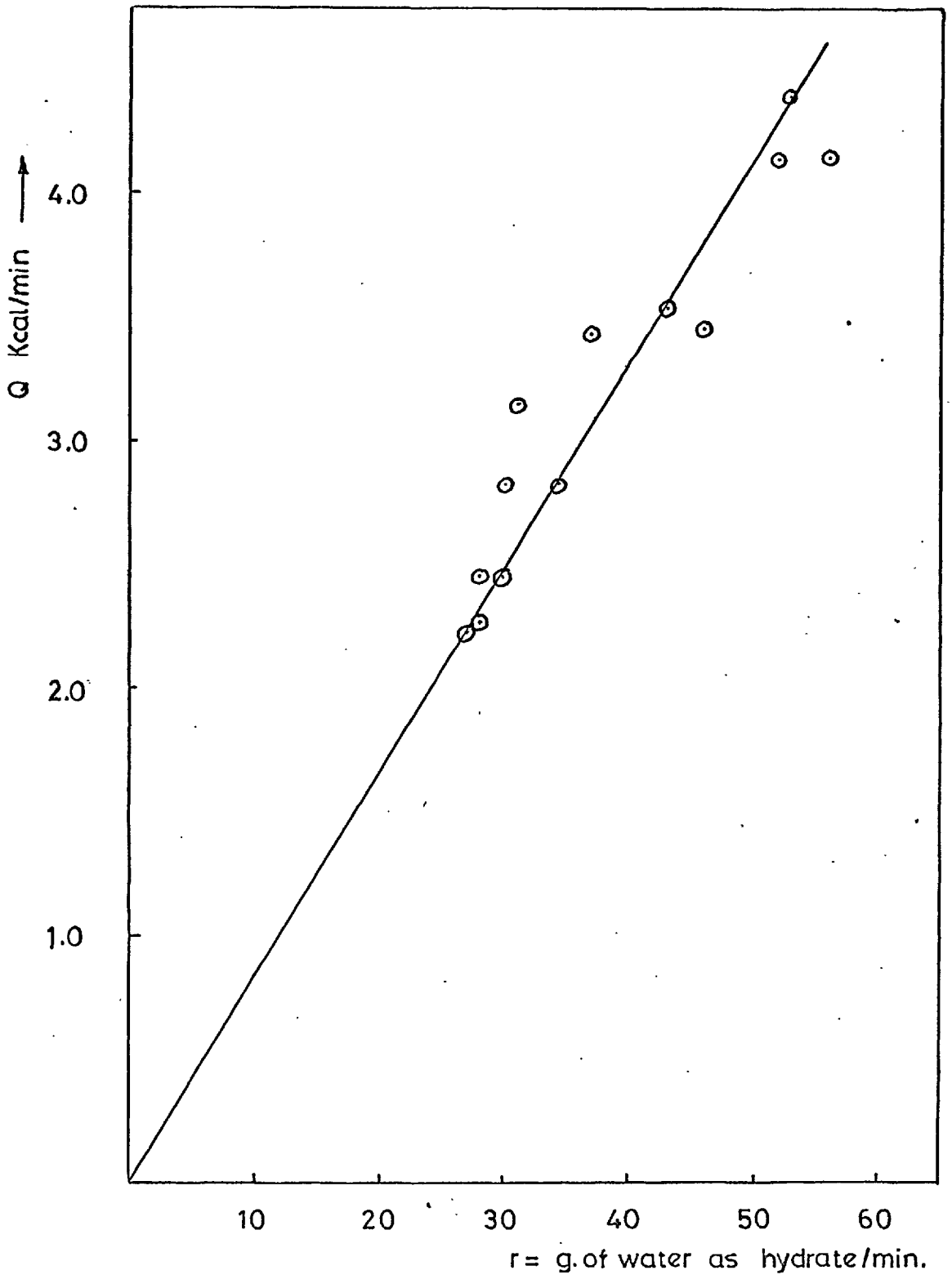


figure A14 Plot of cooling curve versus formation rate of propane hydrate

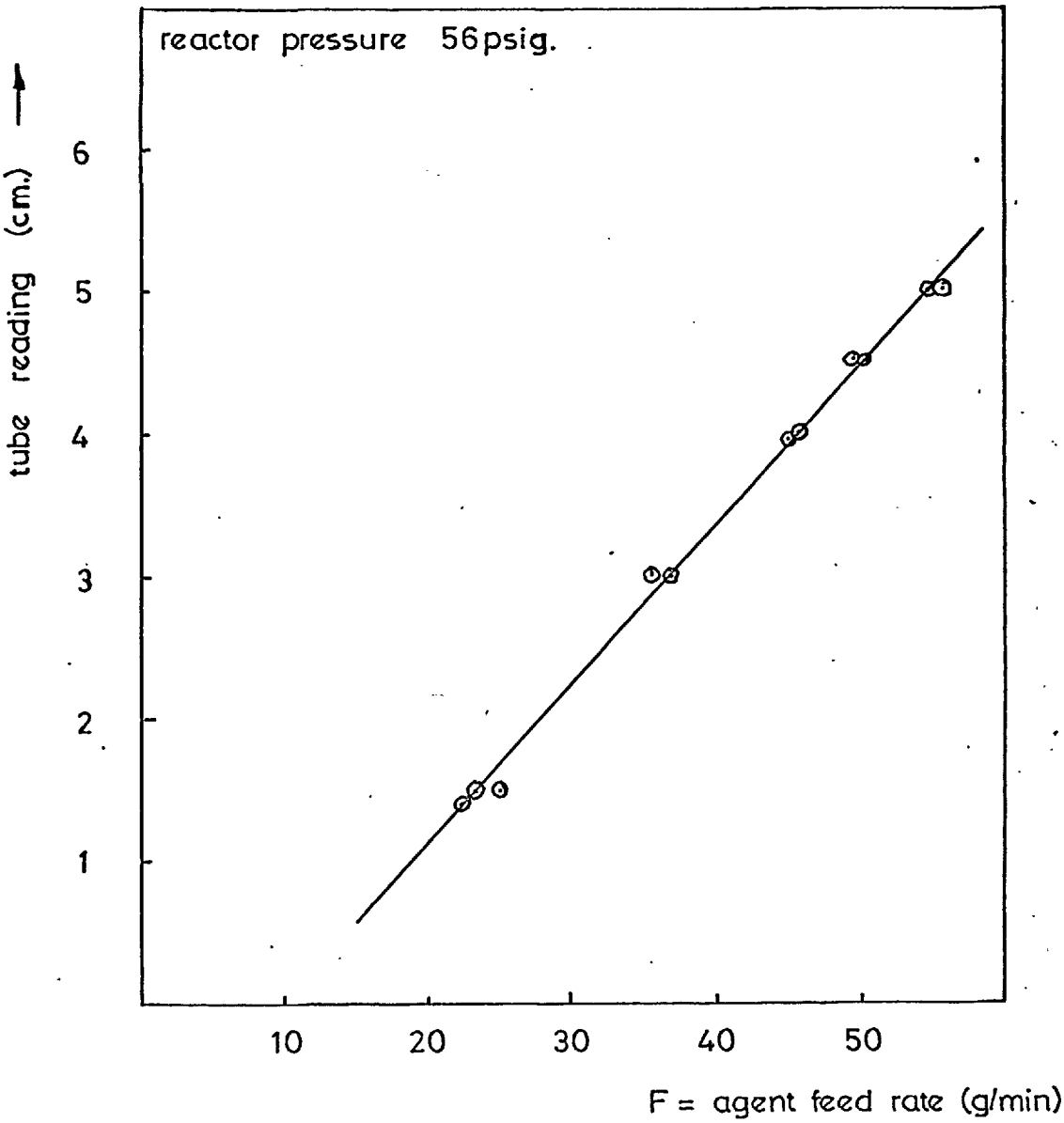


figure A15 Calibration of Propane feed Rotameter

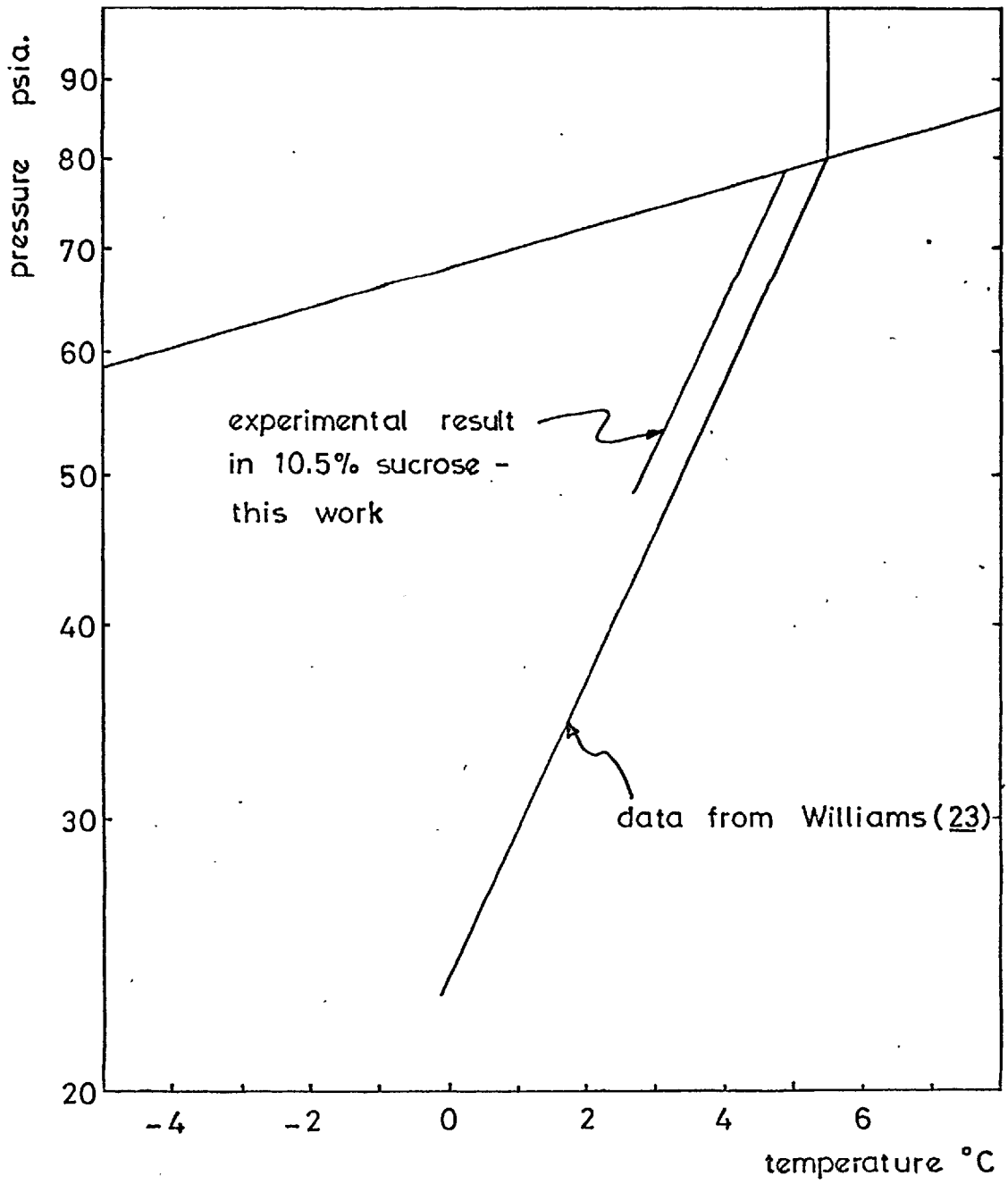


figure A16 Phase diagram: Propane / sucrose system

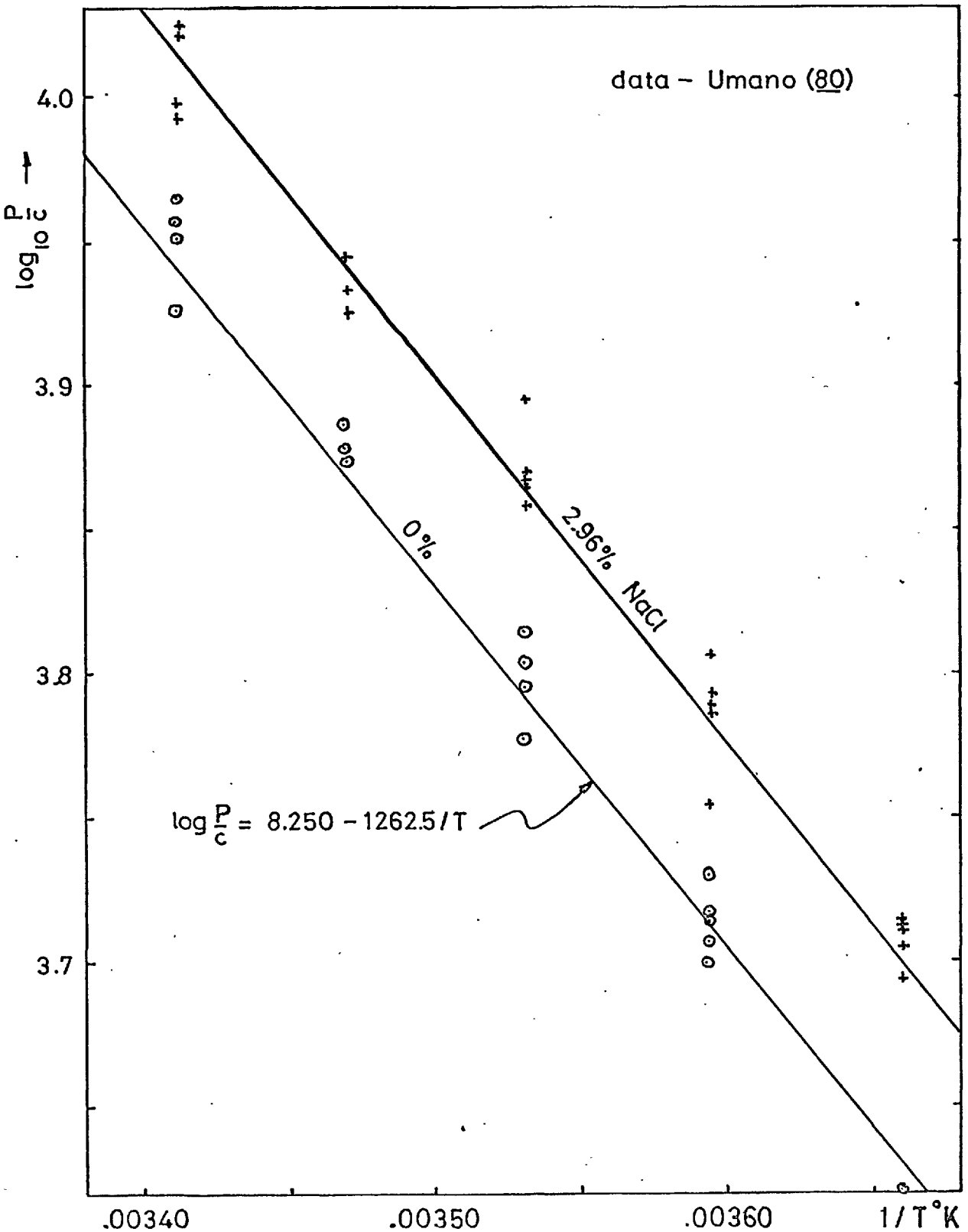


figure A17 Variation of Henry's law constant with temperature for propane in saline solutions

TABLE XV

PROPANE HYDRATE: 1420 RPM (DUAL IMPELLER), V_l = 3.55 l.

RUN	P psig	T_r °C	x_r w/w%	T_c	(T_c-T_r)	(T_r-T_l)	(C_b-C_s) x10^3 g.mol/l	r g/min	P/C*Deviation MODEL 75	Q Kcal/min	Reactor Heat load Kcal/min
101	52.	2.09	10.50	4.00	1.91	2.98	4.46	38.2	3.5	3.17	-
102	56.	2.96	10.50	4.27	1.31	1.89	3.33	37.8	-10.8	3.14	2,58
103	56.	3.11	10.50	4.27	1.16	2.05	2.97	29.4	1.4	2.44	2,49
104	52.	2.35	10.50	4.00	1.65	3.24	3.91	29.4	14.0	2.44	2.32
105	52.	1.54	10.50	4.00	2.46	2.43	5.54	53.0	-2.0	4.40	4.40
106	60.	3.42	10.50	4.52	1.10	0.51	2.97	41.3	6.8	3.43	3.08
107	58.	3.25	10.50	4.40	1.15	1.23	3.02	34.0	2.8	2.82	2.49
108	54.	2.78	10.50	4.14	1.36	3.68	3.35	34.0	-9.4	2.82	2.87
109	56.	2.52	10.50	4.27	1.75	1.46	4.31	50.0	-6.3	4.15	4.65
110	54.	2.00	10.50	4.14	2.14	1.90	5.02	50.0	1.1	4.15	4.32
111	58.	3.11	10.50	4.40	1.29	1.11	3.35	42.5	-6.6	3.53	3.57
112	54.	2.32	10.50	4.14	1.82	2.22	4.36	41.7	1.3	3.46	3.82
113	54.	2.98	10.50	4.14	1.16	2.89	2.89	27.35	-3.7	2.27	2.32
114	56.	3.17	10.50	4.27	1.10	2.11	2.83	26.9	4.9	2.23	2.24

* P/C Deviation = $100\left(\frac{\text{Predicted rate - measured rate}}{\text{Predicted rate}}\right)$

TABLE XVI

Production rate at T_r estimated from sucrose concentration : V_f = 3510.g

RUN	TIME mins	x_r w/w%	$1-x_f/x_r$	y g.	dy/dt g./min
101	0	9.95			-
	3.1	10.36	.0396	139.	
	4.95	10.75	.0744	261.	
	6.9	10.79	.0778	273.	
	8.5	10.95	.0913	321.	
102	0	9.95			31.
	2.8	10.35	.0386	136.	
	4.5	10.46	.0487	171.	
	6.7	10.66	.0666	234.	
	8.8	10.93	.0897	315.	
	11.0	11.13	.1060	372.	
103	0	9.95			30.
	2.5	10.28	.0321	113.	
	5.1	10.60	.0613	215.	
	7.55	10.75	.0744	261.	
	10.0	11.03	.0979	344.	
104	0	9.95			28.
	3.3	10.43	.0460	162.	
	5.75	10.70	.0701	246.	
	7.85	10.88	.0855	300.	
	10.0	11.09	.1028	361.	
105	0	9.95			53.
	2.05	10.36	.0396	139.	
	3.55	10.62	.0631	221.	
	5.65	10.88	.0855	300.	
106	0	9.96			37.
	2.75	10.59	.0595	209.	
	4.35	10.87	.0786	276.	
	6.25	11.02	.0962	338.	

TABLE XVI (continued)

RUN	TIME mins	x_r w/w%	$1-x_{f/x_r}$	y g.	dy/dt g./min
107	0	9.96			
	2.35	10.40	.0423	148.	
	3.45	10.55	.0559	196.	30.
	5.55	10.78	.0761	267.	
	7.6	10.98	.0929	326.	
	9.75	11.22	.1123	394.	
108	0	9.93			
	2.8	10.35	.0406	142.	
	5.0	10.62	.0650	228.	34.5
	7.2	10.87	.0865	303.	
	9.65	11.18	.1118	393.	
109	0	9.95			
	2.0	10.43	.0460	162.	
	3.45	10.68	.0684	240.	56.
	5.60	11.25	.1155	405.	
	7.35	11.45	.1310	460.	
110	0	9.94			
	2.35	10.38	.0424	149.	52.
	4.3	10.70	.0710	249.	
	6.75	11.12	.1061	373.	
111	0	9.94			
	2.45	10.50	.0533	187.	
	3.7	10.74	.0745	261.	43.
	6.05	11.04	.0996	350.	
	7.85	11.22	.1141	400.	
112	0	9.97			
	2.3	10.46	.0468	164.	
	4.35	10.74	.0717	252.	46.
	6.3	11.00	.0936	329.	
	7.75	11.28	.1161	408.	
113	0	9.93			
	3.55	10.42	.0470	165.	
	6.3	10.73	.0746	262.	28.
	9.55	10.99	.0965	339.	
	12.8	11.16	.1102	387.	
	15.9	11.52	.1380	485.	

Appendix D Decomposition results

D1 Heat and Mass Balance during Hydrate Decomposition

The following section outlines the method of checking the actual rate of decomposition of hydrate against the total heat input to the reactor. The method is only valid for a constant slurry temperature.

Hydrate was produced in a volume V_s of aqueous sucrose solution of concentration x_s, to give a hold-up of approximately 15-20% of hydrate. The heater was switched on and, when a steady decomposition temperature was reached, the concentration of mother liquor, x_o, was measured. Thereafter the concentration x was measured at given time intervals.

Take a mass balance on the solvent phase:

$$y_o + V_o\rho_o(1-x_o) = y + V\rho(1-x) \qquad (D1)$$

A mass balance on the solute phase:

$$V_o\rho_o x_o = V\rho x = V_s\rho_s x_s \qquad (D2)$$

where the non-subscripted variables are functions of time and where the subscripts refer to:

s - reactor conditions before hydrate is formed

o - conditions when temperature is constant at T_d.

Hence from (D1) and (D2)

$$y_o - y = V_o \rho_o \left({}^{x_o}/_{x} - 1\right)$$

$$\therefore \quad y_o - y = V_s \rho_o \, {}^{x_s}/_{x_o} \left({}^{x_o}/_{x} - 1\right) \qquad (D3)$$

Experimental values of x and calculated values of $(y_o - y)$ are presented in Table XIX, and $(y_o - y)$ is plotted against time for all runs D1 - D15 in figure A18. The slope of $y_o - y$ with time gives the rate of decomposition of the hydrate.

D2 Calorimetric Check on Total Heat Input

The total heat input was the sum of three terms; the heat leak into the reactor, the power dissipated by the stirrer and the power consumed by the immersion heater. The latter was measured by a watt meter and the other terms were estimated by a calorimetric calibration. Heating curves were obtained for aqueous solution in the stirred reactor, Table XVII, within the temperature range for decomposition and with no hydrate present.

D3 Specimen Calculation of Heat and Mass Balance

Example: 880 RPM, 3.30 litres of 10% sucrose, 100 watts input.

Heat load + stirrer power + heat leak = $(w+w')\ dT/dt$

w = Heat capacity of sucrose solution = 3.15 Kcal/^{o}C

w' = Heat capacity of reactor and fittings. This was estimated by considering dT/dt for different values of the heat load = 0.295 Kcal/^{o}C

$\therefore$ Total heat input = (3.15 + 0.295) 0.475

= 1.63 Kcal/min

Now from figure A18, the rate of decomposition of hydrate is given; = 17.8 g. of water as hydrate as hydrate/min

$\therefore$ rate of absorption of heat = 17.8 x 90. cal/min

= 1.60 Kcal/min

N RPM	Heater load Watts.	Heating Rate dT/dt ^{o}C/min	Total Heat input Kcal/min	Decomposition Rate g/min	Heat Absorption Rate Kcal/min
880	100	0.475	1.63	17.80	1.60
880	200	0.892	3.06	33.75	3.04
1420	200	0.982	3.38	37.25	3.35

Table XVII: Comparison of heat and mass transfer

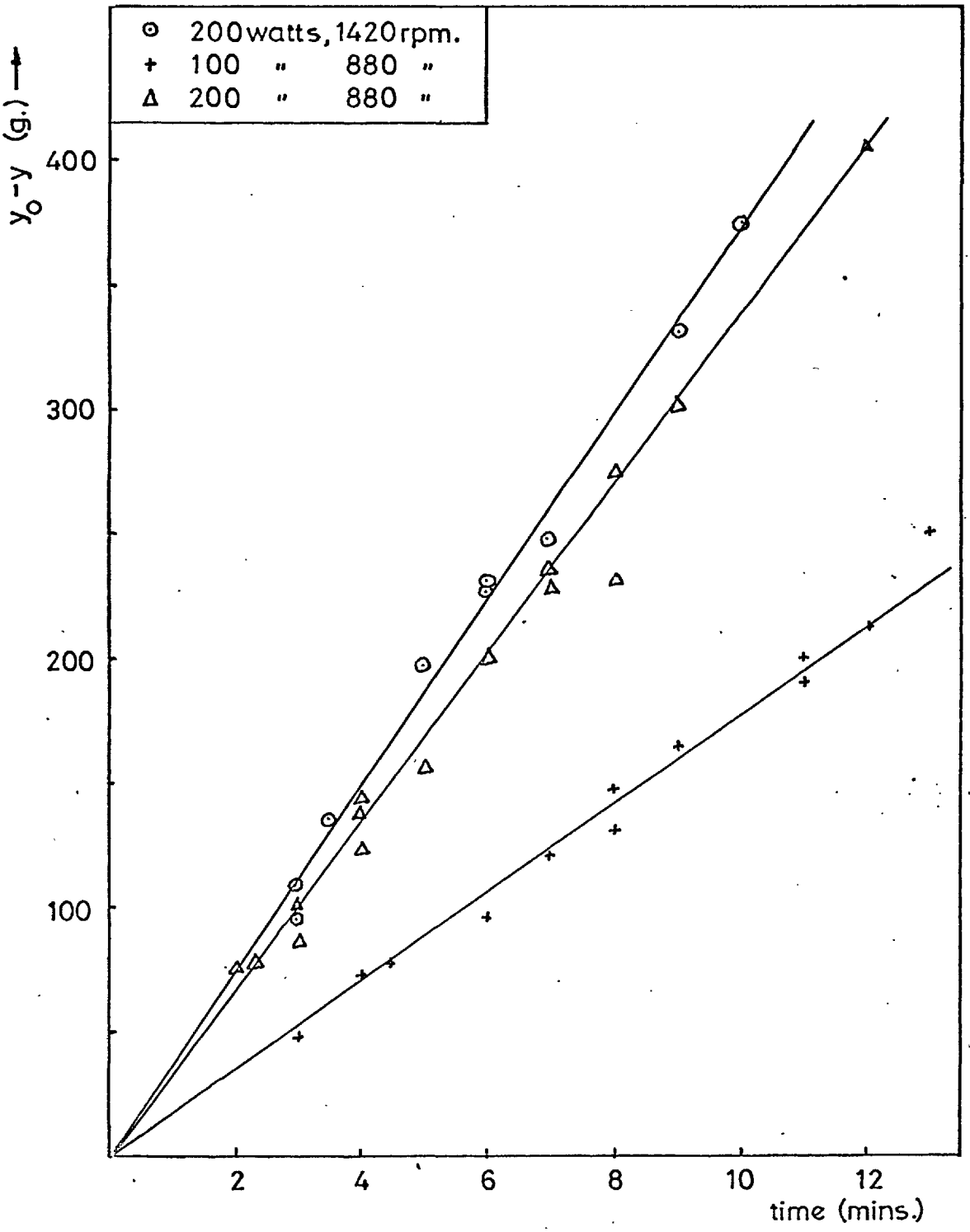


figure A18 Decomposition of hydrate slurry with time

TABLE XVIII

Decomposition Runs D1-D15, summary of reactor conditions

RUN	Heater input (Watts)	N RPM	P psig	T_d °C	T_c °C	Equilibrium C_s Pressure psia	C_s g.mol/l	C_r g.mol/l	C_s-C_r	Pa/p^*
D1	100	880	31.	10.36	9.90	50.54	.01076	.00974	.00102	.700
D2	100	880	34.	10.53	10.20	52.35	.01108	.01030	.00078	.745
D3	100	880	40.	10.87	10.73	56.37	.01174	.01139	.00036	.837
D4	100	880	43.	11.19	10.98	60.44	.01240	.01184	.00056	.882
D5	100	880	46.	11.42	11.21	63.54	.01290	.01232	.00058	.928
D6	200	880	31.	10.68	9.90	54.10	.01137	.00960	.00176	.700
D7	200	880	34.	10.81	10.20	55.64	.01162	.01017	.00145	.745
D8	200	880	37.	11.17	10.47	60.18	.01236	.01062	.00174	.790
D9	200	880	40.	11.30	10.73	61.90	.01264	.01116	.00148	.837
D10	200	880	43.	11.45	10.98	63.96	.01297	.01170	.00127	.882
D11	200	880	46.	11.53	11.21	65.08	.01314	.01226	.00088	.928
D12	200	1420	31.	10.37	9.90	50.56	.01078	.00974	.00103	.700
D13	200	1420	34.	10.58	10.20	52.92	.01117	.01028	.00089	.745
D14	200	1420	43.	11.08	10.89	59.78	.01238	.01189	.00049	.882
D15	200	1420	46.	11.33	11.12	63.12	.01292	.01238	.00054	.928

TABLE XIX

Rate of Mass Transfer during Decomposition

RUN	Time (mins.)	x (w/w)	$V_s \rho_s x_s/x_o$ (gm)	$y-y_o$ (gm)
D1	0.	.1139	2820.	0.
	3.	.1120		49.5
	9.	.1078		165.
	13.	.1048		253.
D2	0.	.1090	3050.	0.
	4.	.1060		68.5
	8.	.1045		131.
	11.	.1026		190.
D3	0.	.1133	2910.	0.
	3.	.1114		49.5
	6.	.1097		96.
	11.	.1060		200.
D4	0.	.1167	2840.	0.
	4.	.1138		72.
	7.	.1119		121.5
	11.	.1092		195.
D5	0.	.1173	2840.	0.
	4.5	.1141		79.5
	8.	.1115		147.
	12.	.1091		213.
	16.	.1078		250.
D6	0.	.1100	3020.	0.
	3.	.1070		85.
	6.	.1032		199.
D7	0.	.1080	3050.	0.
	4.	.1033		139.
	8.	.1006		224.

TABLE XIX (continued)

RUN	Time (mins.)	x (w/w)	$V_s \rho_s x_s/x_o$ (gm)	$y-y_o$ (gm)
D8	0.	.1092	2950.	0.
	2.	.1065		75.
	5.	.1037		157.
D9	0.	.1088	2950.	0.
	2.3	.1060		77.5
	4.	.1045		121.
	7.	.1013		222.
	10.	.0987		300.
D10	0.	.1162	2940.	0.
	4.	.1105		146.
	7.	.1073		235.
D11	0.	.1168	3000.	0.
	4.	.1122		123.
	8.	.1070		275.
	12.	.1030		403.
D12	0.	.1122	2960.	0.
	3.	.1092		81.2
	6.	.1053		193.
	9.	.1016		309.
D13	0.	.1138	2920.	0.
	3.	.1097		109.
	6.	.1056		227.
	9.	.1022		331.
D14	0.	.1282	2600.	0.
	3.	.1236		96.
	5.	.1191		198.
	7.	.1170		248.
D15	0.	.1362	2440.	0.
	3.5	.1291		134.
	6.	.1244		231.
	10.	.1180		376.
	12.	.1131		498.

Appendix E Solubility and Equilibrium Data

E1 Calculation of Solubility

Calibrated System Volume

Total volume of system = 155.76 cc. + burette reading.

(System bounded by valves V2, V3 and mercury surface)

Sample 1

Reactor Pressure	=	61.7 psia.
Reactor Temperature	=	10.49 ^{o}C
Burette Reading	=	23.90 cm^3
Weight of sample in F	=	128.25 g.
Atmospheric pressure	=	760.0 mm. Hg
Ambient temperature	=	20.0 ^{o}C
Vapour pressure of water at ambient T	=	17.5 mm. Hg
Total volume of system	=	155.76 + 23.90 = 179.66 cc
$\therefore$ Volume of Freon flashed from solution	=	(179.66 - 128.25)
	=	51.41 cm^3
$\therefore$ Solubility of Freon in sample above solubility at cell pressure	=	$\frac{51.41}{128.25} \times \frac{1}{22.4} \times \frac{742.5}{760} \times \frac{273.2}{293.2}$
	=	0.0163 g.mole/litre
Solubility of Freon at 742.5 mm Hg & 20°C	=	0.00028 g.mole/litre
$\therefore$ Solubility of Freon at 61.7 psia & 10.49^{o}C	=	0.00191 g.mole/litre

E2 Correction for Heat of Solution

For a volatile solute which obeys Henry's law, the heat of solution is given by Glasstone (83):

$$H_s = -R \left(\frac{\partial \ln c}{\partial 1/T} \right)_p$$

where H_s = Heat of solution

and where the right hand side may be estimated directly from the best-fit equation (10), for freon in water:

$$\left(\frac{\partial \ln c}{\partial 1/T} \right)_p = 2.3026 \times 1633.2$$

$$\therefore \quad H_s = 7472 \text{ cal/gmole.}$$

The correction to the heat of formation calculated in section 4.21 considers the difference between the reactor conditions and the standard states of the reactants. Barduhn (38) gives the correction factors:

$$\Delta H_o = (1 - s + r) \mathcal{Z}_{hf} + r_w - sH_s$$

where ΔH_o = Heat of formation at standard state conditions

s = Moles of freon dissolved in water phase

r = Moles of water evaporated in gas phase

$_w$ = Latent heat of water

Both s and r are evaluated at the critical temperature and pressure, the freon concentration is given by equation (10):

$$c = 0.0188 \text{ gmole/litre}$$

$$c' = 0.00034 \text{ mole fraction}$$

and since the solubility is so low, the estimate of s is given by:

$$s = 17\ (0.00034)$$

since 17 molecules of water are incorporated with one molecule of freon in the hydrate unit cell.

The saturated vapour pressure of water at 12°C is 10.6 mm. Hg, and since the cell pressure is 3435 mm. Hg, by Dalton's law:

$$r = {}^{10.6}/_{3435} = 0.0031$$

Hence:

$$\Delta H_o = -0.9974 \times 31150 + 0.0031 \times 10611 - 0.0057 \times 7472$$

i.e. $\Delta H_o = -31.09$ Kcal/gmole

E3 Relationship between $(c_b - c_s)$ and $(T_c - T_r)$

$$c_b - c_s = c_b\ (1 - {}^{c_s}/_{c_b})$$

From Henry's law for constant T_r and x_r, and the definition of pressures, figure 16a:

$${}^{c_s}/_{c_b} = {}^{P_h}/_{P}$$

From the equilibrium line, equation (7):

$$T_c = 10.58 \ln P + f(x_r)$$

$$T_r = 10.58 \ln P_h + f(x_r)$$

$$\therefore \quad c_b - c_s = c_b\ (1 - 10^{-\frac{(T_c - T_r)}{10.58}})$$

Since the R.H.S. is almost linear with $(T_c - T_r)$ up to $T_c - T_r = 3°C$, over a small range the temperature and concentration driving forces are almost equivalent.

TABLE XX

Freon-12, hydrate, water: Equilibrium Data in Unstirred Cell

Thermocouple T_{mvolts}	Hydrate temperature $T^{o}C$	Cell pressure psia	T_{Bath} ^{o}C
.325	8.30	27.95	5.7
.293	7.55	23.45	6.3
.281	7.24	22.25	6.1
.245	6.35	18.85	5.2
.228	5.95	16.95	4.8
.205	5.35	14.95	4.2
.190	5.00	13.95	3.9
.160	4.25	12.0	3.0
.135	3.60	10.53	2.3
.074	2.10	7.57	1.8
.090	2.50	8.07	4.0
.167	4.40	12.0	5.8
.296	7.60	23.95	9.0
.315	8.10	26.95	10.5
.322	8.27	27.95	11.5
.330	8.45	28.95	12.8
.360	9.20	34.95	12.9
.374	9.50	37.95	13.5
.390	9.95	40.95	13.8
.410	10.40	44.95	14.3
.440	11.10	52.95	14.8
.450	11.35	55.95	15.1
.460	11.60	59.95	15.7
.463	11.65	62.95	16.5
.470	11.80	64.85	16.5

TABLE XXI

Freon-12, hydrate, sucrose: Equilibrium Data in Stirred Reactor

Reactor Pressure Psia	Sucrose Concentration (w/w)	Slurry Temperature °C	Model Temperature Estimate °C	Experimental Temperature Corrected to Rounded Concentration
34.7	.4164	6.16	6.03	6.42 x=.400
38.7	.4085	6.65	6.61	6.78
42.7	.4031	7.10	7.10	7.15
44.7	.4279	6.94	6.86	7.41
48.7	.4216	7.30	7.33	7.66
52.7	.4104	7.77	7.84	7.93
54.7	.4238	7.72	7.76	8.12
56.7	.4156	7.93	8.05	8.18
42.7	.4276	6.71	6.68	7.17
46.7	.4196	7.19	7.19	7.51
50.7	.4104	7.67	7.68	7.83
54.7	.3999	8.10	8.16	8.10
40.7	.3183	7.97	7.96	8.14 x=.300
44.7	.3118	8.46	8.40	8.57
48.7	.3066	8.85	8.80	8.91
52.7	.3014	9.24	9.17	9.26
56.7	.2963	9.61	9.52	9.57
34.7	.3083	7.43	7.40	7.51
38.7	.2988	7.90	7.94	7.89
42.7	.2899	8.36	8.42	8.27
44.7	.3044	8.43	8.48	8.47
48.7	.2977	8.83	8.89	8.81
52.7	.2928	9.20	9.25	9.14
56.7	.2869	9.59	9.61	9.47

TABLE XXI (continued)

Reactor Pressure	Sucrose Concentration	Slurry Temperature	Model Temperature Estimate	Experimental Temperature Corrected to Rounded Concentration
Psia	(w/w)	°C	°C	
38.7	.2030	8.64	8.71	8.66 x=.200
42.7	.1980	9.07	9.15	9.06
46.7	.1933	9.52	9.55	9.47
52.7	.1884	10.08	10.07	10.00
46,7	.2138	9.39	9.40	9.49
50.7	.2089	9.79	9.77	9.86
54.7	.2043	10.17	10.11	10.20
58.7	.1979	10.48	10.45	10.46
34.7	.2102	8.22	8.22	8.29
38.7	.2058	8.68	8.69	8.72
42.7	.2002	9.13	9.13	9.13
46.7	.1953	9.53	9.53	9.50
34.7	.1071	8.87	8.92	8.91 x=.100
38.7	.1048	9.35	9.38	9.38
42.7	.1031	9.78	9.79	9.80
44.7	.1027	9.97	9.98	9.99
42.7	.1187	9.72	9.69	9.84
46.7	.1151	10.10	10.08	10.20
50.7	.1114	10.45	10.45	10.52
54.7	.1083	10.78	10.78	10.83
48.7	.1205	10.24	10.22	10.38
52.7	.1167	10.59	10.57	10.70
56.7	.1127	10.91	10.89	10.99
60.7	.1095	11.21	11.19	11.28
44.7	.0	10.55	10.52	
48.7	.0	10.87	10.87	
54.7	.0	11.36	11.34	
58.7	.0	11.64	11.64	
62.7	.0	11.90	11.90	
36.7	.0	9.70	9.71	
40.7	.0	10.11	10.13	
44.7	.0	10.51	10.51	
50.7	.0	11.00	11.03	
60.7	.0	11.78	11.77	

TABLE XXII

Solubility of Freon-12 in Sucrose

Sample	x	T_r	P	Sample Weight	Freón-12	Ambient Temperature	Ambient Pressure (corrected)	Solubility above Atmospheric	Total Solubility	Estimate from Model (10)
	w/w%	°C	psia	gm	cm^3	°C	mm.Hg.	g.mol/l	g.mol/l	
1	0.	10.49	61.7	128.25	51.41	20.0	742.5	.0163	.0191	.01914
2	0.	7.59	53.7	123.65	48.76	20.0	741.5	.0160	.0188	.0191
3	0.	7.61	53.7	128.15	49.51	20.1	741.5	.0157	.0185	.0191
4	0.	8.61	57.7	120.81	45.85	20.5	739.4	.0153	.0181	.01955
5	0.	9.48	59.7	122.29	54.52	20.5	736.0	.0179	.0207	.0194
6	0.	20.00	69.7	133.90	34.11	21.6	738.0	.0102	.0131	.01405
7	0.	20.05	54.7	133.55	25.81	21.6	738.0	.0078	.0105	.0110
8	0.	18.56	52.7	135.60	25.66	21.7	738.0	.0076	.0104	.0113
9	0.	9.64	28.3*	142.56	24.44	20.0	742.5	.0070	.00975	.0096
10	0.	10.23	41.7*	138.25	37.21	21.3	732.3	.0107	.0135	.0131
11	0.	9.08	31.5*	134.55	27.69	20.2	732.3	.00825	.01105	.01044
12	0.	9.01	30.75*	137.17	25.99	20.2	737.1	.00765	.0104	.0102
13	0.	12.	14.29	120.93	13.43	24.9	738.9		.00442	.00413
14	30.	12.	14.06	129.79	8.22	24.8	726.9		.00279	.00278
15	30.	12.	14.06	136.36	8.30	25.2	726.9		.00268	.00278
16	0.	12.	14.27	121.36	13.93	25.1	737.7		.00456	.00413
17	30.	12.	14.34	135.30	7.86	25.1	741.8		.00265	.00283
18	10.	13.72	50.7	132.79	31.00	20.5	739.4	.0098	.01217	.01225
19	10.	12.96	55.7	139.35	37.62	20.5	739.4	.0113	.0137	.0139
20	10.	5.82	45.2	127.55	41.75	20.7	734.4	.0136	.0160	.0158
21	10.	6.78	48.2	129.50	42.31	20.3	734.9	.0136	.0160	.0161
22	10.	6.79	50.7	131.75	43.10	21.2	730.7	.0135	.0159	.0169
23	10.	10.83	41.7	133.64	28.99	21.0	742.4	.0091	.0115	.0115

* Equilibrium pressure with hydrate crystals

TABLE XXII (continued)

Sample	x	T_r	P	Sample Weight	Freon-12	Ambient Temperature	Ambient Pressure (corrected)	Solubility above Atmospheric	Total Solubility	Estimate from Model (10)
	w/w%	°C	psia	gm	cm^3	°C	cm.Hg.	g.mol/l	g.mol/l	
24	10.	10.80	42.7	134.75	29.82	20.7	734.9	.0092	.0116	.0118
25	10.	12.43	41.7	131.21	26.81	21.2	739.2	.0085	.01093	.0107
26	10.	8.75	50.7	128.19	40.53	21.2	739.2	.0132	.0156	.0154
27	10.	10.20	47.7	133.55	37.10	20.3	739.	.0116	.0140	.0136
28	10.	10.26	46.7	137.75	36.05	20.5	736.	.0109	.0133	.0132
29	10.	10.03	60.7	122.60	45.16	20.0	735.	.0153	.0177	.0174
30	30.	12.79	55.7	142.10	27.91	20.5	732.9	.00885	.0108	.0106
31	30.	10.14	47.7	138.69	27.00	20.8	731.8	.00875	.0107	.0103
32	30.	10.37	53.7	137.55	29.25	20.5	738.3	.00965	.0116	.0114
33	30.	8.48	47.7	136.71	28.69	21.3	734.5	.00945	.0114	.0111
A	0.	25.	90.						.01445	.01465
B	0.	25.	70.						.0111	.0114
C	0.	25.	50.						.00794	.00814
D	0.	25.	30.						.00478	.00488
E	0.	30.	100.						.01293	.01322
F	0.	30.	80.	du Pont data (37) A-N					.01043	.01057
G	0.	30.	60.						.00778	.00793
H	0.	30.	40.						.00516	.00529
I	0.	35.	80.						.00872	.00865
J	0.	35.	60.						.00655	.00649
K	0.	35.	40.						.00418	.00432
L	0.	40.	80.						.00766	.00712
M	0.	40.	60.						.00566	.00534
N	0.	40.	40.						.00368	.00356

Appendix F Filtration data

F1 Calculation of Solids Fraction in Wash Column

The following calculation arrives at a value of the void or interstitial volume of liquor retained within the bed independently of the 'breakthrough' estimate. A total slurry volume, V, is introduced into the wash column to form a drained bed of height 1 cm. The volume of filtrate, V_F, and its concentration, x_F, is measured as the bed is drained. The voids in the bed are filled with sucrose solution of the same concentration as the initial filtrate and occupy a total interstitial volume, V_i. If the true weight of water in the form of hydrate crystals is M_m, then assuming the slurry to be representative of the reactor contents, a mass balance on the slurry may be written:

$$\rho_F(V_F + V_i)(1 - x_F) + M_m = V\rho_f(1 - x_f) \quad \text{solvent}$$

$$\rho_F(V_F + V_i)\, x_F = V\rho_f x_f \quad \text{solute}$$

Hence: $$M_m = \rho_F \{(V_F + V_i)(1 - x_f)(x_F/x_f - 1)\}$$

After washing, consider the void volume to have been replaced by wash water containing a small fraction of sucrose. When the bed is decomposed by heating, a total melt volume V_m is obtained. Hence:

$$M_m + V_i\rho_F = V_m\rho_m$$

where ρ_F = density of final wash effluent

ρ_m = density of decomposed hydrate and wash liquor combined

Hence:

$$V_i\rho_F = V_m\rho_m - \rho_F \{(V_F + V_i)(1 - x_f)(x_F/x_f - 1)\}$$

Example: Run F1

The data is presented in Table XXIII and XXIV

$V_i\rho_F = 115 - 1.038\ (530 + V_i)(0.902)(0.50/9.8)$

Hence $V_i = 87\ cm^3$

Compare with the voidage volume given by the criterion $x_F/x_o = 0.5$ for F1 in figure A19,

i.e. $V_i = 103\ cm^3$

$M_m = 28$ gms. of water as hydrate.

From the composition of freon-12 hydrate:

Total volume of crystals $= 28 \times 427/306 = 39\ cm^3$.

Hence the solids fraction = 21.7%

F2 Calculation of the Dispersion Coefficient

Danckwerts (76) presented a mathematical treatment of the general problem of displacement of one fluid by another in a packed bed. The approximate solution for the diffusion equation is given by:

$$x_F = \frac{x_o}{2}\left(1 - \text{erf}\left(\frac{N-1}{2\sqrt{\frac{DN}{lu}}}\right)\right)$$

where
- x_o = sucrose in initial filtrate
- x_F = sucrose concentration in effluent stream
- N = number of displacements of void volume
- D = dispersion coefficient based on superficial velocity (cm^2/sec)
- u = superficial wash velocity (cm/sec)
- l = bed height (cm)

The ratio ${}^{x}F/x_o$ is tabulated in Table XXV and plotted against the accumulated wash volume V_A in figure A19 to A21. At ${}^{x}F/x_o = 0.5$, $V_A = V_i$, the void volume, i.e. $N' = 1$. The dispersion coefficient may be estimated by using a point taken from the wash curve.

The accumulated wash volume at ${}^{x}F/x_o = 0.01$ is V_A^*, hence $N = V_A^*/V_i$. Substituting in the Danckwerts equation:

$$1 - 2{}^{x}F/x_o = 0.98 = \operatorname{erf}\left(\frac{V_A^*/V_i - 1}{2\sqrt{\frac{D_l V_A^*}{V_i l u}}}\right)$$

Since, from mathematical tables, the argument of the error function of 0.98 is 1.645:

$$D_l^{0.5} = \frac{V_A^*/V_i - 1}{3.29\sqrt{\frac{V_A^*}{V_i l u}}}$$

From Run F1:

$V_A^* = 160 \text{ cm}^3$ $\quad l = 15.8 \text{ cm}$

$V_i = 103 \text{ cm}^3$ $\quad u = 0.0374 \text{ cm/sec}$

$\therefore \quad D_l = 10.65 \times 10^{-3} \text{ cm}^2/\text{sec}$

Alternatively Danckwerts recommended the use of the slope of the wash curve at $V_A = V_i$:

$$\left(\frac{d({}^{x}F/x_o)}{d(V_A/V_i)}\right)_{V_A=V_i} = -\tfrac{1}{2}\left(\frac{lu}{D_2}\right)^{0.5}$$

From Run F1:

Slope at $({}^{x}F/x_o = 0.5) = 1.56$

$\therefore \quad D_2 = 18.8 \times 10^{-3} \ cm^2/sec$

Estimated values of D_1 and D_2 are given in columns 6 and 7 of Table XXIII.

F3 Pressure Drop Measurements Across the Bed

For a selection of runs the pressure drop across the bed of hydrate crystals was measured for a given wash rate. A mercury manometer was attached to pressure probes placed above and at the base of the bed. The probes were provided with filter caps to prevent the ingress of hydrate crystals.

It was considerably difficult to purge the connecting lines efficiently. This was mainly due to the maldistribution of liquid in the bed. At some points the bed was bypassed, leaving the probe isolated in the gas phase. The results below were obtained for the conditions given in Table XXIV.

The Carman equation (86) for fluid flow through packed beds, at a Reynolds number of less than one, gives:

$$D_c^2 = \frac{180 \, lu\eta_l (1 - e)^2}{\Delta P e^3}$$

where e = void fraction

Assuming the crystals to be spheres, the crystal sizes are shown in Table F3. Stable pressure drop readings could be obtained only when the space below the filter disc was flooded and a small head of wash water was maintained above the crystal bed.

Run	ΔP cm. Hg.	Void fraction e	Superficial wash velocity u cm/sec	D_c microns
F10	11.3	0.62	0.028	25
F11	5.5	0.63	0.030	35.5
F12	8.9	0.60	0.035	35
F13	12.4	0.66	0.032	21

Table F3 Estimated Crystal Size

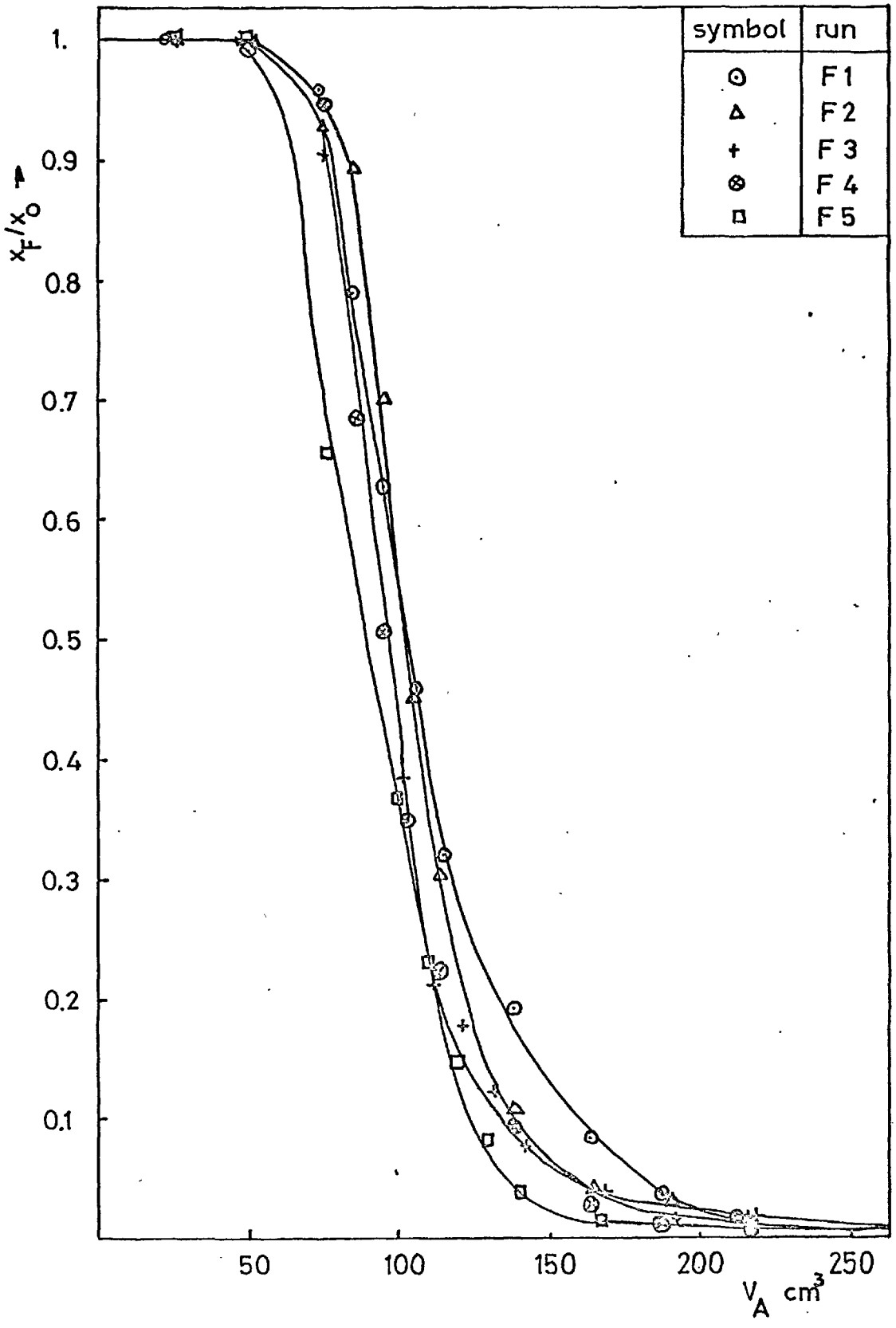


figure A19 Concentration profile in wash effluent – 15.5 cm. bed

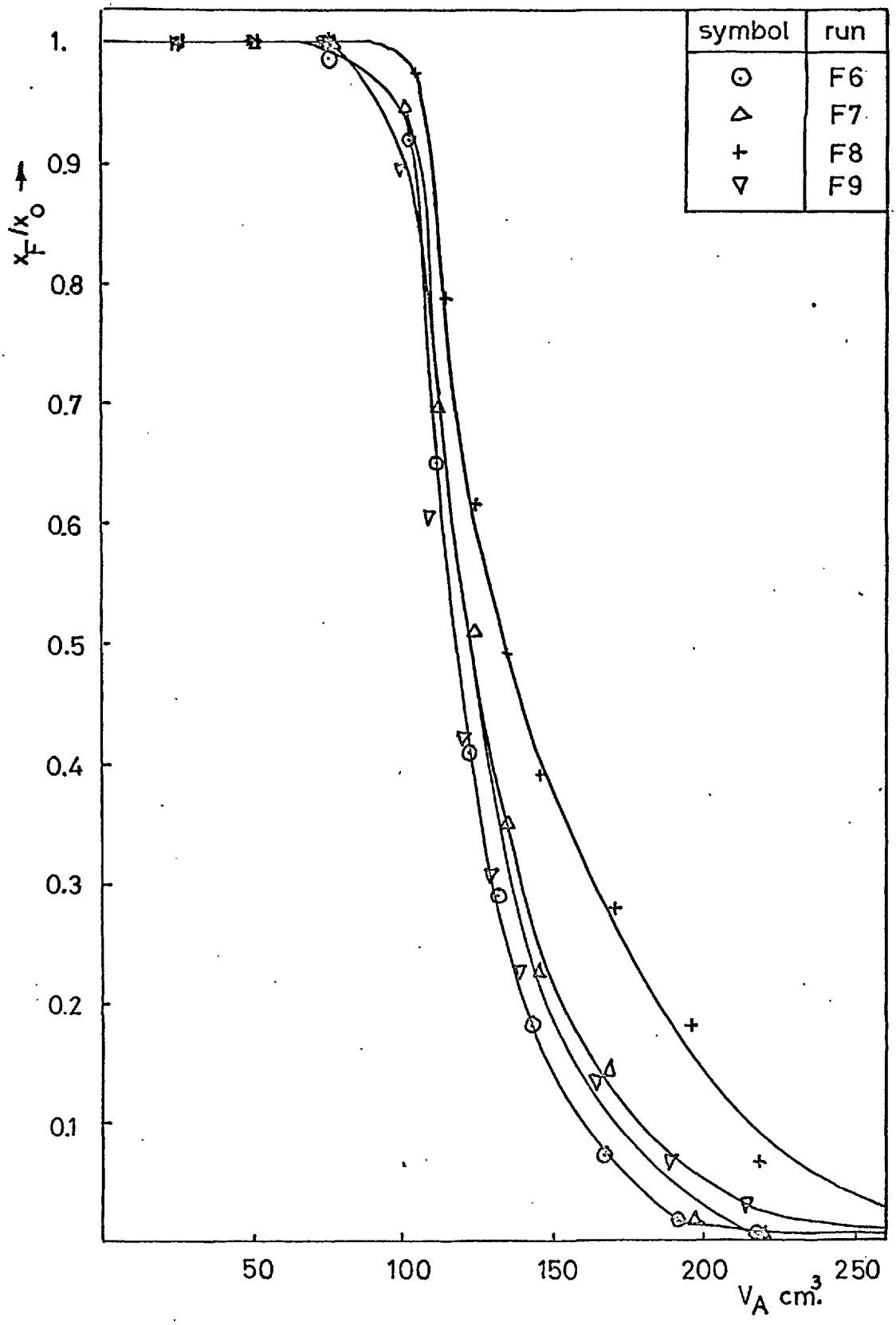


figure A20 Concentration profile in wash effluent - 22 cm. bed

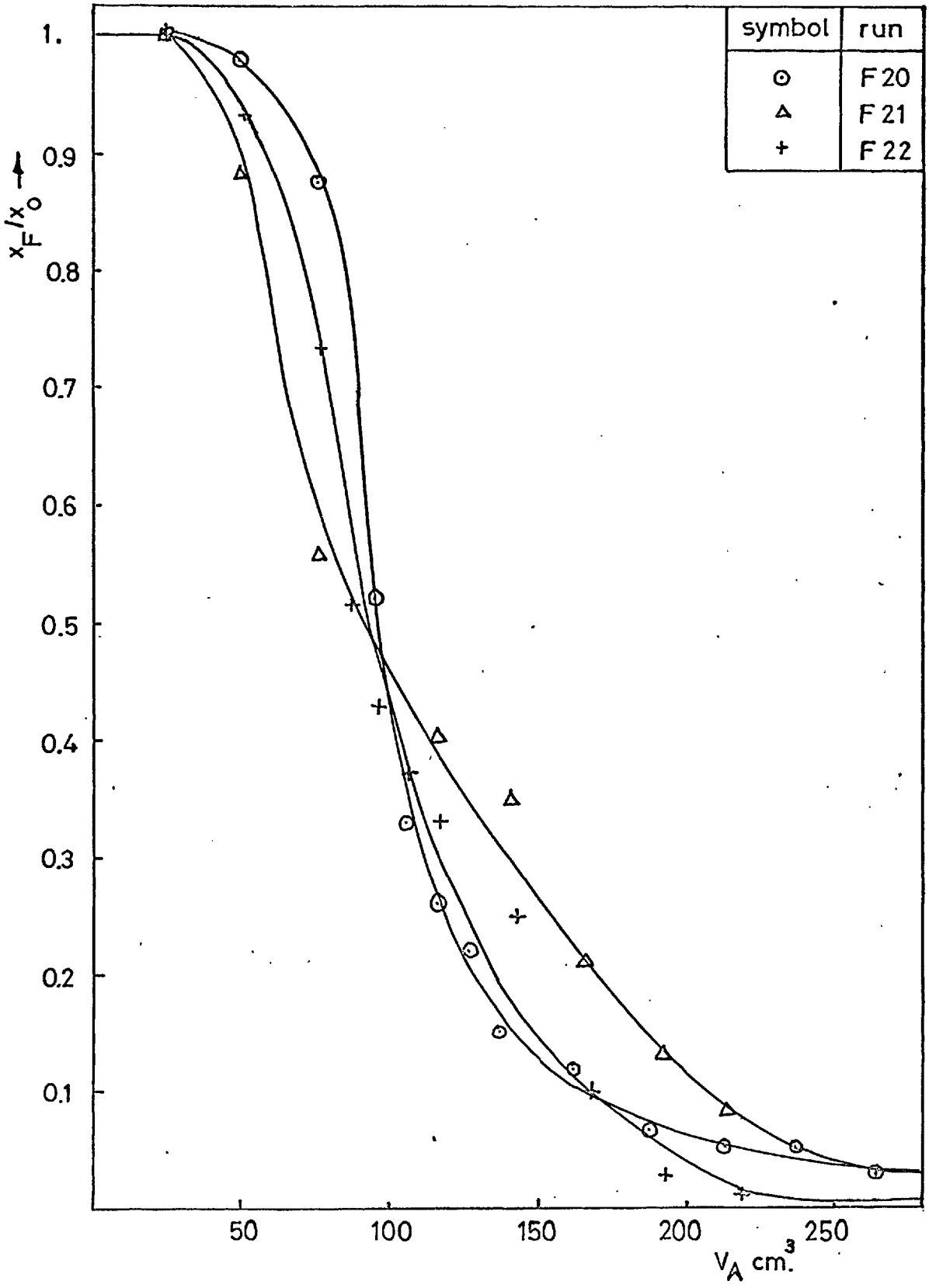


figure A21 Concentration profile in wash effluent – 15.8 cm. bed

TABLE XXIII

Summary of Wash Experiments in 2" dia. Column

Run	Sucrose Feed w/w%	Bed Volume cm^3	Solids Fraction vol.%	Wash Rate cm^3/min	$D_1 x10^3$ cm^2/sec	$D_2 x10^3$ cm^2/sec
F1	9.80	182.	21.7	44.2	10.65	18.8
F2	9.80	179.	27.2	47.7	5.5	11.7
F3	9.80	181.	32.5	45.0	7.2	10.5
F4	9.80	179.	35.7	40.2	6.5	12.3
F5	9.81	181.	35.0	45.8	6.3	20.6
F6	9.82	256.	39.2	39.0	6.4	3.3
F7	9.81	256.	33.3	46.0	8.1	12.3
F8	9.82	256.	25.4	21.6	8.2	15.8
F9	9.80	256.	29.8	38.0	10.8	8.8
F10	9.81	256.	38.0	33.0	11.1	9.6
F11	9.80	260.	37.2	35.5	4.3	4.6
F12	9.82	262.	40.0	41.0	10.6	17.5
F13	9.81	256.	33.7	37.4	3.6	4.8
F20	25.21	182.	-	35.0	13.3	4.4
F21	25.22	182.	24.2	48.0	40.5	29.7
F22	25.21	182.	28.0	48.3	22.9	43.2

TABLE XXIV

Summary of wash and hydrate formation conditions

Run	Wash Conditions							Reactor Conditions			
	Bed Height	Filtrate V_F	Filtrate x_F	Melt V_M	Melt x_M	Crystal Volume	Interstitial Volume	Reactor Pressure	Residence Time	ϕ_h	Impeller S(single) D(Dual)
	cm.	cm^3	w/w%	cm^3	w/w%	cm^3	cm^3	psig.	mins	%	
F1	15.8	530	10.30	115	0.65	39.	87.	40	8.8	4.85	S
F2	15.5	390	10.57	130	0.12	49.	95.	43	8.8	7.3	S
F3	15.8	305	10.94	138	0.22	58.5	96.	46	8.8	10.4	S
F4	15.5	335	10.97	143	0.28	64.2	97.	46	8.8	10.7	S
F5	15.8	740	10.40	135	0.18	63.	90.	46	8.8	5.7	S
F6	22.	655	10.80	205	0.03	100.	133.	43	13.7	9.25	S
F7	22.	580	10.75	192	0.025	85.	131.	40	13.7	8.90	S
F8	22.	355	10.89	166	0.29	65.	119.	46	8.8	10.0	S
F9	22.	420	10.91	171	0.08	76.	117.	46	8.8	10.1	S
F10	22.	530	11.10	175	0.05	97.	106.	43	8.8	10.8	D
F11	22.4	530	10.95	186	0.09	95.	118.	43	8.8	10.4	D
F12	22.5	575	10.95	192	0.05	102.	119.	43	13.7	10.4	D
F13	22.	790	10.54	179	0.04	85.5	118.	43	8.8	6.9	D
F20	15.8	-	-	76	-	-	-	36	13.7	7.32	D
F21	15.8	390	27.38	130	0.48	43.5	98.	36	13.7	7.92	D
F22	15.8	505	27.14	139	0.30	50.5	103.	36	13.7	7.10	D

TABLE XXV

Effluent Wash Liquor concentration with Accumulated Volume

RUN F1, wash : 10 mins.			RUN F2, wash : 10 mins.			RUN F3, wash : 15 mins.		
V_A	x_F	x_F/x_o	V_A	x_F	x_F/x_o	V_A	x_F	x_F/x_o
25.	10.63	1.0	25.	10.9	1.0	25.	11.25	1.0
50.	10.54	0.99	50.	10.9	1.0	75.	11.29	1.01
74.	10.19	0.956	75.	10.14	0.93	101.	10.20	0.905
84.5	8.41	0.790	85.	9.74	0.894	111.5	4.35	0.386
94.5	6.67	0.628	94.5	7.60	0.698	121.	2.4	0.213
105.	4.85	0.456	104.5	5.00	0.459	132.	2.0	0.178
115.	3.36	0.316	114.5	3.32	0.305	142.5	1.4	0.124
135.	2.06	0.194	138.5	1.20	0.11	167.5	0.85	0.075
164.	0.89	0.084	165.5	0.45	0.041	192.5	0.45	0.04
188.	0.38	0.036	190.5	0.35	0.032	218.5	0.20	0.017
212.	0.18	0.017	215.5	0.17	0.015	328.5	0.20	0.017
317.	0.12	0.011	330.5	0.35	0.032	438.5	0.10	0.009
442.	0.07	0.007	477.5	0.04	0.004	558.5	0.07	0.006
						668.5	0.03	0.003

TABLE XXV (continued)

RUN F7, wash : 10 mins.			RUN F8, wash : 17 mins.			RUN F9, wash : 12 mins.		
V_A	x_F	x_F/x_o	V_A	x_F	x_F/x_o	V_A	x_F	x_F/x_o
24.	11.07	1.0	25.	11.2	1.0	24.	11.20	1.0
50.	11.08	1.0	50.	11.2	1.0	49.	11.20	1.0
76.	11.07	1.0	76.	11.2	1.0	74.	11.20	1.0
101.5	10.48	0.945	103.	10.93	0.975	99.	10.07	0.896
111.5	7.70	0.695	113.5	8.83	0.788	109.	6.75	0.602
122.	5.65	0.510	123.5	6.87	0.613	119.	4.70	0.420
132.5	3.85	0.348	133.5	5.50	0.490	129.	3.4	0.303
143.5	2.5	0.226	144.	4.30	0.384	139.	2.5	0.223
169.	1.6	0.144	169.	3.1	0.277	163.	1.5	0.134
195.	0.19	0.017	195.	2.0	0.178	189.	0.75	0.067
220.	0.035	0.003	219.	0.7	0.062	214.	0.33	0.029
343.	0.04	0.003	332.	0.1	0.009	309.	0.105	0.009
461.	0.04	0.003	367.	0.02	0.002	409.	0.030	0.003
						455.	0.010	0.0009

TABLE XXV (continued)

RUN F20, wash : 13 mins.			RUN F21, wash : 20 mins.			RUN F22, wash : 20 mins.		
V_A	x_F	x_F/x_o	V_A	x_F	x_F/x_o	V_A	x_F	x_F/x_o
25.	24.	1.0	25.	28.35	1.0	25.	28.62	1.0
50.	23.5	0.98	51.	25.0	0.882	51.	26.65	0.932
76.	21.0	0.875	76.	15.0	0.53	76.5	20.95	0.733
95.	12.5	0.52	86.			86.5	14.7	0.515
106.	8.0	0.33	96.			96.5	12.20	0.426
117.	6.3	0.263	106.			107.5	10.60	0.37
128.	5.25	0.22	116.	11.30	0.40	117.5	9.4	0.33
138.	3.60	0.15	141.	9.9	0.35	142.5	7.1	0.248
163.	2.85	0.12	166.	6.0	0.212	167.5	2.85	0.10
188.	1.60	0.067	191.	3.85	0.136	192.5	0.85	0.029
213.	1.35	0.056	214.	2.35	0.083	218.5	0.25	0.009
238.	1.35	0.056	331.	0.95	0.033	335.5	0.40	0.014
263.	0.80	0.033	443.	0.18	0.006	450.5	0.13	0.004
373.	0.68	0.028	568.	0.10	0.003	586.5	0.10	0.0035

Appendix G Calibrations and physical constants

G1 Calibration of Thermocouple Probes

The copper-constantin probes were individually calibrated against a standard platinum resistance thermometer in a stirred Dewar flask for the range 5-12°C. The characteristics of the platinum thermometer were known; the maximum possible error in the absolute value of the temperature was $\pm^{1}/_{20}$°C. The thermocouple e.m.f. was linear with temperature in the small range considered, the temperature °C was given by:

$$T = 28.98\ M$$

where M = Potentiometer reading in mv.

G2 Sucrose - Refractive Index

The variation in the refractive index of aqueous solutions with sucrose concentration at 20°C is well documented in the literature; Honig (81) and International Critical Tables. The former reference is most useful since it includes a survey of all physical properties of sucrose solutions.

The Abbe '60' refractometer reads directly in degrees and minutes rather than employing a non-linear refractive index scale. Bellingham and Stanley publish tables for the sodium D_1 line (5896 Å) for converting the critical angle to a refractive index value.

The accuracy with which the refractometer may be read is ±0.1 minute, which corresponds to a refractive index variation of ±0.000016. This in turn represents a change in the sucrose concentration of ±0.01 w/w%, an error which contributes ±1% error to the estimation of the production rate of hydrate in the reactor.

The effect of dissolved freon on the refractive index was checked by conducting a series of experiments with a standard sucrose solution and saturating samples with freon under pressure. The freon had no effect when the sample was brought to equilibrium with atmospheric pressure, expelling residual freon. If the sample was introduced onto the refractometer prism before a period of equilibration, tiny bubbles of freon caused an uneven film of solution to be formed, with gas trapped between the glass surfaces.

G3 Sucrose-Viscosity and other physical constants

Adequate data is available (81) for a large range of sucrose concentrations and solution temperatures. Since the viscosity is an important variable in this work and appears in computer solutions, a mathematical expression for the variation in viscosity was preferred to a graphical interpolation technique.

The equation was based on the Andrade equation quoted by Perry (71), which describes the effect of temperature on liquid viscosity:

$$\eta_l = Ae^{B/T}$$

where A and B are constants for a pure liquid and will become variables for a 2 component system.

Assume:

$$A = a_o + a_1x + a_2x^2 + a_3x^3$$

$$B = b_o + b_1x + b_2x^2 + b_3x^3$$

where a_o, a_1, ... b_o, b_1, ... are constants and x is the weight fraction of sucrose in solution.

Data covering the range 0 to 45% (w/w) and 0-30°C was obtained from Honig (81) and the non-linear model above was fitted to the data by a hill-climbing computer programme, which minimised the sum of squares of the errors. This gave the expression:

$$\eta_l = 10^{-3}(1.154 - 6.32x + 11.88x^2 - 76.51x^3)e^{B/T}$$

where

$$B = 1993.4 + 2347.5x + 1283x^2 + 5343x^3$$

and η_l is given in centipoise and T is measured in °K. The estimate of the standard mean deviation is 0.054 cp, and the mean percentage deviation from the model was ±1.5%. All data fell within ±5% of the estimated viscosity for the range considered.

The surface tensions of sucrose solutions (84) and freon (82) are given in figure A22. It is noteworthy that the interfacial tension varies only slightly over the entire experimental range.

The sucrose density (84) may be expressed:

$$\rho_l = 0.9945 + 0.435x \qquad (g/cm^3)$$

The sucrose specific heat, International Critical Tables;

$$c_p = 0.992 - 0.61x \qquad (cal/g.)$$

G4 Calorimetric determination of power input

It is desirable to estimate the relative power consumed by the dual and the single impeller systems, since the power input is used as the scale-up criterion. Calorimetric tests were run to measure the power dissipated as heat in the reactor. The results were reproduceable, with the reactor operating at ambient temperature in an atmosphere of air. The results are summarised in table XXVI, and presented in graphical form, figure A23. The relevance of the change in power consumed with liquid head is discussed in chapter six.

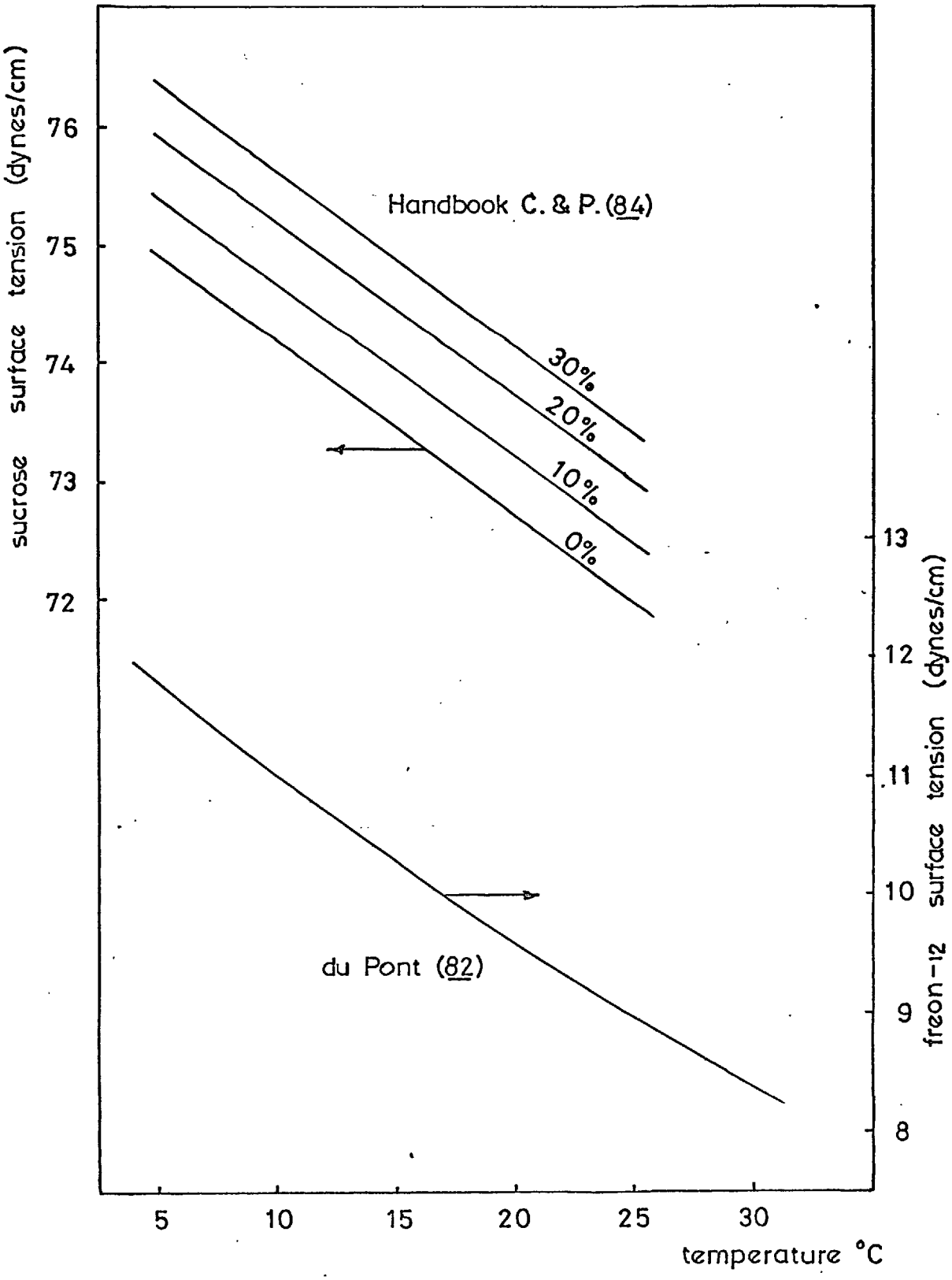


figure A 22 Variation of surface tension with temperature

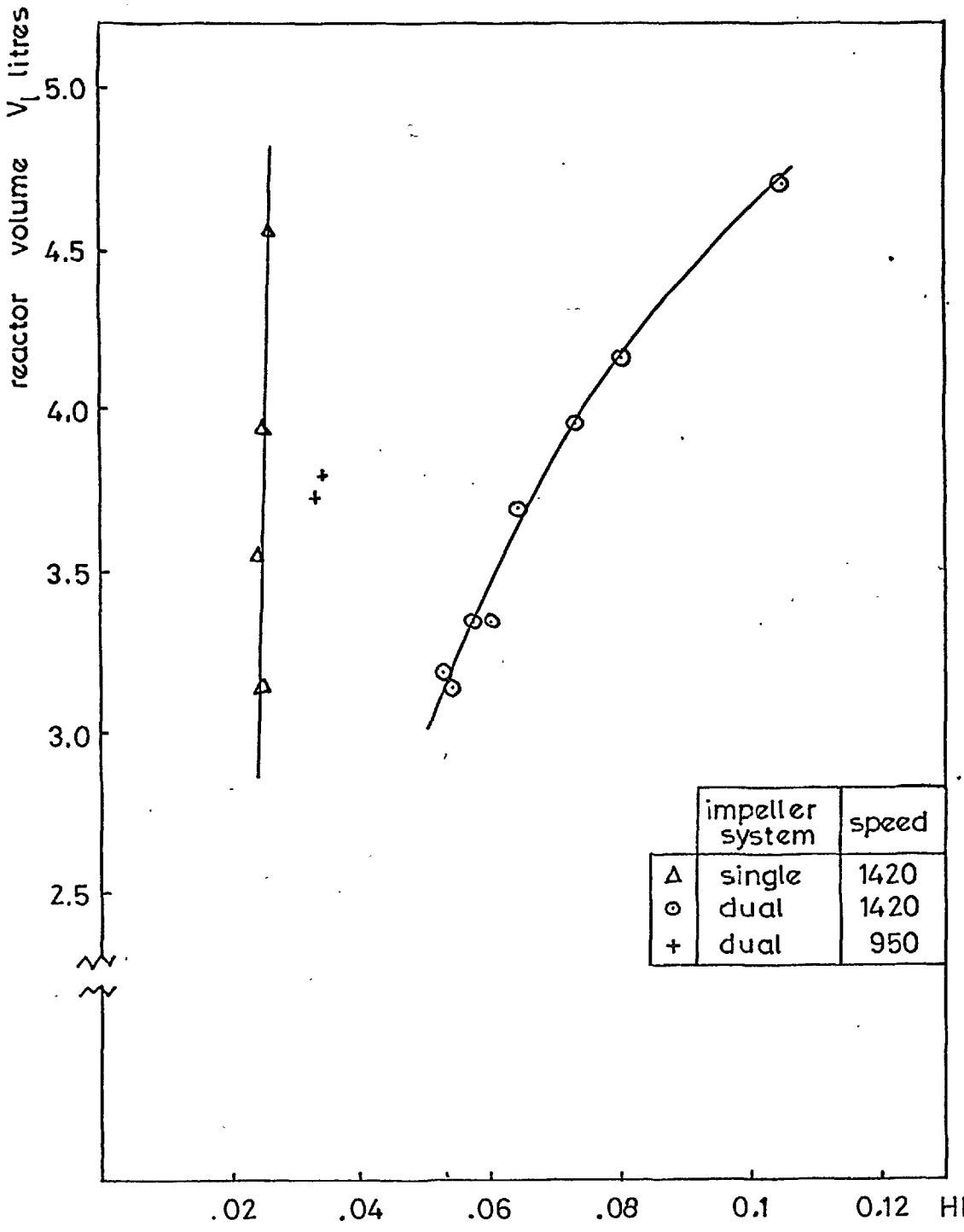


figure A 23 Plot of power consumed in aqueous phase versus volume of phase

Table XXVI

Stirrer power input with liquid depth

Run	Impeller speed and type	Reactor liquid capacity l	Total heat capacity Kcal/°C	Heating rate °C/min	Stirrer HP
G1		4.55	4.69	0.0592	0.026
G2	1420 rpm	3.55	3.72	0.0688	0.024
G3	Single	3.14	3.39	0.0770	0.024
G4		3.95	4.11	0.0650	0.025
G5		3.19	3.37	0.1475	0.053
G6		3.35	3.53	0.1530	0.0575
G7	1420 rpm	3.95	4.11	0.1675	0.0735
G8		4.70	4.88	0.2015	0.105
G9	Dual	4.15	4.31	0.174	0.080
G10		3.70	4.87	0.123	0.064
G11		3.35	3.53	0.159	0.060
G12		3.14	3.33	0.152	0.054
G14	950 rpm	3.74	3.91	0.0790	0.033
G15	Dual	3.80	3.97	0.0803	0.034

Note:

Heat capacity of reactor = 0.295 Kcal/°C

Heat leak into reactor @ 10°C = 0.34 Kcal/min

TABLE XXVII

Data from Sideman (67)

Predicted heat flow rate from model (ii), table 5.41

Q Heat Input (watts)	Q' Predicted heat flow (watts)	N Agitation speed (RPM)	(T_r-T_1) Temperature differential °C
100	127	600	0.95
100	112	700	0.20
100	126	800	0.10
100	136	900	0.05
150	147	600	1.5
150	151	700	0.5
150	136	750	0.2
150	126	800	0.1
150	136	900	0.05
150	132	1000	0.02
175	164	600	2.1
175	172	700	0.75
175	172	750	0.43
175	164	800	0.23
175	170	900	0.10
175	177	1000	0.05
200	181	600	2.90
200	212	700	1.43
200	217	800	0.55
200	193	900	0.15

Notation

A_b	= total surface area of bubbles	(cm^2)
A_v	= total heat transfer area of agent	(cm^2)
a	= specific surface of dispersed phase	(cm^{-1})
c_b	= equilibrium agent concentration at bubble surface	($g.mol/cm^3$)
c_i	= agent concentration at crystal surface	($g.mol/cm^3$)
c_p	= specific heat of aqueous phase	(cal/g^oC)
c_{ph}	= specific heat of hydrate crystal	(cal/g^oC)
c_r	= agent concentration in bulk aqueous phase	($g.mol/cm^3$)
c_s	= agent concentration in equilibrium with hydrate	($g.mol/cm^3$)
D	= impeller diameter	(cm)
D_{as}	= molecular diffusion coefficient of agent in sucrose solution	(cm^2/sec)
D_{ss}	= diffusivity of sucrose in aqueous solution	(cm^2/sec)
D_T	= tank diameter	(cm)
D_1, D_2	= dispersion coefficients based on superficial velocity in wash column	(cm^2/sec)
E	= energy dissipated per unit volume	(HP/ft^3)
E_g	= energy dissipated under gas load	(HP/ft^3)
e	= void fraction	
F	= liquid agent flow rate	(g/min)
G	= gaseous agent flow rate	(cm^3/min)
h	= heat transfer coefficient	($cal/min.cm^2.^oC$)
K_h	= total heat leak into reactor	(cal/min)
k_c	= liquid-film mass transfer coefficient for diffusion to crystal surface	(cm/sec)
k_c'	= rate constant for surface process	(cm/sec)
k_l	= liquid-film mass-transfer coefficient for diffusion from dispersed agent	(cm/sec)
k_l'	= modified liquid-film transfer coefficient	($g.cm/g.mol.min$)

Notation (continued)

Le	= Lewis number $(\frac{k}{\rho_l c_p D_{as}})$	
N	= stirrer speed	(r.p.m.)
P	= reactor pressure	(p.s.i.a.)
P*	= hydrate equilibrium pressure at invariant point	(p.s.i.a.)
P_g	= agitator power input under gas load	(H.P.)
P_h	= hydrate equilibrium pressure at temperature of bulk aqueous phase	(p.s.i.a.)
P_o	= agitator power input in liquid phase	(H.P.)
Q	= reactor heat load, equation (58)	(cal/min)
Q'	= net cooling rate in steady state runs	(cal/min)
Re	= Reynolds number	
r	= rate of hydrate production expressed as water flux	(g/min)
r_A	= agent transfer rate	(g.mol/sec)
r_d	= rate of hydrate decomposition as water flux	(g/min)
Sc	= Schmidt number (ν_l/D_{as})	
T_c	= equilibrium temperature of hydrate at P, x_r	(°C)
T_i	= temperature at crystal surface	(°C)
T_l	= condensation temperature of agent at reactor pressure	(°C)
T_n	= nucleation temperature	(°C)
V_g	= superficial gas velocity in reactor	(ft/sec)
V_l	= volume of liquid in the reactor	(cm^3)
V_r	= total operating volume of four-phase dispersion	(cm^3)
v_c	= reactor recycle rate	(cm^3/min)
v_f	= sucrose feed rate	(cm^3/min)
X	= mole fraction of sucrose in solution	

Notation (continued)

x	= weight fraction of sucrose in solution	(w/w)
x_f	= weight fraction of sucrose in reactor feed	(w/w)
x_s	= sucrose concentration at crystal surface	(w/w)
w	= distance measured from crystal surface	(cm)
y	= hold-up of water in hydrate form	(g)
z	= distance measured from bubble surface	(cm)
α	= mole ratio of water to agent in hydrate molecule, α' refers to weight ratio	
λ_{hf}	= heat of formation of hydrate phase	(cal/g)
λ_l	= latent heat of vaporization of hydrating agent	(cal/g)
η_d	= viscosity of dispersed phase	(g/cm.sec)
η_h	= viscosity of hydrate slurry	(g/cm.sec)
η_l	= viscosity of continuous liquid phase	(g/cm.sec)
ϕ_g	= volume fraction of gas in dispersion	
ϕ_h	= volume fraction of hydrate phase in dispersion	
ϕ_l	= volume fraction of liquid agent in dispersion	
ρ_l	= liquid density	(g/cm^3)
σ	= interfacial surface tension	(dyne/cm)
ξ	= conversion of aqueous feed	
f,r,b,d	= subscripts used throughout to denote feed and reactor conditions, bubble and drop sites respectively.	

References

(1) Muller J.G., "Concentration and Purification by Freezing", International Institute of Refrigeration, Delft, 1966.

(2) Tressler D.K., and Joslyn M.A., "The Chemistry and Technology of Fruit and Vegetable Juice Production", Avi, New York, 1954.

(3) Jacobs M.B., editor "The Chemistry and Technology of Food and Food Products", 2d ed., Interscience, New York, 1951.

(4) Tressler D.K., Joslyn M.A., and Marsh, "Fruit and Vegetable Juices", Avi, New York, 1939.

(5) News Item, European Chemical News 7, 156 (1965).

(6) Stewart E.D., American Brewer 94, 92 (1961).

(7) Dooley J.R., and Lineberry D.D., Chem. Eng. Progr. 62, Symp. Ser., No. 69, 111 (1966).

(8) Strobel J.J., Chem. Eng. Progr. 57, No. 1, 37 (1961).

(9) McKay D.L., Brit. Patent 973,729 Oct. 1964

(10) Ahrel P.J.I., Brit. Patent 688,593 Mar. 1953
Corny J., Brit. Patent 932,215 July 1963
Clark H.E., U.S. Patent 3,098,735 July 1963
Slattery G.H., U.S. Patent 2,764,488 Sept.1956

(11) Dynatech Co., Office of Saline Water, U.S. Dept. of Interior, Res. and Dev. Progress Rept. No. 120, 1964.

(12) Sideman S., and Shabtai H., Canadian J. Chem. Eng. 42, 107 (1964).

(13) Lindblom E.D., U.S. Patent 2,297,786 Oct. 1942

(14) Stinchfield R.M., Sc.D. Thesis, M.I.T., 1952.

(15) Bottoms R.R., U.S. Patent 2,020,719 Nov. 1935
Brown D., Brit.Patent 954,926 Apr. 1964
Gilliland E.R., Brit.Patent 841,374 July 1960
Herman E.R., Brit.Patent 912,772 Dec. 1962
Margiloff I.B., Brit.Patent 919,595 Feb. 1963
Rosenstein L., U.S. Patent 3,098,733 July 1963
Svanoe H., U.S. Patent 3,098,734 July 1963
Zarchin A., U.S. Patent 2,821,304 Jan. 1958

(16) Blaw-Knox Co., Office of Saline Water, U.S. Dept. of Interior, Res. and Dev. Progress Rept. No. 40, 1960.
Wiegandt H.F., Office of Saline Water, U.S. Dept. of Interior, Res. and Dev. Progress Rept. No. 41, 1960.

(17) Shiloh M., and Sideman S., Canadian J. Chem. Eng. 45, 300 (1967).

(18) Donath W.E., U. U.S. Patent 2,904,511 Sept. 1959

(19) Barduhn A.J., Towlson H.E., and Chien Hu Y., A.I. A.I.Ch.E. Journal 8, 176 (1962).

(20) Briggs F.A., and Barduhn A.J., "Saline Water Conversion II", Advances in Chemistry Series, No. 38, Am. Chem. Soc., 1963.

(21) Sourinajan S., Ind. Eng. Chem. Proc. Des. & Dev. 6, 154 (1964).

(22) Barduhn A.J., Chem. Eng. Progr. 63, 99 (1967).

(23) Williams V.C., Roy C.L., and Williams R.A., International Symposium on Water Desalination, Washington, Oct. 1965.

(24) Koppers Co., Office of Saline Water, U.S. Dept. of Interior, Res. and Dev. Progress Repts. No. 90 & No. 125, 1964.

(25) Collot d'Escury F.A.C., M. Sc. Thesis, T.H.Delft, 1964.

(26) de Graauw J., and Rutten J., "Results of some experiments on hydrate formation", Technological University, Delft, Sept. 1965.

(27) Pangborn J.B., "Hydrate reaction kinetics", Syracuse University Research Institute, Sept. 1966.

(28) Luyben W.L., A.I.Ch.E. Journal 12, 662 (1966).

(29) Weisser E.F., Chem. Eng. Progr. 61, No. 4, 86 (1965).

(30) Westerterp K.R., van Dierendonck L.L., and de Kraa J.A., Chem. Eng. Sci. 18, 157 (1963).

(31) Bates R.L., Fondy P.L., and Corpstein R.R., Ind. Eng. Chem. Proc. Des. & Dev. 2, 310 (1963).

(32) Wittstruck T.A., Brey W.S., Buswell A.M., and Rodebush W.H., J. Chem. Eng. Data 6, 345 (1961).

(33) Wilcox W.I., Carson D.B., and Katz D.L., Ind. Eng. Chem. 33, 662 (1941).

(34) Barduhn A.J., Office of Saline Water, U.S. Dept. of Interior, Res. and Dev. Progress Rept. No. 44, 1960.

(35) von Stackelberg M., and Müller H.R., Z. Electrochem. 58, 40 (1954).

(36) Mandel J., "The Statistical Analysis of Experimental Data", Interscience, New York, 1964.

(37) E.I. du Pont de Nemours & Co., Technical Bulletin B-17, 1953.

(38) Barduhn A.J., Office of Saline Water, U.S. Dept. of Interior, Res. and Dev. Progress Repts. No. 59, 1962; No. 88, 1964.

(39) Glew D.N., and Molwyn-Hughes E.A., Disc. Faraday Soc. No. 15, 150 (1953).

(40) Johnson A.I., and Furter W.F., Canadian J. Chem. Eng. 38, 78 (1960).

(41) Sideman S., and Taitel Y., Int. J. Heat & Mass Transfer 7, 1273 (1964).

(42) Gordon K.F., and Sherwood T.K., Chem. Eng. Progr. 50, Symp. Ser., No. 10, 15 (1954).

(43) Noyes A.A., and Whitney W.R., J. Am. Chem. Soc. 19 930 (1897).

(44) Cartier R., Pindzola D., and Burns P.F., Ind. Eng. Chem. 51, 1409 (1959).

(45) Nielson A.E., "Kinetics of Precipitation", Pergammon, 1964.

(46) Chilton T.H., and Colburn A.P., Ind. Eng. Chem. 26, 183 (1934).

(47) Rushton J.E., Costich E.W., and Everett A.J., Chem. Eng. Progr. 46, 395 (1950).

(48) Miller S.A., and Mann C.A., Trans. Am. Inst. Chem. Engr. 40, 709 (1944).

(49) Oyama Y., and Endoh K., Chem. Eng. (Japan) 19, 2 (1955).

(50) Michel B.J., and Miller S.A., A.I.Ch.E. Journal 8, 262 (1962).

(51) Friedman A.M., and Lightfoot E.N., Ind. Eng. Chem. 49, 1227 (1957).

(52) Calderbank P.H., Brit. Chem. Eng. 1, 206 (1956).

(53) Calderbank P.H., Trans. Instn. Chem. Engrs. 36, 443 (1958).

(54) Foust H.C., Mack D.E., and Rushton J.H., Ind. Eng. Chem. 36, 517 (1944).

(55) Vermeulen T., Williams G.M., and Langlois G.E., Chem. Eng. Progr. 51, 85 (1955).

(56) Rodger W.A., Trice V.G., and Rushton J.H., Chem. Eng. Progr. 52, 515 (1956).

(57) Hixson A.W., and Baum S.J., Ind. Eng. Chem. 33, 478 (1941).

(58) Johnson A.I., and Huang C.J., A.I.Ch.E. Journal 2, 413 (1956).

(59) Calderbank P.H., and Moo-Young M.B., Chem. Eng. Sci. 16, 39 (1961).

(60) Harriott P., A.I.Ch.E. Journal 8, 93 (1962).

(61) Middleman S., A.I.Ch.E. Journal 11, 750 (1965).

(62) Wilke C.R., and Chang P., A.I.Ch.E. Journal 1, 264 (1955).

(63) Ratcliffe G.A., and Holdcroft J.G., Trans. Instn. Chem. Engrs. 41, 315 (1963).

(64) Sideman S., Hortascu O., and Fulton J.W., Ind. Eng. Chem. 58, 38 (1966).

(65) Korwat H., Chem. Ing. Technik 31, 588 (1959).

(66) Sideman S., and Gat Y., A.I.Ch.E. Journal 12, 296 (1966).

(67) Sideman S., and Barsky Z., A.I.Ch.E. Journal 11, 539 (1965).

(68) Maude A.D., and Whitmore R.L., Trans. Instn. Chem. Engrs. 36, 296 (1958).

(69) Bonilla C.F., Cervi A., Colven J.J., and Wang S.J., "Preprints of the Heat Transfer Symposium", A.I.Ch.E., Dec. 1951.

(70) Davies O.L., ed. "The Design and Analysis of Industrial Experiments", Oliver and Boyd, 1954.

(71) Perry J.H., ed. "Chemical Engineers' Handbook", 3rd ed., McGraw-Hill, 1963.

(72) Sherwood T.K., Office of Saline Water, U.S. Dept. of Interior, Res. and Dev. Progress Rept. No. 242, 1967.

(73) Melia T.P., and Moffitt W.P., Ind. Eng. Chem. Fund. 3, 313 (1964).

(74) Kitchener S.A., and Strickland-Constable R.F., Proc. Roy. Soc. A 245, 93 (1958).

(75) Lal D.P., Ph.D. Thesis, University of London, 1966.

(76) Danckwerts P.V., Chem. Eng. Sci. 2, 1 (1953).

(77) Dodge B.F., and Eshaya A.M., "Saline Water Conversion", Advances in Chemistry Series, No. 27, Am. Chem. Soc., 1960.

(78) Yoshida F., and Miura Y., Ind. Eng. Chem. Proc. Des. & Dev. 2, 263 (1963).

(79) Clayton W.J., J. Soc. Cosmetic Chemists 18, 333 (1967).

(80) Umano S., Japan. Govt. Chem. Ind. Res. Publ., 54, No. 1, 27 (1959).

(81) Honig P., ed. "Principles of Sugar Technology", Volume I, Elsevier, 1959.

(82) E.I. du Pont de Nemours & Co., Technical Bulletin T-12, 1956.

(83) Glasstone S., "Thermodynamics for Chemists", van Nostrand, 1956.

(84) Hodgeman C.D., ed. "Handbook of Chemistry and Physics", 40th ed., Chemical Rubber Publishing Co.

(85) Ting H.H., and McCabe W.L., Ind. Eng. Chem. 26, 1201 (1934).

(86) Carman P.C., Trans. Instn. Chem. Engrs. 15, 150 (1937).